

## NATIONAL INSTITUTE FOR FUSION SCIENCE

## Review of Zonal Flows

P.H. Diamond, S.-I. Itoh, K. Itoh and T.S. Hahm

(Received - Sep. 9, 2004 )

NIFS-805

Oct. 2004

This report was prepared as a preprint of work performed as a collaboration research of the National Institute for Fusion Science (NIFS) of Japan. The views presented here are solely those of the authors. This document is intended for information only and may be published in a journal after some rearrangement of its contents in the future.

Inquiries about copyright should be addressed to the Research Information Center, National Institute for Fusion Science, Oroshi-cho, Toki-shi, Gifu-ken 509-5292 Japan.

E-mail: [bunken@nifs.ac.jp](mailto:bunken@nifs.ac.jp)

**<Notice about photocopying>**

In order to photocopy any work from this publication, you or your organization must obtain permission from the following organization which has been delegated for copyright for clearance by the copyright owner of this publication.

**Except in the USA**

Japan Academic Association for Copyright Clearance (JAACC)

6-41 Akasaka 9-chome, Minato-ku, Tokyo 107-0052 Japan

Phone: 81-3-3475-5618 FAX: 81-3-3475-5619 E-mail: [jaacc@mtd.biglobe.ne.jp](mailto:jaacc@mtd.biglobe.ne.jp)

**In the USA**

Copyright Clearance Center, Inc.

222 Rosewood Drive, Danvers, MA 01923 USA

Phone: 1-978-750-8400 FAX: 1-978-646-8600

## **Review of Zonal Flows**

P. H. Diamond<sup>1</sup>, S.-I. Itoh<sup>2</sup>, K. Itoh<sup>3</sup>, T. S. Hahm<sup>4</sup>

<sup>1</sup> University of California San Diego, La Jolla, CA 92093-0319, USA

<sup>2</sup> Institute for Applied Mechanics, Kyushu University 87, Kasuga 816-8580, Japan

<sup>3</sup> National Institute for Fusion Science, Toki 509-5292, Japan

<sup>4</sup> Princeton University, Plasma Physics Laboratory, Princeton, NJ 08543, USA

### **Abstract**

A comprehensive review of zonal flow phenomena in plasmas is presented. While the emphasis is on zonal flows in laboratory plasmas, zonal flows in nature are discussed as well. The review presents the status of theory, numerical simulation and experiments relevant to zonal flows. The emphasis is on developing an integrated understanding of the dynamics of drift wave - zonal flow turbulence by combining detailed studies of the generation of zonal flows by drift waves, the back-interaction of zonal flows on the drift waves, and the various feedback loops by which the system regulates and organizes itself. The implications of zonal flow phenomena for confinement in, and the phenomena of fusion devices are discussed. Special attention is given to the comparison of experiment with theory and to identifying directions for progress in future research.

### **Dedication**

This review article is dedicated to the memory of Professor. Marshall N. Rosenbluth.

**Keywords:** zonal flow, geodesic acoustic mode, zonal magnetic field, drift waves, convective cells, turbulence, turbulent transport, turbulence suppression, nonlinear interaction, modulational instability, envelope formalism, nonlocal interaction in Fourier space, coherent structure, statistical property, confinement improvement, dynamo, planetary atmosphere, nonlinear theory, numerical simulation, experimental observation

## **Contents**

1. Introduction
2. Basic Physics of Zonal Flows: A Heuristic Overview
  - 2.1 Introduction
  - 2.2 Basic dynamics of zonal flows
  - 2.3 Self-consistent solution and multiple states
  - 2.4 General comments
  - 2.5 Implications for experiments
3. Theory of zonal flows
  - 3.1 Linear Dynamics of Zonal Flow Modes
  - 3.2 Generation mechanism
  - 3.3 Shearing and back reaction of flows on turbulence
  - 3.4 Nonlinear Damping and Saturation: Low Collisionality Regimes
  - 3.5 The Drift Wave - Zonal Flow System: Self-consistent State
  - 3.6 Suppression of Turbulent Transport
4. Numerical Simulations of Zonal Flow Dynamics
  - 4.1 Introduction
  - 4.2 Ion Temperature Gradient Driven Turbulence
  - 4.3. Electron Temperature Gradient Driven Turbulence
  - 4.4. Fluid Simulations with Zonal Flows
  - 4.5 Edge turbulence
  - 4.6 Short summary of the correspondence between theoretical issues and numerical results
5. Zonal Flows in Planetary Atmospheres
  - 5.1 Waves in rotating sphere.
  - 5.2 Zonal Belts of Jupiter
  - 5.3 Superrotation of the Venusian Atmosphere
6. Extensions of Theoretical Models
  - 6.1 Streamers
  - 6.2 Noise Effects and Probabilistic Formulations
  - 6.3 Statistical properties
  - 6.4 Non-Markovian Theory
  - 6.5 Envelope Formalism
7. Laboratory Experiments on Zonal Flow Physics
  - 7.1 Characteristics of Zonal Flows
  - 7.2. Zonal Flow Dynamics and Interaction with Ambient Turbulence
  - 7.3. Suggestions on future experiments and information needed from simulations and theory
8. Summary and Discussion  
Acknowledgements
- Appendix A Ray of Drift Wave Packet and Trapping
- Appendix B Hierarchy of Nonlinear Governing Equations
- Appendix C Near isomorphism between ETG and ITG

## 1. Introduction

Zonal flows, by which we mean azimuthally symmetric band-like shear flows, are a ubiquitous phenomena in nature and the laboratory. The well-known examples of the Jovian belts and zones, and the terrestrial atmospheric jet stream are familiar to nearly everyone - the latter especially to travelers enduring long, bumpy airplane rides against strong head winds. Zonal flows are also present in the Venusian atmosphere (which rotates faster than the planet does!) and occur in the solar tachocline, where they play a role in the solar dynamo mechanism. In the laboratory, the importance of sheared  $\mathbf{E} \times \mathbf{B}$  flows to the development of L-mode confinement, the L-to-H transition and internal transport barriers (ITBs) is now well and widely appreciated.

While many mechanism can act to trigger and stimulate the growth of sheared electric fields (i.e. profile evolution and transport bifurcation, neoclassical effects, external momentum injection, etc.) certainly one possibility is via the self-generation and amplification of  $\mathbf{E} \times \mathbf{B}$  flows by turbulent stresses (i.e. the turbulent transport of momentum). Of course, this is the same mechanism as that responsible for zonal flow generation. However, it should be emphasized that it is now widely recognized and accepted that zonal flows are a key constituent in virtually *all* cases and regimes of drift wave turbulence - indeed, so much so that this classic problem is now frequently referred to as "drift wave-zonal flow turbulence". This paradigm shift occurred on account of the realization that zonal flows are ubiquitous in dynamical models used for describing fusion plasmas (i.e. ITG, TEM, ETG, resistive ballooning, and interchange, etc.) in all geometries and regimes (i.e. core, edge, etc.), and because of the realization that zonal flows are a critical agent of self-regulation for drift wave transport and turbulence. Both theoretical work and numerical simulation made important contributions to this paradigm shift. Indeed, for the case of low collisionality plasmas, a significant portion of the available free energy is ultimately deposited in the zonal flows. Figure 1.1 presents energy flow charts which illustrate the classic paradigm of drift wave turbulence and the new paradigm of drift wave - zonal flow turbulence. The study of zonal flow has had a profound impact on fusion research. For instance, the proper treatment of the zonal flow physics has partly resolved the confusion concerning the prospect of burning plasma as has been discussed by Rosenbluth and collaborators in conjunction with the design of the International Thermonuclear Experimental Reactor (ITER). At the same time, the understanding of the turbulence-zonal flow system has advanced the understanding of self-organization process in nature.

We note here that, while zonal flows have a strong influence on the formation of transport barriers, the dynamics of barriers and transitions involve evolutions of both the mean  $\mathbf{E} \times \mathbf{B}$  flow as well as the zonal  $\mathbf{E} \times \mathbf{B}$  flow. The topics of mean  $E_r$  dynamics, transport barriers, and confinement regime transitions are beyond the scope of this review.

In the context of tokamak plasmas, zonal flows are  $n = 0$  electrostatic potential fluctuations with finite radial wave number. Zonal flows are elongated, asymmetric vortex modes, and thus have zero frequency. They are predominantly poloidally symmetric as well, though some coupling to low- $m$  sideband modes may occur. On account of their symmetry, zonal flows cannot access expansion free energy stored in temperature, density gradients, etc., and are not subject to Landau damping. These zonal flows are driven *exclusively* by nonlinear interactions, which transfer energy from the finite- $n$  drift waves to the  $n = 0$  flow. Usually, such nonlinear interactions are three-wave triad couplings between two high  $k$  drift waves and one low  $q = q_r \hat{r}$  zonal flow excitation. In position space, this energy transfer process is simply one whereby Reynolds work is performed on the flow by the wave stresses. Two important consequences of this process of generation follow directly. First, since zonal flow production is exclusively via nonlinear transfer from drift waves, zonal flows must eventually decay and vanish if the underlying drift wave drive is extinguished. Thus, zonal flows differ in an important way from mean  $\mathbf{E} \times \mathbf{B}$  flows, which can be sustained (and are, in strong H-mode and ITB regimes) in the absence of turbulence. Second, since zonal flows are generated by nonlinear energy transfer *from* drift waves, their generation naturally acts to *reduce* the intensity and level of transport caused by the primary drift wave turbulence. Thus, zonal flows necessarily act to *regulate and partially suppress* drift wave turbulence and transport. This is clear from numerical simulations, which universally show that turbulence and transport levels are reduced when the zonal flow generation is (properly) allowed. Since zonal flows cannot tap expansion free energy, are generated by nonlinear coupling from drift waves, and damp primarily (but not exclusively) by collisional processes, they constitute a significant and benign (from a confinement viewpoint) reservoir or repository for the available free energy of the system.

Another route to understanding the effects of zonal flow on drift waves is via the shearing paradigm: From this standpoint, zonal flows produce a spatio-temporally complex shearing pattern, which naturally tends to distort drift wave eddies by stretching them, and in the process generates large  $k_r$ . Of course, at smaller scales, coupling to dissipation becomes stronger, resulting in a net stabilizing trend. The treatment of zonal flow shearing differs from that for mean flow shearing on account of the complexity of the flow pattern. Progress here has been facilitated by the realization that a statistical analysis is possible. This follows from the fact that the autocorrelation time of a drift wave packet propagating in a zonal flow field is usually quite short, and because the drift wave rays are chaotic. Hence, significant advances have been made on calculating the 'back reaction' of zonal flows on the underlying drift wave field within the framework of random shearing, using wave kinetics and quasilinear theory. Conservation of energy between drift waves and zonal flows has been proved for the theory, at the level of a

renormalized quasilinear description. Thus, it is possible to close the 'feedback loop' of wave-flow interactions, allowing a self-consistent analysis of the various system states, and enabling an understanding of the mechanisms and routes for bifurcation between them.

From a more theoretical perspective, the drift wave-zonal flow problem is a splendid example of *two* generic types of problems frequently encountered in the dynamics of complex systems. These are the problem of nonlinear interaction between two classes of fluctuations of disparate scale, and the problem of self-organization of structures in turbulence. The drift wave-zonal flow problem is clearly a member of the first class, since drift waves have high frequency and wavenumber ( $k_{\perp} \rho_i \sim 1$ ,  $\omega_k \sim \omega_*$ ) in comparison to zonal flows ( $q \rho_i \ll 1$ ,  $\Omega \sim 0$ ). Another member of this group, familiar to most plasma physicists, is the well known problem of Langmuir turbulence, which is concerned with the interaction between high frequency plasma waves and low frequency ion acoustic waves. As is often the case in such problems, fluctuations on one class of scales can be treated as "slaved" to the other, thus facilitating progress through the use of averaging, adiabatic theory and projection operator techniques. In the case of the drift wave-zonal flow problem, great simplification has been demonstrated via the identification of a conserved drift wave population density (i.e. action-like invariant) which is adiabatically modulated by the sheared flows. Indeed, though superficially paradoxical, it seems fair to say that such disparate scale interaction problems are, in some sense, more tractable than the naively 'simpler' problem of Kolmogorov turbulence, since the ratio of the typical scales of the two classes of fluctuations may be used to constitute a small parameter, which is then exploited via adiabatic methodology.

Of course, it is patently obvious that the zonal flow problem is one of self-organization of large structure in turbulence. Examples of other members of this class include transport barrier and profile formation and dynamics, the origin of the solar differential rotation, the famous magnetic dynamo problem (relevant, in quite different limits, to the sun, earth, galaxy, and Reversed Field Pinch), and the formation of profiles in turbulent and swirling pipe flow. Table 1.1 summarizes these related structure formation phenomena, illustrating the objective of this review. Most of these problems are attacked at the simplest level by considering the stability of an ensemble or 'gas' of ambient turbulence to a seed perturbation. For example, in the dynamo problem, one starts by considering the stability of some state of MHD turbulence to a seed magnetic field. In the zonal flow problem, one correspondingly considers the stability of a gas of drift waves to a seed shear. The incidence of instability means that the initial vortex tilt will be re-enforced, thus amplifying the seed perturbation. It should be noted that the zonal flow formation phenomenon is related to, but not quite the same as, the well known inverse cascade of energy in a 2D fluid, which leads to large scale vortex formation. This is because the inverse cascade proceeds via a local coupling in wavenumber space, while

zonal flow generation occurs via nonlocal transfer of energy between small and large scales. Indeed, zonal shear amplification is rather like the familiar  $\alpha$  -effect from dynamo theory, which describes a nonlocal transfer of magnetic helicity to large scale. We also note that the initial stage of pattern formation instability meets only a part of the challenge to a theoretical description of structure formation, and that one must subsequently 'close the loop' by understanding the mechanisms of saturation of the zonal flow instability. The saturation of zonal flows driven by drift wave turbulence is now a subject of intensive theoretical and computational investigation, worldwide.

As a related phenomena, convective cells have been subject to intensive study for a long time. The convective cell is a perturbation which is constant along the magnetic field line but changes in the direction perpendicular to the magnetic field. Such a structure is known to be induced by background drift wave turbulence. The zonal flow can be considered as a particular example of an anisotropic convective cell. However, the convective cells of greatest interest as agents of transport are localized in the poloidal direction and extended radially, which is the opposite limit of anisotropy from that of the zonal flow. Such cells are commonly referred to as *streamers*.

As the zonal flow problem is a member of a large class of rapidly expanding research topics, the perspective of this review is composed as follows. First, we present detailed explanations of the physical understanding of drift wave-zonal flow turbulence. Second, we also stress the view that studies on toroidal plasma turbulence enhance our understanding of turbulent structure formation in nature. In this sense, this review is a companion article to recent reviews on the magnetic dynamo problem which, taken together, present a unified view that addresses the mystery of structure formation in turbulent media. Third, the impact of direct nonlinear simulation (DNS) is discussed in the context of understanding zonal flow physics, although a survey of DNS techniques themselves is beyond the scope of this review. It is certainly the case that DNS studies have significantly furthered our understanding of drift wave-zonal flow turbulence. For these reasons, examples are mainly chosen from the realm of core plasma (i.e. drift wave) turbulence. In order to maintain transparency and to be concise, this review is limited in scope. Studies of edge turbulence and of general convective cell physics are not treated in depth here. While these topics are closely related to the topic of this review, extensive introductory discussions, which are too lengthy for this paper, are necessary. Hence, details of these important areas are left for future reviews.

This article reviews zonal flow dynamics, with special emphasis on the theory of drift wave-zonal flow turbulence and its role in plasma confinement. The remainder of this review article is organized as follows. Chapter 2 presents a heuristic overview of the essentials of zonal flow physics, including shearing, generation mechanisms, and multiple states and bifurcations. Chapter 2 is aimed at general readers and non-specialists. Chapter 3 presents a detailed description of the theory of drift wave-zonal

flow turbulence. Section 3.1 discusses neoclassical collisional friction damping. Section 3.2 is concerned with drive and amplification, from a number of perspectives and approaches. In particular, both coherent and broad-band modulational stability calculations are explained in detail, and extensions to regimes where waves are trapped in the flows are discussed as well. Section 3.3 describes the feed back of zonal flows on drift waves, while Section 3.4 discusses nonlinear saturation mechanisms. An emphasis is placed upon unifying the various limiting models. Section 3.5 presents a unified, self-consistent description of the various systems and the bifurcation transitions between them. Section 3.6 deals with the effect of the zonal flows on transport. Chapter 4 gives an overview of what numerical simulations have elucidated about zonal flow dynamics in magnetized plasmas. Chapter 5 gives an introduction to zonal flow phenomena in nature. Special emphasis is placed upon the well known and visually compelling example of belt and band formation in the atmosphere of Jupiter. Chapter 6 discusses advanced extensions of the theory, including statistical and probabilistic approaches, application to general convective cell phenomena (including "streamers") and non-Markovian models. Chapter 7 surveys the state of experimental studies of zonal flow phenomena in magnetically confined plasma. Chapter 8 gives a statement of conclusions, an assessment of the current state of our understanding and presents suggestions for the future direction of research. These structures are illustrated in the roadmap of Fig.1.2.



## 2. Basic Physics of Zonal Flows: A Heuristic Overview

### 2.1 Introduction

We present an introduction to the basic physics of zonal flows. This section is directed toward a general audience, which may include plasma and fusion experimentalists and other non-specialists. Some of the relevant, early work on zonal flows can be found in [2.1-2.6]. The emphasis here is on physical reasoning and intuition, rather than on formalism and rigorous deduction. This section begins with a discussion of shearing [2.7-2.11] by a spectrum of zonal flows and its effect on the primary drift wave spectrum. Considerations of energetics, specifically the conservation of energy between drift waves and zonal flows (which is explicitly proved in Section III), in the quasi-linear approximation [2.12-2.13] are then used to describe and calculate the rate of amplification of zonal shears by turbulence. We then discuss some basic features of the dynamical system of waves and zonal flows, and its various states. (Fig.2.1) The final part of this section discusses aspects of experimental investigations of zonal flow physics. Taking as an example drift wave turbulence with a spatial scale length of  $\rho_i$ , the basic characteristics of zonal flows are summarized in Table 2.1. This table serves as a guide for the explanations in the following chapters. In the study of zonal flows, three principal theoretical approaches have been applied. These are: (i) the wave kinetic and adiabatic theory, (ii) the parametric (modulational) theory, and (iii) the envelope formalism. In this chapter, an explanation in the spirit of wave kinetics and adiabatic theory is given. The wave kinetic theory as well as parametric theory are described in Chapter 3. The envelope formalism is discussed in Chapter 6.

### 2.2 Basic dynamics of zonal flows

The zonal flow is a toroidally symmetric electric field perturbation in a toroidal plasma, which is constant on the magnetic surface but rapidly varies in the radial direction, as is illustrated in Fig.2.2. The associated  $\mathbf{E} \times \mathbf{B}$  flow is in the poloidal direction, and its sign changes with radius. The zonal flow corresponds to a strongly asymmetric limit of a convective cell. The key element in the dynamics of zonal flows is the process of shearing of turbulent eddies by flows with a larger scale (i.e., with shear lengths  $L_s > \Delta x_c$ , where  $\Delta x_c$  is the eddy scale). The fact that such shearing acts to reduce turbulence and transport is what drives the strong current interest in zonal flows. In the case of a smooth, mean shear flow, it is well known that shearing tilts eddies, narrowing their radial extent and elongating them. (Fig.2.3). In some simulations, sheared flows are observed to break up the large eddys associated with extended modes. At the level of eikonal theory, this implies that the radial wavenumber of the turbulence increases linearly in time, i.e.

$$\frac{d}{dt} k_r = - \frac{d}{dr} (k_\theta V_\theta(r)), \quad (2.1a)$$

$$k_r = k_r^{(0)} - k_\theta \frac{\partial V_\theta(r)}{\partial r} t. \quad (2.1b)$$

As a consequence, the eddies necessarily must increase the strength of their coupling to small scale dissipation, thus tending to a quench of the driving process. In addition, the increase in  $k_r$  implies a decrease in  $\Delta x_c$ , thus reducing the effective step size for turbulent transport [2.14].

In the case of zonal flows, the physics is closely related, but different in detail, since zonal flow shears nearly always appear as elements of a spatially complex (and frequently temporally complex) pattern. (Fig.2.4) [2.15-2.17] This presents a significant complication to any theoretical description. Fortunately, the problem is greatly simplified by two observations. First, the drift wave spectrum is quite broad, encompassing a range of spatial scales from the profile scale  $L_\perp$  to the ion gyro-radius  $\rho_i$ , and a range of time scales from  $(D_B/L_\perp^2)^{-1}$  to  $L_\perp/c_s$ . Here  $D_B = \rho_s c_s$ . In contrast, the dynamically relevant part of the zonal flow spectrum has quite a low frequency and large extent, so that a scale separation between the drift waves and zonal flows clearly exists. Second, the 'rays' along which the drift waves propagate can easily be demonstrated to be chaotic, which is not surprising, in view of the highly turbulent state of the drift wave spectrum.  $\Delta k$ , the width of the drift wave spectrum satisfies  $\Delta k \rho_i \sim 1$ . Thus, the effective lifetime of the instantaneous pattern 'seen' by a propagating drift wave group packet is  $|\Delta q_r v_g|^{-1}$ . Here,  $q_r$  is the radial wave number of the zonal flow and  $v_g$  is the group velocity of the drift waves. This implies that the effective lifetime of the instantaneous shearing pattern, as seen by the wave packet, is  $\tau_{ac} \sim |\Delta q_r v_g|^{-1}$ . Note that, on account of ray chaos, no 'random phase' assumption for zonal flow shears is necessary [2.18]. For virtually any relevant parameters, this time scale is shorter than the time scale for shearing, trapping, etc. of the wave packet. Thus, the shearing process in a zonal flow field can be treated as a random, diffusive process, consisting of a succession of many short kicks, which correspond to shearing events. Thus, the mean square wavenumber increases as

$$\langle \delta k_r^2 \rangle = D_k t, \quad (2.2a)$$

$$D_k = \sum_q |k_\theta V_{\theta,q}|^2 \tau_{k,q}, \quad (2.2b)$$

where  $\langle \dots \rangle$  represents the average,  $V_{\theta,q}$  represents the  $q$ -Fourier components of the poloidal flow velocity and  $\tau_{k,q}$  is the time of (triad) interaction between the zonal flow

and the drift wave packet. This diffusion coefficient  $D_k$  is simply the mean square shear in the flow-induced Doppler shift of the wave [weighted by the correlation time of the wave packet element with the zonal flow shear], on the scale of zonal flow wavenumber  $q$  [2.19]. Thus, in contrast to the case of coherent shearing for which the radial wavenumber increases linearly with time, the rms wavenumber increases  $\sim t^{1/2}$ . However, the basic trend toward coupling to smaller scales in the drift wave spectrum persists. Furthermore, this evolution is adiabatic, on account of the separation in time and space scales between drift waves and zonal flows mentioned above. The use of adiabatic approximation methods greatly simplifies the calculations [2.20-2.22].

As noted above, much of the interest in zonal flows is driven by the fact that they regulate turbulence via shearing. However, it is certainly true that all low- $n$  modes in a spectrum of drift wave turbulence will shear and strain the larger- $n$ , smaller-scale fluctuations. Indeed, non-local shearing-straining interactions are characteristic of 2D turbulence once large scale vortices are established, as argued by Kraichnan and shown in simulations by Borue and Orszag. This, in turn, naturally motivates the questions: "What is so special about zonal flows (with  $n = 0$ )?" and "Why aren't other low- $n$  modes given equal consideration as regulators of drift wave turbulence?" There are at least *three* answers to this very relevant and interesting question. These are discussed below.

First, zonal flows may be said to be the '*modes of minimal inertia*'. This is because zonal flows, with  $n = 0$  and  $k_{\parallel} = 0$ , are not screened by Boltzmann electrons, as are the usual drift-ITG modes. Hence, the potential vorticity of a zonal flow mode is simply  $q_r^2 \rho_s^2 \hat{\phi}_q$ , as opposed to  $(1 + k_{\perp}^2 \rho_s^2) \hat{\phi}_k$ , so that zonal flows have lower effective inertia than standard drift waves do. The comparatively low effective inertia of zonal flows means that large zonal flow velocities develop in response to drift wave drive, unless damping intervenes. In this regard, it is also worthwhile to point out that in the case of ETG turbulence, *both* zonal flows and ETG modes involve a Boltzmann ion response  $\hat{n}_i/n_o = -|e|\hat{\phi}/T_i$ , since  $k_{\perp} \rho_i \gg 1$  for ETG. Hence, it is no surprise that zonal flow effects are less dramatic for ETG turbulence than for its drift-ITG counterpart, since for ETG, zonal flows have an effective inertia *comparable* to other modes.

Second, zonal flows, with  $n = 0$  and  $k_{\parallel} = 0$ , are *modes of minimal Landau damping*. This means that the only linear dissipation acting on zonal flows for asymptotic times (i.e.,  $t \rightarrow \infty$ ) is due to collisions. In particular, no linear, time-asymptotic dissipation acts on zonal flows in a collisionless system.

Third, since zonal flows have  $n = 0$ , they are intrinsically incapable of driving radial  $E \times B$  flow perturbations. Thus, they cannot tap expansion free energy stored in radial gradients. Thus, zonal flows do not cause transport or relaxation, and so constitute a *benign repository* for free energy. In contrast, other low  $n$ -modes necessarily involve a

trade-off between shearing (a "plus" for confinement) and enhanced transport (a "minus").

Having established the physics of shearing, it is illuminating to present a short, 'back-of-an-envelope' type demonstration of zonal flow instability. For other approaches, see the cited literature [2.23-2.29]. Consider a packet of drift waves propagating in an ensemble of quasi-stationary, random zonal flow shear layers, as shown in Fig. 2.4(b). Take the zonal flows as slowly varying with respect to the drift waves (i.e.,  $\Omega \ll \omega_k$ ), i.e., as quasi-stationary. Here,  $\Omega$  is the rate of the change or frequency of the zonal flow and  $\omega_k$  is the characteristic frequency of drift waves. The spatially complex shearing flow will result in an increase in  $\langle k_r^2 \rangle$ , the mean square radial wave vector (i.e., consider a random walk of  $k_r$ , as described above). In turn the drift wave frequency  $\omega_k / (1 + k_\perp^2 \rho_s^2)$  must then decrease. Here,  $\rho_s$  is the ion gyroradius at the electron temperature. Since  $\Omega \ll \omega_k$ , the drift wave action density  $N_k = \mathcal{E}(k) / \omega_k$  is conserved, so that *drift wave energy must also decrease*. As the total energy of the system of waves and flows is also conserved (i.e.,  $\mathcal{E}_{\text{wave}} + \mathcal{E}_{\text{flow}} = \text{const.}$ , as shown in Section 3.2.2), *it thus follows that the zonal flow energy must, in turn, increase*. Hence, the *initial perturbation is reinforced*, suggestive of *instability*. Note that the simplicity and clarity of this argument support the assertion that zonal flow generation is a robust and ubiquitous phenomenon.

A slightly larger envelope is required for a 'physical argument' which is also quantitatively predictive. Consider a drift wave packet propagating in a sheared flow field, as shown in Fig. 2.5. Take  $\omega_k > |V_E'|$  and  $|k| > |V_E'/V_E|$ , so that wave action density is conserved (i.e.,  $N(k) = N_0$ ), a constant. [ $V_E$  is the  $E \times B$  velocity and  $V_E'$  is its radial derivative.] Thus, wave energy density evolves according to:

$$\begin{aligned} \frac{d}{dt} \mathcal{E}(k) &= N_0 \frac{d\omega_k}{dt} \\ &= N_0 \left( \frac{\partial \omega_k}{\partial t} + V_s \cdot \frac{\partial \omega_k}{\partial x} + \frac{\partial \omega_k}{\partial k} \cdot \frac{dk}{dt} \right) \\ &\equiv \left( \frac{2k_r k_\theta \rho_s^2}{1 + k_\perp^2 \rho_s^2} \right) V_E' \mathcal{E}(k). \end{aligned} \quad (2.3)$$

Here we have assumed stationary, isotropic turbulence and have used the eikonal equation  $dk/dt = -k_\theta \partial V_\theta / \partial x$ . Equation (2.3) just states that the drift wave packet loses or gains energy due to work on the mean flow via wave induced Reynolds stress [2.30]. Note that  $k_r k_\theta \mathcal{E}(k) \sim \langle \tilde{V}_r \tilde{V}_\theta \rangle$ , the Reynolds stress produced by  $E \times B$  velocity fluctuations. Note as well that the factor  $k_r k_\theta \mathcal{E}(k) V_E'$  is rather obviously suggestive of

the role of triad interactions in controlling fluctuation-flow energy exchange. For zonal flows, the shear is random and broad-band, so that  $V_E \rightarrow \tilde{V}_E$ ,  $N \rightarrow \langle N \rangle + \tilde{N}$  and  $NV_E' \rightarrow \langle \tilde{N} \tilde{V}_E' \rangle$ . Hence, Eq.(2.3) may be rewritten as:

$$\frac{d}{dt} \varepsilon(k) = -V_{R,r} k_\theta (\tilde{V}_E' \tilde{N}). \quad (2.4)$$

To complete the argument, the correlator  $\langle \tilde{N} \tilde{V}_E' \rangle$  must now be calculated. To this end, we use the wave kinetic equation (WKE)

$$\begin{aligned} \frac{\partial N}{\partial t} + (V_g + V) \cdot \nabla N - \frac{\partial}{\partial x} (\omega + k_\theta V_E) \cdot \frac{\partial N}{\partial k} \\ = \gamma_k N - \Delta \omega_k N^2 / N_0 \end{aligned} \quad (2.5)$$

and the methodology of quasi-linear theory to obtain:

$$k_\theta \langle V_E' \tilde{N} \rangle = D_K \frac{\partial \langle N \rangle}{\partial k_r} \quad (2.6a)$$

$$D_K = k_\theta^2 \sum_q q^2 |V_{Eq}|^2 R(k, q) \quad (2.6b)$$

$$R(k, q) = \gamma_k / \left( (q V_{R,r})^2 + \gamma_k^2 \right). \quad (2.6c)$$

The term  $\Delta \omega_k N^2 / N_0$  represents drift wave non-linear damping via self-interaction of the drift waves (i.e., inverse cascade by *local* interaction). Here  $q$  is the radial wavenumber of the zonal flow, and equilibrium balance in the absence of flow has been used to relate  $\Delta \omega_k$  to  $\gamma_k$ .  $\gamma_k$  is the growth rate of the drift mode. The wave energy then evolves according to:

$$\frac{d\varepsilon(k)}{dt} = \frac{2\rho_s^2 D_K k_r}{(1 + k_\perp^2 \rho_s^2)^2} \frac{\partial \langle N \rangle}{\partial k_r}. \quad (2.7)$$

As the total energy of the stationary wave-flow system is conserved,

$$d/dt \left( \sum_k \varepsilon(k) + \sum_q |\tilde{v}_q|^2 \right) = 0.$$

The zonal flow generation rate is thus determined to be:

$$\gamma_q = -2q^2 c_s^2 \sum_q \frac{k_\theta^2 \rho_s^2}{(1+k_\perp^2 \rho_s^2)^2} R(k, q) k_r \left( \frac{\partial \langle \eta \rangle}{\partial k_r} \right) \quad (2.8a)$$

$$\langle \eta \rangle = (1+k_\perp^2 \rho_s^2) \langle \epsilon \rangle. \quad (2.8b)$$

Here  $\langle \eta \rangle$  is the mean potential enstrophy density of the drift wave turbulence, (i.e.,  $\eta(k) = (1+k_\perp^2 \rho_s^2)^2 |\phi_k|^2$ ) and may be thought of as the population density of drift wave vortices. Note that for toroidally and poloidally symmetric shears,  $dk_\theta/dt = 0$ , so that the conventional wave action density  $N(k)$  and the potential enstrophy density  $\eta(k)$  are *identical*, up to a constant factor.

The result given above in Eq. (2.8a), obtained by transparent physical reasoning, is identical to that derived previously by formal modulational stability arguments. Note that  $\partial \langle \eta \rangle / \partial k_r < 0$  (a condition which is virtually always satisfied in 2D or drift wave turbulence) is required for zonal flow growth. In addition, the argument above reveals that drift wave ray chaos provides the key element of irreversibility, which is crucial to the wave-flow energy transfer dynamics. Here ray chaos requires overlap of the  $\Omega/q_r = V_k$  resonances in  $D_k$ , a condition easily satisfied for finite lifetime drift wave eddies and (nearly) zero frequency zonal flows (i.e.,  $\Delta\omega_k \gg \Omega$ ) [2.31]. Under these conditions a positive Lyapunov exponent is present and neighbouring drift wave rays diverge exponentially in time. Ray chaos in turn ensures that zonal flow shearing and wave refraction are random, thus validating the use of the stochastic methodology employed here [2.32]. In the case where rays are not chaotic, envelope perturbation formalism [2.33, 2.34], methods from the theory of trapping [2.35-2.37] or parametric instability theory [2.38] must be used to calculate zonal flow generation.

### 2.3 Self-consistent solution and multiple states

At this point, we have identified the two principal elements of the physics of the drift wave - zonal flow system. These are:

- i) The shearing of drift wave eddies by the complex zonal flow field, resulting in a diffusive increase in  $\langle k_r^2 \rangle$  and coupling to dissipation, reduction in transport, etc.,
- ii) the amplification of zonal flow shears by modulational instability of the drift wave to a 'test' or seed shear.

Note that i) and ii) are, to some extent, different views of the same process of energy transfer from the short wavelength drift wave spectrum to the long wavelength zonal flow spectrum. This process of drift wave energy depletion results in a diffusive *increase* in the mean square radial wavenumber of drift waves, and a transfer of drift wave

population density to small scale. In view of the fact that the drift wave population density is equivalent to the potential enstrophy density, we see that the process of zonal flow generation is not unlike the dual cascade phenomenon familiar from 2D hydrodynamics. Here, the growth of zonal flow shears corresponds to the inverse energy cascade, while the increase in RMS of  $k_r$  is similar to the forward enstrophy cascade [2.39]. Unlike the case of 2D hydrodynamics, zonal shear amplification is a *non-local* coupling process in wavenumber space. (See Fig.2.6.)

To proceed, we now examine the coupled evolution for  $\langle N \rangle$ , the drift wave quanta density, and the zonal flow spectrum. These evolve according to:

$$\frac{\partial}{\partial t} \langle N \rangle - \frac{\partial}{\partial k_r} D_k \frac{\partial}{\partial k_r} \langle N \rangle = \gamma_k \langle N \rangle - \frac{\Delta \omega_k}{N_0} \langle N \rangle^2, \quad (2.9a)$$

$$\frac{\partial}{\partial t} |\phi_q|^2 = \Gamma_q \left[ \partial \langle N \rangle / \partial k_r \right] |\phi_q|^2 - \gamma_d |\phi_q|^2 - \gamma_{NL} \left[ |\phi_q|^2 \right] |\phi_q|^2. \quad (2.9b)$$

Equation (2.9a) is simply the quasi-linear Boltzmann equation for  $\langle N \rangle$ , while Eq. (2.9b) describes zonal flow potential growth and damping by modulational instability (the first term - proportional to the drift wave population gradient  $\partial \langle N \rangle / \partial k_r$ ), collisional damping (the second term - due to the friction between trapped and circulating ions) [2.40, 2.41] and nonlinear damping of zonal flows (the third term - which schematically represents a number of different candidate zonal flow saturation processes). Note here that  $\gamma_{NL}$  is an unspecified function of zonal flow intensity, and thus can represent nonlinear damping process such as turbulent viscous damping, etc. Together, Eqs.(2.9a) and (2.9b) constitute a simple model of the coupled evolution dynamics. This 'minimal' model could be supplemented by transport equations which evolve the profiles used to calculate  $\gamma_k$ , the drift wave growth rate (i.e.,  $\gamma_k = \gamma_k \left[ n^{-1} dn/dr, T^{-1} dT/dr, \dots \right]$ ) [2.42]. The minimal system has the generic structure of a 'predator-prey' model, where the drift waves correspond to the prey population and the zonal flows correspond to the predator population [2.43-2.47]. As usual, the prey breeds rapidly (i.e.,  $\gamma_k$  is fast), and supports the predator population as the food supply for the latter (i.e.,  $\Gamma_q = \Gamma_q \left[ \langle N \rangle \right]$ ). The predators regulate the prey by feeding upon them (i.e.,  $\Gamma_q$  and  $D_k$  conserve energy with each other) and are themselves regulated by predator death (at rate  $\gamma_d$ ) and predator-predator competition ( $\gamma_{NL} \left[ |\phi_q|^2 \right]$ ). Taken together, Eqs.(2.9a) and (2.9b) describe a self-regulating system with multiple states.

The dynamics of the two population system are more easily grasped by considering a zero-dimensional model for population  $N$  and  $V^2$ , instead of the one-dimensional model equations for  $\langle N(k) \rangle$  and  $|\phi_q|^2$ . The 0-D simplified model is this:

$$\frac{d}{dt} N = \gamma N - \alpha V^2 N - \Delta\omega N^2, \quad (2.10a)$$

$$\frac{d}{dt} V^2 = \alpha N V^2 - \gamma_d V^2 - \gamma_{NL}(V^2) V^2. \quad (2.10b)$$

The states of the system are set by the fixed points of the model, and in turn are determined by

$$0 = \gamma - \alpha V^2 - \Delta\omega N, \quad (2.11a)$$

$$0 = \alpha N - \gamma_d - \gamma_{NL}(V^2). \quad (2.11b)$$

There are (at least) two classes of fixed points for the system. The state with finite fluctuations and transport, but no flow is that with

$$N = \gamma/\Delta\omega, \quad (2.12a)$$

$$V^2 = 0. \quad (2.12b)$$

This corresponds to a state where turbulence saturates by local, nonlinear interactions. A second state, with flow, is that with

$$N = \alpha^{-1} \left( \gamma_d + \gamma_{NL}(V^2) \right), \quad (2.13a)$$

$$V^2 + \alpha^{-2} \Delta\omega \gamma_{NL}(V^2) = \alpha^{-1} (\gamma - \Delta\omega \gamma_d \alpha^{-1}). \quad (2.13b)$$

Note that the general form  $\gamma_{NL}(V^2)$  certainly allows limit cycle solutions. Given the physically plausible assumption that  $\gamma_{NL}(V^2) > 0$  and increases with  $V^2$  as  $V^2 \rightarrow \infty$ , the Poincare-Bendixon theorem implies that limit cycle solutions to (2.10a,b) can be identified by the appearance of unstable centers as fixed points of those equations. In general, the appearance of such limit cycle attractors is due to the effects of time delays in the dynamical system of zonal flows and drift waves. For the especially simple case where  $\gamma_{NL}(V^2) \sim \alpha_2 V^2$ , this system is reduced to:

$$N = \frac{\gamma_d + \alpha_2 \gamma \alpha^{-1}}{\alpha + \Delta\omega \alpha_2 \alpha^{-1}} \quad (2.14a)$$



$$V^2 = \left[ \frac{\gamma - \Delta\omega\gamma_d\alpha^{-1}}{\alpha + \alpha_2\Delta\omega\alpha^{-1}} \right]. \quad (2.14b)$$

Even this highly over-simplified model contains a wealth of interesting physics. The properties of the two states are summarized in Table 2.2, which we now discuss. Access to the state of no flow requires only primary linear instability, i.e.,  $\gamma > 0$ , while access to states with finite flow requires  $\gamma > \Delta\omega\gamma_d/\alpha$ , so that the excitation of the underlying drift waves is sufficient to amplify the flow shear against collisional damping. In the no flow state,  $N \sim \gamma/\Delta\omega$ , consistent with the traditional picture of saturation of turbulence and transport via the balance of linear growth with nonlinear damping. With the presence of flow,  $N \sim \gamma_d\alpha^{-1}$ , which directly ties the *turbulence level* to the *flow damping* [2.48]. This follows the fact that *in the finite flow state, the turbulence level is regulated by the shear flow, which is, in turn, itself controlled by the flow damping. Thus, the fluctuation level is ultimately set by the flow damping!* This prediction has been confirmed by several numerical simulations [2.49]. In the finite flow state,  $V^2$  is set by the *difference* between the wave growth and flow damping. Thus, the branching ratio of the zonal flow to drift wave energy scales as  $\gamma/\gamma_d$ . In particular, for  $\gamma_d \rightarrow 0$ , the *dominant ultimate repository of expansion free energy are the zonal flows, whose energy exceeds that of the drift waves*. Note that the ratio  $\gamma/\gamma_d$  is the key control parameter for manipulating the fluctuation energy branching ratio. It is interesting to note that the rather special 'Dimits shift' regime [2.50], which is a state very close to marginal stability in an effectively collisionless system, corresponds to the somewhat ill-defined case where both  $\gamma \rightarrow 0$  and  $\gamma_d \rightarrow 0$ , i.e., weak flow damping and drift waves near their marginal point. The Dimits shift was discovered by direct nonlinear simulation of ion-temperature-gradient (ITG) mode-driven turbulence in the collisionless limit. In the Dimits shift regime, the drift wave fluctuations are just above the linear stability threshold and nearly quenched by zonal flow effects which are large, on account of weak flow damping at low collisionality. The Dimits shift regime is characterized by a large imbalance between the energy in zonal flows and in  $n \neq 0$  fluctuations (with zonal flow energy much larger), which gives the appearance of a 'shift' (i.e., increase) in the effective threshold for ITG turbulence and transport. Thus, it is not surprising that the Dimits shift regime merits special attention. Detailed discussion of the Dimits shift regime is given in Chapter 3.

It is especially interesting to comment on the effects of nonlinear zonal flow damping, for which  $\alpha_2 \neq 0$ . The details of this process are a subject of intense ongoing research, and will be discussed extensively later in this review. Candidate mechanisms include Kelvin-Helmholtz-like instabilities of the zonal flows (which could produce a turbulent viscosity, resulting in flow damping) [2.51-2.53], drift wave trapping, etc. Whatever the details, the effect of nonlinear flow damping is to limit the intensity of the zonal flow spectrum. Since energy is conserved between drift waves and zonal flows

(within the time scales of the evolution of zonal flow), this is equivalent to enhancing the fluctuation levels, in comparison to the case where  $\alpha_2 = 0$ . This is, indeed, the case in the RHS column of Table 2.2, where we see the effect of finite  $\alpha_2$  is to enhance  $N$  and reduce  $V^2$  in comparison to the case where  $\alpha_2 = 0$ . Thus, nonlinear flow damping may be viewed as a "return" of expansion free energy to the drift wave 'channel', which thus lowers the branching ratio  $V^2 / N$ .

## 2.4 General Comments

It should be clear that the drift wave- zonal flow problem is a particular example of the more general problem of describing the nonlinear interaction between, and turbulence in, two classes of phenomena of disparate-scale, and of understanding structure formation and self-organization in such systems. Such problems are ubiquitous, and notable examples in plasma physics are Langmuir turbulence and caviton formation, magnetic field generation and the dynamo problem, and the formation of ionospheric structures, just to name a few. It is interesting to note that the separation in spatio-temporal scales often facilitates progress on such problems, via the use of adiabatic invariants, or systematic elimination of degrees of freedom using the methodology of Zwanzig-Mori theory, etc. Thus, such nominally "more complex" problems are often easier than the so-called classic "simple" problems, such as homogeneous turbulence. The general theory of turbulence in systems with multiple bands of interacting disparate scales is reviewed in ref. [2.54]. The Langmuir turbulence and collapse problems are reviewed in [2.55]. The theory of the dynamo problem is discussed in great detail in [2.56-2.61].

## 2.5 Implications for experiments

Experimental investigation of zonal flow physics is an urgent task, because the zonal flow has a decisive impact on the turbulent transport in confined plasmas. So far, progress on zonal flow physics has been made primarily by theoretical or simulation studies. The interpretation and critical tests of the theoretical findings in physical experiments are, although ongoing, important and merit special emphasis.

Although the system of drift waves and zonal flow shows a complex behaviour and provides a fruitful example of the complex dynamics of turbulent media, it is still highly simplified when compared to real experiments. For instance, noise occurs in real plasmas and can play an important role in their dynamics, particularly near bifurcation thresholds. A brief discussion on the role of noise in the problem of zonal flows is presented in the later chapters. In addition, convective cells, which in general are not constant in the poloidal direction, can be driven by a mesoscale electric field. A typical example of such poloidally-inhomogeneous mesoscale structure is the streamer. The

general theory of convective cells and streamers is beyond the scope of this review, but a short discussion thereof is given in the later chapters.

### Chapter 3 Theory of Zonal Flow Dynamics

In this chapter, the theory of zonal flow dynamics is discussed in detail. As shown in the heuristic discussion of Chapter 2, the essence of the drift wave - zonal flow system dynamics is that several mechanisms are simultaneously at work. The synergy of these mechanisms results in the (self) organization of the self-regulating state. Here, we present a step-by-step discussion of the theory of the basic elements, which are:

- (i) linear damping (especially collisional) of the zonal flow
- (ii) mechanisms for the excitation of zonal flows by background turbulence
- (iii) mechanisms by which the spectrum of zonal flow shears limits and reacts back upon the underlying drift wave turbulence
- (iv) nonlinear damping and saturation mechanisms for zonal flow, especially in collisionless or very low collisionality regimes
- (v) the type of self-organized states which are realized from the interaction of elements (i)-(iv)
- (vi) the effect of zonal flows on turbulent transport.

Elements (i)-(vi) are discussed below. Related illustrations, tests and analyses utilizing numerical simulation are presented in Chapter 4.

The remainder of Chapter 3 is organized as follows. Section 3.1 presents the theory of linear collisional damping of zonal flows - the collisional damping is a key energy sink. Special emphasis is placed upon the key, pioneering work of Rosenbluth and collaborators. Section 3.2 presents the theory of zonal flow generation by modulational instability of the ambient drift wave spectrum. The theory is developed for both the coherent (i.e., parametric modulational) and broadband, turbulent (i.e., wave kinetic) limits. Critical time scales which quantitatively identify these regimes are identified and discussed. The relations between, and connections (vis-a-vis energetics) between modulational instability and shearing,  $k$ -space diffusion, etc., are discussed and a unifying framework is proposed. Emphasis here is an electrostatic turbulence and zonal flows, but related discussions of electromagnetic turbulence, zonal flows and GAMs (Geodesic Acoustic Modes) are also included. The relationship between zonal magnetic field dynamics and the classical dynamo problem is discussed. In section 3.3, the theory of shearing and its effects on turbulence are discussed, for both mean field and random

(i.e. zonal flow) shearing. This discussion is important in its own right (as an element in system self-regulation) and as a foundation for understanding the impact of zonal flows on turbulent transport, etc. In section 3.4, zonal flow saturation is discussed, with special emphasis placed upon collisionless or low collisionality regimes. As with generation, several different applicable models are discussed, each in the context of its regime of relevance as defined by time scales, degrees of freedom, etc. In particular, tertiary instability, nonlinear wave packet scattering, wave trapping and other mechanisms are discussed. After explaining the elementary processes, a unifying classification of various possible system states is suggested in terms of the Chirikov parameter and Kubo number, which characterize the turbulent state. This classification scheme gives a global perspective on the nonlinear theory of zonal flows. In section 3.5, the system dynamics of zonal flows and turbulence are presented. In the final section 3.6, the effects of zonal flows on turbulent transport are discussed. Special attention is given to zonal-flow-induced modification of the cross phase and upon the scaling of the turbulent transport flux with zonal flow parameters, such as shear strength, flow correlation time, etc.

### 3.1 Linear Dynamics of Zonal Flow Modes

Zonal flows are, first and foremost, plasma eigenmodes, albeit modes which are linearly stable. In this subsection, we discuss the linear response of the plasma to low frequency electric field perturbation which is constant on a magnetic surface. This corresponds to the  $m = n = 0$  component, where  $m$  and  $n$  are the poloidal and toroidal mode numbers, respectively. The issue is how the toroidal effects influence the response. Two relevant regimes are explained. One is that of the slowly varying response, for which  $|\partial/\partial t| \ll \omega_i \equiv v_{Ti}/qR$ , where  $\omega_i$  is the ion transit frequency and  $v_{Thi}$  is the thermal velocity of ions,  $v_{Thi} = \sqrt{T/m_i}$ . In this case, the perturbation is called a zonal flow. The plasma response is incompressible, and the poloidal  $E \times B$  velocity is associated with a toroidal return flow. The other is a fast-varying regime, where  $|\partial/\partial t| \sim \omega_i$ . In this case, the poloidal asymmetry leads to plasma compression so as to induce an oscillation in the range of  $\omega \sim \omega_i$ . This oscillation is called the geodesic acoustic mode (GAM). We first describe the zonal flow and then explain the geodesic acoustic mode. The damping of these modes by collisions and ion Landau damping is explained. In this section (and throughout the review), we use the word 'damping' for the linear response mechanisms (e.g., collisional damping or collisionless damping, like Landau damping). The nonlinear mechanisms that induce the decay of regulate the flow are called 'saturation mechanisms' or, if necessary for clarity, 'nonlinear damping mechanisms'.)

### 3.1.1 Zonal flow eigenmode

In drift-ITG mode (ion temperature gradient turbulence [3.1]), zonal flows have an electrostatic potential  $\tilde{\phi}$  which is constant on a magnetic surface, and so have  $m = n = 0$ ,  $k_{\parallel} = 0$ . Because of the vanishing  $k_{\parallel}$ , the electron response is no longer a Boltzmann response, so that the relation  $\tilde{n}/n = e\tilde{\phi}/T$  no longer holds. The density perturbation is usually a small correction, in comparison with the potential perturbation. Certain CTEM (collisionless trapped electron mode) regimes may be an exception to this. Thus, zonal flows correspond to a highly anisotropic limit of the more general "convective cell mode" [2.3, 3.2]. As discussed in Chapter 2, zonal flows (but not GAMs) can be thought of as convective cells of minimum inertia, minimum Landau damping and minimum transport [3.3].

The spatial structure of the zonal flow is described here. The electrostatic perturbation is constant on each magnetic surface. If it is decomposed as

$$\tilde{\phi} = \sum_{q_r} \tilde{\phi}(q_r) \exp(i q_r (r - r_0)) \quad (3.1.1)$$

where  $r_0$  is a radius of reference, each  $q_r$  component has the linear dispersion relation [2.3, 3.2]

$$\omega = 0. \quad (3.1.2)$$

The vanishing real frequency is easily understood. The electrostatic perturbation with  $m = n = 0$  does not cause acceleration along the magnetic surface. The polarization drift disappears, consistent with the ordering of  $\omega \ll \omega_i$ . For completeness, we note that there arises small but finite real frequency because of collisional damping, which is explained in §3.1.3.

The plasma produces an  $E \times B$  flow,

$$V_{E \times B} = -\frac{E_r}{B}. \quad (3.1.3)$$

This flow is directed mainly in the poloidal direction. Because of toroidicity, this flow component induces the compression of plasma. To maintain incompressibility, this compression is compensated by a return flow along the field line, so:

$$\mathbf{V} = -\frac{E_r}{B} \begin{pmatrix} 0 \\ 1 \\ -2q \cos \theta \end{pmatrix} \quad (3.1.4)$$

to the leading order in the inverse aspect ratio  $\epsilon = r/R$  [2.46]. This flow pattern is illustrated in Fig.3.1.1. On account of the secondary flow along the magnetic field line, the zonal flow in a toroidal plasma is subject to a stronger damping rate as compared to those in slab plasmas.

The density perturbation remains to small correction. For the range of scales comparable to the ion gyroradius, it can be given as:

$$\frac{\tilde{n}_i}{n} \approx q^2 r^2 \rho_i^2 \frac{e\tilde{\phi}}{T} . \quad (3.1.5)$$

### 3.1.2 Geodesic acoustic mode (GAM)

The dynamics of plasma rotation are influenced by toroidal geometry. Toroidal effects have been studied in conjunction with the neoclassical transport theory [3.4-3.12], as reviewed in [3.13-3.15]. When one constructs an eigenmode in the regime of fast variation,  $|\partial/\partial t| \sim \omega_i$ , one finds the geodesic acoustic mode (GAM) [3.5]. The GAM is a perturbation for which the  $m = n = 0$  electrostatic potential is linearly coupled (by toroidal effects) to the  $m = 1/n = 0$  sideband density perturbation. A brief description of GAM is presented here.

Working in the framework of standard fluid equations, one begins with, as governing equations, the continuity equation and the equation of motion

$$\frac{\partial}{\partial t} n + \nabla \cdot n \mathbf{V}_\perp + \nabla_\parallel n V_\parallel = S - \nabla \cdot \Gamma , \quad (3.1.6)$$

$$nm_i \left( \frac{\partial}{\partial t} \mathbf{V} + \mathbf{V} \cdot \nabla \mathbf{V} \right) = -\nabla p + \mathbf{J} \times \mathbf{B} + Sm_i \mathbf{V} , \quad (3.1.7)$$

together with the charge neutrality condition  $\nabla \cdot \mathbf{J} = 0$  and Ohm's law

$$\mathbf{E} + \mathbf{V} \times \mathbf{B} = 0 . \quad (3.1.8)$$

$p = nT$  is the pressure, and the temperature gradient is neglected for simplicity. The source terms  $S$  and  $\Gamma$  represent the (equilibrium) particle source and flux, respectively. These can induce acceleration of the zonal flow if they are not homogeneous on a magnetic surface. The so-called Stringer spin-up [3.6] is such an acceleration phenomenon. In this subsection, we do not describe the response to  $S$  and  $\Gamma$ , but restrict ourselves to the dynamics of GAM eigenmode.

The key mechanism for generating the GAM is seen in Eq.(3.1.7) [3.5, 3.16]. If one takes the poloidal component of Eq.(3.1.7), one obtains

$$\mathbf{B}_p \cdot \left( nm_i \frac{d}{dt} \mathbf{V} + T \nabla n \right) = B_t R^{-1} \mathbf{J} \cdot \nabla \psi \quad (3.1.9)$$

where  $\mathbf{B}_p$  and  $B_t$  denote the poloidal and toroidal magnetic fields, and  $\nabla \psi$  denotes a unit vector in the direction across the magnetic surface. Because of the charge neutrality, the net current across the magnetic surface vanishes. Using Eq.(3.1.9), the condition  $\int ds \cdot \mathbf{J} = 0$  may be rewritten as:

$$\int \frac{ds R^2}{|\nabla \psi|} \mathbf{B}_p \cdot \left( nm_i \frac{d}{dt} \mathbf{V} + T \nabla n \right) = 0 \quad (3.1.10)$$

This relation is trivial in a cylindrical plasma. However, in toroidal plasmas, toroidicity induces coupling between the  $m = n = 0$  component of the electrostatic potential and the  $m = 1, n = 0$  component of the density perturbation. It may be convenient to use the notation of [3.16], i.e.,

$$\tilde{V}_{E \times B}(r; t), \tilde{N}(r, \theta; t) = \tilde{n} / n_0 \text{ and } \tilde{V}_{\parallel}(r, \theta; t), \quad (3.1.11)$$

where all the fields have toroidal symmetry. To leading order in  $\epsilon$ , one can rewrite Eq.(3.1.6), the parallel component of Eq.(3.1.7), and Eq.(3.1.10) as:

$$\frac{\partial}{\partial t} \tilde{N} - \frac{2}{R} \sin \theta \tilde{V}_{E \times B} + \nabla_{\parallel} \tilde{V}_{\parallel} = 0, \quad (3.1.12a)$$

$$\frac{\partial}{\partial t} \tilde{V}_{\parallel} + c_s^2 \nabla_{\parallel} \tilde{N} = 0, \quad (3.1.12b)$$

$$\frac{\partial}{\partial t} \tilde{V}_{E \times B} + \frac{2}{R} c_s^2 \oint \frac{d\theta}{2\pi} \sin \theta \tilde{N} = 0, \quad (3.1.12c)$$

respectively. This set of equations describes two classes of oscillations. One is a particular case for which the density perturbation has a  $\sin \theta$  dependence, i.e.,

$$\tilde{N}(r, \theta; t) = N_1(r; t) \sin \theta. \quad (3.1.13)$$

In this case, the dispersion relation given from Eq.(3.1.12) is:

$$\Omega^2 - \frac{2c_s^2}{R^2} - q_{\parallel}^2 c_s^2 = 0. \quad (3.1.14)$$



The second term on the right hand side comes from the combination of the second terms in Eq.(3.1.12a) and in (3.1.12c). The third term in Eq.(3.1.14) is a contribution of the usual parallel ion sound wave response. The resulting mode is the geodesic acoustic mode, the frequency of which is higher than the ion acoustic wave and is given by:

$$\omega_{\text{GAM}}^2 \approx 2c_s^2 R^{-2} (1 + q^{-2}/2) . \quad (3.1.15)$$

The eigenfunction is given by the relation  $N_1 = \sqrt{2} c_s^{-1} \tilde{V}_{E \times B}$  from Eq.(3.1.12). The phase of  $N_1$  is shifted  $\pi/2$  behind the phase of the radial electric field. The density perturbation can be rewritten as

$$\frac{\tilde{n}}{n_0} = - \left( \sqrt{2} q r \rho_s \frac{e\tilde{\Phi}}{T_e} \right) \sin \theta . \quad (3.1.16)$$

The normalized density perturbation is  $q r \rho_s$  -times smaller than the normalized electrostatic potential perturbation  $e\tilde{\Phi}/T_e$ . This dependence is of lower order with respect to  $q r \rho_s$ , in comparison to that of the zonal flow Eq.(3.1.5). The higher relative density perturbation characteristic of a GAM may render it comparatively easier to detect than pure zonal flow.

If the density perturbation has dependence other than  $\sin \theta$ , the equation (3.1.12) reduces to

$$\Omega^2 - q_{\parallel}^2 c_s^2 = 0 , \text{ and } \Omega = 0 , \quad (3.1.17)$$

i.e., the conventional ion sound wave and the zonal flow. Note that if one chooses the zonal flow branch  $\Omega = 0$ , Eq.(3.1.12a) gives the parallel flow

$$V_{\parallel} = -2q \cos \theta V_{E \times B} . \quad (3.1.18)$$

This is the return flow along the magnetic field line given in Eq.(3.1.4).

The dispersion relation Eq.(3.1.14) was derived for general toroidal magnetic configurations in [3.5]. The second term was given as the product of an integral of the geodesic curvature multiplied by a relative perturbation amplitude. This is the reason that this mode is called the geodesic acoustic mode or GAM. It can be explained pictorially as follows. Equation (3.1.9) states that the diamagnetic current must be compensated by the polarization drift current of the ions. The density perturbation couples to the inhomogeneous  $E \times B$  motion on the magnetic surface. The geodesic curvature is the curvature of the magnetic field line measured on the magnetic surface. (The geodesic line

is a 'straight line' on a toroidal surface, i.e., the line connecting two points of minimum length. See Fig.3.1.3.) If the magnetic field line (locally) coincides with the geodesic line, the  $E \times B$  flow velocity on the magnetic surface does not compress the plasma element. However, if the field line has a finite local geodesic curvature, the  $E \times B$  motion induces compression. This local compression turns into a density perturbation, if the frequency is in the range of  $c_s/qR$  or higher. (If  $\omega$  is much smaller, the compression is compensated by the dc asymmetric parallel flow as is shown in Eq.(3.1.18).) A schematic drawing is given in Fig.3.1.3.

It has been noted that the dispersion relation Eq.(3.1.15) seems not to explicitly include the effect of toroidicity. However, the GAM disappears in the cylindrical limit. If one takes  $c_s r^{-1}$  as the basic unit of frequency, the GAM driving term (the second term) vanishes as  $\epsilon \rightarrow 0$ . In the limit of  $\epsilon \rightarrow 0$  for a fixed value of  $B_p/B_t$ , the ion sound term dominates and the GAM frequency (the second term in Eq.(3.1.14)) is negligibly small. The physics is straightforward: in cylindrical plasma with  $B_p/B_t$  given, the magnetic field line is a geodesic line on a cylindrical, circular-cross-section magnetic surface.

### 3.1.3 Collisional damping process

The process of collisional damping of zonal flow is now explained. In a slab plasma, the damping rate of the zonal flow is given by  $\mu_i q_r^2$ , i.e., in proportion to  $v_{ii} \rho_i^2 q_r^2$  (here  $\mu_i$  is the ion viscosity). However, in toroidal plasmas, the damping rate remains independent of scale. (See, e.g., for a review, [3.13-3.15].) Progress in the theory of the H-mode, [2.30, 3.17, 3.18] has stimulated a revival of the detailed calculation [2.30, 2.40, 3.17-3.29]. In this subsection, we first describe stationary flow which is realized by the balance of collisional drag with pressure gradient drive. Then relaxation processes are discussed. The case with  $|\partial/\partial t| \ll \omega_i \equiv v_{Th}/qR$  is discussed first. The case of rapidly varying response (GAM),  $|\partial/\partial t| \sim \omega_i$ , is explained next.

#### (i) Stationary flow driven by pressure gradient

The fluid velocity in an inhomogeneous toroidal flow, projected on the poloidal cross-section is expressed as

$$V_\theta = \frac{\epsilon}{q} \bar{V}_\parallel + V_{E \times B} + V_d + V_{dT} \quad (3.1.19)$$

Here  $V_{E \times B}$  is the  $E \times B$  drift velocity,  $V_d$  is the diamagnetic drift velocity,  $V_{dT}$  is the ion-temperature-gradient drift velocity, so that

$$V_d = \frac{T}{eBL_n}, \quad V_{dT} = \frac{T}{eBL_T}, \quad \frac{1}{L_n} = -\frac{d}{dr} \ln n \quad \text{and} \quad \frac{1}{L_T} = -\frac{d}{dr} \ln T_i,$$

$$(3.1.20)$$

and  $\bar{V}_{\parallel}$  is the average of  $V_{\parallel}$  on a magnetic surface. In the absence of torques (e.g., orbit loss, external momentum injection, etc.),  $\epsilon q^{-1} \bar{V}_{\parallel}$  is an  $O(\epsilon^2)$  correction with respect to  $V_{E \times B}$ . (See, e.g., [3.29].) The equilibrium velocity is obtained as

$$V_{\theta} = C_H V_{dT} \quad (3.1.21)$$

where  $C_H$  is a numerical coefficient, shown by Hazeltine to be [3.10]

$$C_H \approx 1.17 \text{ (banana)}, C_H \approx -0.5 \text{ (plateau)}, C_H \approx -2.1 \text{ (Pfirsch-Schluter)}. \quad (3.1.22)$$

From Eqs.(3.1.19) and (3.1.21), the  $E \times B$  drift velocity is given as

$$V_{E \times B} = (C_H - 1) V_{dT} - V_d, \quad (3.1.23)$$

if there is no other force to drive plasma poloidal rotation. The velocity scales with the (density and temperature) diamagnetic drift velocity. The radial electric field is easily deduced from this relation, and is given by:

$$E_r = (C_H - 1) \frac{T}{eL_T} - \frac{T}{eL_n} \quad (3.1.24)$$

The radial electric field is of the order of ion temperature gradient divided by the electron charge, if the stationary state is governed by collisional transport processes.

## (ii) Damping rate

The deviation of radial electric field from the result given by Eq.(3.1.24) is determined by the balance between the damping and driving torques. Here we survey the theories of collisional damping.

Collisional damping of zonal flows is controlled by ion-ion collision processes. The transit-time-magnetic-pumping process is explained below.

Figure 3.1.4 illustrates the change of the phase space distribution of ions when poloidal rotation occurs. When a small element of a phase space in the low field side moves to the high field side, it is 'stretched' in the direction of the perpendicular velocity,  $v_{\perp}$ , since  $v_{\perp}$  increases due to the conservation of magnetic moment. On account of ion-ion collisions, the deformed distribution tends to recover isotropy, which is shown by a thick solid line. In this relaxation process, the thermalization of ordered poloidal motion occurs, and the poloidal velocity is damped. From this argument, it is clear that this

damping rate is independent of the radial structure of the flow. This is *not* diffusive damping.

In the Pfirsch-Schluter regime, [3. 11]

$$\frac{d}{dt} V_\theta = -\gamma_{\text{damp}} (V_\theta - C_H V_{dT}) \quad (3.1.25)$$

where the damping rate is given as

$$\gamma_{\text{damp}} = \omega_i^2 \nu_{ii}^{-1} . \quad (3.1.26)$$

The mean free length in poloidal direction, which is determined by ion collisions, is inversely proportional to  $\nu_{ii}$ . Note that here  $\gamma_{\text{damp}} = D_{||}/(qR)^2 = \omega_i^2/\nu_{ii}$  is simply the time for parallel diffusion of one connection length. The dependence on the toroidicity is explained as follows. The normalization time is taken to be

$$\omega_\perp = v_{Ti}/a , \quad (3.1.27)$$

$v_{Ti} = \sqrt{T_i/m_i}$ , i.e., the ion thermal transit rate across the minor radius, Eq.(3.1.27) states that  $\gamma_{\text{damp}} = \epsilon^2 q^{-2} \omega_\perp^2 \nu_{ii}^{-1}$ . This explicitly shows that the damping disappears in the limit of  $\epsilon \rightarrow 0$ . In the limit of  $\epsilon \rightarrow 0$ , the magnetic field is constant, and transit-time magnetic pumping disappears.

In the banana regime, stronger damping occurs due to collisions between transiting ions and banana ions, because magnetically trapped particles do not rotate freely in the poloidal direction. (See Fig.3.1.5.) The poloidal rotation velocity, which is carried by the untrapped particles, is impeded by collisional friction with poloidally stationary trapped particle bananas. The damping rate associated with this process has been calculated by various authors. For the ordering  $|\partial/\partial t| \ll \omega_i$ , the drift-kinetic equation was solved by analytic methods. (The other limit of ordering,  $|\partial/\partial t| \sim \omega_i$ , is relevant to the other limit of the characteristic dynamics, namely the geodesic acoustic mode (GAM). This is discussed later.) Reference [3.20] found, by using an improved evaluation of eigenfunctions, that the damping rate increases as the toroidicity  $\epsilon$  becomes small. A fitting formula was proposed as,

$$\gamma_{\text{damp}} \approx 1.5 \nu_{ii}^D(v)/\sqrt{\epsilon} \quad (3.1.28)$$

where  $\nu_{ii}^D(v)$  is the energy-dependent pitch-angle scattering coefficient. In [3.22], an evaluation of the damping rate showed that the  $\epsilon$ -dependence is much stronger than that

given by Eq.(3.1.28). (The numerical solution in [3.22] can be fit by  $\gamma_{\text{damp}}/v_{ii} \propto \epsilon^{-\alpha}$  with  $\alpha \simeq 0.85$  for  $0.2 < \epsilon < 0.8$ .) An alternative fit

$$\gamma_{\text{damp}} \simeq v_{ii}^D(v)/\epsilon \quad (3.1.29)$$

was proposed. Direct numerical solution of the drift kinetic equation [3.29] has supported the conclusion that  $\gamma_{\text{damp}}$  is a decreasing function of  $\epsilon$ . The damping rate is in the range predicted by Eqs.(3.1.28) and (3.1.29). (The discrepancy between Eqs.(3.1.28) and (3.1.29) becomes large in the limit of  $\epsilon \rightarrow 0$ . In this limit, the banana regime reverts to the plateau regime and Eqs.(3.1.28) and (3.1.29) do not apply.) It has also been pointed out that collisional damping induces a real part of the total oscillation frequency for the zonal flow, so that [3.22]

$$\omega = \omega_r + i\gamma_{\text{damp}}, \quad (3.1.30a)$$

$$\omega_r \simeq v_{ii}. \quad (3.1.30b)$$

In the plateau regime, the dissipation rate is controlled by the transit frequency  $\omega_t$  and

$$\gamma_{\text{damp}} \simeq \omega_t h(\epsilon) \quad (3.1.31)$$

where  $h(\epsilon)$  is weakly dependent on toroidicity. Direct numerical calculation has shown that  $h(\epsilon) \sim \epsilon^\alpha$ , and a small positive parameter is observed in the range of  $\alpha \sim 1/3$  [3.29].

It should be noted that the damping rate in the banana regime, Eq.(3.1.28) or (3.1.29), *increases* if  $\epsilon$  decreases. However, this does not contradict the requirement of  $\gamma_{\text{damp}} \rightarrow 0$  as  $\epsilon \rightarrow 0$ . In the limit of  $\epsilon \rightarrow 0$ , the banana regime metamorphosizes into the plateau regime. In the plateau regime, one has  $\gamma_{\text{damp}} \sim \epsilon^{1+\alpha} q^{-1} \omega_\perp$ . Thus, the damping rate vanishes explicitly as toroidicity disappears,  $\epsilon \rightarrow 0$ .

Collisionless damping, if it exists, would influence poloidal rotation in the high temperature plasmas. The damping rate vanishes in the limit of  $v_{ii} \rightarrow 0$ , in quiescent plasmas [2.40]. The drive by turbulence (zonal flow drive) and other torque (e.g., orbit loss, external force, etc.) can balance the collisional damping. Figure 3.1.6 summarizes the scaling trends of the collisional damping rate.

The question of what the collisional damping rate is in the limit of the high poloidal velocity has attracted attention. It was noted that the damping rate  $\gamma_{\text{damp}}$  can depend on the poloidal velocity, if  $V_\theta$  becomes of the order of  $\epsilon v_{Th}/q$ . The damping rate then becomes a *decreasing function* of  $V_\theta$  [3.18, 3.31]. This is a possible origin of

a bifurcation of the radial electric field. (Examples include [3.32].) This mechanism, and the consequences, are explained in [2.46].

### (iii) Geodesic acoustic mode (GAM)

The geodesic acoustic mode (GAM) is also subject to collisional damping. After solving the drift kinetic equation with the ordering of  $|\partial/\partial t| \sim \omega_i$ , the dispersion relation has been obtained in [3.29] as

$$\omega^2 - \frac{7}{8} \frac{c_s^2}{R^2} + i \frac{v_{ii}}{\omega} \frac{c_s^2}{R^2} = 0. \quad (3.1.32)$$

(As compared to Eq.(3.1.14), the GAM frequency is evaluated with a slightly different numerical coefficient. This arises because the velocity moment is taken after the drift kinetic equation is solved. It is in contrast to Eq.(3.1.14), which was derived from the fluid equations, for which the velocity moments are calculated *before* solving the dynamical equation.) The damping rate of the GAM is estimated from Eq.(3.1.32) to be

$$\gamma_{\text{damp}}^{\text{GAM}} \approx \frac{4}{7} \nu_{ii}. \quad (3.1.33)$$

The banana ions do not explicitly play a role in damping, because the GAM frequency is much faster than the bounce frequency of banana ions.

### 3.1.4. Rosenbluth-Hinton Undamped Component of Zonal Flows in Collisionless Plasmas

Both nonlinear simulations and theories of ITG modes have shown that turbulence-generated, axisymmetric, radially-sheared zonal flows play a dominant role in regulating the level of turbulence and transport. Therefore, an accurate treatment of the damping of self-generated zonal flows is an outstanding issue in predicting confinement. Asymptotic behavior in the collisionless limit is of particular interest regarding future devices. The adequacy of gyrofluid models for calculating the zonal flow damping, in view of the "first principles" claim of their pessimistic prediction on ITER confinement, has been questioned by Rosenbluth and Hinton (RH) [2.40]. Their analytic calculation has shown that linear collisionless kinetic mechanisms do not damp the zonal flows completely. This prediction was verified later by various gyrokinetic codes [2.50, 3.33-3.35] while gyrofluid models [3.36, 3.37] incorrectly predicted a total collisionless decay of poloidal rotation. A modification of the gyrofluid approximation was attempted later, but only a part of RH undamped flow has been recovered to date [3.38].

As discussed at the beginning of this chapter, zonal flow can be viewed as a superposition of GAMs with a characteristic real frequency on the order of  $\omega_r \sim V_{Th}/R$  and with a corresponding ion Landau damping rate  $\omega_r \exp(-q^2/2)$ , and a zero frequency component to which RH calculation applies. (An example of the time evolution history of zonal flows which are allowed to relax in the absence of turbulence in a collisionless toroidal plasma is shown by DNS, and is explained in Chapter 4. Its poloidal component is damped due to the variation of  $B$  in the poloidal direction. The damping occurs due to the transit time magnetic pumping [3.9]. One can identify the oscillation and decay of GAMs as well as the non-zero asymptotic level of zonal flows predicted by RH.)

The RH calculation, which is based on the gyrokinetic equation, consists of following the long term evolution of the zonal flow with an assigned finite initial value. Concentrating on the long term behavior  $t \gg \omega_{b,i}^{-1}$ , RH calculates the bounce-averaged gyrokinetic response to an initial perturbation. The nonlinear gyrokinetic Vlasov equation for zonal flow component with  $q = (q_r, 0, 0)$ , i.e.,  $n = m = 0$  can be written as

$$\left[ \frac{\partial}{\partial t} + (\mathbf{v}_{\parallel} \hat{b} + \mathbf{v}_d) \cdot \nabla - C_{ii} \right] f_{i,q} + \frac{e}{T} F_0 (\mathbf{v}_{\parallel} \hat{b} \cdot \nabla + \mathbf{v}_d \cdot \nabla) \phi_q = S_{i,q}, \quad (3.1.34)$$

where  $\phi_q$  is the electrostatic potential of the zonal flow;  $f_{i,q}$  and  $F_0$  are the perturbed and unperturbed distribution functions of ions, respectively; and nonlinear interactions of ITGs with  $\mathbf{k}$ ,  $\mathbf{k}'$  are considered as a noise source  $S_{i,q}$  for zonal flows. Of course, Eq.(3.1.34) should include a response renormalization, as well as noise. The corresponding gyrokinetic Poisson's equation (i.e., the quasi-neutrality condition expressed in terms of the guiding center density  $n_{i,q}$  and polarization density) is

$$-n_0 \frac{e}{T_i} \rho_i^2 q_r^2 \phi_q + n_{i,q} = n_{e,q}, \quad (3.1.35)$$

where  $n_{e,q} = 0$ , for the adiabatic electron response with zonal flows, and the long wavelength approximation for zonal flow  $\rho_i^2 q_r^2 \ll 1$  have been used.

In RH, a bounce-average of Eq. (3.1.34) has been performed for a high aspect ratio circular tokamak geometry. In particular  $\rho_i^2 q_r^2 \ll \rho_{\theta,i}^2 q_r^2 \ll 1$  is assumed. ( $\rho_{\theta,i}$  is the ion gyroradius at the poloidal magnetic field.) The detailed calculation is not repeated here. The main result is that an initial zonal flow potential  $\phi_q(0)$  will be reduced to a level  $\phi_q(t)$  as  $t \rightarrow \infty$ , due to the neoclassical enhancement of polarization shielding:

$$\frac{\phi_q(t)}{\phi_q(0)} = \frac{1}{1 + 1.6\epsilon^{-1/2} q^2}. \quad (3.1.36)$$

In physical terms, the usual polarization shielding associated with finite Larmor radius effect in a short term (after a few gyro-periods)  $\sim \rho_i^2 q_r^2$  is replaced by the neoclassical polarization shielding associated with the finite banana width of trapped ions at long time (after a few bounce periods)  $\sim \epsilon^{1/2} \rho_{b,i}^2 q_r^2 \sim \epsilon^{-1/2} \rho_{b,i}^2 q_r^2$ . ( $\rho_{b,i}$  is the banana width of ions.) An accurate calculation of the coefficient 1.6 requires a kinetic calculation which includes the contribution from passing particles, but the correct scaling can be deduced from considering trapped ions only.

The result in Eq. (3.1.36) has been useful in benchmarking various gyrokinetic codes. For that purpose it suffices to solve Eqs. (3.1.34) and (3.1.35) with initial values  $f(0)$  and  $\phi(0)$ . After a such test, which is explained in Chapter 4, the RH result has turned out to be highly relevant, as indicated by numerous nonlinear simulations.

### 3.1.5 Further Details of Collisional Damping of Zonal Flows

A frequently-asked question about zonal flow in toroidal geometry is: "why isn't the radial electric field  $E_r$  associated with zonal flow balanced by the toroidal flow, eventually satisfying the radial force balance  $E_r = V_\theta B_t$ ?"

To elucidate the relation between the RH result and this question, one should recall that the RH calculation is purely collisionless, and that one should consider the ion-ion collisional effect for the longer-term behavior of zonal flows. The collisional damping process of zonal flows has been examined in detail by Hinton and Rosenbluth (HR) in their follow-up paper [2.41]. HR identified several temporal-asymptotic phases of zonal flow response to an initial zonal flow potential  $\phi_q(0)$ , which consist of:

- i) For times longer than a few ion bounce-times, the zonal flow potential reduces to a non-zero residual value given by Eq. (3.1.36) due to a collisionless kinetic process which includes the ion Landau damping of GAMs, transit time magnetic pumping, and neoclassical enhancement of polarization shielding.
- ii) For times of the order of  $\epsilon \tau_{ii}$ , where  $\tau_{ii}$  is the ion-ion collisional time, the potential and poloidal flow decay due to pitch-angle scattering in a trapped-passing boundary layer. Most of collisional poloidal flow decay occurs in this phase (as confirmed by simulation [2.48]), and zonal flow is mostly in the poloidal direction, up to this phase.
- iii) For times comparable to  $\epsilon^{1/2} \tau_{ii}$ , the potential approaches a non-zero steady state value  $\phi_q(t) = \phi_q(0) B_p^2 B_t^{-2}$ , consistent with  $E_r = V_\theta B_t$ , and the poloidal flows decays approximately exponentially.
- iv) For times longer than  $\tau_{ii}$ , damping of poloidal flow is due to energetic ions with small collisional rates, resulting in a slow non-exponential decay due to ion drag. Note that the collisional damping of the toroidal flow is a higher order process.



The main conclusion is that the most of collisional decay occurs on the time scale in phase ii). Thus *one can define the net effective collisional decay time of zonal flow as  $1.5 \epsilon \tau_{ii}$* , following HR .

As illustrated in Appendix C, there exists a near isomorphism between ITG turbulence and ETG turbulence. One crucial difference is that, while the adiabatic electron density response due to electron thermalization along the magnetic field is zero for ITG zonal flows (see Eq. (3.1.35), the adiabatic ion density response due to demagnetization is non-zero for ETG zonal flows. Interesting consequences for ETG zonal flow damping, related to this difference, have been investigated in Ref. [3.39].

### 3.2 Generation mechanism

The zonal flow is driven by nonlinear processes in the spectrum or wave packet ensemble of fluctuations in the range of the drift wave frequency. In this subsection, several elementary processes for generation of zonal flow are presented. We have previously discussed the linear response of stable zonal flow modes. As these are intrinsically incapable of trapping available expansion free energy since  $n = 0$ , they must be excited by nonlinear pumping by drift waves. Here we discuss the mechanisms of nonlinear excitation. The mechanism for zonal flow generation includes both parametric instability of a single drift wave and modulational instability of a spectrum of drift waves. The modulational instability can be calculated via both eikonal theory and wave kinetics, and by envelope formalism.

#### 3.2.1 Generation by parametric instability

A single drift wave (plane wave) is shown to be unstable to parametric perturbations [2.3, 3.40]. By parametric instability, the drift wave can generate convective cells for which the parallel wavenumber vanishes,  $k_{\parallel} = 0$ . The zonal flow is a special example, corresponding to extreme anisotropy with  $q_r \gg q_{\theta} \sim q_{\parallel} \sim 0$ , of a convective cell. A schematic diagram of the parametric instability process which generates the zonal flow is given in Fig.3.2.1. The structure of the wavenumbers is illustrated in Fig.3.2.1. Note that the parametric instability process is the usual one, familiar from weak turbulence theory, with the feature that one of the 'daughter waves' has zero frequency. In this subsection, parametric instability of a simple drift wave

$$\tilde{\phi}(\mathbf{x}, t) = \tilde{\phi}_{d0} \exp(i\mathbf{k}_{d0} \cdot \mathbf{x} - i\omega_d t) + \text{c.c.}$$

is discussed.

#### (i) Zonal flow in slab plasma

Two possible parametric instabilities occur for a plane drift wave. (See Fig.3.2.1.) In the study of parametric instability in slab plasmas, we use the coordinates  $(x, y, z)$  where  $x$  is in the direction of the radius and  $z$  is in the direction of magnetic field. One is the parametric decay instability [2.3, 3.40]. The primary drift wave, denoted by the wavenumber  $k_{d0}$  and frequency  $\omega_{d0}$ , where the suffix d stands the drift wave, can induce a pairing of a convective cell (wavenumber  $q$  and frequency  $\Omega$ ) and a secondary drift wave (wavenumber  $k_{d1}$  and frequency  $\omega_{d1}$ ). This process occurs if conditions

$$k_{d1} + q = k_{d0}, \quad \omega_{d1} + \Omega = \omega_{d0} \quad (3.2.1)$$

and

$$k_{d0}^2 > k_{d1}^2 \quad (3.2.2)$$

are satisfied. The growth rate of parametric decay instability is easily shown to be:

$$\gamma_{di} = c_s \rho_s |k_{d0} \times q| \sqrt{\frac{T_e}{T_i} \frac{k_{d0}^2 - k_{d1}^2}{q^2}} \frac{e\tilde{\Phi}_{d0}}{T_e}, \quad (3.2.3)$$

where  $\tilde{\Phi}_{d0}$  is the amplitude of the electrostatic potential perturbation associated with the primary drift wave.

The parametric decay instability is not effective for generating zonal flow. The beat condition requires

$$k_{d1,y} = k_{d0,y} \text{ and } k_{d1,x} = k_{d0,x} - q_x, \text{ with } \omega_{d1} = \omega_{d0}, \quad (3.2.4)$$

because  $\Omega \approx 0$  applies as explained in §3.1. The dispersion relation for drift waves

$$\omega_d = \frac{V_{dn} k_{d,y}}{1 + \rho_s^2 k_d^2}, \quad (3.2.5)$$

( $V_{dn}$  is the diamagnetic drift velocity), together with Eq.(3.2.4) requires,

$$q_x = 2 k_{d0,x} \quad (3.2.6a)$$

and

$$k_{d1,x} = -k_{d0,x}. \quad (3.2.6b)$$

Parametric decay is possible if Eq.(3.2.6) is satisfied. However, for this combination of wave vectors, the relation  $k_{d0}^2 = k_{d1}^2$  is forced, so the growth rate of parametric decay vanishes. Thus, the zonal flow is not driven by the parametric decay instability.

The other possible parametric process is the modulational instability [2.23, 3.41]. In this case, the primary drift wave (denoted by  $k_{d0}$  and  $\omega_{d0}$ ) couples to the (modulating) zonal flow ( $q$  and  $\Omega$ ) and so induces two secondary drift waves. The two induced drift waves are denoted by  $d+$  and  $d-$ , and have wavenumbers

$$k_{d+} = k_{d0} + q, \quad \text{and} \quad k_{d-} = q - k_{d0}. \quad (3.2.7)$$

The modulational instability means that the radial structure of the wave function primary drift wave is modified when the zonal flow is excited. As in the case of the parametric decay process, we study the growth rate of the parametric modulational instability starting from a reduced set of equations. We employ a potential vorticity conservation equation (ala the Charney-Hasegawa-Mima equation)

$$\frac{\partial}{\partial t} (n - \Delta_{\perp} \phi) + \left[ \phi, (n - \Delta_{\perp} \phi) \right] + \frac{\partial}{\partial y} \phi = 0 \quad (3.2.8)$$

where  $[\phi, g] \equiv (\hat{b} \times \nabla_{\perp} \phi) \cdot \nabla g$  ( $\hat{b}$  : unit vector in the direction of the magnetic field) represents the advective nonlinear term, and the normalizations of space in unit of  $\rho_s$  and time in units of  $L_n c_s^{-1}$ , together with

$$n \equiv \frac{\tilde{n}}{n_0} \frac{L_n}{\rho_s}, \quad \phi \equiv \frac{e \tilde{\phi}}{T_e} \frac{L_n}{\rho_s} \quad (3.2.9)$$

are employed for simplicity. In the case of co-existing drift waves and zonal flows,

$$\phi = \phi_d + \phi_{ZF} \quad \text{and} \quad n = n_d + n_{ZF},$$

Eq.(3.2.8) is then separated into the vorticity equation for drift waves

$$\frac{\partial}{\partial t} (n_d - \Delta_{\perp} \phi_d) + \left[ \phi, (n - \Delta_{\perp} \phi) \right] - \left\langle \left[ \phi, (n - \Delta_{\perp} \phi) \right] \right\rangle + \frac{\partial}{\partial y} \phi_d = 0 \quad (3.2.10)$$

and that of the zonal flow

$$\frac{\partial}{\partial t} (n_{ZF} - \Delta_{\perp} \phi_{ZF}) + \left\langle \left[ \phi, (n - \Delta_{\perp} \phi) \right] \right\rangle = 0, \quad (3.2.11)$$

where  $\langle \dots \rangle$  denotes the average over the magnetic surface. The density response is given by the Boltzmann relation for drift waves

$$n_d = \phi_d . \quad (3.2.12)$$

For zonal flows, the continuity equation holds, so that

$$\frac{\partial}{\partial t} n_{ZF} + \langle [\phi, n] \rangle = 0 . \quad (3.2.13)$$

Equations (3.2.10), (3.2.11), (3.2.12) and (3.2.11) govern how the set of perturbations (zonal flow and secondary drift waves) grow in the presence of the primary plane drift wave. Writing the temporal evolution of these secondary modes as  $\exp(-i\Omega t)$ , and linearizing Eqs.(3.2.10)-(3.2.13) with respect to the amplitudes of the secondary mode implies

$$n_{ZF} = 0 \quad (3.2.14)$$

so long as  $\Omega \neq 0$ . Thus the vorticity equation for the zonal flow reduces to the Euler equation for a 2D fluid. By use of Eq.(3.2.12) and (3.2.14), the linearized forms of Eqs.(3.2.10) and (3.2.11) can be written as

$$\phi_{d+} = \frac{-i |k_{d0\perp} \times q|}{\omega_d - \omega_{d+} + \Omega} \frac{(1 + k_{d0\perp}^2 - q^2)}{(1 + k_{d+ \perp}^2)} \phi_{d0} \phi_{ZF} , \quad (3.2.15a)$$

$$\phi_{d-} = \frac{-i |k_{d0\perp} \times q|}{\omega_{d-} + \omega_d - \Omega} \frac{(1 + k_{d0\perp}^2 - q^2)}{(1 + k_{d- \perp}^2)} \phi_{d0}^* \phi_{ZF} . \quad (3.2.15b)$$

We also obtain:

$$\Omega q_{\perp}^2 \phi_{ZF} = i |k_{d0\perp} \times q| \left[ (k_{d0\perp}^2 - k_{d+ \perp}^2) \phi_{d0}^* \phi_{d+} - (k_{d0\perp}^2 - k_{d- \perp}^2) \phi_{d0} \phi_{d-} \right] \quad (3.2.16a)$$

where

$$\omega_{d+} = \frac{k_{d0,y}}{1 + k_{d+}^2} , \quad \text{and} \quad \omega_{d-} = \frac{-k_{d0,y}}{1 + k_{d-}^2} , \quad (3.2.16b)$$

are the natural frequencies of the secondary drift waves. (Particular cases with  $\omega_{d+} - \omega_d - \Omega = 0$  or  $\omega_{d-} - \omega_d - \Omega = 0$ , for which the denominators in Eq.(3.2.15a) or in Eq.(3.2.15b) vanish, correspond to the parametric decay instability. They are discussed above.) The eigenfrequency is illustrated in Fig.3.2.2.

Equations (3.2.15) and (3.2.16) yield the parametric modulational dispersion relation

$$\left(\omega_d - \omega_{d+} + \Omega\right)\left(\omega_d + \omega_{d-} - \Omega\right) = \frac{|k_{d0\perp} \times q|^2}{q^2} \left(1 + k_{d0\perp}^2 - q^2\right)^2 \left(\frac{k_{d+\perp}^2 - k_{d0\perp}^2}{1 + k_{d+\perp}^2} + \frac{k_{d-\perp}^2 - k_{d0\perp}^2}{1 + k_{d-\perp}^2}\right) |\phi_{d0}|^2. \quad (3.2.17)$$

The left hand side of Eq.(3.2.17) is a quadratic function of  $\Omega$ . The condition for the instability to exist, i.e., the solution for complex  $\Omega$ , is given as

$$\left(\omega_d - \frac{\omega_{d+} - \omega_{d-}}{2}\right)^2 < \frac{|k_{d0\perp} \times q|^2}{q^2} \left(1 + k_{d0\perp}^2 - q^2\right)^2 \left(\frac{k_{d+\perp}^2 - k_{d0\perp}^2}{1 + k_{d+\perp}^2} + \frac{k_{d-\perp}^2 - k_{d0\perp}^2}{1 + k_{d-\perp}^2}\right) |\phi_{d0}|^2 \quad (3.2.18a)$$

In the limit of a long wavelength of the zonal flow,  $|q| \ll |k_{d\perp}|$ , this condition can be simplified to

$$|\phi_{d0}| > \frac{|k_{d0,y}| q^2}{\sqrt{2} |k_{d0\perp} \times q|}. \quad (3.2.18b)$$

Parametric modulational instability can occur if the condition (3.2.18) is satisfied. The growth rate of the secondary perturbation is given from Eq.(3.2.17) and is expressed in the long wavelength limit as

$$\gamma_{ZF} = \sqrt{2} |k_{d0\perp} \times q| \sqrt{\phi_{d0}^2 - \frac{|k_{d0,y}|^2 q^4}{2 |k_{d0\perp} \times q|^2}}. \quad (3.2.19)$$

In the case that the drift wave is propagating nearly in the poloidal direction,  $k_{d,x} \approx 0$ , Eq.(3.2.19) is simplified to

$$\gamma_{ZF} \approx k_{d0\perp} q_x \sqrt{2 \phi_{d0}^2 - q_x^2}. \quad (3.2.20)$$

The maximum growth rate is given as

$$\gamma_{ZF} \approx k_{d0\perp} \Phi_{d0}^2 \quad (3.2.21)$$

for  $|q| = \Phi_{d0}$ . Expressed in dimensional form, Eq.(3.2.20) is rewritten as

$$\gamma_{ZF} = \rho_s^2 k_{d0\perp} q_x \sqrt{2 \left( \frac{e \tilde{\Phi}_{d0}}{T_e} \frac{L_n}{\rho_s} \right)^2 - q_x^2 \rho_s^2} \frac{c_s}{L_n} = q_x \rho_s \omega_* \sqrt{2 \left( \frac{e \tilde{\Phi}_{d0}}{T_e} \frac{L_n}{\rho_s} \right)^2 - q_x^2 \rho_s^2}.$$

Figure 3.2.3 shows a plot of the growth rate of the modulational instability as a function of the wavenumber of the zonal flow. It is unstable in the long wavelength region. If the growth rate of the parametric instability is larger than the collisional damping, growth of the zonal flow can occur.

### (ii) Tokamak plasma

In tokamak plasma, a single drift wave eigenmode is not a plane wave but is given by a ballooning eigenfunction. Ballooning modes are similar to Bloch wavefunctions, familiar from condensed matter physics. A ballooning mode has a single  $n$ -value (toroidal mode number - the 'good' quantum number in the direction of symmetry), and consists of a set of coupled poloidal harmonics, vibrating together with a fixed phase relation, which defines the radial wave number. Coupling of poloidal harmonics occurs on account of the poloidal angle dependence of the  $\nabla B$  and curvature drifts. A ballooning mode can be viewed as a particular poloidal harmonic linearly coupled (by toroidal effects) to neighbouring side-bands. When written in terms of the extended poloidal coordinate used in the ballooning mode formalism, ballooning modes are seen to extend along the magnetic field line. A similar analysis has been developed, and toroidal effects influence the coupling coefficients [2.23]. Here, the parametric modulational instability calculation of section (i) is extended to toroidal geometry. The pump wave is expressed as [3.42]

$$\tilde{\Phi}_0(\mathbf{r}, t) = \exp(-in\zeta - i\omega_0 t) \sum_m \Phi_0(m - nq) \exp(im\theta) + c.c. \quad (3.2.22)$$

where  $m$  and  $n$  are the poloidal and toroidal mode numbers, respectively, and  $\Phi_0(m - nq)$  represents the poloidal harmonic wavefunction. As in the case of slab plasma, a single toroidal mode number  $n$  is kept. The zonal flow  $\tilde{\Phi}_{ZF}$  and two nonlinear side bands of the toroidal drift waves ( $\tilde{\Phi}_+$  and  $\tilde{\Phi}_-$ ) may occur by the modulational instability. Note that in this analysis, it is important to distinguish between nonlinear

sidebands (driven by nonlinear beats) and linear sidebands which result from toroidicity-induced coupling. They are given as

$$\tilde{\Phi}_{ZF}(r, t) = \exp(iq_r r - i\Omega t) \Phi_{ZF} + c.c. \quad (3.2.23)$$

$$\tilde{\Phi}_+(r, t) = \exp(-in\zeta - i\omega_0 t + iq_r r - i\Omega t) \sum_m \Phi_+(m - nq) \exp(im\theta) + c.c. \quad (3.2.24a)$$

$$\tilde{\Phi}_-(r, t) = \exp(in\zeta + i\omega_0 t + iq_r r - i\Omega t) \sum_m \Phi_-(m - nq) \exp(im\theta) + c.c. \quad (3.2.24b)$$

This form is physically equivalent to the corresponding one in subsection (i), but the toroidicity-induced coupling affects the structure of the eigenfunction. (The suffix "d" denoting drift waves is dropped in order to reduce the complexity of notation.)

The modulational instability is analyzed by a procedure similar to that for the slab plasma. The response of the zonal flow to the modulation (equivalent to (3.2.11)) is

$$-i\Omega \Phi_{ZF} = g \left\langle \sum_m (a_+ \Phi_0^* \Phi_+ - a_- \Phi_0 \Phi_-) \right\rangle, \quad (3.2.25)$$

where

$$g = \frac{(2 + \eta_i)}{2B} \frac{k_\theta}{q_r} \frac{B_\theta^2}{1.6\epsilon^{3/2} B_\xi^2}, \quad a_\pm = k_{0\perp}^2 - k_{\pm\perp}^2, \quad (3.2.26)$$

$k_\theta = nq / r_0$ ,  $r_0$  is a reference radius,  $k_{0\perp} = \hat{\theta} k_\theta + inq' \partial / \partial \xi$ ,  $\xi = m - nq$ , and  $k_{\pm\perp} = \pm k_{0\perp} + \hat{r} q_r$ .

The side band components are calculated by use of the linear response to the drive by the beat between the primary wave and the zonal flow. The drive is proportional to  $\Phi_0 \Phi_{ZF}$  and has the frequency  $\omega_0 + \Omega$ . The amplitude of  $\Phi_+$  is given by:

$$\mathcal{L}_+(\omega_0 + \Omega) \Phi_+ = \frac{-i}{B} k_\theta q_r \Phi_0 \Phi_{ZF}, \quad (3.2.27a)$$

where  $\mathcal{L}_+$  is the linear operator representing the linear response,

$$\mathcal{L}_+(\omega_0 + \Omega)\Phi_+ = (\omega_0 + \Omega) \left( 2\Phi_+ - \left\langle \int dv \frac{(\omega_0 + \Omega - \omega_{*i}) F_M J_0^2 \Phi_+}{v_{\parallel} \nabla_{\parallel} - i(\omega_0 + \Omega) + i\mathbf{k}_{+\perp} \cdot \mathbf{V}_{dM}} \right\rangle \right), \quad (3.2.27b)$$

where  $\omega_{*i}$  is the ion diamagnetic drift frequency (including the temperature gradient),  $V_{dM}$  is the drift due to the inhomogeneity of magnetic field and  $\langle \dots \rangle$  indicates the average over  $\xi$ . The operator  $\mathcal{L}_+(\omega)$  determines the eigenfrequency of the beat mode,  $\omega_+$ , through the dispersion relation

$$\mathcal{L}_+(\omega_+)\Phi_+ = 0. \quad (3.2.28)$$

As is discussed in subsection (i), the beat frequency  $\omega_0 + \Omega$  is not equal to the eigenfrequency  $\omega_+$ . To facilitate analytic approximation, the solution is assumed to have a form of  $\Phi_+(\xi) = A_+ \Phi_0(\xi)$ . Substituting this form into Eq.(3.2.27a) and averaging over  $\xi$ , determines the proportionality constant  $A_+$ , so:

$$\Phi_+(\xi) = \frac{-i k_{\theta} q_r}{B D_+} \Phi_{ZF} \Phi_0(\xi) \quad (3.2.29)$$

where

$$D_+ = \left\langle \Phi_0^* \mathcal{L}_+(\omega_0 + \Omega) \Phi_0 \right\rangle \left\langle |\Phi_0|^2 \right\rangle^{-1}. \quad (3.2.30)$$

Because the frequency mismatch  $\omega_0 + \Omega - \omega_+$  is small, a Taylor expansion is used to obtain

$$D_+(\omega_0 + \Omega) = \left. \frac{\partial D_+}{\partial \omega} \right|_{\omega_+} (\omega_0 + \Omega - \omega_+) + \dots \approx (\omega_0 - \omega_+ + \Omega), \quad (3.2.31)$$

(The second parenthesis of the right hand side of Eq.(3.2.27b) has a leading term  $2\Phi_+$ . Therefore, to leading order, one has the estimate  $\partial D_+ / \partial \omega \sim 1$ .) Thus Eq.(3.2.29) is simplified to

$$\Phi_+(\xi) = \frac{-i k_{\theta} q_r}{B (\omega_0 - \omega_+ + \Omega)} \Phi_{ZF} \Phi_0(\xi) \quad (3.2.32)$$



A similar procedure gives

$$\Phi_{-}(\xi) = \frac{-i k_{\theta} q_r}{B(\omega_0 - \omega_{-} - \Omega)} \Phi_{ZF} \Phi_0(\xi) \quad (3.2.33)$$

and  $\omega_{+} = \omega_{-}$  is used (due to up-down symmetry). Equations (3.2.32) and (3.2.33) are equivalent to Eq.(3.2.15). Because of toroidicity, the coupling coefficient is controlled by geometric factors. Substituting Eqs.(3.2.32) and (3.2.33) into Eq.(3.2.25), one obtains a dispersion relation for the modulational instability, namely

$$(\omega_0 - \omega_{+} + \Omega)(\omega_0 - \omega_{-} - \Omega) = \gamma_{\text{mod}}^2 \quad (3.2.34a)$$

where

$$\gamma_{\text{mod}}^2 = \frac{(2 + \eta_i)}{1.6\epsilon^{3/2}} \frac{B_{\theta}^2}{B_{\xi}^2} k_{\theta}^2 q_r^2 c_s^2 \rho_s^2 |\tilde{\Phi}_0|^2 \quad (3.2.34b)$$

and  $|\tilde{\Phi}_0|^2 = \left\langle \sum_m |\Phi_0|^2 \right\rangle$  is the amplitude of the primary drift wave. It is worth noting that the difference of the eigenfrequencies is second order in the wavenumber of the zonal flow  $q_r$ , i.e.,

$$|\omega_0 - \omega_{+}| \approx \omega_0 q_r^2 \rho_s^2. \quad (3.2.35)$$

The factor of  $B_{\theta}^2/(1.6\epsilon^{3/2}B_{\xi}^2)$  is a consequence of the structure of the dielectric constant of the plasma in toroidal geometry. The result has a similar structure to that of Eq.(3.2.18) with similar scalings with the amplitude and the wavenumbers of the pump drift wave and the zonal flow. If  $\gamma_{\text{mod}}^2 > (\omega_0 - \omega_{+})^2$  holds, one obtains the growth rate

$$\Omega = i\sqrt{\gamma_{\text{mod}}^2 - (\omega_0 - \omega_{+})^2}, \quad (3.2.36)$$

using  $\omega_{+} = \omega_{-}$ . The growth rate of the zonal flow has a similar dependence on  $q_r$  as is illustrated in Fig.3.2.3. An estimate of the wavenumber at which the growth rate has maximum is estimated to be  $q_r \approx k_{\theta} \hat{s}$ , where  $\hat{s}$  is the shear parameter. Finally, on account of the confluence of nonlinear beat-induced coupling with linear, toroidicity-induced coupling, interaction with neighbouring poloidal harmonics is possible, and has

no slab counter-part. For this reason, parametric modulational instability in a tokamak has sometimes been referred to as "four-wave coupling". This name is slightly confusing, and the reader should keep in mind that, really, only *three* independent  $n$  modes are involved, as in the case of parametric modulational instability in a slab. The 'fourth wave' enters via linear, toroidicity-induced coupling.

As is the case for the slab plasmas, the zonal flow is expected to be amplified if the growth rate Eq.(3.2.36) is larger than the collisional damping, as explained in § 3.1.3.

$$\sqrt{\gamma_{\text{mod}}^2 - (\omega_0 - \omega_+)^2} > \gamma_{\text{damp}}. \quad (3.2.37)$$

### 3.2.2 Zonal Flow Generation by a Spectrum of Drift Wave Turbulence

While the simplified, truncated-degree-of-freedom models discussed in Chapter 2 can elucidate and encapsulate some aspects of the physics of zonal flow generation, the physically relevant problem requires an understanding of the answer to the question: "Under what conditions is a *spectrum* of drift wave turbulence unstable to a test zonal shear?". By a 'test zonal shear', we mean a weakly sheared seed flow  $V_z(x)$ , such that  $dV_z(x)/dx \neq 0$ . In principle,  $V_z(x)$  itself can support a spectrum of scales. Note that in this respect, the zonal flow generation problem resembles the well-known magnetic dynamo problem, which seeks to answer the question of: "When is a spectrum of MHD turbulence unstable to a 'test' magnetic field?" In the (relevant) case of generation by a spectrum of drift waves, the test zonal flow might interact with a broad spectrum of primary drift wave fluctuations, each of which has a finite self-correlation time. Thus, a statistical, RPA-type theory is necessary. The essence of such a theory is to derive the zonal flow growth rate by:

- a.) first averaging the zonal flow evolution equation (i.e. mean field evolution equation) over an ensemble of drift wave realizations to relate  $\partial \phi_{ZF}/\partial t$  to  $\langle \tilde{\phi}_{DW}^2 \rangle$ , thus obtaining an equation for mean field evolution in the presence of wave (i.e. pondermotive) pressures and stresses,
- b.) then computing the response of the drift wave spectrum to the test zonal flow shear, thus 'closing the feedback loop'.

This procedure, which is typical of that followed in the course of modulational stability calculations, ultimately rests upon:

- a.) the separation in *time* scales between the low-frequency zonal flow and the higher frequency drift waves (i.e.  $\Omega_{ZF} \ll \omega_k$ ). This time scale separation enables the use of adiabatic theory (i.e. eikonal theory and wave kinetics) to compute the response of the primary drift wave spectrum to the test shear, and justifies the neglect of drift wave diffraction. Note that the parametric instability calculation, discussed in Section 3.2, also rests upon such an assumption of time scale separation.
- b.) the assumption of quasi-Gaussian distribution of drift wave phases.

It is worthwhile to note that the weak turbulence theory of zonal flow growth is quite closely related to the classic problem of weak Langmuir turbulence [3.43]. In Langmuir turbulence, low frequency test phonons (i.e. ion acoustic waves) grow by depleting the energy of a bath of ambient plasmons (i.e. plasma waves). Since  $\omega_{pe} \gg q c_s$ , the zonal flow is the analogue of the ion-acoustic wave, while the drift waves are the analogue of the plasma wave. Table 3.2.1 presents a detailed comparison and contrast of the weak Langmuir turbulence and zonal flow problems. The interested reader who is familiar with the weak turbulence theory of Langmuir turbulence may find it helpful to review Table 3.2.1 now. We will return to Table 3.2.1 later, after discussing the theory of zonal flow growth.

### i) Zonal flow growth

As previously noted, the basic dynamics of zonal flows are governed by the 2D Navier-Stokes equation, since the density perturbation associated with the zonal flow is negligibly small. Alternatively, the zonal flow structure is essentially two dimensional, as is a convective cell. Thus, in de-dimensionalized units, the zonal flow potential evolves according to a 2D fluid equation:

$$\frac{\partial}{\partial t} \nabla_r^2 \phi_{ZF} = \frac{-\partial}{\partial r} \langle \tilde{v}_{rd} \nabla^2 \tilde{\phi}_d \rangle - \underline{\underline{\gamma}}_d \nabla_r^2 \phi_{ZF}. \quad (3.2.38)$$

Here  $\underline{\underline{\gamma}}_d$  is a generic damping operator, which may be a scalar coefficient or an integro-differential operator. Physically, Eq. (3.2.38) tells us that zonal flow vorticity evolves due to the spatial flux of drift wave vorticity  $\Gamma_u = \langle \tilde{v}_{rd} \nabla^2 \tilde{\phi}_d \rangle$ . This observation is important, as it establishes there is no *net* flow generation or momentum increase, up to boundary through put terms. Rather, zonal 'flow generation' is really a process of flow *shear amplification*. Zonal flow evolution (i.e., velocity profile evolution) is transparently a process driven by vorticity *transport*, just as temperature and density

profile evolution are driven by thermal and particle fluxes. Eq. (3.2.38) may be rewritten as:

$$\frac{\partial}{\partial t} \nabla_r^2 \tilde{\phi}_{ZF} = \frac{1}{B} \frac{\partial^2}{\partial r^2} \langle \nabla_\theta \tilde{\phi}_d \nabla_r \tilde{\phi}_d \rangle - \gamma_d (\nabla_r^2 \tilde{\phi}_{ZF}), \quad (3.2.39)$$

or, in spectral form, as:

$$\frac{\partial}{\partial t} \nabla_r^2 \tilde{\phi}_{ZF} = \frac{1}{B} \frac{\partial^2}{\partial r^2} \int d^2 k \, k_r k_\theta |\phi_k^d|^2 - \gamma_d (\nabla_r^2 \tilde{\phi}_{ZF}). \quad (3.2.40)$$

Equation (3.2.40) directly relates the evolution of zonal flow potential to the slow variation of the drift wave intensity envelope. By "slow variation" we refer to the fact that  $|\phi_k^d|^2$  varies on a scale larger than upon which  $\phi_k^d$  does, i.e.  $k_r > \left(1/|\phi_k^d|^2\right) \partial |\phi_k^d|^2 / \partial r$ .

Also, it is now clear that the scale of the drift wave intensity envelope is what sets the scale of the zonal flow.

Since wave population density (alternatively the "density of waves") is conserved along wave ray trajectories, tracking the evolution of  $N$ , the density of waves, is particularly useful in evaluating the response of the drift wave spectrum to modulation by a test shear. Thus, it is considerably more convenient to work with  $N(\mathbf{k}, \mathbf{r}, t)$  than with  $|\phi_k^d|^2$ . The convenience of  $N(\mathbf{k}, \mathbf{r}, t)$  follows, of course, from the fact that  $N$  obeys a Boltzmann equation, with characteristic equations given by the eikonal equations for a drift wave. The question then becomes, 'just what exactly is  $N(\mathbf{k}, \mathbf{r}, t)$ , the wave population density?' In most cases,  $N(\mathbf{k}, \mathbf{r}, t)$  is the wave action density  $N = \mathcal{E}/\omega_k$ , where  $\mathcal{E}$  is the wave energy density. In the case of drift wave turbulence, this question is complicated by the fact that drift wave turbulence supports *two* quadratic conserved quantities, namely the energy density  $\mathcal{E} = (1 + k_\perp^2 \rho_s^2)^2 |\phi_k^d|^2$  and the potential enstrophy density  $Z = (1 + k_\perp^2 \rho_s^2)^2 |\phi_k^d|^2$ . Thus, one can count either the local 'wave' density, given by the action density  $N = (1 + k_\perp^2 \rho_s^2)^2 |\phi_k^d|^2 / \omega_k$ , or the local 'vortex density' (i.e. 'roton' number), given by  $N_r = (1 + k_\perp^2 \rho_s^2)^2 |\phi_k^d|^2$ . However, for zonal flow shears (which have  $q_\theta = 0$ ),  $k_\theta$  is unchanged by flow shearing, since  $dk_y/dt = -\partial(k_\theta V_{ZF}(x))/\partial y = 0$ . The action density then becomes  $N = (1 + k_\perp^2 \rho_s^2)^2 |\phi_k^d|^2 / \omega_{*e}$  where  $\omega_{*e}$  is an irrelevant constant multiplier, thus rendering both counts of exciton density the same! Hence, we can rewrite the zonal flow evolution equation Eq.(3.2.40) as [2.13, 2.17, 3.44]:

$$\int d^2k \frac{k_\theta^2 k_x}{(1 + k_\perp^2 \rho_s^2)^2} \frac{\partial N_k}{\partial k_r} = - \int d^2k k_\theta^2 |\phi_k^d|^2 = - k_\theta^2 |\tilde{\phi}_d|^2. \quad (3.2.41)$$

In Eq. (3.2.41) above, the amplification of the zonal flow shear  $\tilde{v}_{ZF}$  is related to the density of waves  $N(\mathbf{k}, \mathbf{r}, t)$  which is, in turn, a functional of the zonal flow field. At the level of a linear response theory for modulation of  $N$  by  $\tilde{v}_{ZF}$ ,  $\tilde{N}$  is given by

$$\tilde{N}(\mathbf{k}, \mathbf{r}, t) = \left( \frac{\delta N}{\delta \tilde{v}_{ZF}} \right) \tilde{v}_{ZF}', \quad (3.2.42)$$

where  $\tilde{v}_{ZF}' = \partial \tilde{v}_{ZF} / \partial r$ , so that  $\tilde{v}_{ZF}'$  evolution is then related to the modulation response  $\delta N / \delta \tilde{v}_{ZF}'$  as:

$$\frac{\partial}{\partial t} v_{ZF}' = \frac{1}{B^2} \frac{\partial^2}{\partial r^2} \int d^2k \frac{k_r k_\theta}{(1 + k_\perp^2 \rho_s^2)^2} \left( \frac{\delta N}{\delta v_{ZF}'}(\mathbf{k}, \mathbf{r}, t) \right) v_{ZF}' - \gamma_d [v_{ZF}']. \quad (3.2.43)$$

Note that Eq. (3.2.43) relates shear amplification to the extent to which the modulation, induced in the drift wave population  $N$  by  $\tilde{v}_{ZF}'$ , tends to drive a Reynolds stress, which *re-enforces* the initial perturbation. An *affirmative answer* to this question establishes that the drift wave spectrum is *unstable* to the growth of a seed zonal velocity shear.

The modulational response  $\delta N / \delta \tilde{v}_{ZF}'$  may now be calculated by linearizing the wave kinetic equation for  $N$ , which can formally be written as (by taking a model of nonlinear damping as  $\gamma_{NL} N = \Delta \omega_k N^2 / N_0$ ):

$$\frac{\partial N}{\partial t} + (\underline{v}_r + \tilde{\underline{v}}_{ZF}) \cdot \underline{\nabla} N - \frac{\partial}{\partial \underline{x}} (\omega + \underline{k} \cdot \tilde{\underline{v}}_{ZF}) \cdot \frac{\partial N}{\partial \underline{k}} = \gamma_k N - \frac{\Delta \omega_k}{N_0} N^2, \quad (3.2.44)$$

with characteristic equations for  $\underline{x}$  and  $\underline{k}$  evolution given by:

$$\frac{d\underline{x}}{dt} = \underline{v}_r + \tilde{\underline{v}}_{ZF}, \quad (3.2.45a)$$

$$\frac{d\underline{k}}{dt} = - \frac{\partial}{\partial \underline{x}} (\omega + \underline{k} \cdot \tilde{\underline{v}}_{ZF}). \quad (3.2.45b)$$

The RHS of Eq. (3.2.44) may be simplified by noting that, in the absence of modulation and inhomogeneities,  $N$  must reduce to an equilibrium value determined by local

interactions, which do not conserve population density. Thus, in the spirit of the Chapman-Enskog expansion, to lowest order  $N = N_0 \gamma_k / \Delta \omega_k$ . For an ansatz reference equilibrium spectrum  $N_0(k)$ , this forces  $\gamma_k = \Delta \omega_k$ , so that the linearized form of the wave kinetic equation for zonal flow shears becomes:

$$\frac{\partial \tilde{N}}{\partial t} + v_r \frac{\partial \tilde{N}}{\partial r} + \gamma_k \tilde{N} = \frac{\partial}{\partial x} (k_\theta \tilde{V}_{ZF}) \frac{\partial \langle N \rangle}{\partial k_r}. \quad (3.2.46)$$

Here  $\langle N \rangle$  is the equilibrium value of the wave spectrum. Note that the  $+\gamma_k \tilde{N}$  damping term arises from a partial cancellation between  $\gamma_k \tilde{N}$  and  $-2\Delta \omega_k \langle N \rangle \tilde{N} / N_0$ , after using  $\Delta \omega_k = \gamma_k$  and  $N_0 = \langle N \rangle$ . It follows then that the modulation  $\tilde{N}_{q,\Omega}$  induced by  $\tilde{V}_{ZF}$  is given by:

$$\tilde{N}_{q,\Omega} = \frac{-q k_\theta \tilde{V}_{ZF}}{(\Omega - q v_r + i \gamma_k)} \frac{\partial \langle N \rangle}{\partial k_r}, \quad (3.2.47)$$

so the modulational instability eigenfrequency is given by:

$$\Omega = \frac{+q^2}{B^2} \int \frac{d^2 k k_\theta^2}{(\Omega - q v_r + i \gamma_k)} k_r \frac{\partial \langle N \rangle / \partial k_r}{(1 + k_\perp^2 \rho_s^2)^2} - i \gamma_d. \quad (3.2.48)$$

This finally implies that the zonal flow growth rate is given by:

$$\Gamma_q = \frac{-q^2}{B^2} \int dk^2 \frac{k_\theta^2}{(1 + k_\perp^2 \rho_s^2)^2} \frac{\gamma_k}{(\Omega - q v_r)^2 + \gamma_k^2} (k_r \partial \langle N \rangle / \partial k_r) - \gamma_d. \quad (3.2.49)$$

Several aspects of the structure of the zonal flow growth are apparent from Eq. (3.2.49). First, *note that growth requires  $\partial N / \partial k_r < 0$ !* This condition is satisfied for virtually any realistic equilibrium spectral density for drift wave turbulence. In contrast to the well-known case of Langmuir turbulence, a population inversion (i.e.  $\partial N / \partial k_r > 0$ ) is *not* required for growth of zonal flows by RPA modulational instability. This is a consequence of the fact that  $\omega_k$  *decreases* with increasing  $k_r$  for drift waves, while  $\omega_k$  *increases* with increasing  $k$  for Langmuir waves (i.e., see Section 2). Thus, induced diffusion of  $k_r$  will deplete the drift wave population and drive zonal flows for  $d \langle N \rangle / dk_r < 0$ , while induced diffusion of  $k_r$  will deplete the plasmon population for  $d \langle N \rangle / dk > 0$ .

It is also interesting to note that the leading behavior of the zonal flow growth has the form of negative viscosity or negative diffusion, i.e.

$$\Gamma_q \approx q^2 D(q), \quad (3.2.50)$$

where

$$D(q) \equiv \frac{-1}{B^2} \int d^2k \frac{k_\theta^2 \gamma_k}{(1 + k_\perp^2 \rho_s^2)^2} \frac{k_r}{(\Omega - q v_k)^2 + \gamma_k^2} \partial \langle N \rangle / \partial k_r. \quad (3.2.51)$$

This is, of course, consistent with expectations based upon the well-known inverse cascade of energy in 2D, although we emphasize that zonal flow growth is non-local in wave number, and strongly anisotropic, in contrast to the inverse cascade. See Fig.3.2.4 for the illustration of the integrand of Eq.(3.2.51). Note also that  $D(q) \sim 1/q^2$  when the drift wave packet transit-time through the zonal flow approaches  $\gamma_k^{-1}$ , so that an interpretation based purely upon the negative viscosity concept is over-simplified. An order-of-magnitude estimate of Eq. (3.2.50) is given with the help of Eq. (3.2.51). Assuming that  $k_\perp^2 \rho_s^2 < 1$  and that  $\gamma_k > q v_k$ , integration by parts yields

$$\int d^2k \frac{k_\theta^2 k_r}{(1 + k_\perp^2 \rho_s^2)^2} \frac{\partial N_k}{\partial k_r} \approx - \int d^2k k_\theta^2 |\phi_k|^2 \approx - k_\theta^2 |\tilde{\phi}_d|^2. \quad (3.2.52)$$

Combining Eqs. (3.2.51) and (3.2.52),  $D(q)$  is evaluated as

$$D(q) \approx \frac{k_\theta^2}{B^2} |\tilde{\phi}_d|^2 = \frac{c_s^2 \rho_s^2}{\gamma_{drift}} k_\theta^2 \left| \frac{e \tilde{\phi}_d}{T} \right|^2. \quad (3.2.53)$$

This value is of the same order of magnitude in comparison to other transport coefficients driven by turbulent drift waves. However, it should be noted that zonal flow growth occurs over a region of size  $q^{-1}$ , while conventional transport coefficients quantify the rate of diffusion across a profile scale length. Thus, zonal flow dynamics are *mesoscopic* phenomena, occurring on spatial scales between those of the turbulence correlation length and characteristic scale lengths of the profiles.

## (ii) Energy Conservation property

It is appropriate to demonstrate here that the RPA theory of zonal flow growth, presented above, manifestly conserves energy. Eq. (3.2.51) gives the zonal flow production rate as

$$\Gamma_q = \frac{-q^2}{B^2} \int d^2k \frac{k_\theta^2}{(1 + k_\perp^2 \rho_s^2)^2} R(q, \Omega) k_r \frac{\partial \langle N \rangle}{\partial k_r}, \quad (3.2.54a)$$

$$R(q, \Omega) = \frac{\gamma_k}{(\Omega - qV_E)^2 + \gamma_k^2}. \quad (3.2.54b)$$

(The role of nonlinear damping is explained again in Chap.6.) Thus, the time rate of change of zonal flow energy, due to interaction with drift waves, is

$$\frac{d}{dt} |\tilde{V}_{ZF}|^2 = \sum_q 2\Gamma_q |\tilde{V}_{ZFq}|^2 = \frac{-2}{B^2} \sum_q \int d^2k \frac{q^2 |k_\theta V_{ZFq}|^2}{(1 + k_\perp^2 \rho_s^2)^2} R(q, \Omega) \frac{\partial \langle N \rangle}{\partial k_r}. \quad (3.2.55)$$

The corresponding rate of change of the mean drift wave energy is

$$\frac{d}{dt} \langle \mathcal{E} \rangle = \frac{d}{dt} \int d^2k \frac{1}{(1 + k_\perp^2 \rho_s^2)} \frac{d}{dt} \langle N(k, t) \rangle. \quad (3.2.56)$$

It is understood here that  $\langle N(k, t) \rangle$  corresponds to the mean drift wave potential enstrophy ( $N = (1 + k_\perp^2 \rho_s^2)^2 |\phi_k|^2$ ). Since a spectrum of sheared zonal flows induces diffusion of the drift wave population in radial wave number, one can write:

$$\frac{d \langle N \rangle}{dt} = \frac{\partial}{\partial r} D_{K,K} \frac{\partial \langle N \rangle}{\partial r}. \quad (3.2.57)$$

Proceeding to integrate by parts, we obtain

$$\frac{d \langle \mathcal{E} \rangle}{dt} = \int d^2k \frac{2k_r}{(1 + k_\perp^2 \rho_s^2)} D_{K,K} \frac{\partial \langle N \rangle}{\partial k_r}, \quad (3.2.58)$$

where:

$$D_{K,K} = \sum_q \frac{1}{B^2} k_\theta^2 |\tilde{V}_{ZF}|^2 q^2 R(q, \Omega). \quad (3.2.59)$$

It is thus abundantly clear that



$$d\left(\left|\tilde{V}_{ZF}\right|^2 + \langle \mathcal{E} \rangle\right)/dt = 0,$$

so the theory conserves energy. Having thus rigorously established energy conservation, we will make use of this actively in the future to simplify calculations.

### 3.2.3 Relation between the RPA and single mode description

It is appropriate, at this point, to establish some connection or correspondence between the coherent modulation instability calculation discussed in Section 3.2.1 and the RPA calculation discussed here in Subsection 3.2.2. To this end, it is interesting to note that the zonal flow growth rate Eq.(3.2.48) may be re-expressed as a frequency, i.e.

$$\Omega = -\int d^2k \frac{\gamma_{coh}^2(q, k)}{(\Omega - q v_g + i \gamma_k)}, \quad (3.2.60a)$$

where

$$\gamma_{coh}^2(q, k) = \frac{k_\theta^2 q^2 k_r}{B^2 (1 + k_\perp^2 \rho_s^2)^2} \partial \langle N \rangle / \partial k_r, \quad (3.2.60b)$$

or, after integration by parts

$$\gamma_{coh}^2 \equiv \frac{-q^2 k_\theta^2 \langle N \rangle}{B^2 (1 + k_\perp^2 \rho_s^2)^2}. \quad (3.2.60c)$$

Here the effect of  $\partial / \partial k_r$  on  $(1 + k_\perp^2 \rho_s^2)^{-2} (1 + k_\perp^2 \rho_s^2)^{-2}$  and  $R$  has been neglected. In this limit, then Eq.(3.2.60a) can be rewritten as

$$\Omega(\Omega - q v_g) = -\gamma_{mod}^2, \quad (3.2.61a)$$

where

$$\gamma_{coh}^2 \equiv \frac{k_\theta^2 q^2 \langle N \rangle}{(1 + k_\perp^2 \rho_s^2)^2}. \quad (3.2.61b)$$

This form is essentially the same as those obtained from the parametric analyses of modulational instability, and gives the zonal flow growth rate as

$$\gamma_{ZF}^2 = \gamma_{\text{mod}}^2 - (q v_k)^2,$$

which is equivalent to Eq. (3.2.20). In this case, the growth rate  $\gamma_{ZF} \approx \gamma_{\text{mod}}$  is linearly proportional to the wavenumber of zonal flow and the amplitude of the drift wave. The result in the case of the plane drift wave corresponds to the limiting case where the lifetime of the primary drift waves,  $\gamma_{\text{drift}}^{-1}$ , is much longer than the growth rate of the zonal flow. We emphasize, however, that the validity of the coherent calculation not only requires that  $\gamma_{\text{mod}} > \gamma_k$ , but also  $\gamma_{\text{mod}} > q \frac{d v_k}{dk} \Delta k$ . Here  $\left( q \left( d v_k / dk \right) \Delta k \right)^{-1}$  is the autocorrelation of a drift wave packet with the zonal flow strain field, in that it measures the time for a packet to disperse as it propagates radially across a zonal flow of scale  $q^{-1}$ . Thus, validity of the coherent modulational theory requires *both* proximity to marginal stability of the primary drift wave spectrum (so  $\gamma_{\text{mod}} > \gamma_k$ ), and a narrow spectrum (so that  $\gamma_{\text{mod}} > q (d v_{kr} / dk) \Delta k$ ).

Building upon these considerations, one may construct an interpolation formula:

$$\Omega \left( \Omega - q \frac{\partial \omega}{\partial k_r} + i \gamma_{\text{drift}} \right) = -\gamma_{\text{mod}}^2, \quad (3.2.62)$$

with the growth rate

$$\gamma_{ZF} = \frac{\sqrt{(4\gamma_{\text{mod}}^2 + \gamma_{\text{drift}}^2)^{1/2}} - \gamma_{\text{drift}}}{2}, \quad (3.2.63)$$

for the case of  $\gamma_{\text{mod}}^2 > 0$ . Noticing that the coefficient  $D_{k_r, k_r}$  defined by Eq. (3.2.59) satisfies the relation

$$D_{k_r, k_r} \approx q_r^{-2} \gamma_{\text{mod}}^2 \gamma_{\text{drift}}^{-1}, \quad (3.2.64)$$

within the approximation of Eq. (3.2.61). Equation (3.2.63) covers various ranges. In the limit of plane wave,  $\gamma_{\text{drift}} < \gamma_{\text{mod}}$ , the reactive instability Eq.(3.2.20) or (3.2.36) is recovered, where  $\gamma_{ZF} \sim \gamma_{\text{mod}} \propto q_r$  holds. In the opposite limit,  $\gamma_{\text{drift}} > \gamma_{\text{mod}}$ , diffusive growth ( $\gamma_{ZF} \sim \gamma_{\text{mod}}^2 \propto q_r^2$ ) is found. Figure 3.2.5 illustrates the transition between regimes.

It might be useful here to note the cut-off of the zonal flow growth at large  $q_r$ . It is explained in the case of plane drift wave (parametric modulational instability) as Eq.(3.2.20) or Fig.3.2.3. A similar expression is obtained in the limit of RPA. In the

expression of the zonal flow growth rate in the RPA limit, e.g., Eq.(3.2.54), the response function is evaluated by  $R(q, \Omega) \sim 1/\gamma_k$ . The lowest order correction of the wave dispersion is written as  $R(q, \Omega) \sim \gamma_k^{-1} \left( 1 - q_r^2 v_{gr}^2 \gamma_k^{-2} + \dots \right)$ . Thus one has an expression of  $\gamma_{ZF}$ ,

$$\gamma_{ZF} = D(q_r = 0) q_r^2 \left( 1 - q_r^2 q_{r0}^2 \right)$$

where

$$q_{r0}^2 = v_{gr}^{-2} \gamma_k^2$$

represents the effect of the dispersion of the drift waves. This is an expansion of Eq.(3.2.50) with respect to  $q_r^2 q_{r0}^2$ .

### 3.2.4 Zonal Flow Drive by Poloidal Asymmetry

The particle flux driven by drift-wave fluctuations could be poloidally asymmetric. If such an asymmetry exists in the background drift waves, a poloidal flow is induced in tokamak plasmas. This mechanism was first noted by Stringer [3.6] and is called the Stringer spin-up. We briefly explain it here.

The continuity equation (3.1.6) describes the flow on the magnetic surface if there is poloidal asymmetry in the net source term  $S - \nabla \cdot \Gamma$ . Poloidal asymmetry of  $S - \nabla \cdot \Gamma$  appears, if the particle flux is not uniform in  $\theta$ . For instance, the local neoclassical flux has  $\theta$ -dependence. In addition, the turbulence driven flux can, in principle, be poloidally asymmetric, on account of poloidal dependence of the turbulence intensity. We write

$$S - \nabla \cdot \Gamma = \langle S - \nabla \cdot \Gamma \rangle + (S - \nabla \cdot \Gamma)_a F(\theta) \quad (3.2.65)$$

where  $\langle \dots \rangle$  is a poloidal average, and  $F(\theta)$  is a function describing the poloidally-inhomogeneous part, so  $\langle F(\theta) \rangle = 0$ . The magnitude of poloidal asymmetry,  $(S - \nabla \cdot \Gamma)_a$ , and the shape of  $F(\theta)$  are taken as prescribed here. In steady-state, this inhomogeneity induces a secondary flow on the magnetic surface  $V_{a,\parallel}$  which compensates the asymmetry of the source as is illustrated in Fig.3.2.6. The asymmetric flow  $V_{a,\parallel}$  is given by:

$$V_{a,\parallel} = \frac{qR}{n_0} (S - \nabla \cdot \Gamma)_a \int_0^{2\pi} d\theta F(\theta). \quad (3.2.66)$$

In the presence of this flow, the parallel component of Eq.(3.1.7) is affected, in that the  $r^{-1} V_\theta \partial V_\parallel / \partial \theta$  term in  $\mathbf{V} \cdot \nabla \mathbf{V}$  does not vanish. As a result, one has

$$\frac{\partial}{\partial t} \tilde{V}_\parallel + \frac{1}{r} \tilde{V}_{E \times B, \theta} \frac{\partial}{\partial \theta} V_{a, \parallel} + c_s^2 \nabla_\parallel \tilde{N} = 0 . \quad (3.2.67)$$

This relation, together with Eqs.(3.1.12a) and (3.1.12c),

$$\frac{\partial}{\partial t} \tilde{N} - \frac{2}{R} \sin \theta \tilde{V}_{E \times B} + \nabla_\parallel \tilde{V}_\parallel = 0 ,$$

$$\frac{\partial}{\partial t} \tilde{V}_{E \times B} + \frac{2}{R} c_s^2 \oint \frac{d\theta}{2\pi} \sin \theta \tilde{N} = 0 ,$$

yield the dispersion relation in the presence of the asymmetry  $(S - \nabla \cdot \Gamma)_a$ . As in Eq.(3.1.11), one may choose the poloidal dependencies in  $\tilde{N}(r, \theta; t)$  and  $\tilde{V}_\parallel(r, \theta; t)$  but the  $\mathbf{E} \times \mathbf{B}$  flow is symmetric,  $\tilde{V}_E = \tilde{V}_{E \times B}(r; t)$ . Writing the temporal dependence as  $\exp(-i\Omega t)$  for these perturbation variables, the set of equations (3.2.65), (3.1.12a) and (3.1.12c) give the dispersion relation

$$\Omega^3 - \omega_{\text{GAM}}^2 \Omega = -i \frac{2c_s^2}{Rr} \gamma_{\text{as}} , \quad (3.2.68)$$

where  $\gamma_{\text{as}}$  is the net particle "production" rate of the asymmetric source, i.e.,

$$\gamma_{\text{as}} = \frac{1}{n_0} (S - \nabla \cdot \Gamma)_a \int_0^{2\pi} \frac{d\theta}{2\pi} \cos \theta F(\theta) . \quad (3.2.69)$$

This result shows that instability is possible if  $F(\theta)$  has an in-out asymmetry, like  $F(\theta) \sim \cos \theta$ .

Equation (3.2.69) predicts two possible types of instabilities. One is growth of the zero frequency zonal flow with  $\Omega \ll \omega_{\text{GAM}}$ . In this case, Eq.(3.2.69) reduces to

$$\Omega \approx i \frac{1}{\omega_{\text{GAM}}^2} \frac{2c_s^2}{Rr} \gamma_{\text{as}} \approx i \frac{R}{r} \gamma_{\text{as}} , \quad (3.2.70)$$

which shows that poloidally-symmetric flow spins up if  $\gamma_{\text{as}} > 0$ . Figure 3.2.6 shows the case of  $\gamma_{\text{as}} > 0$ . The other case corresponds to the excitation of the geodesic acoustic mode (GAM). For the branch with  $\Omega \approx \omega_{\text{GAM}}$ , Eq.(3.2.68) gives an approximate solution

$$\Omega = \omega_{\text{GAM}} - i \frac{1}{\omega_{\text{GAM}}^2} \frac{c_s^2}{R r} \gamma_{\text{as}} = \omega_{\text{GAM}} - i \frac{R}{2r} \gamma_{\text{as}} . \quad (3.2.71)$$

The geodesic acoustic mode is destabilized if  $\gamma_{\text{as}} < 0$ . We note that the growth rate of the axisymmetric flow, Eq.(3.2.70) or (3.2.71) does not depend on the radial extent of the flow, i.e.,

$$\gamma_{\text{as}} \propto (q_r)^0 . \quad (3.2.72)$$

where  $q_r$  is the radial wavenumber of the zonal flow. Hence, the Stringer spin-up mechanism can be important for the case of small  $q_r$ . The collisional damping rate in §3.1.3 is also independent of  $q_r$ . Comparing Eqs.(3.1.28) or (3.1.29) with (3.1.33), the excitation of a GAM with long radial wavelength is expected to occur if  $\gamma_{\text{as}} < \nu_{ii}$ .

When the radial wavelength is short, GAMs are stabilized by the turbulent viscous damping of parallel flow, which is explained by the next subsection. Thus turbulent transport plays two roles in the Stringer spin-up. Poloidal asymmetry of the particle flux  $\Gamma$  can drive the process while the radial dependence of the momentum flux can damp it. (It has recently been pointed out that the shearing of the background turbulence by GAM induces poloidal asymmetry of the particle flux  $\Gamma$  and that this mechanism can cause the GAM instability. In this case, the growth rate is proportional to  $q_r^2$ . [3.45])

### 3.2.5 Influence of turbulent momentum transport on the secondary flow

As is shown in 3.1.1, the zonal flow is associated with a secondary flow along the magnetic field line that cancels the divergence of the perpendicular flow. The viscous damping of this secondary flow due to toroidicity acts as a damping rate of the zonal flow, in addition to the collisional damping. This damping rate is rewritten as [2.46]

$$\gamma_{\text{damp}} = \mu_{\parallel} (1 + 2q^2) q_r^2 \quad (3.2.73)$$

where  $\mu_{\parallel}$  is the turbulent shear viscosity for the flow along the field line, and  $q$  is the safety factor. Of course,  $\mu_{\parallel}$  is a function of the drift wave intensity, and thus can be suppressed in the regime of strong zonal flows, such as the Dimits shift. The Pfirsch-Schlüter coefficient  $1 + 2q^2$  is replaced by  $1 + 1.6q^2/\sqrt{\epsilon}$  in the collisionless limit. This damping term has dependencies on the wavenumber  $q_r$  and the intensity of the primary drift wave turbulence, which are similar to the growth rate, given in subsection 3.2.3. The dependence on geometrical factors differs from  $\gamma_{\text{ZF}}$ . Therefore the safety factor  $q$  (and thus the  $B_{\theta}(r)$  profile!) can play an important role in determining the domain of zonal flow growth.

### 3.2.6 Electromagnetic effects

The discussion in the previous subsections is cast in the framework of the electrostatic limit, in the interest of transparency of argument. Plasma turbulence supports magnetic perturbations, and electromagnetic effects also have important roles in the physics of zonal flows. One of the effects is known as the 'finite- $\beta$  effect' on drift waves [3.46], where  $\beta$  is the ratio of the plasma pressure to the magnetic field pressure,  $\beta = 2\mu_0 B^{-2} p$ . In particular, the phrase "finite- $\beta$  effect" includes the effects of magnetic stresses (dependent on the  $\beta$  since  $\tilde{B}/B_0$  scales with  $\beta$ ) on zonal flow growth.

Frequently, the magnetic stress tends to compete against the Reynolds stress, thus reducing zonal flow growth. The other is the generation of the (poloidally symmetric) magnetic field bands by plasma turbulence. The generation of the magnetic field that has a symmetry (on a larger scale than that of the background turbulence) has been known as the mean field dynamo. This dynamo is more akin to a 'mesoscale dynamo'. Since the magnetic fields so generated have zonal symmetry and structure, we refer to them as *zonal fields*. As is the case of the zonal flow, the generated magnetic field may be constant on the magnetic surface but is rapidly changing in radial direction. The study of zonal fields is a new direction from which to approach the dynamo problem [2.58, 2.60, 2.61].

In the broad context of the zonal flows, two directions of research are explained here. One is finite- $\beta$  effects on drift waves and the zonal flow generation by them. This is discussed in the context of parametric decay instability. The other is the magnetic field generation by drift-Alfven waves. The zonal field calculation is approached using the methods of statistical theory. Here, two examples are arranged as follows:

subject	mechanisms for zonal flow growth
zonal flow generation by finite- $\beta$ drift waves	modulational instability of a plane drift Alfven wave
zonal magnetic field generation	Random Alfven wave refraction of Alfven wave turbulence

#### (i) finite- $\beta$ effect on the drift waves

In the finite- $\beta$  plasmas, coupling between the drift wave and shear Alfven wave occurs so as to form a drift-Alfven mode. The dispersion relation of this mode has been given as

$$1 + k_y^2 \rho_s^2 - \frac{\omega_*}{\omega} - \frac{\omega(\omega - \omega_*)}{k_{\parallel}^2 V_A^2} = 0, \quad (3.2.72)$$

where  $V_A$  is Alfvén wave velocity.

The plane drift Alfvén mode is also unstable to modulations. The method explained in §3.2.1 has been applied to the finite- $\beta$  case [3.47, 3.48]. Introducing the vector potential perturbation  $\Psi$  (the component of the vector potential in the direction of main magnetic field), one writes the plane wave as

$$\begin{pmatrix} \phi \\ \Psi \end{pmatrix}_0 = \begin{pmatrix} \phi_0 \\ \Psi_0 \end{pmatrix} \exp \left( i k_y y + i k_{\parallel} z - i \omega_0 t \right) \quad (3.2.73)$$

where the suffix 0 stands for the primary wave with real frequency  $\omega_0$  given by (3.2.72). The modulational perturbation thus follows

$$\begin{aligned} \begin{pmatrix} \phi \\ \Psi \end{pmatrix}_m &= \begin{pmatrix} \phi_{ZF} \\ \Psi_{ZF} \end{pmatrix} \exp \left( i q_x x - i \Omega t \right) \\ &+ \begin{pmatrix} \phi_+ \\ \Psi_+ \end{pmatrix} \exp \left( i q_x x + i k_y y + i k_{\parallel} z - i \omega_+ t \right) + \begin{pmatrix} \phi_- \\ \Psi_- \end{pmatrix} \exp \left( i q_x x - i k_y y - i k_{\parallel} z - i \omega_- t \right) \end{aligned} \quad (3.2.74)$$

where  $\phi_{ZF}$  is the electrostatic potential perturbation that induces zonal flow,  $\Psi_{ZF}$  generates the zonal magnetic field,  $\Omega$  is the frequency of the zonal flow and field, and  $(\phi_+, \Psi_+)$  and  $(\phi_-, \Psi_-)$  are the upper and lower drift-Alfvén mode sidebands.

As was explained in §3.2.1, nonlinearity induces the coupling between the primary wave and the modulations. In the electromagnetic case, the primary nonlinearities consist of the convective nonlinearity  $V_{\perp} \cdot \nabla$  in the Lagrange time derivative, and the nonlinearity in  $\nabla_{\parallel}$ , due to the bending of magnetic field lines [3.49, 3.50]. A set of bilinear equations for the variables  $(\phi_0, \Psi_0)$ ,  $(\phi_{ZF}, \Psi_{ZF})$ ,  $(\phi_+, \Psi_+)$ , and  $(\phi_-, \Psi_-)$  was derived. By using the estimate of  $k_{\parallel} \sim 1/qR$ , the growth rate of the zonal flow together with the zonal field  $\gamma_{ZF} = \text{Im} \Omega$  is given by

$$\gamma_{ZF} = q_x k_y \rho_s^2 \omega_{ci} |\phi_0| \left( M_A \left( 1 - \omega_0^2 k_y^2 \rho_s^2 \beta \right) + M_B \omega_0^2 q_x^2 k_y^2 \rho_s^4 \beta - \frac{q_x^2 \rho_s^4 \omega_0^2}{2 L_n^2 |\phi_0|^2} \right)^{1/2} \quad (3.2.75)$$

with coefficients

$$M_A = C^{-1} \left( 1 - \hat{\omega}_0 (2\hat{\omega}_0 - 1) k_y^2 \rho_s^2 \hat{\beta} + \frac{q_x^2 - k_y^2}{k_\perp^2} \left( 1 - \frac{1}{\hat{\omega}_0} - k_y^2 \rho_s^2 \right) \right), \quad (3.2.76a)$$

$$M_B = -\frac{2k_y^2}{C k_\perp^2} \left( 1 - \frac{1}{\hat{\omega}_0} + k_y^2 \rho_s^2 \right), \quad (3.2.76b)$$

$$C = 1 + k_y^2 \rho_s^2 - \hat{\omega}_0 (3\hat{\omega}_0 - 2) k_y^2 \rho_s^2 \hat{\beta} \quad (3.2.76c)$$

where  $|\phi_0| = |e\tilde{\phi}_0/T|$ ,  $\hat{\omega}_0 = \omega_0/\omega_*$ , and  $\hat{\beta} = \beta(qR/L_n)^2/2$  are used for convenience to elucidate finite- $\beta$  effects. The coefficient  $\hat{\beta}$  represents the ratio of the frequency to the shear-Alfven wave frequency, i.e.,  $(\omega_*/k_\parallel V_A)^2 \simeq k_y^2 \rho_s^2 \hat{\beta}$ .

This set of equations are cast in terms of the parameters we now list: the amplitude of the pump wave  $|\phi_0| = |e\tilde{\phi}_0/T|$ ; the wavenumber of the pump wave  $k_y \rho_s$ ; the wave number of the zonal flow  $q_x \rho_s$ ; and the normalized pressure,  $\hat{\beta}$ . The fourth parameter appears as a result of finite  $\beta$ . In the limit of  $\hat{\beta} \rightarrow 0$ , the result of §3.2.2 are recovered. Equation (3.2.75) describes how the growth rate of the zonal flow (via parametric modulational instability) is altered by finite- $\beta$  effects. In the limit of small  $\hat{\beta}$ , Eq.(3.2.75) tells that the growth rate of the zonal flow decreases as  $\hat{\beta}$  increases. This has also been discussed in terms of 'Alfvenization' of the zonal flow drive [3.51]. In addition to the Reynolds stress, the divergence of the Maxwell stress is known to induce a force on plasmas. The signs of the divergences of the Reynolds stress and Maxwell stress are opposite for the drift-Alfven waves. For the shear-Alfven wave, the relation  $\tilde{v} \propto \tilde{B}$  holds. This implies a cancellation of the Reynolds stress and Maxwell stress, and the consequent quenching of the zonal flow drive. Thus, the finite- $\beta$  effect, which introduces a coupling between the shear-Alfven wave and drift wave, causes magnetic field perturbations that reduce the drive of the zonal flow for fixed value of  $|\phi_0| = |e\tilde{\phi}_0/T|$ . Equation (3.2.75) includes terms quadratic in  $\hat{\beta}$ , which exceeds the linear term on  $\hat{\beta}$ , as  $\hat{\beta}$  increases. In [3.48], it has been shown that the zonal flow growth rate starts to increase if  $\hat{\beta}$  exceeds a critical value,  $\hat{\beta} > \hat{\beta}_c$ ,

$$\hat{\beta}_c \simeq 2k_y^{-2} \rho_s^{-2}. \quad (3.2.77)$$

The origin of the reduction of turbulent transport at high beta value that has been observed in direct numerical simulations [3.48] is attributed to this.



Another application of this type of analyses has been given for the Alfvén ITG mode [3.52]. The same structure of the modulational instability (3.2.20) was found [3.47].

## (ii) Zonal Magnetic Field Generation

The amplitude of the zonal magnetic field  $\psi_{ZF}$  is shown to 'seed' the growth of modulational instability [3.47]. This effect is important for zonal field growth. In the problem of the dynamo in space and astrophysical objects, the electric resistance by collisions along the field line is weak enough that zonal magnetic field generation can have substantial impact. The regime of low resistivity is also relevant to toroidal plasmas. In addition, nonlinear MHD instability, like the neoclassical tearing mode [3.53], which illustrates the critical role of the current profile in turbulent plasmas, can be 'seeded' by zonal field. Thus, the study of zonal magnetic field that is associated with, and similar to, the zonal flow has attracted attention.

An analysis of zonal field modulational instability is briefly illustrated here, and provides an introduction to further study of dynamo and field amplification problems. The equation for the "mean field" is here considered to be that for vector potential component in the direction of the strong (toroidal) magnetic field [3.54]. The equation is given by the  $V_{\parallel}$  moment of the electron drift kinetic equation, which is:

$$\left(1 - \delta_e^2 \nabla_{\perp}^2\right) \frac{\partial}{\partial t} \psi_{ZF} - \left\langle \tilde{E}_{\parallel} \tilde{n} \right\rangle + \frac{\partial}{\partial r} \Gamma_{J,r} = \eta_{\parallel} \nabla_{\perp}^2 \psi_{ZF} \quad (3.2.78)$$

Here  $\delta_e$  is the collisionless electron skin depth,  $c/\omega_{pe}$ ,  $\left\langle \tilde{E}_{\parallel} \tilde{n} \right\rangle$  gives the average parallel acceleration,  $\Gamma_{J,r}$  stands for the turbulent flux of current in the  $x$  direction, and  $\eta_{\parallel}$  is the collisional resistivity.  $\Gamma_{J,r}$  is closely related to the mean magnetic helicity flux. By using quasilinear theory as applied to the drift-kinetic equation, the terms  $\left\langle \tilde{E}_{\parallel} \tilde{n} \right\rangle$  and  $\Gamma_{J,r}$ , which contribute to the generation of the mean magnetic field, are easily shown to be

$$\left\langle \tilde{E}_{\parallel} \tilde{n} \right\rangle = -\frac{\pi T_e}{e} \sum_k \frac{2k_{\perp}^2 \rho_s^2}{2 + k_{\perp}^2 \rho_s^2} \frac{k_{\parallel}}{|k_{\parallel}|} \omega_k^2 f_0(\omega_k/k_{\parallel}) N_k, \quad (3.2.79a)$$

$$\Gamma_{J,r} = \frac{\pi T_e}{\Omega} \sum_k \frac{2k_{\perp}^2 \rho_s^2}{2 + k_{\perp}^2 \rho_s^2} \frac{k_y \omega_k^3}{k_{\parallel} |k_{\parallel}|} f_0(\omega_k/k_{\parallel}) N_k, \quad (3.2.79b)$$

where  $\Omega$  is the time derivative of the zonal field,  $\frac{\partial}{\partial t} \psi_{ZF} = -i\Omega \psi_{ZF}$ ,  $f_0(\omega_k/k_{\parallel})$  is the unperturbed distribution function of plasma particles at the resonant phase velocity,

$v_{\parallel} = \omega_k/k_{\parallel}$ , and  $N_k$  is the action density of the kinetic shear-Alfven wave (i.e., the ratio of the wave energy density divided by the wave frequency) given by;

$$N_k = \frac{2 + k_{\perp}^2 \rho_s^2}{2\omega_k} k_{\perp}^2 \rho_s^2 \left| \frac{e\tilde{\Phi}_k}{T_e} \right|^2. \quad (3.2.80)$$

Note that  $\Gamma_{J,r} \rightarrow 0$  as  $k_{\perp} \rho \rightarrow 0$  (i.e., in the ideal MHD limit). This is a consequence of the fact that, on resonance,  $\Gamma_{J,r} \propto |\tilde{E}_{\parallel}|^2$ , which vanishes for ideal Alfven waves. Thus, zonal field dynamics are explicitly dependent on  $\tilde{E}_{\parallel}$  of the underlying waves. As usual,  $N$  may be thought of as a wave population density. The sensitivity of the weighting factor to finite-gyroradius effects is due to the influence of the dispersion relation  $\omega_k^2 = k_{\parallel}^2 v_A^2 (1 + k_{\perp}^2 \rho_s^2)$  on the phase relation  $\psi/\phi$  for kinetic shear Alfven waves. The modulation of the action density  $N_k$  resulting to the imposition of a seed zonal magnetic field is calculated by the same procedure of §3.2.2. The wave packet evolves according to the wave kinetic equation

$$\frac{\partial}{\partial t} N_k + v_g \cdot \frac{\partial N}{\partial x} - \frac{\partial}{\partial x} \omega_k \cdot \frac{\partial N}{\partial k_x} = C(N), \quad (3.2.81)$$

where  $C(N)$  stands for wave damping. The dispersion relation for the kinetic Alfven wave satisfies

$$\omega_k^2 = k_{\parallel}^2 v_A^2 (1 + k_{\perp}^2 \rho_s^2), \quad (3.2.82a)$$

and the group velocity is given as

$$v_{g,r} = \frac{k_{\parallel}^2 v_A^2}{\omega_k} k_x \rho_s^2. \quad (3.2.82b)$$

(The kinetic shear Alfven wave is a forward-going wave.) Therefore the perturbation in the wave frequency caused by the imposition of the zonal magnetic field  $\delta B_x$  is given by

$$\frac{\delta \omega_k}{\omega_k} = \frac{k_y}{k_{\parallel} B_0} \delta B_x, \quad (3.2.83)$$

where  $B_0$  stands for the unperturbed magnetic field and the relation  $\delta k_{\parallel} = k_y \delta B_x B_0^{-1}$  is used. Note that Eq.(3.2.83) results from a simple modulation of Alfven speed. By use

of this frequency modulation, the modulation of the wave action density  $\delta N_k$  is easily shown to be

$$\delta N_k = \frac{i\omega_k}{\Omega - q_x v_{g,x} + i\gamma_{\text{KSAW}}} \frac{k_y}{k_{\parallel}} \frac{q_x^2}{B_0} \frac{\delta \psi_{\text{ZF}}}{\partial k_x}, \quad (3.2.84)$$

where damping rate  $\gamma_{\text{KSAW}}$  is introduced as  $C(N) = -\gamma_{\text{KSAW}}N$  in Eq.(3.2.81). Substitution of Eq.(3.2.84) into Eq.(3.2.79) gives the response of  $\langle \tilde{E}_{\parallel} \tilde{n}/n \rangle$  and  $\Gamma_{J,r}$ , to the imposition of  $\psi_{\text{ZF}}$ , i.e.,  $\delta \langle \tilde{E}_{\parallel} \tilde{n}/n \rangle$  and  $\delta \Gamma_{J,r}$ . If the forms of  $\delta \langle \tilde{E}_{\parallel} \tilde{n}/n \rangle$  and  $\delta \Gamma_{J,r}$  are substituted into Eq.(3.2.78), a closed equation for  $\psi_{\text{ZF}}$  follows. This equation determines the eigenvalue  $\Omega$ , by which Eq.(3.2.78) is rewritten as

$$\frac{\partial}{\partial t} \psi_{\text{ZF}} = -i\Omega \psi_{\text{ZF}} - \frac{q_r^2 \eta_{\parallel}}{1 + q_r^2 \delta_e^2} \psi_{\text{ZF}}. \quad (3.2.85)$$

The growth rate  $\text{Im } \Omega$  can be re-expressed as [3.54];

$$\text{Im } \Omega = \frac{4\pi c_s^2 \delta_e^2 q_r^2}{v_{\text{th},e} (1 + q_r^2 \delta_e^2)} \sum_k \frac{(1 + k_{\perp}^2 \rho_s^2)^{5/2}}{2 + k_{\perp}^2 \rho_s^2} \frac{k_{\perp}^2 k_y^2}{|k_{\parallel}|} \frac{\partial^2}{\partial k_x^2} \left( \frac{\langle \omega_k N_k \rangle}{\sqrt{1 + k_{\perp}^2 \rho_s^2}} \right) f_0 \quad (3.2.86)$$

This result has a similar structure to the case of zonal flow generation, Eqs.(3.2.50) and (3.2.51) in its dependence on  $q_r^2$ , and on the wave population spectrum (i.e.,  $k_x$ -derivative of  $N_k$ ). It shows that zonal magnetic field instability is driven by a negative slope of  $\langle \omega_k N_k \rangle / \sqrt{1 + k_{\perp}^2 \rho_s^2}$ . This condition is usually satisfied, without inversion of populations for Alfvénic MHD.

As was the case for zonal flow drive by drift waves, the drive of zonal magnetic field is also subject to damping by the collisional resistivity. If the growth rate  $\gamma_{\text{ZF}} = \text{Im } \Omega$  Eq.(3.2.85) exceeds the resistive damping rate,

$$\gamma_{\text{ZF}} > \frac{q_r^2 \eta_{\parallel}}{1 + q_r^2 \delta_e^2} \quad (3.2.87)$$

the zonal magnetic field grows. This driving mechanism of mesoscale magnetic perturbation by microscopic turbulence can have an impact on global MHD instabilities in toroidal plasmas by secondary perturbations, such as neoclassical tearing modes.

### 3.2.7 Comparison with MHD mean field dynamo theory

It is instructive to compare the results for zonal field growth with those of dynamo theory, in MHD, which is another outstanding problem in structure formation in an axial vector field due to turbulence.

In the mean field MHD dynamo theory, the mean magnetic field  $\langle \mathbf{B} \rangle$  and vorticity  $\langle \boldsymbol{\omega} \rangle$  evolve (for incompressible turbulence) according to: [2.58, 2.60, 2.61]

$$\frac{d\langle \mathbf{B} \rangle}{dt} = \nabla \times \langle \tilde{\mathbf{v}} \times \tilde{\mathbf{B}} \rangle + \eta_{\parallel} \nabla^2 \langle \mathbf{B} \rangle \quad (3.2.88a)$$

$$\frac{d\langle \boldsymbol{\omega} \rangle}{dt} = \nabla \times \left\langle \frac{\tilde{\mathbf{B}} \cdot \nabla \tilde{\mathbf{B}}}{4\pi n_i m_i} - \tilde{\mathbf{v}} \cdot \nabla \tilde{\mathbf{v}} \right\rangle, \quad (3.2.88b)$$

where  $\nu$  is a molecular viscosity. The essence of the mean field electrodynamic theory is to approximate the averages of the nonlinear terms, quadratic in fluctuation amplitude, by some effective transport coefficient times a mean field quantity. In many ways this procedure for a closure approximation is quite similar to the familiar case of quasilinear theory, which is a closure of the Vlasov hierarchy. While relatively minor, technical variations abound, most mean field dynamo theories predict

$$\frac{d\langle \mathbf{B} \rangle}{dt} = \nabla \times \left( \alpha \langle \mathbf{B} \rangle - \beta \langle \mathbf{J} \rangle \right) + \eta_{\parallel} \nabla^2 \langle \mathbf{B} \rangle \quad (3.2.88c)$$

$$\frac{d\langle \boldsymbol{\omega} \rangle}{dt} = \nu_{\text{eff}} \nabla^2 \langle \boldsymbol{\omega} \rangle + \nu \nabla^2 \langle \boldsymbol{\omega} \rangle. \quad (3.2.88d)$$

Here  $\alpha$  is the familiar pseudo-scalar, proportional to turbulent helicity, and  $\beta$  and  $\nu_T$  are turbulent resistivity and viscosity, respectively. Note that  $\beta$  is positive but  $\nu_{\text{eff}}$  is *not* positive definite, since it is clear from Eq.(3.2.88b) that turbulence effects on  $\langle \boldsymbol{\omega} \rangle$  must vanish if  $\tilde{\mathbf{v}} = \tilde{\mathbf{B}} / \sqrt{4\pi n_i m_i}$ , i.e., a state of maximal cross helicity. This is identical to the cancellation of the Reynolds and Maxwell stresses which occurs for zonal flow generation by Alfvén waves. Additional contributions to  $\langle \tilde{\mathbf{v}} \times \tilde{\mathbf{B}} \rangle$  and  $\langle \tilde{\mathbf{B}} \cdot \nabla \tilde{\mathbf{B}} / 4\pi n_i m_i - \tilde{\mathbf{v}} \cdot \nabla \tilde{\mathbf{v}} \rangle$  may enter. These correspond to mean vorticity effects on  $\langle \mathbf{B} \rangle$  and mean magnetic field effects on  $\langle \boldsymbol{\omega} \rangle$ , respectively.

An important, relatively recent development in the theory of mean field electrodynamics was motivated by questions of self-consistency and conservation of magnetic helicity. These considerations together suggest that  $\alpha$  should be quenched, as compared to its kinematic value, and that the quench should be proportional to the

magnetic Reynolds number  $R_M$ . While this question is still controversial, both theory and computation suggest that

$$\alpha = \frac{\alpha_{\text{kin}}}{\left(1 + R_M^\sigma \langle V_A \rangle^2 / \langle \tilde{v}^2 \rangle\right)} \quad (3.2.88e)$$

where  $\alpha_{\text{kin}}$  is the kinematic alpha coefficient  $\alpha_{\text{kin}} \simeq \langle \tilde{v} \cdot \tilde{\omega} \rangle \tau_c$ ,  $\tau_c$  is the correlation time and  $\sigma \simeq 1$ . It is useful to note that Eq.(3.2.88e) may be rewritten as

$$\alpha = \frac{\alpha_{\text{kin}} \eta_{\parallel}}{\eta_{\parallel} + \tau_c \langle V_A \rangle^2} \quad (3.2.88f)$$

This expression emphasizes that mean field growth is ultimately tied to *collisional resistivity*, as it is only the latter which breaks the freezing-in of field and fluid in MHD.

### (i) Correspondence of driving terms

Comparing the results of Eq.(3.2.86) with Eq.(3.2.88c), one finds that the physics of zonal field generation in part-(ii) of subsection 3.2.6 has a deep connection to the physics of mean field dynamos. In order to clarify the relation of zonal magnetic field generation, Eqs.(3.2.85) and (3.2.86), to the MHD dynamo problem, Eqs.(3.2.85) and (3.2.86) may be rewritten by the use of  $B_\theta = d\psi_{ZF}/dr$ , so

$$\frac{\partial}{\partial t} B_\theta = -\eta_{ZF} \nabla^2 B_\theta, \quad (3.2.89)$$

where

$$\eta_{ZF} = -\frac{4\pi c_s^2 \delta_e^2}{v_{th,e} (1 + q_r^2 \delta_e^2)} \sum_k \frac{(1 + k_\perp^2 \rho_s^2)^{5/2}}{2 + k_\perp^2 \rho_s^2} \frac{k_\perp^2 k_y}{|k_\parallel|} \frac{\partial^2}{\partial k_x^2} \left( \frac{\langle \omega_k N_k \rangle}{\sqrt{1 + k_\perp^2 \rho_s^2}} \right) f_0 \quad (3.2.90)$$

Here, the collisional resistivity  $\eta_{\parallel}$  is dropped and the  $q_r^2$  in Eq.(3.2.86) is rewritten as  $-\nabla^2$ , noting that the generated field depends only on the radius  $r$ . The sign of  $\eta_{ZF}$  (i.e., corresponding to a *negative resistivity*) is positive for 'normal', i.e., one with  $\partial^2/\partial k_x^2 \left( \langle \omega_k N_k \rangle / \sqrt{1 + k_\perp^2 \rho_s^2} \right) < 0$ , but becomes negative (corresponding to positive dissipation) if  $\partial^2/\partial k_x^2 \left( \langle \omega_k N_k \rangle / \sqrt{1 + k_\perp^2 \rho_s^2} \right) > 0$ , as for a population inversion. If one considers the  $\beta J$  term in Eq.(3.2.88c), the induction equation can be written as

$$\left. \frac{dB}{dt} \right|_{\beta\text{-dynamo}} = \beta \nabla^2 B . \quad (3.2.91)$$

Comparing Eqs.(3.2.89) and (3.2.91), one finds that the electromotive force for zonal field generation corresponds to the  $\beta \mathbf{J}$  -term in the mean field induction equation. The driving takes the form of a coefficient  $\eta_{ZF}$  of *negative* turbulent resistivity. What is interesting is that the sign of the turbulent resistivity varies with the spectrum slope. Thus, the zonal field 'dynamo' is really a process of flux or current coalescence, somewhat akin to the inverse cascade of mean-square magnetic flux predicted for 2D and 3D reduced MHD. This process conserves total magnetic flux, unlike an alpha dynamo, which amplifies magnetic flux via the stretch-twist-fold cycle. Note that there is a clear correspondence between zonal flow and zonal field generation. Zonal field generation is, simply put, related to the inverse cascade of magnetic flux while zonal flow generation is related to the inverse cascade of fluid energy.

The relationship to the drive of zonal flow vorticity is also discussed. The growth of the zonal flow vorticity, e.g., Equations (3.4.21) and (3.4.22), can be written as

$$\frac{\partial}{\partial t} U_q = - D_{\pi} \nabla^2 U_q , \quad (3.2.92a)$$

and

$$D_{\pi} = - \frac{1}{2B^2} \sum_k \frac{k_{\theta}^2 k_r}{(1 + k_{\perp}^2 \rho_s^2)^2} R(q, k) \frac{\partial N_k}{\partial k_r} . \quad (3.2.92b)$$

where  $U_q$  is the vorticity of the zonal flow, and the collisional damping term  $\gamma_{\text{damp}}$  is dropped in order to highlight the turbulent drive term. Comparing Eqs.(3.2.92a) with (3.2.88), we see that the drive of zonal flow vorticity by drift waves corresponds to a turbulent viscosity in mean field MHD (the first term in RHS of Eq.(3.2.88d). As in the case of the magnetic field, the viscosity-like term ( $D_{\pi} \nabla^2 U_q$ ) in Eq.(3.2.92a) has the opposite sign to the usual turbulent viscosity, ala Prandtl. The MHD dynamo theory has also shown that the zonal flow can be driven by the curvature of plasma current, and its possible role in the ITB formation has been discussed [3.55]. A corresponding term in the zonal flow problem will be obtained by retaining the  $\psi_{ZF}$  -term in Eq.(3.2.74) in calculating the evolution of  $\phi_{ZF}$ . This is a subject for future research.

## (ii) Other contrasts

*Meso-scale character:*

The zonal magnetic field and zonal flow both have a meso-scale character. That is, while they can have a coherence length on a mesoscale, i.e., is equal to the system size, in the poloidal and toroidal directions, along the magnetic field, the radial wave length can be really as short as that of the microscopic fluctuations. In MHD dynamo theory, research has concentrated on the large scale dynamo having a characteristic scale length of the system size or at the small scale dynamo, which has a microscopic scale length usually set by the dissipation scale. The problem of the zonal field and zonal flow generation sits in an intermediate regime that connects both of large- and small-scales. However, zonal structures are highly anisotropic.

In addition, the symmetry of the generated field also influences the turbulent driving terms. For instance, the generated zonal magnetic field in §3.2.6 is dependent on only one radial dimension, and the toroidal magnetic field is unchanged. Under such constraints of symmetry, Cowling's theorem guarantees that the  $\alpha$ -dynamo term can not possibly appear.

#### *Collisionless dynamo*

Both zonal magnetic field and zonal flow couple to collisionless dissipation. In the case of zonal fields, collisionless dissipation (i.e., in particular, Landau damping) regulates both magnetic helicity and current transport. This first, genuinely 'collisionless dynamo' theory is notable since Landau resonance is a natural alternative to resistive diffusion for decoupling the magnetic field and plasma, in low-collisionality regimes. Of course, one should also recognize that Landau damping is not a panacea for the problems confronting dynamo theory. For example, here zonal magnetic field growth occurs via the product of the  $|\tilde{E}_{\parallel}|^2$  spectrum and Landau damping, i.e.,  

$$\eta_{ZF} \sim \sum |\tilde{E}_{\parallel}|^2 \delta(\omega - k_{\parallel} V_{\parallel})$$
As a consequence, zonal field growth is limited by the size of  $\tilde{E}_{\parallel}$  (which vanishes in ideal MHD), since coupling of fields to particles enters via the latter. Thus in progressing from MHD to kinetics, one in a sense exchanges the 'freezing-in law' difficulty for the  $\tilde{E}_{\parallel} \sim 0$  difficulty.

#### *Tertiary instability*

As is discussed in Section 3.5, one possible route to zonal flow saturation is via generalized Kelvin-Helmholtz instability of the flow. Such an instability is an example of a tertiary instability, i.e., parasitic instability driven by a secondary instability. Zonal fields can also exhibit tertiary instabilities, since zonal fields correspond to localized current layers, with regions of steep electron temperature gradients, we may speculate that the tertiary instability of the zonal field is similar to a 'micro-tearing mode', and is driven by relaxation of the current and temperature profile of the zonal field. Of course, given the narrow radial extent of the zonal field, such tertiary micro-tearing modes are almost

certainly temperature gradient driven. Note that such instabilities will also produce zonal current filamentation, which may contribute to the seeding of neoclassical tearing modes, as well. More generally, tertiary micro tearing instabilities offer another possible route to dynamo saturation. Of course, just as magnetic shear severely inhibits the generalized Kelvin-Helmholtz instability of zonal flows, it also can be expected to restrict the viability of tertiary micro-tearing. Detailed research on tertiary micro-tearing is necessary to quantitatively address the speculations presented here.

#### *Role of global parameters in turbulent coefficients*

One of the goals of the study of structure formation in turbulent media is to relate the turbulent driving coefficients (e. g.,  $\alpha$ ,  $\beta$ ,  $v_{\text{eff}}$  in MHD turbulence theory, or  $\gamma_{\text{ZF}}$  and  $\chi_{\text{turb}}$  in the problem of zonal flow and drift wave turbulence) to relevant dimensionless parameters characteristic of the system, such as  $\rho/a$ , Rayleigh number, Taylor number, etc. In this direction of research, explicit analytic formulae have been obtained for the problem of zonal flow and drift wave turbulence. This is a significant achievement of the cumulative research effort on turbulence theory. In addition, in this area of research, one can find cross-disciplinary similarities, such as transport suppression by the inhomogeneous  $E \times B$  flow and ' $\alpha$ -suppression' in MHD dynamo theory.

The noticeable difference in the sign of corresponding terms in the zonal flow problem and the dynamo problem may be viewed as originating from the differences in the nature of the turbulence. In the MHD dynamo, turbulent dynamo coefficients are evaluated based on three-dimensional turbulence, since the theory is constructed for a weak magnetic field. On the other hand, the turbulence which is analyzed for the source of zonal flow is quasi-two-dimensional, on account of the strong toroidal field, which is externally imposed. The unification of the dynamo problem and the zonal flow problem is an outstanding key future challenge for turbulence theory.

### **3.3 Shearing and back reaction of flows on turbulence**

In magnetized plasmas, if flow shear exists together with a pressure gradient (a source of turbulence) the flow shear may suppress the turbulence driven by pressure-gradient relaxation. The back reaction, both externally-generated and self-generated shear flow on pressure-gradient-driven turbulence, is a key mechanism that governs the turbulent state and the transport. Of course, flow shear itself may be a source of instability, such as the familiar Kelvin-Helmholtz instability. However, magnetic shear



tends to mitigate or quench velocity-shear-driven instabilities, so they are not of too great a concern to confinement systems.

### 3.3.1 Effect of flow shear on linear stability

The first step in analyzing the back interaction of sheared flow on turbulence is linear stability theory. The linear effect of sheared flow on the pressure-gradient-driven instability has been exhaustively surveyed in literature [2.14]. Indeed, the Richardson problem of shear flow and buoyancy, which leads to the definition of the Richardson number  $R_i \equiv (g/L_n)(dV_y/dx)^{-2}$ , is a classic example of the competition between processes (i.e., density or potential temperature-gradient-driven buoyancy and shearing). (Here the gravity  $g$  is in the direction of density gradient, x-direction.) Readers are recommended to refer to [2.14] for details of the various linear mechanisms. Some key elementary processes are explained here.

One characteristic mechanism for shear suppression is via a deformation of the eigenfunction. The eigenfunction of the least stable mode at thermal convection instability typically has the longest wave length in the direction of the gradient. In the presence of velocity shear, as is shown in Fig.3.3.1, the eigenfunctions are deformed, so that the wave length in the direction of the gradient becomes smaller. As a result of this, the linear growth rate decreases. (In other words, the fundamental mode, which has the largest growth rate, is forced to couple to higher modes, which are much more stable than the fundamental.) The scale for radial transport and mixing is also reduced by this effect. Consideration of the symmetry explains how the stabilizing effect usually appears at second order in velocity shear, i.e.,  $\sim (dV_y/dx)^2$ , so the stabilizing trend does not depend on the sign of  $dV_y/dx$ . This mechanism works for the Rayleigh-Benard instability in neutral fluids [3.56-3.58] and for plasma instabilities driven by pressure, density and temperature inhomogeneities [3.59-3.68]. For non-resonant or hydrodynamic process, stabilization is possible, if the heuristic condition

$$|V'_{E \times B}| \sim \gamma_{L0} \quad (3.3.1)$$

is satisfied, where  $\gamma_{L0}$  is the linear growth rate in the limit of  $V'_{E \times B} = 0$ . It is *very important* to realize that *this is only an approximate criterion*. This order-of-magnitude estimate is consistent with the results of simulations of *linear-dynamics* with sheared flow [2.17, 3.69].

In collisionless plasmas, there are other routes by which velocity shear leads to stabilization. Another type of stabilization mechanism occurs via wave-particle resonance. The ion orbit can be modified by an inhomogeneous electric field, so Landau damping may be enhanced, and very strong ion Landau resonance takes place if the

electric field shear is large enough [3.70]. For instance, ion Landau damping, which is usually a stabilizing effect, enters via the wave-particle resonant denominator  $i/(\omega - k_{\parallel} v_{\parallel})$ , so that wave-ion resonance occurs at  $x_i = \omega / v_{Th} k'_{\parallel}$  ( $k'_{\parallel} = \partial k_{\parallel} / \partial x$ ). In the presence of sheared  $E \times B$  flow, the shear flow Doppler shift renders the resonance equal to  $i/(\omega - k_{\parallel} v_{\parallel} - k_{\theta} x \partial V_{\theta} / \partial x)$ . Here, it is understood that  $\partial V_{\theta} / \partial x$  is expanded about the resonant surface  $r_{mn}$ , i.e.,  $V_{E \times B} = V_{\theta}(r_{mn}) + (r - r_{mn}) \partial V_{\theta} / \partial x + \dots$ , where  $x = (r - r_{mn})$ . The resonant Doppler shift is absorbed into  $\omega$ . Then, with velocity shear, the ion Landau resonance point is shifted to  $x_i = \omega / (v_{Th} k'_{\parallel} + k_{\theta} \partial V_{\theta} / \partial x)$ , so that the resonance is stronger. Thus, electric field shear can significantly enhance the effect of ion Landau damping. Drift reversal of trapped particles due to an inhomogeneous electric field also influences stability. The toroidal drift velocity of trapped ions is modified by a factor  $(1 + 2u_g)$ , where  $u_g = \rho_p v_{th}^{-1} B_p^{-1} (dE_r / dr)$ . If the condition  $u_g < -1/2$  is satisfied, trapped particles drift as if the magnetic curvature were favourable. The trapped-ion mode is thus stabilized by drift reversal in the range of  $u_g < -1$ . Note that this stabilization mechanism is asymmetric with respect to the sign of  $E_r$  [3.71].

If flow shear becomes too strong, KH type instability may occur [3.58]. The evolution from drift instability to K-H instability has been confirmed for drift wave - zonal flow and other plasma systems [3.63].

### 3.3.2 Effect on turbulence amplitude

In the model equation for a passive scalar advected by background fluctuations, the effects of rapidly-changing fluctuations are included in the turbulent transport coefficient, which is a measure of turbulent mixing. The equation of the test field  $\tilde{X}$  in the presence of the sheared flow thus has the form

$$\frac{\partial}{\partial t} \tilde{X} + \bar{V}_y(x) \frac{\partial}{\partial y} \tilde{X} - D \nabla^2 \tilde{X} = \tilde{S}^{\text{ext}} \quad (3.3.2)$$

where  $\bar{V}_y(x)$  is the sheared flow in Fig.3.3.2,  $D$  is the diffusion coefficient due to the small scale fluctuations, and  $\tilde{S}^{\text{ext}}$  represents the source. The stretching of contours of constant test perturbations occurs, and the turbulence level (i.e.,  $\tilde{X}$ ), the cross phase, and the flux are suppressed by  $\partial \bar{V}_y / \partial x$  (i.e.,  $E_r'$  in magnetized plasmas). The mean velocity is in the y-direction (poloidal direction), and is sheared in the x-direction (radial direction). The sheared velocity is expressed as

$$\bar{V}_y = S_v x \quad (3.3.3)$$

in local coordinates. The flow shear is interpreted as  $S_v = r d(E/Br)/dr$  in a cylindrical geometry. The expression for toroidal plasmas has been derived [2.9] and is

$$S_v = \frac{r}{q} \frac{d}{dr} \left( \frac{q E_r}{r B} \right). \quad (3.3.4)$$

**(i) Mean-flow - constant stretching and decorrelation rate**

We first consider the case where the mean flow shear  $S_v$  varies much more slowly than the autocorrelation time of turbulent fluctuations, and varies smoothly in space (i.e., on scales longer than that of the turbulence correlation function). In this case,  $S_v$  may be taken as constant. The influence of the convection term  $\bar{V}_y(x) \frac{\partial}{\partial y}$  in (3.3.2) is treated by using shearing coordinates [3.72]. The Lagrangian time derivative in Eq.(3.3.2) is given as

$$\frac{\partial}{\partial t} + \bar{V}_y(x) \frac{\partial}{\partial y} \rightarrow \frac{\partial}{\partial t} + S_v x \frac{\partial}{\partial y}, \quad (3.3.5)$$

Shearing coordinates annihilate the operator  $(\partial/\partial t + S_v x \partial/\partial y)$  via the transformation

$$k_x \rightarrow k_x^{(0)} + k_y S_v t \quad (3.3.6)$$

where  $k_x^{(0)}$  is defined at  $t = 0$ . Note that shearing coordinates are quite analogous to Roberts and Taylor twisted slicing coordinates, which annihilates the operator  $\mathbf{B} \cdot \nabla$ .

The increase in the perpendicular wave number is also observed in the laboratory frame. After time  $t$ , a circular element is stretched to an ellipse with a major axis of length

$$L_{\parallel} \approx \sqrt{L^2 + (LS_v t)^2} \quad (3.3.7)$$

Since area is preserved by this stretching, the length of the minor axis is given by

$$L_{\perp} = \frac{L}{\sqrt{1 + S_v^2 t^2}} \quad (3.3.8)$$

The reduction in  $L_{\perp}$  is equivalent to the growth of the perpendicular wave number, so that the characteristic perpendicular wave number for the test field  $\tilde{X}$  is effectively enhanced by a factor  $(1 + S_v^2 t^2)$  [2.7, 3.73-3.75],

$$k_{\perp \text{eff}}^2 = k_{\perp}^2 (1 + S_v^2 t^2) . \quad (3.3.9)$$

Again, this is quite analogous to the familiar expression for  $k_{\perp}^2$  of ballooning modes, i.e.,

$$k_{\perp}^2 = k_{\theta}^2 (1 + s^2 (\theta - \theta_0)^2) .$$

Time-asymptotically, then

$$k_{\perp \text{eff}} \propto k_{\perp} S_v t . \quad (3.3.11)$$

The change of the wave number is linear in time, i.e., *ballistic*.

The diffusivity  $D$  implies a random walk due to the background fluctuations. The influence of the shear flow on diffusivity will be discussed in §3.6. One simple, direct method to determine the relevant time scales is to analyze the random motion in shearing coordinates. The correlation time  $\tau_{\text{cor}}$  in the presence of random motion but in the absence of shear is

$$\frac{1}{\tau_{\text{cor}}} = k_{\perp}^2 D \quad (3.3.12)$$

The wavenumber increases in time so that the correlation time becomes shorter in the presence of the shear flow, since  $k_{\perp}$  is stretched, as shown in Eq.(3.3.9). Equation (3.3.11) holds for long times, if  $k_{\perp} S_v t > 1$ . Then the effective correlation time is just

$$\frac{1}{\tau_{\text{cor, eff}}} = D k_{\perp}^{(0)2} (1 + S_v^2 \tau_{\text{cor, eff}}^2) \quad (3.3.13)$$

Thus, if  $S_v \tau_{\text{cor, eff}} > 1$ ,

$$\frac{1}{\tau_{\text{cor, eff}}} = k_{\perp}^{(0)2/3} D^{1/3} S_v^{2/3} \quad (3.3.14)$$

which is the enhanced decorrelation rate, resulting from the coupling of shearing and turbulent decorrelation. This result is similar to Dupree 1966 and Hirshman-Molvig 1979 [3.76], all of which involve decorrelation via scattering of action coupled to differentially rotating phase space flow. If  $S_v \tau_{\text{cor, eff}} < 1$ ,

$$\frac{1}{\tau_{\text{cor, eff}}} = k_{\perp}^{(0)2} D \left( 1 + S_v^2 \tau_{\text{cor}}^{(0)2} + \dots \right), \quad (3.3.15)$$

which recovers the shear-free result. Note that the hybrid decorrelation due to the shear flow is effective if  $S_v$  reaches the level  $Dk_{\perp 0}^2$ . For a constant  $D$ , the relation

$$S_v \geq Dk_{\perp 0}^2 \quad (3.3.16)$$

indicates when decorrelation by shear flow is more effective.

The reduction of the correlation length leads to suppression of the fluctuation amplitude of the test field  $\tilde{X}$ , as

$$\langle \tilde{X}^2 \rangle \approx \frac{1}{1 + S_v^2 \tau_{\text{cor}}^2} \langle \tilde{X}^2 \rangle_{\text{ref}} = \frac{1}{1 + S_v^2 \tau_{\text{cor}}^2} \tau_{\text{cor}}^{(0)} \lim_{\ell \rightarrow 0} \mathcal{J}^{\text{ext}}(\ell) \quad (3.3.17)$$

assuming that the magnitude of the source term  $\lim_{\ell \rightarrow 0} \mathcal{J}^{\text{ext}}(\ell)$  is unaffected.

## (ii) Random stretching and decorrelation rate

In the presence of zonal flows or the GAMs, the shearing velocity is *not* constant in time. Moreover, even a slowly-varying ensemble of zonal flow modes can result in drift-wave-ray chaos due to overlap of  $\Omega = q_r V_g$  resonances, thus validating the assumption of stochastic dynamics. As an analytic idealization then, we take  $S_v$  as a stochastic variable

$$\langle S_v \rangle = 0, \quad (3.3.18)$$

where  $\langle S_v \rangle$  is a long-time average of  $S_v$ ,  $\langle \dots \rangle = \lim_{t \rightarrow \infty} \frac{1}{t} \int_0^t dt \dots$ . We write

$$S_v = \gamma_v \sqrt{\tau_{\text{ac}}} w(t), \quad (3.3.19)$$

where  $\gamma_v$  denotes the instantaneous magnitude of the zonal flow shear,  $w(t)$  is the temporal coherence function and  $\tau_{\text{ac}}$  is the autocorrelation time of the (random) zonal flow. Obviously  $w(t)$  is constant for  $t < \tau_{\text{ac}}$  and fluctuates drastically for  $t > \tau_{\text{ac}}$ .

The stretching of an eddy in the y-direction is now a stochastic process. Therefore  $\left\langle \int_0^t S_v dt \right\rangle$  vanishes, but its mean square linearly increases in time, so

$$\lim_{t \rightarrow \infty} \frac{1}{t} \int_0^t dt \left( \int_0^t S_v dt' \right)^2 = \gamma_v^2 \tau_{ac} t . \quad (3.3.20)$$

The stretching process is now diffusive. The length of the axis of stretching is

$$L_t^2 \approx L^2 + L^2 \left( \int_0^t S_v dt' \right)^2 \quad (3.3.21)$$

and is stochastic. Its statistical average is given by

$$\langle L_t^2 \rangle \approx L^2 + L^2 \gamma_v^2 \tau_{ac} t , \quad (3.3.22a)$$

or

$$\langle k_{\perp}^2 \rangle = k_{\perp}^{(0)2} + D(K) t , \text{ where } D(K) = k_{\perp}^{(0)2} \gamma_v^2 \tau_{ac} . \quad (3.3.22b)$$

A similar argument as in the previous subsection applies to this diffusive shearing case. We have an equation for the decorrelation rate in the presence of the stochastic shear flow as

$$\frac{1}{\tau_{cor}} = D k_{\perp}^{(0)2} (1 + \gamma_v^2 \tau_{ac} t) , \quad (3.3.23a)$$

and

$$\frac{1}{\tau_{cor}} \approx D k_{\perp}^{(0)2} \gamma_v^2 \tau_{ac} t \quad (3.3.23b)$$

for long times. Thus, if  $\tau_{cor} > \gamma_v^{-2} \tau_{ac}^{-1}$ , we have

$$\frac{1}{\tau_{cor}} \approx \left( D k_{\perp}^{(0)2} \gamma_v^2 \tau_{ac} \right)^{1/2} . \quad (3.3.24)$$

Note that this is a 'doubly-diffusive' hybrid decorrelation rate, combining a random walk in radius with one in  $k_r$ . If, on the other hand,  $\tau_{cor} < \gamma_v^{-2} \tau_{ac}^{-1}$

$$\frac{1}{\tau_{cor}} \approx D k_{\perp}^{(0)2} \quad (3.3.25)$$

as usual. It is important to note here that  $\tau_{ac}$ , the autocorrelation time of the pattern of zonal flow shears that a drift wave packet actually sees, is given by  $\min \left\{ \Delta\Omega, \Delta q_r v_g(k) \right\}$ . Thus, the strength of zonal flow induced shear decorrelation is sensitive to the structure of the zonal flow spectrum.

### (iii) Stochastic Doppler shift

There might be a case in which the radial wave length of the GAM is much longer than the wave length of the test mode, while the flow changes in time very rapidly. In such a case, in addition to the flow shear (as is discussed in (ii), in this subsection), the stochastic Doppler shift is also effective in reducing the turbulence level [2.14, 3.77, 3.78].

In the forced stochastic oscillator equation (3.3.1), the Doppler shift term is given by the random Doppler shift,

$$\frac{d}{dt} \tilde{X}_k + i\tilde{\omega}_k \tilde{X}_k - D_k \nabla^2 \tilde{X}_k = \tilde{S}_k^{\text{ext}}. \quad (3.3.26)$$

The impact of stochastic frequency shift is characterized by the parameter

$$\Gamma_l = \tau_{ac,l} \langle \tilde{\omega}_k^2 \rangle \quad (3.3.27)$$

where  $\tau_{ac,l}$  is the autocorrelation time of the longer wavelength fluctuations  $\tilde{v}_l$ . The statistical property of the response function of equation (3.3.26)

$$G(t; t') = \exp \left( - \int_{t'}^t d\tau (i\tilde{\omega}_k + \Gamma_s) \right) \quad (3.3.28)$$

has been studied when the correlation  $\langle \tilde{\omega}_k(t) \tilde{\omega}_k(0) \rangle$  decays as [3.79]

$$\langle \tilde{\omega}_k(t) \tilde{\omega}_k(0) \rangle = \langle \tilde{\omega}_k^2 \rangle \exp \left( - t/\tau_{ac,l} \right). \quad (3.3.29)$$

In the opposite limit, i.e., the limit of rapidly changing background fluctuations,

$$\tau_{ac,l} \ll \tau_{cor}, \quad (3.3.30)$$

one obtains

$$\langle G(t; 0)G(t'; 0) \rangle = \exp \left( -2(\Gamma_l + \tau_{\text{cor}}^{-1})|t - t'| \right). \quad (3.3.31)$$

The decorrelation of the test field occurs with the rate of  $\tau_{\text{cor}}^{-1} + \Gamma_l$ . The statistical average of the fluctuating field  $\tilde{X}$  is calculated. One finds that the fluctuation level is suppressed by the stochastic Doppler shift, due to the longer wavelength fluctuations, by the factor of

$$\frac{1}{1 + \tau_D \Gamma_l} = \frac{1}{1 + \tau_D \tau_{\text{ac}, l} \langle \tilde{\omega}_k^2 \rangle} \quad (\text{for } \tau_{\text{ac}, l} \ll \tau_D) \quad (3.3.32)$$

assuming that the source  $\lim_{\ell \rightarrow 0} \mathcal{J}^{\text{ext}}(\ell)$  is unchanged.

In the large amplitude limit of random oscillation (or long correlation time  $\tau_{\text{ac}, l}$ ),

$$\tau_{\text{ac}, l}^2 \langle \tilde{\omega}_k^2 \rangle > 1, \quad (3.3.33)$$

the Gaussian response is given by

$$\langle G(t; 0)G(t'; 0) \rangle \propto \exp \left( -2\langle \tilde{\omega}_k^2 \rangle (t - t')^2 \right). \quad (3.3.34)$$

Equation (3.3.34), when compared to equation (3.3.31), is called motional narrowing. This results in

$$J \sim \sqrt{\frac{\pi}{2}} \frac{1}{\sqrt{\langle \tilde{\omega}_k^2 \rangle}} \lim_{\ell \rightarrow 0} \mathcal{J}^{\text{ext}}(\ell) \quad (3.3.35)$$

A reduction by the factor  $1 / \tau_{\text{cor}} \sqrt{\langle \tilde{\omega}_k^2 \rangle}$  is obtained.

### 3.3.3 Symmetry between zonal flow drive and turbulence suppression

After overviewing the back-interaction of flows on turbulence, we now visit the issue of symmetry between zonal flow drive and turbulence suppression.

When the drift waves are stochastic in time, the random stretching induces diffusion of drift wave fluctuations in  $k_r$  space. One then has

$$\frac{\partial}{\partial t} \langle N_k \rangle - \frac{\partial}{\partial k_r} D(k) \frac{\partial}{\partial k_r} \langle N_k \rangle = \gamma_L \langle N_k \rangle - \Delta \omega_k \langle N_k \rangle^2 \quad (3.3.36)$$

where the  $k$ -space diffusion coefficient in Eq.(3.3.22b) is written as



$$D(k) = k_{\theta}^{(0)^2} q_x^2 \mathcal{V}_{ZF}^2 \tau_{ac} . \quad (3.3.37)$$

In this expression, an oscillating shear is rewritten in terms of the zonal flow velocity as

$$\gamma_V^2 = \sum_{q_x} q_x^2 \mathcal{V}_{ZF}^2 . \quad (3.3.38)$$

The terms on the right-hand-side of Eq.(3.3.36) denote the linear growth and nonlinear damping of turbulence by like-scale interaction. The effect of  $k$ -space diffusion on the evolution of drift wave energy,  $W_{\text{drift}} = \sum_k \omega_k \langle N_k \rangle$ , is thus given as

$$\frac{\partial}{\partial t} \sum_k \omega_k \langle N_k \rangle = - \sum_k \frac{\partial \omega_k}{\partial k_r} D(k) \frac{\partial}{\partial k_r} \langle N_k \rangle + \sum_k \left( \gamma_L \langle N_k \rangle - \Delta \omega_k \langle N_k \rangle^2 \right) . \quad (3.3.39)$$

The second term, i.e., the contribution of the zonal flows, is given as

$$\frac{\partial}{\partial t} W_{\text{drift}} \Big|_{ZF} = - \sum_{q_x} \sum_k \frac{\partial \omega_k}{\partial k_r} k_{\theta}^{(0)^2} \tau_{ac} \frac{\partial}{\partial k_r} \langle N_k \rangle q_x^2 \mathcal{V}_{ZF, q_x}^2 . \quad (3.3.40)$$

This term may be written as

$$\frac{\partial}{\partial t} W_{\text{drift}} \Big|_Z = - \sum_{q_x} D_{rr, q_x} q_x^2 \mathcal{V}_{ZF, q_x}^2 , \quad (3.3.41)$$

where

$$D_{rr} = \sum_k \frac{\partial \omega_k}{\partial k_r} k_{\theta}^{(0)^2} \tau_{ac} \frac{\partial}{\partial k_r} \langle N_k \rangle . \quad (3.3.42)$$

Note that  $\tau_{ac}$  of Eq.(3.3.42) is really an estimate of the response function  $R(K, \Omega)$  in the propagator:

$$R(K, \Omega) = \tau_{ac} . \quad (3.3.43)$$

The kinetic energy of the zonal flow  $W_{ZF} = \sum_{q_x} \mathcal{V}_{ZF, q_x}^2$  increases, within the framework of quasilinear theory, at the expense of the zonal flow, i.e.,

$$\left. \frac{\partial}{\partial t} W_{ZF} \right|_{\text{drift}} = \sum_{q, \alpha} D_{rr, q, \alpha} q_x^2 \tilde{V}_{ZF, q, \alpha}^2. \quad (3.3.44)$$

This proves

$$\left. \frac{\partial}{\partial t} W_{\text{drift}} \right|_{ZF} = - \left. \frac{\partial}{\partial t} W_{ZF} \right|_{\text{drift}} \quad (3.3.45)$$

From these considerations, we see that symmetry between the coefficient  $\alpha$  in Eqs.(2.10a) and (2.10b) comes from the conservation of energy in the coupling between the drift wave fluctuations and zonal flow. The suppression of drift wave fluctuations by the shear associated with the zonal flow can be alternatively described as an energy transfer from drift wave fluctuations to zonal flow fluctuations. This relation holds for the case where the quasilinear theory for  $N$  is applicable.

### 3.3.4 Poloidal Asymmetry

While we focus almost exclusively on zonal flows which are symmetric in both the toroidal and poloidal directions in this review article, sometimes it is necessary to take into account a weak poloidal variation of zonal flows, or a poloidally-varying large-scale convective cell, when we study the shearing of smaller turbulence eddies by larger coherent structures. The examples include:

- (i) Strong-toroidal-rotation-induced centrifugal force can introduce the poloidal-angle dependence of the electrostatic potential associated with the mean  $\mathbf{E} \times \mathbf{B}$  flow. [3.80, 3.81]
- (ii) Shearing of smaller-scale eddies by larger-scale convective cells ( $n \sim m \sim O(1)$ ) including a side band of zonal flows such as  $\phi_{n=0, m=1}$ , etc.
- (iii) Shearing of smaller scale turbulence (originating from high- $k$  instabilities) by larger scale turbulence (originating from low- $k$  instabilities); for instance, shearing of ETG or CDBM turbulence by ITG-TIM (trapped ion mode) turbulence. (A more detailed discussion is made in §3.4.6.)
- (iv) Poloidally inhomogeneous toroidal flow induced by pressure anisotropy. [3.82]

The steep poloidal variation, rather than radial change, is associated with the streamer, (which is beyond the scope of this review), briefly discussed in §6. For these situations,

one could construct a model problem of shearing by considering an electrostatic potential  $\phi(r, \theta)$  which varies in both radius and poloidal angle. Then the two-point correlation function evolution is not only governed by the usual ambient turbulence-induced diffusion and the radial shear of the poloidal  $E \times B$  flow, but also by the poloidal shear of the radial  $E \times B$  flow, as well as the radial shear and the poloidal shear of the radial  $E \times B$  flow.[3.83] These quantities in the order of appearance are:

$$\omega_{E, rr} = -\frac{\partial^2}{\partial r^2} \phi(r, \theta) \quad (3.3.46a)$$

$$\omega_{E, \theta r} = -\frac{1}{r} \frac{\partial^2}{\partial \theta \partial r} \phi(r, \theta) \quad (3.3.46b)$$

$$\omega_{E, r\theta} = -\frac{\partial^2}{\partial r \partial \theta} \phi(r, \theta) \quad (3.3.46c)$$

$$\omega_{E, \theta\theta} = -\frac{1}{qr^2} \frac{\partial^2}{\partial \theta^2} \phi(r, \theta) \quad (3.3.46d)$$

where  $q$  is the safety factor. These illustrate the "tensor" nature of the shearing  $\omega_E$  by convective cells. From these generalizations, the standard theories of shearing, addressing the reduction of the radial correlation length, can be extended to study the deformations of eddies in every direction [3.83] including the change in the correlation length in the direction parallel to the magnetic field.[3.82]

Following a procedure in [2.7], the two-point correlation evolution equation has been derived in general toroidal geometry [3.83]

$$\begin{aligned} \frac{d}{dt} C_{12} + \left\{ \left( \psi_- \omega_{E, \psi\psi} + \eta_- \omega_{E, \theta\psi} \right) \frac{\partial}{\partial \zeta_-} + \left( \psi_- \omega_{E, \psi\theta} + \eta_- \omega_{E, \theta\theta} \right) \frac{\partial}{\partial \psi_-} - D_{eff} \frac{\partial^2}{\partial \zeta_-^2} \right\} C_{12} \\ = S_2 \end{aligned} \quad (3.3.47)$$

Here,  $C_{12} = \langle \delta H(1) \delta H(2) \rangle$  is a correlation function of fluctuating quantity  $\delta H$ , and  $D_{eff}$  is the ambient turbulence-induced relative diffusion of two nearby points:  $(\psi_1, \eta_1, \zeta_1)$  and  $(\psi_2, \eta_2, \zeta_2)$  in flux coordinates. Other notations follow those of [3.83]. In contrast to the usual case of a flux function  $\phi(r)$ , where only the radial shear of the  $E \times B$  angular frequency, mainly in the poloidal direction,  $\omega_{E, \psi\psi} = -\partial^2 \phi / \partial \psi^2 = \partial(E_r / RB_\theta) / \partial \psi$  appears in the two point correlation evolution, (3.3.47) describes the "tensor" character of the shearing process when  $\phi$  is a function of both  $\psi$  and  $\theta$ .

$\omega_{E, \alpha\beta}$  with subscripts  $\psi$  and  $\theta$  for  $\alpha, \beta$  is a natural flux coordinate generalization of Eq.(3.3.46). By taking the moments and following the standard procedure of calculating the exponentiation rate of two nearby points, one can derive that the shape of turbulent eddies are distorted due to the various components of the shear tensor in the following way [3.83]:

$$\Delta r^2 = \Delta r_0^2 \left( 1 + \frac{\omega_E^2}{\Delta\omega_k (\Delta\omega_k + \omega_{E, \psi\theta})} \right)^{-1} \quad (3.3.48a)$$

and

$$\Delta \eta^2 = \Delta \eta_0^2 \left( 1 + \frac{\left( \frac{\Delta \eta_0}{\Delta \zeta_0} \right)^2 \omega_{E, \theta\psi}^2}{\Delta\omega_k (\Delta\omega_k + \omega_{E, \psi\theta})} \right)^{-1} \quad (3.3.48b)$$

where  $\Delta\omega_k$  is the decorrelation rate of ambient turbulence and

$\omega_E = - \left( \Delta\psi_0 / \Delta\zeta_0 \right) \left( \partial^2 \phi / \partial \psi^2 \right)$  is the  $\mathbf{E} \times \mathbf{B}$  shearing rate in general toroidal geometry.

Note that Eq.(3.3.48b) shows the reduction in parallel correlation length due to poloidal asymmetry which has been independently found in [3.82]. The tensor character of the shearing process has been also recognized in the problem of the shearing of small ETG eddies by larger ITG eddies, which is discussed in §3.4.6.

Unlike decorrelation via the shear in  $\mathbf{E} \times \mathbf{B}$  zonal flow, it can be shown that from a symmetry argument on the two point-correlation function that there is no net decorrelation mechanism due to the flow curvature associated with the second radial derivative of the zonal flow [3.84].

### 3.4 Nonlinear Damping and Saturation: Low Collisionality Regimes

In this section, nonlinear mechanisms which limit or saturate the growth of zonal flows are described. Research in this direction has been particularly stimulated by the challenge of understanding how zonal flow growth is controlled in low or zero collisionality regimes, for which the energy density of zonal flows can substantially exceed the energy density of drift waves, i.e.,  $|\tilde{V}_{ZF}^2| \gg \int \omega_k N_k dk$ . Several possibilities exist, including:

- a) tertiary instability - i.e., a secondary instability of the zonal flow (itself a product of the secondary instability), rather like the familiar Kelvin-Helmholtz (KH) instability of a sheared flow. Such a tertiary KH instability will *return* energy to the  $m \neq 0$  fluctuations, thus limiting zonal flow growth.
- b) nonlinear wave packet scattering - i.e., a process by which a drift wave packet undergoes multiple nonlinear interactions with the zonal flow, thereby exchanging energy with, and thus regulating the growth of the zonal flows. Such scattering processes are quite similar to nonlinear wave-particle interaction, familiar from weak turbulence theory. This process also returns energy to  $m \neq 0$  fluctuations.
- c) nonlinear wave packet trapping - i.e., the process by which modulational instability is saturated due to deflection of drift wave trajectories by finite amplitude zonal flows. This process is analogous to the trapping of particles by a finite amplitude waves in a Vlasov plasma, and acts to nonlinearly quench the zonal flow growth process by terminating the *input of energy* to the zonal flow.
- d) adjustment of system dynamics - i.e., an 'umbrella label' under which the various routes by which the system evolves toward a stationary state via adjustment of the global dynamics may be collectively described. Examples include the possibility of either multi-dimensional (i.e., repetitive bursts or limit cycle) or strange (i.e., chaotic) attractors, in contrast to the naively expected fixed point. Another possibility is adjustment (via predator-prey dynamics) to exploit available, albeit weak, dissipation. Generally, mechanisms in (d) work in synergy with mechanisms in (a)-(c).

sub-section	key concept	Degrees of freedom		correlation time		coherent structure	next sub-section
		<i>drift wave</i>	<i>zonal flow</i>	<i>drift wave</i>	<i>zonal flow</i>		
3.4.1	tertiary inst.	-	1	long	long	-	-
3.4.2	dithering	small	1	long	long	dynamics	3.5.2
3.4.4	diffusion model	large	large	short	short	no	3.5.3
3.4.5	predator-prey model						3.5.1
3.4.6	wave trapping	large	large	long	long	yes	3.5.4
3.4.7	collisionless satu.	large	large	short	long	yes	3.5.5

### 3.4.1 Tertiary instability

One mechanism for nonlinear saturation of zonal flows is turbulent viscous damping of the flow, originating either from background drift wave turbulence, or from instability of the zonal flow. As the zonal flow is itself the product of a 'secondary' instability in the ensemble of 'primary' drift waves, instability of the zonal flow is called *tertiary* instability [3.85]. These tertiary instabilities of the flow may be thought of as generalized Kelvin-Helmholtz (GKH) instabilities, which relax the profile of generalized potential vorticity and so mix and transport zonal flow momentum, thus damping the flow. Interest in GKH instabilities was sparked by consideration of the so-called Dimits shift regime, where the overwhelming preponderance of available free energy is channeled into zonal flows (i.e.,  $E_{ZF}/E_{DW} = \gamma_L/\gamma_{damp}$ ), in turn naturally raising the question of what sort of consideration of stability will *ultimately limit* zonal flow shears. Of course, proximity to, or exceedence of, the GKH stability boundary results in the onset of momentum transport and turbulent viscosity.

The actual GKH is driven by both  $\mathbf{E} \times \mathbf{B}$  velocity and ion temperature gradients, since both enter the total potential vorticity  $\nabla^2(\phi + \tau T_e/2)$  (where  $\tau = T_e/T_i$ ). However, it is instructive to first consider the simpler limit of  $\tau \rightarrow 0$ . In that case, flute-like ( $k_{\parallel} \rightarrow 0$ ) modes with low but finite  $m$  (i.e.,  $m \neq 0$ ) evolve according to

$$\left(\frac{\partial}{\partial t} + V_{ZF} \cdot \nabla\right) \nabla^2 \phi_{KH} + V_{KH} \cdot \nabla \nabla^2 \phi_{ZF} = \left(\frac{\partial^2}{\partial x^2} - \frac{\partial^2}{\partial y^2}\right) \langle \varphi_x \varphi_y \rangle + \frac{1}{2} \frac{\partial^2}{\partial x \partial y} \left( \langle \varphi_y^2 \rangle - \langle \varphi_x^2 \rangle \right) \quad (3.4.1)$$

Here the LHS describes the linear growth of the KH instabilities and the RHS represents drive by drift wave stresses. Equation (3.4.1) thus states that  $m \neq 0$  GKH fluctuations (which transport and mix zonal flow momentum) can be excited *either* by instability of the zonal flow *or* by drift wave Reynolds stress. This suggests that, in contrast to the hierarchical scenario (Fig.3.4.1(a)) of primary  $\rightarrow$  secondary  $\rightarrow$  tertiary instability described above, the process for generation of  $m \neq 0$  modes may be non-hierarchical (Fig.3.4.1(b)), whereby low but non-zero  $m$  modes are generated *both* by KH instability of the zonal flow *and* by modulational instability of the drift wave spectrum. Here, we focus primarily on the hierarchical scenario and its implications. The direct drive by drift waves is briefly discussed in Chap.6. The relative importance of the hierarchical and non-hierarchical scenarios is a topic of on-going research. An existing result indicates that the modulational drive of  $m \neq 0$  modes results in momentum transport significantly in excess of the KH driven transport, but further research into this question is necessary before reaching a definitive conclusion.

Regarding KH instabilities, it is instructive to start by considering a simple case with zonal potential  $\phi_{ZF} = \bar{\phi} \cos(q_x x)$ , perturbed by a KH perturbation

$$\phi_{KH} = \sum_n \hat{\phi}_n \cos(nq_x x + q_y y) \quad (3.4.2)$$

( $q_x$  is the wave number of the zonal flow, and  $q_y$  is the poloidal wavenumber of the KH instability.) The perturbation is easily shown to grow at the rate

$$\gamma_{KH}^2 = \bar{\phi}^2 q_x^2 q_y^2 \left( \frac{q_x^2 - q_y^2}{q_x^2 + q_y^2} \right). \quad (3.4.3a)$$

Thus,  $\gamma_{KH} > 0$  requires  $q_x^2 > q_y^2$ , i.e., *the poloidal wavelength of the KH mode must exceed the radial scale of the zonal flow*. This of course favors long-wavelength instability. For  $q_y^2 \ll q_x^2$ , note that  $\gamma_{KH}$  reduces to

$$\gamma_{KH} \sim |q_y V_{ZF}|. \quad (3.4.3b)$$

Note that  $\gamma_{KH}$  scales with  $V_{ZF}$ , not with  $dV_{ZF}/dx$ . [3.41, 3.86]

Of course, the example discussed above is over-simplified, as it omits magnetic shear, electron dissipation, and many other effects. In particular, magnetic shear is quite strongly stabilizing, as it works against the interchange of vorticities at an inflection point, which is the basic mechanism of the KH and the elementary process which underlies the well-known Rayleigh inflection-point criterion. Figure 3.4.2 illustrates the basic effect - in a sheared magnetic field, the changing local angle of tilt of magnetic field lines requires that vortex tubes rotate upon interchange. This imposes an energy penalty for the interchange process, thus tending to stabilize the KH. The strong sensitivity of the KH to magnetic shear is nicely illustrated later in Chapter 4. (The figure 4.18 of Chap.4 shows the disruption of the zonal flow pattern in the regimes of weak magnetic shear and its persistence in regions of strong magnetic shear [2.52].) In order to examine the effect of shear on tertiary KH modes, the energy transfer budget and zonal flow pattern of a shearless and sheared system were compared in [3.87]. In the shear-free system, transfers of energy from zonal flows to drift waves occurred, and disruption of the zonal flow pattern was evident in the flow visualizations. In the sheared system, no back-transfer of energy occurred and the flow pattern persisted.

In the plasma of interest,  $\tau \neq 0$ , so the generalized potential vorticity is  $\nabla^2(\Phi)$ , where  $\Phi \equiv \phi + \tau T/2$ . The system is described by the equations

$$\frac{\partial}{\partial t} \nabla^2 \Phi + [\Phi, \nabla^2 \Phi] = \frac{\tau^2}{4} [T, \nabla^2 T] \quad (3.4.4a)$$

$$\frac{\partial}{\partial t} T + [\Phi, T] = 0 \quad (3.4.4b)$$

Here  $[g, h]$  is the Poisson bracket. Note that, to the lowest order in  $\tau$ , this system corresponds to a statement of conservation of potential vorticity in flows with generalized velocity  $\mathbf{V} = \nabla \Phi \times \hat{\mathbf{z}}$ . Here, the temperature gradient, as well as  $\mathbf{E} \times \mathbf{B}$  shear, can drive instability. A similar analysis as before gives

$$\gamma_{KH}^2 = \frac{1}{2} \left( \bar{\Phi} + \frac{\tau}{2} \bar{T} \right)^2 q_x^2 q_y^2 \left( \frac{q_x^2 - q_y^2}{q_x^2 + q_y^2} \right). \quad (3.4.5)$$

Note that the *phase* between the zonal potential and zonal temperature is *crucial* to the result. This phase is determined by several factors, including the zonal flow generation mechanism (i.e., which sets the ratio of growth for  $\bar{\Phi}$  and  $\bar{T}$ ) and the Rosenbluth-Hinton damping mechanism (i.e., which suggests that certain values of phase damp more rapidly than others). While one study suggests a good correlation between the stability boundary for GKH and the termination of the Dimits shift regime (see, e.g., Fig.4.16 in Chapter 4 [3.88]), the parameter space for this problem has not been systematically explored so the "bottom line" remains controversial. Moreover, other linear stability studies which retain ion Landau damping suggest that even for steep  $\partial T / \partial x$ , tertiary instability growth is very weak and the scale of mixing is quite small. [3.89] Thus, tertiary instability and its effect on zonal flow saturation remain open problems, where further study is needed.

With the as-yet-inconclusive findings described above in mind, it is interesting to note that another, related, route to exciting momentum transport and the back-transfer of energy from zonal flows to waves exists and has not been explored. This mechanism exploits the situation that GKH modes, while not strongly unstable, are not heavily damped either, and the fact that noise emission from primary drift waves is abundant. Thus, one has a situation of noise emission into slow modes, sitting close to criticality, so that large transport can occur *without* linear instability. Moreover, the effective noise bath will be enhanced by self-consistent inclusion of the GKH effect. Finally, noise emission can also produce localized defects in the flow, which in turn drive small scale relaxation and momentum transport.

### 3.4.2 Model of small plane waves

As is explained in §3.2.2, dynamics of a plane drift wave explain the zonal flow growth if the decorrelation rate of drift waves  $\gamma_{\text{drift}}$  is very small. One nonlinear



mechanism is the back-interaction of excited secondary waves (zonal flow and side-band drift waves) on the primary drift waves. Within this framework, one can construct a model composed of three drift waves and one zonal flow. The example of toroidal drift waves of §3.2.2 is explained.

The quasi-linear effects of the secondary waves on the primary drift wave are given by [2.23]

$$\left(\frac{\partial}{\partial t} - \gamma_L\right) \left\langle \left(\frac{e\Phi_0}{T}\right)^2 \right\rangle = -\frac{T}{eB} \frac{k_{\theta} q_r}{\partial D / \partial \omega_0} \left( \frac{\Phi_{-}(\xi)}{\Phi_0(\xi)} \Phi_{ZF} + \frac{\Phi_{+}(\xi)}{\Phi_0(\xi)} \Phi_{ZF}^{*} \right) \quad (3.4.6)$$

where  $\gamma_L$  is the linear growth rate of the primary mode, representing the energy source. (See §3.2.1(ii) for definition of variables.) Replacing variables from a set of  $\{\Phi_0(\xi), \Phi_{ZF}, \Phi_{+}(\xi) \text{ and } \Phi_{-}(\xi)\}$  to  $[P, Z, S \text{ and } \Psi]$  which are defined as

$$P = \left\langle \left(\frac{e\Phi_0}{T}\right)^2 \right\rangle, Z = \Phi_{ZF} \text{ and } \frac{\Phi_{+}(\xi)}{\Phi_0(\xi)} = S \exp(i\Psi) \quad (3.4.7)$$

with suitable normalizations, a closed set of equations results. These are:

$$\frac{dP}{d\tau} = P - 2 Z S \cos(\Psi) \quad (3.4.8)$$

$$\frac{dZ}{d\tau} = -\frac{\gamma_{\text{damp}}}{\gamma_L} Z + 2 P S \cos(\Psi) \quad (3.4.9)$$

$$\frac{dS}{d\tau} = -\frac{\gamma_{\text{side}}}{\gamma_L} S + Z P \cos(\Psi) \quad (3.4.10)$$

$$\frac{d\Psi}{d\tau} = \frac{(\omega_0 - \Omega_{+})}{\gamma_L} - \frac{Z P}{S} \sin(\Psi) \quad (3.4.11)$$

where the normalized time is  $\tau = \gamma_L t$ ,  $\gamma_{\text{damp}}$  is the collisional damping rate of the zonal flow,  $\gamma_{\text{side}}$  is the side-band damping rate, and  $\omega_0 - \Omega_{+}$  is the frequency mismatch of the side-band and primary mode.

Equations (3.4.9)-(3.4.11) describe the parametric excitation for a fixed pump amplitude. The coupling to the primary wave, Eq.(3.4.8), describes the nonlinear stabilizing effect of the driven zonal flow on the growth rate of the zonal flow  $\gamma_{ZF}$ .

### 3.4.3 Nonlinear coupled equation for a large number of drift waves

If the number of excited drift wave modes are very small, so that the drift wave can be treated as a monochromatic pump, a simple model like §3.4.2 applies. In real plasmas, however, the primary fluctuations (drift waves) have a large number of degrees of freedom, and an analysis treating the drift wave spectrum is necessary.

Equations (3.2.40) and (3.2.45) describe the coupled dynamics of the drift wave action and the vorticity of the zonal flow,

$$N_k = \left(1 + k_{\perp}^2 \rho_s^2\right)^2 |\phi_k|^2 \quad \text{and} \quad U \equiv \frac{d}{dr} V_{ZF}$$

respectively. Taking into account of the collisional damping of zonal flow (§3.1.3), the dynamical equation for the zonal flow vorticity

$$\left(\frac{\partial}{\partial t} + \gamma_{\text{damp}}\right) U = \frac{\partial^2}{\partial r^2} \frac{c^2}{B^2} \int d^2k \frac{k_{\theta} k_r}{\left(1 + k_{\perp}^2 \rho_s^2\right)^2} N_k \quad (3.4.12)$$

and that of the drift wave spectrum

$$\frac{\partial}{\partial t} N_k + \mathbf{v}_g \cdot \frac{\partial N_k}{\partial \mathbf{x}} - \frac{\partial \omega_{k0}}{\partial \mathbf{x}} \cdot \frac{\partial N_k}{\partial \mathbf{k}} - \gamma_{\text{drift}} N_k = k_{\theta} \frac{\partial N_k}{\partial k_r} U \quad (3.4.13)$$

are derived, where  $\mathbf{v}_g \equiv \frac{\partial \omega_k}{\partial \mathbf{k}}$  is the group velocity of the drift wave, and  $\gamma_{\text{drift}}$  represents the linear instability and the nonlinear damping rate that causes saturation of the drift wave (in the absence of zonal flow).

In the following subsections, the evolution of drift waves and zonal flow is explained in several limiting cases.

#### 3.4.4 Diffusion limit

We first discuss the case where the autocorrelation time of the drift wave  $\tau_{\text{ac}, d}$  and that of the zonal flow  $\tau_{\text{ac}, ZF}$  are much shorter than the time scale determined by  $\gamma_{ZF}^{-1}$ , where  $\gamma_{ZF}^{-1}$  is the characteristic time scale of the linear zonal flow instability. It is very important to keep in mind that we also use this ordering as a tractable model of the case where the zonal flow spectrum is slowly varying, but spatially complex. Thus, this limit is of broader interest than one may initially think. Note that the validity of the equivalence between spatial complexity and short autocorrelation time follows from the fact that it is the net dispersion in  $\Omega - q_r v_{gr}$  which is of interests. Thus, even if  $\Delta\Omega$  is small, the existence of fine scale zonal flows can guarantee that  $v_{gr} \Delta k$  is large, so that the zonal flow-drift wave autocorrelation time is correspondingly short. The autocorrelation

time of the drift wave,  $\tau_{ac, d} \approx \gamma_{drift}^{-1}$ ; is determined by the drift wave self-nonlinearity, and is taken as prescribed in this review. The time scale orderings are written as

$$\gamma_{drift} \gg \gamma_{ZF} \quad (3.4.14)$$

$$\tau_{ac, ZF}^{-1} \gg \gamma_{ZF} \quad (3.4.15)$$

In this case, the phase of each mode composing the drift wave fluctuation is considered to be random and the distribution function  $N_k$  is treated. Fourier components of the zonal flow,  $U_{q_r}$ ,

$$U = \sum_{q_r} U_{q_r} \exp(iq_r r) \quad (3.4.16)$$

induce random Doppler shifts in the drift waves, because the autocorrelation time of  $U_{q_r}$  is short. The coefficient  $k_{\theta} U$  in the right hand side of Eq.(3.4.13) can be considered as a random frequency modulation.

The term  $k_{\theta} U \partial N_k / \partial k_r$  in Eq.(3.4.13) changes rapidly in time and is approximated as random. The average within the 'long time scale',  $\gamma_{ZF}^{-1}$ , is evaluated according to the analysis of §3.3.2. By employing a quasi-linear treatment for random stretching from §3.3.2(ii), one has [3.44]

$$\overline{k_{\theta} U \frac{\partial N_k}{\partial k_r}} = \frac{\partial}{\partial k_r} \left( D_K \frac{\partial N_k}{\partial k_r} \right) \quad (3.4.17)$$

where

$$D_K = \sum_{q_r} R(k, q_r) k_{\theta}^2 q_r^2 U_{q_r}^2 \quad (3.4.18)$$

is the diffusion coefficient in the wavenumber space that determines the straining of the drift wave due to the random Doppler shift. For further simplification, the response of drift waves on the left hand side of Eq.(3.4.13) can be rewritten, in terms of the linear growth term and nonlinear self-interaction term, as

$$\frac{\partial N_k}{\partial t} + \mathbf{v}_g \cdot \frac{\partial N_k}{\partial \mathbf{x}} - \frac{\partial \omega_{k0}}{\partial \mathbf{x}} \cdot \frac{\partial N_k}{\partial \mathbf{k}} = \gamma_L N_k - \gamma_{NL} N_k \quad (3.4.19)$$

where  $\gamma_L$  is the linear growth rate and  $\gamma_{NL}$  is the nonlinear damping rate. With this formal expression, Eq.(3.4.13) reduces to the diffusion equation for the drift wave spectrum

$$\left(\frac{\partial}{\partial t} - \gamma_L + \gamma_{NL}\right) N_k - \frac{\partial}{\partial k_r} \left( D_K \frac{\partial N_k}{\partial k_r} \right) = 0. \quad (3.4.20)$$

The evolution of the zonal flow is given by the negative diffusion effect and collisional damping, as is explained in §3.2.2, as

$$\left(\frac{\partial}{\partial t} + \gamma_{\text{damp}}\right) |U_{q_r}|^2 = \frac{\partial^2}{\partial r^2} \sum_k D_q \frac{\partial}{\partial k_r} N_k |U_{q_r}|^2 \quad (3.4.21)$$

where the coefficient  $D_K$  is calculated in §3.2.2 to be

$$D_q = \frac{1}{B^2} \frac{k_{\theta}^2 k_r}{(1 + k_{\perp}^2 \rho_s^2)^2} R(q_r, k). \quad (3.4.22)$$

### 3.4.5 Predator-prey model

The system of Eqs.(3.4.21) and (3.4.22) describes the interaction between the drift-wave and zonal flow. This is an example of a two-component, self-regulating system. As the 'primary' fluctuation, the drift wave grows by its own instability mechanism. The drift wave fluctuation energy is transformed into the energy of the zonal flow via the secondary instability process. In this sense, a correspondence of the form:

$$\begin{aligned} \text{drift wave fluctuation } \langle N \rangle &= \sum_k N_k && \leftrightarrow \text{prey} \\ \text{zonal flow energy } \langle U^2 \rangle &= \sum_{q_r} |U_{q_r}|^2 && \leftrightarrow \text{predator} \end{aligned} \quad (3.4.23)$$

holds.

A low-degree of freedom model can be deduced from Eqs.(3.4.21) and (3.4.22). Integrating Eqs.(3.4.21) and (3.4.22) in wavenumber space, one finds

$$\sum_k \left( \frac{\partial}{\partial t} - \gamma_L + \gamma_{NL} \right) N_k = \sum_k \frac{\partial}{\partial k_r} \left( D_K \frac{\partial N_k}{\partial k_r} \right) \quad (3.4.24)$$

and

$$\left(\frac{\partial}{\partial t} + \gamma_{\text{damp}}\right) \langle U^2 \rangle = - \sum_{k, q_i} q_r^2 D_q \frac{\partial}{\partial k_r} N_k |U_{q_i}|^2. \quad (3.4.25)$$

A Krook approximation is used to write:

$$\sum_k \frac{\partial}{\partial k_r} \left( D_K \frac{\partial N_k}{\partial k_r} \right) \approx - C_{Z \rightarrow d} \langle U^2 \rangle \langle N \rangle \quad (3.4.26)$$

$$- \sum_{k, q_r} q_r^2 D_q \frac{\partial}{\partial k_r} N_k |U_{q_r}|^2 \approx C_{d \rightarrow Z} \langle U^2 \rangle \langle N \rangle \quad (3.4.27)$$

where  $C_{Z \rightarrow d}$  and  $C_{d \rightarrow Z}$  are positive numbers. With this simplification, Eqs.(3.4.24) (3.4.25) can be modelled as

$$\left(\frac{\partial}{\partial t} - \gamma_L + \gamma_{\text{NL}}\right) \langle N \rangle = - C_{Z \rightarrow d} \langle U^2 \rangle \langle N \rangle, \quad (3.4.28)$$

$$\left(\frac{\partial}{\partial t} + \gamma_{\text{damp}}\right) \langle U^2 \rangle = C_{d \rightarrow Z} \langle U^2 \rangle \langle N \rangle. \quad (3.4.29)$$

where  $\gamma_L$  and  $\gamma_{\text{NL}}$  are typical numbers for the linear and nonlinear rates. As is explained, the collisional damping rate  $\gamma_{\text{damp}}$  does *not* depend on the scale  $q_r$ , as it is a drag, not a viscosity. The conservation of the total energy among drift wave and zonal flow requires

$$C_{d \rightarrow Z} = C_{Z \rightarrow d}. \quad (3.4.30)$$

The evolution of the wave-zonal flow system critically depends on the nonlinear damping of drift waves. The simplest form of the nonlinear damping rate of the drift wave may be chosen as

$$\gamma_{\text{NL}} \langle N \rangle = \gamma_2 \langle N \rangle^2. \quad (3.4.31)$$

By these simplifications, one has a two-dimensional predator-prey model of the form

$$\frac{d}{dt} \langle N \rangle = \gamma_L \langle N \rangle - \gamma_2 \langle N \rangle^2 - C_{d \rightarrow Z} \langle U^2 \rangle \langle N \rangle, \quad (3.4.32a)$$

$$\frac{d}{dt} \langle U^2 \rangle = - \gamma_{\text{damp}} \langle U^2 \rangle + C_{d \rightarrow Z} \langle U^2 \rangle \langle N \rangle. \quad (3.4.32b)$$

A tractable model with a small number of degrees of freedom can be constructed in the diffusion limit, as well.

### 3.4.6 Coherent Nonlinear Drift Wave- Zonal Flow Interactions (1) - Wave Trapping

The growth of the zonal flow is influenced by the finite amplitude zonal flow on the drift waves, even if tertiary instability is not induced. The presence of the zonal flow induces higher order deformation of the drift wave spectra, which causes the modification of the growth rate of the zonal flow. This is, of course, analogous to the modification of the distribution function structure due to nonlinear resonant particle dynamics in Vlasov plasma problems. An analogy holds, and may be summarized by:

Drift wave -zonal flow problem	1D Vlasov problem
$N_k \leftrightarrow \tilde{f}(v)$	
$k_r \leftrightarrow v$	(3.4.33)
$k_\theta U(x) \leftrightarrow e\tilde{E}(x)$	

where  $U$  is the vorticity of the zonal flow,  $U = \partial V_{ZF} / \partial x$ . A more thorough comparison is summarized in the Table 3.4,1.

As in the case of particle trapping in a wave field, the trapping of drift wave packet in the zonal flow field can take place, this phenomena thus has an influence on the evolution of zonal flow. The bounce motion of drift wave rays occurs, as is explained in Appendix A. In this subsection, we review the nonlinear process that is relevant when the lifetime of the drift wave and that of zonal flow are long compared to both  $\gamma_{ZF}$  and the bounce frequency  $\omega_{\text{bounce}}$  (the explicit form of which is given in Appendix A), i.e., when

$$\gamma_{\text{drift}} \ll \gamma_{ZF}, \omega_{\text{bounce}} \quad (3.4.34a)$$

$$\tau_{\text{ac}, ZF}^{-1} \ll \gamma_{ZF}, \omega_{\text{bounce}} \quad (3.4.34b)$$

This is the opposite limit to §3.4.4, where waves and zonal flows are assumed to be randomized rapidly during the interaction between them, as in the quasilinear problems. Another limit is that the life time of drift waves is much shorter than the trapping time, but the coherence time of the zonal flow is longer than  $\gamma_{ZF}^{-1}$ . This limit is discussed in the next subsection. (§3.4.7).

The coupled dynamical equations for the drift-wave fluctuations and the zonal flow component are given following the argument of Eqs. (3.4.12) and (3.4.13). The

vorticity equation that relates the zonal flow to the wave population, (3.4.12) and the wave kinetic equation, together form a nonlinear dynamical system

$$\left( \frac{\partial}{\partial t} + \gamma_{\text{damp}} \right) U = \frac{\partial^2}{\partial r^2} \frac{1}{B^2} \int d^2 k \frac{k_\theta k_r}{(1 + k_\perp^2 \rho_s^2)^2} N_k, \quad (3.4.35a)$$

$$\frac{\partial}{\partial t} N_k + \mathbf{v}_g \cdot \frac{\partial N_k}{\partial \mathbf{x}} = k_\theta \frac{\partial N_k}{\partial k_r} (1 + k_\perp^2 \rho_i^2) U, \quad (3.4.35b)$$

where the 'screening' effect of a finite gyroradius is retained,  $\bar{U} = U + \rho_s^2 \frac{d^2}{dr^2} U$ . In comparison with Eq.(3.4.13), the linear growth and nonlinear damping of drift waves are dropped, because the case of coherent waves is studied here.

This set of equations (3.4.35a) and (3.4.35b) has a similar structure to the Vlasov equation that describes wave-particle interactions (such as plasma waves, etc.). The term  $k_\theta U(x)$  in Eq.(3.4.35b) is the counterpart of acceleration in the phase space. That is, Eq.(3.4.35b) has a similar structure to the one-dimensional Vlasov equation, and Eq.(3.4.35a) is the analogue of the Poisson equation. With this analogy in mind, one can study a BGK-like solution with finite-amplitude zonal flow.

Consideration of drift wave ray dynamics (details are given in Appendix A) leads us to conclude that the drift wave-packet can be labeled by the two invariants of motion  $\omega_{k0}$  and  $k_{y0}$ , i.e.,

$$\omega_k - u k_x - k_y V_{ZF} \equiv \omega_{k0} \quad \text{and} \quad k_y = k_{y0}, \quad (3.4.36)$$

where  $u$  is a uniform velocity  $\frac{d}{dt} \rightarrow -u \frac{d}{dx}$ . Note that the wavefrequency  $\omega_k$  and the wavenumber  $k_x$  are modified along the path of the drift wave-packet according to the relation which is simply the dispersion relation

$$\omega_k = k_{y0} (1 + k_{y0}^2 + k_x^2)^{-1}. \quad (3.4.37)$$

By use of these two integrals of motion, ( $\omega_{k0}$  and  $k_{y0}$ ), an exact solution for the distribution function is given in the form:

$$N(x, k_x, k_y) = N(\omega_{k0}(x, k_x), k_{y0}). \quad (3.4.38)$$

Combining Eq.(A.37) and Eq.(A.44) describes the coherent structure of the system of zonal flow and drift waves.

The trapping of the drift wave-packet occurs in the trough of the zonal flow, as is explained in the Appendix A. Figure 3.4.3 illustrates the rays of drift wave-packets in phase space for the case in which the screened velocity  $\bar{V}_{ZF}$  has a sinusoidal dependence in the  $x$ -direction. The trapped region is determined by the difference  $\Delta\bar{V}_{ZF}$  between the maximum and minimum of  $\bar{V}_{ZF}$ . The wavenumber on the separatrix at the minimum of  $\bar{V}_{ZF}$  is given as

$$k_{x0, sep}^2 = \frac{\Delta\bar{V}_{ZF} (1 + k_{y0}^2)^2}{1 - \Delta\bar{V}_{ZF} (1 + k_{y0}^2)} \quad (3.4.39)$$

for a simple case of stationary zonal flow structure. Wave packets which satisfy  $k_{x0}^2 < k_{x0, sep}^2$  are trapped in the inhomogeneous zonal flow. The bounce frequency at the bottom of the trough is seen to be

$$\omega_{bounce}^2 = \frac{2\rho_s^2 k_y q_r}{1 + \rho_s^2 k_y^2} \omega_{k0} \frac{d\bar{V}_{ZF}}{dr} \quad (3.4.40)$$

As is the case for the trapping of resonant particles by waves in collisionless plasmas, the bounce frequency of quasi-particles (wave-packets) has a dependence like  $\omega_{bounce} \propto \sqrt{\bar{V}_{ZF}}$ . The bounce frequency away from the O-point can be evaluated by use of elliptic functions. The bounce frequency becomes lower as the trajectory approaches the separatrix. The assumption in this line of thought, Eq.(3.4.34a), means that  $\gamma_{drift} < \omega_{bounce}$  is necessary in order that the wave-packet trapping is relevant. Thus, trapping of wave packets is particularly relevant near marginal stability of the drift waves.

If the trapping of the wave-packet is effective, the growth of the zonal flow stops. On a trapped trajectory, the distribution function tends to approach the same value. The distribution function  $N_k$  finally recovers a symmetry with respect to  $k_r$ , and the RHS of Eq.(3.4.35a) vanishes. The trapping of the drift wave tends to terminate the growth of the zonal flow.

### 3.4.7 Coherent Nonlinear Drift Wave- Zonal Flow Interactions (2) - zonal flow quenching

If the zonal flow has a long life time, it is possible to form a coherent spatial structure through a strongly nonlinear deformation of the drift wave population density. However, the condition of Eq.(3.4.34a) does not always hold. That is, the



autocorrelation time of drift waves can be shorter than the life time of zonal flow structures, while the zonal flows maintain their coherence, i.e.,

$$\gamma_{\text{drift}} > \gamma_{\text{ZF}}, \omega_{\text{bounce}}, \quad (3.4.41a)$$

$$\tau_{\text{ac, ZF}}^{-1} \ll \gamma_{\text{ZF}}. \quad (3.4.41b)$$

In this subsection, we study the case where the turbulent drift wave spectrum forms a spatially coherent zonal flow structure.

The wave kinetic equations as in §3.4.4, Eq. (3.4.35a) and Eq.(3.4.35b), are employed. An asymmetric part of  $N_k$  with respect to  $k_x$ ,  $\hat{N}_k$ , contributes to the time evolution of  $U$  through Eq.(3.4.35a). Solving Eq.(3.4.35b) and expressing  $\hat{N}_k$  in the form of a perturbation expansion

$$\hat{N}_k = \hat{N}_k^{(1)}U + \hat{N}_k^{(2)}U^2 + \hat{N}_k^{(3)}U^3 + \dots, \quad (3.4.42)$$

and substituting it into Eq.(3.4.35a), a nonlinear equation of the zonal flow vorticity  $U$  is obtained. The linear response has been obtained, as is explained in §3.2.1, i.e.,

$$\hat{N}_k^{(1)} = \frac{\partial}{\partial r} (k_\theta V_c) R(q_r, \Omega) \frac{\partial N_k}{\partial k_r},$$

where  $R(q_r, \Omega) = i/(\Omega - q_r v_g + i\gamma_{\text{drift}})$  is the response function. The first-order term gives the negative-diffusion-like form  $\gamma_{\text{ZF}} = D_{rr} q_r^2$ , i.e., the basic zonal flow growth. The higher order responses with respect to  $U$ ,  $\hat{N}_k^{(2)}$  and  $\hat{N}_k^{(3)}$  can be calculated using the formal relation

$$\hat{N}_k^{(n)} = k_\theta U R(q_r, \Omega) \frac{\partial \hat{N}_k^{(n-1)}}{\partial k_r}. \quad (3.4.43)$$

This simplification is based on the assumption that the relaxation of drift wave spectrum by its own self-nonlinear interaction is *fast*. Equation (3.4.43) is based on a formal expansion in the parameter  $U R(q_r, \Omega) \approx U/\gamma_{\text{drift}}$ . Thus, all resonance functions, both  $R(q_r, \Omega) = i/(\Omega - q_r v_g + i\gamma_{\text{drift}})$ , and those corresponding to higher resonances, reduce to the simple form  $R(q_r, \Omega) \sim 1/\gamma_{\text{drift}}$ . Note that this approximation clearly fails close to marginal stability of the primary drift waves, where  $\gamma_{\text{drift}} \rightarrow 0$ . Quantitatively, the competition between  $\gamma_L$  and the dispersion (spread) in  $\Omega - q_r v_g$ , is given by

$\Delta(\Omega - q_r v_g)$ . For  $\gamma_{\text{drift}} < \Delta(\Omega - q_r v_g)$ , resonance structure becomes important, and the analogue of phase-space density granulations form in N.

For a wide spectrum of fluctuations, one has  $R(q_r, \Omega) \rightarrow 1/\gamma_{\text{drift}}$  and obtains the leading diffusion term of Eq.(3.2.51) of §3.2.2. In such a case,  $R(q_r, \Omega)$  has an approximate symmetry with respect to  $k_r$ . The contribution from the second-order term is small, from the consideration of this symmetry, so the first contributing order is the one comes from the third-order term:

$$\hat{N}_k^{(3)} = U^3 R(q_r, \Omega)^3 k_\theta^3 \frac{\partial^3 N_k}{\partial k_r^3} . \quad (3.4.44)$$

Note that this is equivalent to the term which gives nonlinear Landau damping in the Vlasov problem. Recall that nonlinear Landau damping is also third order in the perturbation amplitude, involves contributions at beat wave resonances, where  $\omega + \omega' = (k + k')v$ , and may be obtained from 'higher-order quasilinear theory'. Here, the explicit beat wave resonance is absent, since  $R(q_r, \Omega) \sim 1/\gamma_{\text{drift}}$  - i.e., large  $\gamma_{\text{drift}}$  smears them out. Figure 3.4.4 illustrates the linear response  $\hat{N}_k^{(1)}$  and third order response  $\hat{N}_k^{(3)}$  for the case of a monotonically decreasing drift wave spectrum. The nonlinear term works against the linear term, so as to cause nonlinear saturation. Substituting Eq.(3.4.44) into Eq.(3.4.35a), one obtains a nonlinear equation for the drift wave vorticity [3.90]

$$\frac{\partial}{\partial t} U = -D_{rr} \frac{\partial^2}{\partial r^2} U + D_3 \frac{\partial^2}{\partial r^2} U^3 - \gamma_{\text{damp}} U . \quad (3.4.45)$$

with

$$D_3 = -\frac{c^2}{B^2} \int d^2k \frac{R(q_r, \Omega)^3 k_\theta^4 k_r}{(1 + k_\perp^2 \rho_s^2)^2} \frac{\partial^3 N_k}{\partial k_r^3} . \quad (3.4.46)$$

As the spectral function is peaked near  $k_r \approx 0$ , the sign in the definition of  $D_3$  is chosen such that  $D_3$  is positive when  $D_{rr}$  is positive.

Equation (3.4.45) shows that the drive of the zonal flow is reduced (and can even be quenched) when the amplitude of the zonal flow becomes larger. The quenching of the drive of the zonal flow is a characteristic mechanism in the problem of generation of the axial-vector field through turbulent transport of energy (such as dynamo problems). In the case of magnetic field generation via a dynamo, the coefficient  $\alpha$  for the mean

electro-motive force is known to be suppressed by the generated magnetic field. The so-called  $\alpha$ -suppression problem has been investigated [3.91]. Equation (3.4.45) is an explicit expression for the quench of the driving force of the axial vector field.

Equation (3.4.45) governs the dynamics of the (coherent) structure of the zonal flow. Further exploration of this result follows. The most unstable wavenumber of the zonal flow is derived in §3.2. The zonal flow growth rate  $\gamma_{ZF}$  (the first term in the RHS of Eq.(3.4.45)) does not continue to growth at larger  $q_r$  when the dispersion effect of the drift waves on the zonal flow is introduced:  $\gamma_Z = D_{rr} q_r^2 \left(1 - q_r^2 / q_{r0}^2\right)$ , where  $q_{r0}^{-1}$

represents the characteristic scale where the dispersion suppresses the zonal flow instability. An explicit form of  $q_{r0}$  is explained in §3.2.2. Of course, flow growth must slow down on scales smaller than the neoclassical or collective (screening) lengths, namely,  $\rho_{\theta i}$  and  $\rho_i$ . Damping is induced by collisional processes (§3.1.3) and by the turbulent diffusion of a secondary parallel flow (§3.2.6), via

$\gamma_{\text{damp}} = \gamma_{\text{damp}}^{\text{coll}} + \mu_{\parallel} (1 + 2q^2) q_r^2$ , where  $\gamma_{\text{damp}}^{\text{coll}}$  is the collisional damping explained in §3.1.3, and  $\mu_{\parallel}$  is the turbulent shear viscosity for the flow along the field line, and  $q$  is the safety factor. (The coefficient  $1 + 2q^2$  takes a slightly different form, depending on the plasma parameters.) Thus, Eq.(3.4.45) can be written in the explicit form

$$\frac{\partial}{\partial t} U + D_{rr} \left( \frac{\partial^2}{\partial r^2} U + q_{r0}^2 \frac{\partial^4}{\partial r^4} U \right) - D_3 \frac{\partial^2}{\partial r^2} U^3 - \mu_{\parallel} (1 + 2q^2) \frac{\partial^2}{\partial r^2} U + \gamma_{\text{damp}}^{\text{coll}} U = 0 \quad (3.4.47)$$

The zonal flow is excited if the condition  $D_{rr} > \mu_{\parallel} (1 + 2q^2)$  is satisfied. Both the zonal-flow driving coefficient  $D_{rr}$  and the shear viscosity  $\mu_{\parallel}$  are given by the drift wave spectrum  $N_k$ . Equation (3.4.47) explains that the zonal flow is generated by the background turbulence and is stabilized by collisional damping, higher-order dispersion and by the nonlinearity.

### Section 3.4.8 A Unifying Framework - Shearing and Wave Kinetics

Building upon the studies of particular nonlinear mechanisms in various limiting cases, which are explained individually in the preceding subsections, we now propose a unifying framework for understanding the zonal flow problem. This framework is one of shearing and wave kinetics.

We now discuss the physics of stochastic shearing of primary drift waves by a spatio-temporally complex spectrum of zonal flows, in particular, and also survey the wave kinetics of drift waves in a slowly evolving spectrum of zonal flows, in general. Extensive use is made of an instructive and far-reaching analogy between the wave kinetics of a drift wave packet in a zonal flow field and the kinetics of a particle in a

Langmuir wave field in a one-dimensional Vlasov plasma. On account of the particular symmetry of the zonal flow field, both the drift wave - zonal flow and 1D Vlasov problem can be reduced to 2D phase space dynamics, for  $x, V$  and  $x, k_r$ , respectively. In each case, the effective frequency of the motion  $\omega(J)$  is a function of the action variable  $J$ , so that the dynamics are non-degenerate, and differentially rotating flow in phase space results. The analogy enables a unification of many analyses of shearing effects, both in the stochastic and coherent regimes. Of course, shearing dynamics are of great interest, as they constitute the mechanism by which the zonal flows regulate transport and turbulence levels, and thus merit detailed attention.

The analogy between zonal flow and Vlasov plasma is motivated by the observation of the obvious similarities between the wave-kinetic equation for  $N(\mathbf{k}, \mathbf{x}, t)$  in the presence of a zonal flow spectrum  $|\tilde{V}_q|^2$  and the Boltzmann equation for  $f(\mathbf{V}, \mathbf{x}, t)$  in the presence of a Langmuir wave spectrum  $|\tilde{E}_{k, \omega}|^2$ . These equations are

$$\frac{\partial}{\partial t} N + \mathbf{v}_g \cdot \frac{\partial N}{\partial \mathbf{x}} - \frac{\partial}{\partial \mathbf{x}} (k_y \tilde{V}) \cdot \frac{\partial N}{\partial k_x} = C(N) = \gamma_{\text{drift}} N, \quad (3.4.48a)$$

and

$$\frac{\partial}{\partial t} f + \mathbf{V} \cdot \frac{\partial f}{\partial \mathbf{x}} - \frac{\partial}{\partial \mathbf{x}} \left( \frac{e}{m} \tilde{\Phi} \right) \cdot \frac{\partial f}{\partial \mathbf{v}} = C(f), \quad (3.4.48b)$$

where  $\tilde{E}_{k, \omega} = -\partial \tilde{\Phi}_L / \partial x$  for Langmuir wave turbulence. (The suffix L stands for the Langmuir waves.) The analogy is summarized in Table 3.4.1, which we now discuss. Rather clearly, the analogue of the 'particle' with velocity  $\mathbf{V}$  in the Vlasov case is the drift wave packet with group velocity  $\mathbf{v}_g(k)$ , which is sheared by the zonal flow field  $\tilde{V}$ , itself the analogue of the Langmuir wave field. The analogue of the Boltzmann collision integral  $C(f)$ , which maintains a near-Maxwellian average distribution function is the wave kinetic collision integral  $C(N)$ , taken to have the form

$$\gamma_{\text{drift}} N = \gamma_k N - \Delta \omega_k \frac{N^2}{N_0}$$

in some cases which require an equilibrium spectrum of turbulence in the absence of zonal flows.

Aspects of the dynamics can be elucidated by consideration of resonances and time scales. The analogue of the well known wave-particle resonance

$$\omega/k = V$$

is that for which the phase velocity of the shearing flows equals the wave packet group velocity

$$v_g(k) = \Omega/q_x.$$

Just as in the particle case, chaos occurs when the zonal flow - wave group resonances overlap, resulting in stochastic drift-wave-ray dynamics. Stochasticity of ray trajectories provides the crucial element of *irreversibility* in the drift wave - zonal flow interactions. Note that since zonal flow energy is concentrated at very low frequency, while the dispersion in  $v_g(k)$  is large, overlap of  $v_g(k) = \Omega/q_x$  resonances occurs at quite modest zonal flow amplitudes. Such a state of *ray chaos* naturally necessitates a stochastic description. At least four time scales govern both the wave - particle and zonal shear - wave group dynamics. These are:

i) *The spectral autocorrelation times*  $\tau_{ac}$ . In the case of the Vlasov plasma,

$$\tau_{ac} = \min \left\{ \left( k \Delta(\omega/k) \right)^{-1}, V \Delta k \right\}.$$

These times correspond to the lifetimes of the instantaneous electric field pattern 'seen' or traversed by a particle. For the zonal shear,

$$\tau_{ac} = \min \left\{ (\Delta\Omega)^{-1}, \left( \Delta(q_x v_g) \right)^{-1} \right\}. \quad (3.4.49)$$

Here,  $(\Delta\Omega)^{-1}$  gives the flow pattern lifetime, which is usually quite long, since  $\Omega \sim 0$ .

However, the dispersion in the Doppler frequency shift of the wave in a propagating packet (i.e.,  $\Delta(q_x v_g)$ ) is usually quite large, resulting in short auto-correlation time, and suggests that a stochastic analysis is relevant. It is important to again stress the fact that no *a priori* postulate of randomness or noise in the zonal flow spectrum is required.

ii) *the nonlinear orbit times*, which correspond to the vortex circulation times in phase or eikonal space. These correspond to the particle bounce or trapping time  $(e\tilde{\Phi}_L/m)^{-1}$  in the case of the Vlasov plasma, and the shearing rate of a fluid element in a zonal flow,

$$\tau_{\perp} = (q_x \tilde{v}_{ZF})^{-1} \quad (3.4.50a)$$

or the bounce time  $(\omega_{\text{bounce}}^{-1})$  of a trapped wave packet, where

$$\omega_{\text{bounce}} = \sqrt{\frac{2\rho_s^2 k_y q_r^2}{1 + \rho_s^2 k_y^2}} \omega_{k0} V_{ZF}, \quad (3.4.50b)$$

whichever shorter. In the event that resonances do not overlap, and that the nonlinear orbit time is shorter than the autocorrelation time, a coherent interaction analysis of the dynamics is required.

iii) *the nonlinear decorrelation time*, which quantifies the scattering time for an individual trajectory of coherence time for a resonant triad. For the Vlasov plasma,

$\tau_c = (k^2 D_V)^{-1/3}$ , the well-known result first obtained by Dupree. Here  $D_V$  is the quasi-linear diffusivity in velocity space. For the zonal amplification problem,

$$\tau_c = \min \left\{ \gamma_k^{-1}, k^2/D_k, \left( q_x^2 D_k (dv_g/dk)^2 \right)^{-1/3} \right\}. \quad (3.4.51)$$

Here  $\gamma_k$  controls the triad coherence time. Note that  $\gamma_k$  appears in place of a nonlinear self-decorrelation rate  $\Delta\omega_k$  via the requirement that  $C(N) = 0$ , to determine  $N$  in the absence of zonal flow.  $D_k k^{-2}$  is the rate of diffusive scattering (i.e., random refraction) and  $\left( q_x^2 D_k (dv_g/dk)^2 \right)^{1/3}$  is the analogue of the Dupree decorrelation rate  $(k^2 D_V)^{1/3}$  for the eikonal problem. [Note that  $D_k$  has the dimension of  $m^{-2}s^{-1}$ .] This arises as a consequence of coupling between scattering in  $k_x$  (due to  $D_k$ ) and the propagation at the wave group speed  $v_g(k)$ .

iv) *the time scale for evolution of the average population density*, i.e., the macroscopic relaxation time. For the Vlasov plasma, this is  $\tau_{\text{relax}} = \Delta v^2 D_V^{-1}$ , where  $\Delta v$  is the extent of phase velocities excited, and  $D_V$  is the quasi-linear velocity space diffusion coefficient. Similarly, for the zonal flow problem,

$$\tau_{\text{relax}} = \Delta k^2 / D_k. \quad (3.4.52)$$

The possible dynamical states of the system are classified by the ordering of the various time scales, and by whether or not the trajectories are chaotic or not. The four basic time scales can nearly always be ordered as

$$\min(\tau_{\text{ac}}, \tau_{\perp}) < \max(\tau_{\text{ac}}, \tau_{\perp}) \leq \tau_c < \tau_{\text{relax}}. \quad (3.4.53)$$

Thus, the possible system states can be classified by:

i) *the Chirikov overlap parameter*

$$S = \frac{\Delta v_g}{\Delta(\Omega/q_r)} \quad (3.4.54)$$

Here,  $\Delta v_g$  is the width of the wave group - zonal shear resonance, and  $\Delta(\Omega/q_r)$  is the spacing between resonances.

ii) the effective Kubo number

$$\mathcal{K} = \tau_{ac}/\tau_{\perp}, \quad (3.4.55)$$

the ratio of the autocorrelation time  $\tau_{ac}$  to the zonal flow shearing time  $\tau_{\perp}$ .

These ratios immediately divide the system states into three categories, which are analyzed in Table 3.4.2. For  $S > 1$ , and  $\mathcal{K} \ll 1$ , the dynamics are stochastic, with stochastic rays, and random shearing and refraction of drift waves by zonal flows constituting the principal effect of zonal flows on the turbulence. This regime may be treated by using the method of quasi-linear theory, yielding a picture of diffusive refraction (Section 3.5.4). Extensions to higher order expansions in population density perturbations  $\tilde{N}$  have been implemented, and are analogous to induced scattering (i.e., nonlinear Landau damping), familiar from weak turbulence theory for the Vlasov plasma. (Section 3.5.7 discusses such an extension.) For  $S \ll 1$  and  $\mathcal{K} > 1$ , the dynamics are coherent, with strongly deflected rays tracing vorticities in the  $(x, k_x)$  space. In this regime, the wave population density evolution will exhibit oscillations due to the 'bouncing' of trapped rays, and will asymptote to the formation of wave packets corresponding to BGK solutions of the wave kinetic equation. In this regime zonal flow shear and wave packets adjust to form a self-trapping state. (Section 3.5.6. Some extensions are discussed in Chapter 6.) A third regime is that with  $S > 1$  and  $\mathcal{K} \leq 1$ , which corresponds to the regime of turbulent trapping. The dynamics here resembles those of the stochastic regime, except that consistent with  $\mathcal{K} \leq 1$ , closely separated wave packets remain correlated for times  $t > \tau_c$ . These correlated, small-scale packets are analogous to clumps in the 1D Vlasov plasma, and result in granulation of the wave packet population density  $N$ . Such granulations necessitate the calculation of a Fokker-Planck drag, as well as diffusion, for describing the evolution of  $\langle N \rangle$ , i.e., the long time average. (This issue is discussed in Chapter 6.) Likewise, self-trapped wave packets correspond to holes or cavitons in the Vlasov plasma. Figure 3.4.5 illustrates the parameter domain and various theoretical approaches.

Having outlined the general structure of the dynamics of shearing in wave kinetics, we now proceed to discuss the regime of stochastic ray dynamics in some detail. Here, we are primarily concerned with the evolution of the mean drift wave population  $\langle N(k, t) \rangle$  in the presence of the zonal flow spectrum. The salient features of the

stochastic dynamics regime are given in Table 3.4.3, along with their analogies for the 1D Vlasov turbulence problem. Averaging the wave kinetic equation yields the mean field equation for  $\langle N \rangle$

$$\frac{\partial}{\partial t} \langle N \rangle - \frac{\partial}{\partial k_r} \left\langle \frac{\partial}{\partial x} (k_\theta \tilde{V}) N \right\rangle = \langle C(N) \rangle \quad (3.4.56a)$$

where the mean refraction-induced flux of  $\langle N \rangle$  in  $k_r$  is given by

$$\Gamma_{k_r} = \left\langle \frac{\partial}{\partial x} (k_\theta \tilde{V}) N \right\rangle = -i \sum_{q_x} q_x k_\theta \tilde{V}_{-q} \tilde{N}_q \quad (3.4.56b)$$

Proceeding in the spirit of quasi-linear theory, the expression for

$\Gamma_{k_r} = \left\langle \frac{\partial}{\partial x} (k_\theta \tilde{V}) N \right\rangle = -i \sum_{q_x} q_x k_\theta \tilde{V}_{-q} \tilde{N}_q$  may be calculated by iteratively substituting the response of  $N$  to  $V$ ,  $\delta N / \delta \tilde{V}$ . Proceeding as in Section 3.2,

$$\tilde{N}_q = \frac{q_x k_\theta \tilde{V}_q}{\Omega - q_x v_g + i\gamma_{\text{drift}}} \frac{\partial \langle N \rangle}{\partial k_x}, \quad (3.4.57a)$$

so that the wave number space flux is

$$\Gamma_{k_r} = -D_{k_r} \frac{\partial \langle N \rangle}{\partial k_x} \quad (3.4.57b)$$

with the  $k$ -space diffusion coefficient

$$D_{k_r} = \sum_{q_x} q_x^2 k_\theta^2 |\tilde{V}_q|^2 R(k, q_x) \quad (3.4.57c)$$

and resonance function

$$R(k, q_x) = \frac{\gamma_{\text{drift}}}{(\Omega - q_x v_g)^2 + \gamma_{\text{drift}}^2} \quad (3.4.57d)$$

As noted above, the resonance in question is that between the drift wave packet with group speed  $v_g(k)$  and the phase speed of the zonal shear  $\Omega/q_x$ . It is interesting to observe that this resonance appears as a limiting case of the well known 3-wave resonance denominator



$$R_{k, q, k+q} = \frac{i}{\omega_k + \omega_q - \omega_{k+q} + i(\Delta\omega_k + \Delta\omega_q - \Delta\omega_{k+q})} \quad (3.4.58)$$

Expanding for  $|q| < |k|$  and replacing the broadenings by  $\gamma_{\text{drift}}$  then yields

$$R_{k, q, k+q} = \frac{i}{\omega_q - q \cdot \partial\omega_k / \partial k + i\gamma_{\text{drift}}} \quad (3.4.59)$$

Finally, specializing to the case  $q = q_x \hat{x}$  and rewriting  $\omega_q = \Omega$  then finally gives

$$R_{k, q, k+q} = \frac{i}{\Omega - q_x v_g + i\gamma_{\text{drift}}} = R(k, q_x) \quad (3.4.60)$$

This is no surprise, since zonal flow generation is due to the Reynolds work on the flow shear (i.e.,  $\langle \tilde{V}_x \tilde{V}_y \rangle dV_{ZF}/dx$ ) which is intrinsically a three-wave process. The diffusion equation for  $\langle N \rangle$  may also be straightforwardly derived by a Fokker-Planck calculation.

Here, one should recall that, in the absence of additional physics, the analogue of Liouville's theorem for a stochastic Hamiltonian system implies a partial cancellation between diffusion and drag terms, leaving a result equivalent to the quasi-linear equation derived above.

In the stochastic regime, the evolution of the drift wave spectrum is simple. The  $k_r$  spectrum spreads diffusively, with  $\langle \delta k_r^2 \rangle = D_k t$ . The random walk to larger  $k_r$  just reflects the random shearing at work on waves. The self-consistent dynamics of the drift-wave - zonal flow system are then described by the mean field equation for  $\langle N \rangle$  (rewriting Eq.(3.4.56))

$$\frac{\partial}{\partial t} \langle N \rangle - \frac{\partial}{\partial k_r} D_k \frac{\partial}{\partial k_r} \langle N \rangle = \langle C(N) \rangle \quad (3.4.61)$$

with Eq.(3.4.57c) and equations for the zonal flow intensity evolution.

### 3.5 The Drift Wave - Zonal Flow System: Self-Consistent State

In previous subsections, elementary processes for zonal flow dynamics were explained. These included the linear damping process, the bi-linear growth process, the back-reaction of zonal flows on drift waves, the nonlinear saturation mechanism and electromagnetic effects. Combining these elementary processes as building blocks, self-consistent states of the system are now discussed. As in the description in §3.4, explanations here are given which note the differences in the number of degrees of

freedom and in the correlation times of drift waves and zonal flows. Useful modelling of self-consistent states depends on these key factors, and the correspondence is listed in Table 3.5.1.

First, models with few degrees-of-freedom are explained by focusing on two examples. One is the quite generic predator-prey model (§3.4.5), which is valid for the case where many drift wave modes and zonal flow components are randomly excited, and their correlation times are much shorter than the characteristic time of evolution of the system. This basic model is explained in §3.5.1. The other is the opposite case where only one drift wave is unstable (with side-band modes linearly stable). The coupled modes are thus assumed to have long coherence times (§3.4.2), as in simple dynamical systems such as the Lorenz model. This case is explained in §3.5.2

Next, more detailed descriptions follow. The spectral shape is of considerable importance (as discussed in §3.4.3 and §3.4.4), and is explained within the scope of the induced diffusion model in §3.5.3. Coherent spatial structure is discussed in §3.5.4 and §3.5.5. These discussions correspond to the nonlinear mechanisms in §3.4.6 and §3.4.7, respectively.

### 3.5.1 Predator-Prey model

Drift waves excite zonal flows, while zonal flows suppress drift waves. The degree of excitation or suppression depends upon the amplitudes of the drift wave and zonal flow. These interactions are modelled as a predator-prey dynamical system, for zonal flow mean square shear  $\langle U^2 \rangle = \sum_{q_r} |U_{q_r}|^2$  and drift wave population density  $\langle N \rangle = \sum_k N_k$ . (See Eq.(3.4.23) and (3.4.32).)

#### (i) Stationary states

This system of Eqs.(3.4.32a) and (3.4.32b) has two types of steady-state solution. One is the solution without zonal flow

$$\langle N \rangle = \frac{\gamma_L}{\gamma_2}, \quad (3.5.1a)$$

$$\langle U^2 \rangle = 0, \quad (3.5.1b)$$

which results in the case of strong damping of the zonal flow,

$$\gamma_{\text{damp}} > \frac{C_{d \rightarrow Z}}{\gamma_2} \gamma_L. \quad (3.5.2)$$

The other is the state with zonal flow,

$$\langle N \rangle = \frac{\gamma_{\text{damp}}}{C_{d \rightarrow Z}}, \quad (3.5.3a)$$

$$\langle U^2 \rangle = \frac{1}{C_{d \rightarrow Z}} \left( \gamma_L - \frac{\gamma_2}{C_{d \rightarrow Z}} \gamma_{\text{damp}} \right), \quad (3.5.3b)$$

which is relevant when the damping rate of the zonal flow is weak,

$$0 < \gamma_{\text{damp}} < \frac{C_{d \rightarrow Z}}{\gamma_2} \gamma_L. \quad (3.5.4)$$

(The case of  $\gamma_{\text{damp}} = 0$  needs special consideration, as is explained later.)

This system is controlled by two important parameters, i.e., the linear growth rate of the drift wave  $\gamma_L$  and the damping rate of the zonal flow  $\gamma_{\text{damp}}$ . In the region of low zonal flow damping rate (as for Eq.(3.5.4)), the zonal flow coexists with the drift wave. The phase diagram is illustrated in Fig.3.5.1. The other important result is the role of  $(\gamma_L, \gamma_{\text{damp}})$  in determining the partition of the energy. In the region of low collisionality, where the zonal flow is excited, the drift wave amplitude is independent of the linear growth rate  $\gamma_L$ , but is controlled by the zonal flow damping rate  $\gamma_{\text{damp}}$ . The magnitude of the zonal flow increases if  $\gamma_L$  increases. The dependence on  $\gamma_L$  illustrates the importance of the self-nonlinearity effect of the zonal flow, which is discussed in Eq.(2.13). By use of a generic form  $\gamma_{NL}(U^2) \sim \alpha_2 U^2$ , the partition between the waves and zonal flows is explained in Eq.(2.14). The dependencies are shown, in Fig.3.5.2 for the case of fixed  $\gamma_L$  (Fig.3.5.2(a)) and the case of fixed  $\gamma_{\text{damp}}$  (Fig.3.5.2(b)), when the self-nonlinearity effect is present. The predator-prey model thus explains the most prominent features of the role of zonal flows in determining system behaviour. The possible shift of the boundary for the appearance of turbulence from  $\gamma_L = 0$  to  $\gamma_L = \gamma_{\text{excite}} > 0$  (so called Dimits shift for ITG turbulence) is discussed later.

## (ii) Dynamical behaviour

Equation (3.4.32) also describes the characteristic dynamics of the system. The fixed points Eqs.(3.5.1) and (3.5.3) are stable for a wide range of parameters. In some particular circumstances, different types of dynamics appear, as is categorized in [3.92].

**Stable fixed point:** At first, the stability of fixed points is explained. In cases where all of the coefficients (i.e.,  $\gamma_L$ ,  $\gamma_{\text{damp}}$ ,  $C_{d \rightarrow Z}$ ,  $\gamma_2$ ) are non-negative values,

$$\gamma_L \neq 0, \gamma_{\text{damp}} \neq 0, C_{d \rightarrow Z} \neq 0, \gamma_2 \neq 0 \quad (3.5.5)$$

the fixed points are stable. For instance, the perturbation near the stationary state of the solution Eq.(3.5.3),  $\{\delta\langle N \rangle, \delta\langle U^2 \rangle\} \propto \exp(i\omega t)$ , shows a damped oscillation with the frequency

$$\omega = \frac{-i\gamma_{\text{damp}}\gamma_2 + i\sqrt{\gamma_{\text{damp}}^2\gamma_2^2 - 4\gamma_{\text{damp}}\gamma_L(C_{d \rightarrow Z}^2 - C_{d \rightarrow Z})}}{2C_{d \rightarrow Z}} \quad (3.5.6)$$

The imaginary part of  $\omega$  is negative. Equation (3.5.3) predicts a stable fixed point. Depending on the initial conditions, transient oscillations of drift wave and zonal flow can occur. However, they decay in time and the system converges to a stationary solution.

**Repetitive bursts:** When the nonlinear self-stabilization effect of the drift waves is absent, i.e.,

$$\gamma_2 = 0, \quad (3.5.7)$$

periodic bursts of the wave and flow occur. In this case, Eqs.(3.4.32) has an integral of the motion; namely

$$\langle N \rangle - \frac{\gamma_{\text{damp}}}{\gamma_L} \ln \langle N \rangle + \langle U^2 \rangle - \ln \langle U^2 \rangle = \text{const.} \quad (3.5.8)$$

[3.93, 3.94]. A phase portrait for the system is given in Fig.3.5.3. Periodic bursts appear. The burst of the drift wave spectrum is followed by one of the zonal flow shear. However, this is unphysical for real drift wave turbulence, since the nonlinear self-interaction effects are essential to the turbulence dynamics.

**Single burst and quenching of waves:** When collisional damping of the zonal flow is absent, i.e.,

$$\gamma_{\text{damp}} = 0, \quad (3.5.9)$$

Eq.(3.5.1) requires particular care, because the relation  $\langle N \rangle = 0$  satisfies the RHS of Eq.(3.4.32). As is pointed out in [3.92, 3.44], the problem is a transient one, and the final, steady state depends on the initial condition. The trajectory  $(\langle N \rangle, \langle U^2 \rangle)$  satisfies

$$\frac{d\langle N \rangle}{d\langle U^2 \rangle} = \frac{\gamma_L - \gamma_2 \langle N \rangle - C_{d \rightarrow Z} \langle U^2 \rangle}{C_{d \rightarrow Z} \langle U^2 \rangle}, \quad (3.5.10)$$

which is solved to yield

$$\langle N \rangle = \frac{\gamma_L}{\gamma_2} - \frac{C_{d \rightarrow Z}}{\gamma_2 + C_{d \rightarrow Z}} \langle U^2 \rangle - c_0 \langle U^2 \rangle^{-\gamma_2/C_{d \rightarrow Z}}. \quad (3.5.11)$$

Here  $c_0$  is a constant which is determined by the value of  $(\langle N \rangle, \langle U^2 \rangle)$  at  $t = 0$ . The trajectory  $(\langle N \rangle, \langle U^2 \rangle)$  is shown in Fig.3.5.4 for various values of the initial condition.

The drift wave amplitude increases at first. Then energy is transferred to the mean square flow shear, and the wave energy is finally quenched, at a constant value of the amplitude of the flow. The state is related to the complete quench of wave energy near marginal stability, i.e., the so-called Dimits shift [2.50]. It may be viewed as the continuation of the trend  $N/\langle U^2 \rangle \sim \gamma_{\text{damp}}/\gamma_L$  to the limit where  $\gamma_{\text{damp}} = 0$ .

These features are also seen in the nonlinear coupling of different modes, being studied in relation with the L-H transition problems (e.g., [2.44, 3.95-3.106]). The phase portraits show differences in the underlying dynamics.

### 3.5.2 Single instability model

When only one drift wave is unstable, the primary drift wave and side-bands maintain a long coherence time. This is the opposite limit from the case (i), for which a reduced variable model applies. This case is explained in §3.4.2. A closed set of equations is derived for the amplitude of only one unstable mode,  $P$ , the amplitude of zonal flow,  $Z$ , the relative amplitude of side-band drift wave  $S$  and the frequency mismatch  $\Psi$  as Eqs.(3.4.8)-(3.4.11). This type of coherent interaction of model amplitudes appears in the Lorenz model, and other dynamical systems.

Equations (3.4.8)-(3.4.11) describe the parametric excitation for a fixed pump amplitude  $P$ , and give the zonal flow growth rate  $\gamma_{ZF}$ . The coupling to the primary wave, Eq.(3.4.8) accounts for the stabilizing effect of (nonlinearly driven) zonal flow on the primary drift wave. This system of equations has been analyzed for the problem of three-wave coupling [3.107]. The fixed point is given [2.23] by

$$P_* = \sqrt{\frac{\gamma_{\text{damp}}}{\gamma_L}} Z_* \quad (3.5.12a)$$

$$Z_* = \sqrt{\frac{(\omega_0 - \Omega_+)^2 + \gamma_{\text{side}}^2}{2 \gamma_L \gamma_{\text{side}}}} \quad (3.5.12b)$$

$$S_* = \sqrt{\frac{\gamma_{\text{damp}}}{2 \gamma_{\text{side}}}} Z_* \quad (3.5.12c)$$

$$\sin \Psi_* = \frac{\omega_0 - \Omega_+}{\sqrt{(\omega_0 - \Omega_+)^2 + \gamma_{\text{side}}^2}} \quad (3.5.12d)$$

For a fixed value of  $\gamma_L$  ( $\gamma_L$  is used as a normalizing parameter for obtaining Eqs.(3.4.8)-(3.4.11)), the dependence of the saturation amplitude on the damping rate of zonal flow is explained by Eq.(3.5.12). The amplitude of the primary unstable drift wave increases as  $\gamma_{\text{damp}}$  according to:

$$P \propto \sqrt{\gamma_{\text{damp}}}.$$

In the small  $\gamma_{\text{damp}}$  limit, the zonal flow amplitude  $Z_*$  remains constant, but the amplitudes of the primary wave and sidebands,  $P_*$  and  $S_*$ , vanish. These results are qualitatively the same as those of the model in §3.5.1. In this model, a forward Hopf bifurcation takes place, when  $\gamma_{\text{damp}}$  exceeds a threshold. Figure 3.5.5 illustrates the numerical calculation of the long time behaviour of the solution of Eqs.(3.4.8)-(3.4.11). In the case of small  $\gamma_{\text{damp}}$ , the solution converges to the fixed point in the phase space. In a limit of large  $\gamma_{\text{damp}}$ , the system exhibits chaos.

### 3.5.3 Saturation: determining the Drift Wave Spectrum

The wave spectrum contains additional freedom, and can influence the self-consistent state. Equations (3.4.20)-(3.4.22) form a set of nonlinear diffusion equations that determine the spectra of zonal flow and drift wave. [3.44]

The stationary state of the zonal flow is realized, as is seen from Eq.(3.4.21), by the balance between collisional damping and the bi-linear drive by the drift waves,

$$q_r^2 \sum_k D_q \frac{\partial}{\partial k_r} N_k = \gamma_{\text{damp}}. \quad (3.5.13)$$

On the other hand, the stationary state of the drift waves arises, as seen from Eq.(3.4.20), by the balance between linear drive and damping, nonlinear damping and  $k$  - space diffusion by the random zonal flows. Linear instability sits in the region of small  $|k_r|$ . In the absence of diffusion, the local (in  $k$ -space) balance

$$\gamma_L = \gamma_{NL} \quad (3.5.14)$$

gives the saturated state of drift waves. For a simple case of  $\gamma_{NL} = \gamma_2 N_k$ , Eq.(3.5.14) yields the saturation level

$$N_k = \gamma_L / \gamma_2 . \quad (3.5.15)$$

In the presence of random shearing by zonal flows, diffusion in the  $k$ -space occurs, and fluctuation energy is transferred to stable regions of  $k$ -space, as is illustrated in Fig.3.5.6.

### (i) Constant diffusivity

The case of constant diffusivity illustrates the competition between various effects. The simplest case of  $\gamma_{NL} = \gamma_2 N_k$  is chosen. The coefficients ( $\gamma_2$ ,  $D_k$ ) are independent of  $k_r$ . The linear growth rate is also independent of  $k_r$ , in both the stable region ( $|k_r| > k_{rc}$ ) and unstable region ( $|k_r| < k_{rc}$ ). (Such as the case of Fig.3.5.6.)

In this limit, Eq.(3.4.20) is modelled by a simple diffusion equation

$$-\gamma_L N_k + \gamma_2 N_k^2 - D_k \frac{d^2 N_k}{dk_r^2} = 0 . \quad (3.5.16)$$

This equation is solved by constructing a Sagdeev potential. Multiplying  $dN_k/dk_r$  by Eq.(3.5.16) and integrating over  $k_r$ , one has

$$\int^N \left( -\gamma_L N_k + \gamma_2 N_k^2 \right) dN_k - \frac{1}{2} D_k \left( \frac{dN_k}{dk_r} \right)^2 = \text{const} . \quad (3.5.17)$$

The boundary conditions:

$$\frac{dN_k}{dk_r} = 0 \quad \text{at } N_k = 0 \quad (\text{stable region, } |k_r| > k_{rc}) \quad (3.5.18a)$$

$$\frac{dN_k}{dk_r} = 0 \quad \text{at } k_r = 0 \quad (\text{unstable region, } |k_r| < k_{rc}) \quad (3.5.18b)$$

are natural choices. Equation.(3.5.17) yields integrals in two regions, namely  $|k_r| > k_{rc}$ , for which:

$$\frac{dN_k}{dk_r} = \pm \sqrt{\frac{1}{D_k} \left( -\gamma_L N_k^2 + \frac{2\gamma_2}{3} N_k^3 \right)} . \quad (|k_r| > k_{rc}) , \quad (3.5.19a)$$

and  $|k_r| < k_{rc}$  , for which

$$\frac{dN_k}{dk_r} = \pm \sqrt{\frac{1}{D_k} \left( -\gamma_L N_k^2 + \frac{2\gamma_2}{3} N_k^3 + \gamma_L N(0)^2 - \frac{2\gamma_2}{3} N(0)^3 \right)} , \quad (|k_r| < k_{rc}) \quad (3.5.19b)$$

respectively, where  $N_k = N(0)$  at  $k_r = 0$  . The relation Eq.(3.5.21) is illustrated in Fig.3.5.7.

Equations (3.5.19a) and (3.5.19b) are solved and reduced to quadrature as

$$\int_N^{\infty} \frac{dN_k \sqrt{D_k}}{\sqrt{\left( \gamma_L N_k^2 + \frac{2\gamma_2}{3} N_k^3 \right)}} = k_r \quad (|k_r| > k_{rc}) , \quad (3.5.20a)$$

$$\int_N^{N(0)} \frac{dN_k \sqrt{D_k}}{\sqrt{\left( -\gamma_L N_k^2 + \frac{2\gamma_2}{3} N_k^3 + \gamma_L N(0)^2 - \frac{2\gamma_2}{3} N(0)^3 \right)}} = k_r \quad (|k_r| < k_{rc}) . \quad (3.5.20b)$$

Two solutions to Eqs. (3.5.20a) and (3.5.20b) must be connected at

$$|k_r| = k_{rc} . \quad (3.5.21)$$

*This continuity condition determines  $N(0)$  as an eigenvalue.* As an illustration, a case of strong linear stability in the region  $|k_r| > k_{rc}$  is described here. In this case, the connection at  $|k_r| = k_{rc}$  requires

$$N(k_{rc}) = 0 . \quad (3.5.22)$$



That is,

$$\int_0^1 \frac{dn}{\sqrt{\left(1 - n^2 + \frac{2\gamma_L N(0)}{3\gamma_L} (n^3 - 1)\right)}} = k_{rc} \sqrt{\frac{D_k}{\gamma_L}} \quad (3.5.23)$$

where  $n(k_r) = N_k/N(0)$  is a normalized function that describes the shape of the spectrum. This relation (3.5.23) gives a relation between  $N(0)$ ,  $\gamma_L$  and  $D_k$  (i.e., the zonal flow amplitude), as

$$D_k = \frac{\gamma_L}{k_{rc}^2} \left( \text{LHS of Eq.(3.5.18)} \right)^2. \quad (3.5.24)$$

Equation (3.5.8) requires

$$\left[ q_r^2 \sum_k \frac{1}{B^2} \frac{k_{\theta}^2 k_r}{(1 + k_{\perp}^2 \rho_s^2)^2} R(q_r, k) \frac{\partial}{\partial k_r} n(k) \right] N(0) = \gamma_{\text{damp}}. \quad (3.5.25)$$

Equations (3.5.23) or (3.5.24) and (3.5.25) describes the self-consistent solution. Equation (3.5.19) shows that  $D_k$  (i.e., the mean square zonal flow amplitude) is an increasing function of  $\gamma_L$  but is a decreasing function of  $N(0)$ . Although the coefficient in the square bracket in Eq.(3.5.25) depends on  $\gamma_{\text{damp}}$  through the spectral shape function  $N(k_r)$ , Eq.(3.5.25) tells us that  $N(0)$  increases nearly linearly with respect to  $\gamma_{\text{damp}}$ , in the limit of small  $\gamma_{\text{damp}}$ .

Figure 3.5.8 illustrates the solution of Eqs.(3.5.23) or (3.5.24) and (3.5.25). The gradual change of the drift wave spectrum with the collisional damping is demonstrated. The features in Eqs.(3.5.23) - (3.5.25) are the ones clarified by the low-dimensional model in §3.5.1. Direct calculation of diffusion equation gives a smooth continuation from the collisionless regime to the regime of strong collisionality.

## (ii) Numerical solution

In more realistic examples, for which  $\gamma_L$  and  $D_k$  depend upon the wave-number  $k_r$ , a numerical solution of Eq.(3.5.20) is required. Examples of such a numerical solution of Eqs.(3.5.23)-(3.5.25) are quoted in Fig.3.5.9. The linear growth rate  $\gamma_L$  (right vertical axis) is assumed to be a smoothly decreasing function of  $k_r$ . The drift

wave spectrum  $N(k_r)$  is also shown for two time slices. One is in the early phase of the (temporal) growth of the wave energy. The other is at the time where the zonal flow reaches its peak and the waves are already subject to back reaction. In the early phase, the spectrum is concentrated in the region  $k_r \sim 0$ , where the mode has the largest growth rate. After being sheared by the driven zonal flow, the width of the spectrum increases. (i.e., about 1.5 times, measured by the half width at half maximum.)

The solution of the full diffusion equation recovers the basic trends of the low-degrees-of-freedom model. The drift wave amplitude goes to zero if  $\gamma_{\text{damp}}$  approaches to zero. However, there is a quantitative difference between the two models. The result of solution for the spectrum gives an empirical fit as [3.92]

$$\langle N \rangle \propto \gamma_{\text{damp}}^{0.75}. \quad (3.5.26)$$

This dependence is slightly weaker than that predicted by the predator-prey model, and than the analytical result in (i). This may be due to the fact that the change in spectrum shape due to finite  $\gamma_{\text{damp}}$  leads to the modification of the effective coupling coefficient  $C_{d \rightarrow z}$  which is averaged over the drift wave spectrum.

Temporal evolution is also investigated by the numerical solution for  $\langle N \rangle$  distribution function. In this case, the coupling coefficient  $C_{d \rightarrow z}$  is not constant in time, on account of the change of the spectral shape, and the result in §3.5.1 must be re-examined. By solution of the diffusion equation, the qualitative conclusion of the low-dimensional model is confirmed. Specifically:

- (a) the steady state is a stable fixed point, and the temporal solution converges after transient oscillations [ $\gamma_L \neq 0$ ,  $\gamma_{\text{damp}} \neq 0$ ,  $\gamma_2 \neq 0$  as is in Eq.(3.5.5)];
- (b) periodic bursts appear for  $\gamma_L \neq 0$ ,  $\gamma_{\text{damp}} \neq 0$ ,  $\gamma_2 = 0$  as is in Eq.(3.5.7), corresponding to a limit cycle attractor;
- (c) a single transient burst of drift waves is quenched by zonal flow for  $\gamma_L \neq 0$ ,  $\gamma_{\text{damp}} = 0$ ,  $\gamma_2 \neq 0$  as is in Eq.(3.5.9), corresponding to the Dimits shift regime.

The results are demonstrated in Fig.3.5.10. Figures.3.5.10(b) and (c) correspond to the trajectories in Figs. 3.5.3 and 3.5.4, respectively. They confirm the understanding which is obtained by use of a simple model in §3.5.1. Study of the transient phenomena by simulation [3.108, 3.109] is explained in Chapter 4.

### 3.5.4 Wave trapping and BGK solution

When the coherence time of the zonal flow and drift waves is much longer than the time scale of drift wave spectral evolution, trapping of drift waves by the zonal flow

may occur [2.36, 3.110-3.112]. For this, the relations  $\gamma_{\text{drift}} \ll \omega_{\text{bounce}}$  and  $\tau_{\text{ac, ZF}}^{-1} \ll \omega_{\text{bounce}}$  apply. In this case, the drift wave-packets have constants of the motions  $(k_{y0}, \omega_{k0})$  as is shown in Appendix A. Note that in this regime, the drift wave ray dynamics resemble those of a particle trapped in a single, large-amplitude plasma wave. Time asymptotically, then, the solution for  $N$  corresponds to a BGK solution, i.e., a time-independent solution parameterized by a finite set of constants of (in this case) the motion of the ray trajectory. As with all BGK solutions, there is no guarantee a particular solution is stable or is physically accessible. Additional physical considerations must be introduced or addressed to determine stability.

In this system, there are infinite number of constants of motion, because the wave kinetic equation (for  $\text{RHS} = 0$ ), like the Vlasov equation, is time reversible. Just as irreversibility enters the collisionless Vlasov problem when phase mixing of undamped Case-Van Kampen modes leads to Landau damping of (macroscopic - i.e., velocity integrated) Langmuir wave perturbations, irreversibility enters here when spectral integrals of  $N$  are computed. The BGK solution corresponds, in principle, to the finite amplitude, time-asymptotic state of such solutions. The distribution function can thus be written in terms of the constants of motion as Eq.(3.4.38). Noting that the trajectories are classified into untrapped and trapped orbits, Eq.(3.4.38) can be rewritten as

$$N(x, k_x, k_y) = N_U(\omega_{k0}(x, k_x), k_{y0}) + N_T(\omega_{k0}(x, k_x), k_{y0}) \quad (3.5.27)$$

where the suffixes  $U$  and  $T$  denote the untrapped and trapped wave-packets.

The self-consistent solution is given by Eqs.(3.4.37) and (3.5.27). Rewriting the integration variable in the RHS of Eq.(3.4.37) from  $(k_x, k_y)$  to  $(\omega_{k0}, k_{y0})$ , one has

$$\left(u \frac{d}{dx} - \gamma_{\text{damp}}\right) V_{\text{ZF}} = -\frac{d}{dx} \int_{-\infty}^{\infty} dk_y k_y \left\{ \int_{w_m}^{\infty} dw J N_U + \int_{w_{\min}}^{w_m} dw J N_T \right\} \quad (3.5.28)$$

where  $w = -\omega_{k0}/k_{y0}$ ,  $J$  is the Jacobian of the transformation of variables,  $w_m$  is the value of  $w$  at the separatrix, and  $w_{\min}$  is  $w$  at  $k_x = 0$  [2.36].

The distribution functions  $N_U$  and  $N_T$  have infinite degrees of freedom, and flattening (i.e., plateau formation) might take place (and likely *does*) in  $N_T(\omega_{k0}(x, k_x), k_{y0})$ . Schematic distribution may be the one in Fig.3.5.11. Choosing a particular class of the functions  $N_U(\omega_{k0}(x, k_x), k_{y0})$  and  $N_T(\omega_{k0}(x, k_x), k_{y0})$ , a self-consistent solution  $V_{\text{ZF}}$  has been obtained from Eq.(3.5.28). For instance,

$N_U(\omega_{k0}(x, k_x), k_{y0})$  is chosen to have a Lorentzian shape with respect to the constant of motion  $w = -\omega_{k0}/k_{y0}$ . In Fig.3.5.11, the distribution function in the trough (solid line) and that at the peak (dashed line) are shown, when the zonal flow is given as in Fig.3.4.2. Trapping of wave-packets in the well of  $V_{ZF}$  means that the wave density is high at the trough.

The accessibility and stability of a particular distribution function require future research.

### 3.5.5 Zonal flow quenching and coherent structure

If wave trapping is not complete, a coherent structure of the zonal flow is formed by drift wave turbulence. This is the case for  $\gamma_{\text{drift}} > \gamma_{ZF}$ ,  $\omega_{\text{bounce}}$ , and  $\tau_{ac, ZF}^{-1} \ll \gamma_{ZF}$ . The case where the turbulent drift wave spectrum forms such a spatially coherent zonal flow structure is discussed in this section.

If the asymmetric deformation of the distribution function  $N(k_x)$  is calculated to higher order in the zonal flow vorticity  $U$ , the correction of order  $U^3$  tends to reduce asymmetry. This is reasonable, since the third order contribution is stabilizing. This situation is illustrated in Fig.3.5.12. For the case of  $U > 0$ , modification of  $\delta N$  is positive for  $k_x > 0$ , so as to increase  $U$ . The third order term has the opposite sign, so as to suppress the growth of the zonal flow. [3.90, 3.113]

Taking into account the modification of the growth rate of the zonal flow, the dynamical equation for the zonal flow is written in an explicit form as Eq.(3.4.47). By use of normalized variables  $x = r/L$ ,  $\tau = t/t_Z$  and  $\hat{U} = U/U_0$ , where  $L^{-2} = q_{r0}^2(1 - \mu)$ ,  $t_Z = D_{rr}^{-1} q_{r0}^{-2}(1 - \mu)^{-2}$  and  $U_0^2 = D_{rr} D_3^{-1}(1 - \mu)$ , Eq. (3.4.47) is rewritten in the collisionless limit as

$$\frac{\partial}{\partial \tau} \hat{U} + \frac{\partial^2}{\partial x^2} \hat{U} - \frac{\partial^2}{\partial x^2} \hat{U}^3 + \frac{\partial^4}{\partial x^4} \hat{U} = 0. \quad (3.5.29)$$

The short wavelength components with  $q_r^2 L^2 > 1$  are stabilized by the higher-order derivative term. The flow is generated at the large scale  $q_r^2 L^2 < 1$ , and the zonal flow energy is saturated by nonlinear coupling to higher-order dissipation, via  $\hat{U}$  steepening. Note that Eq.(3.5.29) is a 1D nonlinear wave equation for  $\hat{U}$ , which states that  $\hat{U}$  grows and nonlinearly couples to small scale dissipation via 'wave function' steepening (i.e., nonlinear flow shear amplifications.).

The case that the flow is generated from a state with low noise level, where no net flow momentum exists, ( $\int dx \hat{U} = 0$ ), is studied. Here the flow evolves satisfying the

condition  $\int dx \hat{U} = 0$ . A stationary solution of Eq.(3.5.29) in the domain  $0 < x < d$ , for the periodic boundary condition, is given by an elliptic integral as

$$\int_{-u_c}^0 (1 - 2u^2 + u^4 - \kappa^2)^{-1/2} du = \pm \frac{x}{\sqrt{2}}, \quad (3.5.30)$$

where  $\kappa$  is an integral constant ( $0 \leq \kappa < 1$ ) given by the periodicity constraint

$\int_{-u_c}^{u_c} (1 - 2u^2 + u^4 - \kappa^2)^{-1/2} du = d/2\sqrt{2}n$  ( $n = 1, 2, 3, \dots$ ). The integer  $n$  is the one which is closest to  $d/n = 4\sqrt{2}\pi$ .) Numerical solution of Eq.(3.5.29) has shown that the solution (3.5.30) is stable and is an attractor. Figure 3.5.13 illustrates the stable stationary state. Compared to a simple sinusoidal function (eigenfunction of the linear operator), the result in Fig.3.5.13 has much weaker curvature at the peak, and is closer to a piecewise constant function.

The normalized function  $u(x)$  is of the order of unity, so that the characteristic values of vorticity and scale length  $l$  are given as

$$U_0 = D_{rr}^{1/2} D_3^{-1/2} (1 - \mu)^{1/2}, \quad (3.5.31)$$

$$l = q\bar{\tau}_0^{-1} (1 - \mu)^{-1/2}. \quad (3.5.32)$$

The amplitude of zonal flow is given as  $V_0 = lU_0$ . From Eqs.(3.2.51) and (3.4.46), one can obtain an order of magnitude estimate of  $D_3/D_{rr}$ . The ratio  $D_3/D_{rr}$  is characterized by  $D_3 \sim k_\theta^2 l^2 \Delta\omega_k^{-2} D_{rr}$ . One has an estimate  $U_0 = v_z l^{-1} (1 - \mu)^{1/2}$ , where  $v_z = \Delta\omega_k k_\theta^{-1}$ . The flow velocity  $V_0 = U_0 l$  is given as

$$V_0 = v_z (1 - \mu)^{1/2}. \quad (3.5.33)$$

This result gives an expression for the zonal flow in terms of the decorrelation rates of drift waves. Combining this with the dynamical equation which dictates the drift wave fluctuations, e.g., Eq.(3.5.16), the amplitude of the self-consistent state may be derived. Further research is necessary to understand the significance of these results..

### 3.5.6 Shift of the boundary for drift wave excitation

When coupling with zonal flow is taken into account, the boundary in the parameter space for the excitation of turbulent transport is modified. The shift of the excitation boundary is one aspect of characteristic nonlinear interactions. The shift is

noticed in the context of subcritical excitation of turbulence (see, e.g., [3.114-3.116] and a review [3.117]). The shift also appears for supercritical excitation [3.118-3.123]. The case of ITG coupled with zonal flow also belongs to this class of stability boundary shifts.

The mutual interaction of fluctuations with different scale lengths has been studied [3.118]. The component with longer wave length is called 'intermediate scale' and that with shorter wave length is called 'micro'. In the presence of mutual interaction, the phase diagram is illustrated in Fig.3.5.14. The boundary for the excitation of the micro mode is no longer  $\gamma_L^{\text{micro}} = 0$  but shifted to a positive value of  $\gamma_L^{\text{micro}}$ . In the absence of the intermediate scale mode, the micro mode is excited for  $\gamma_L^{\text{micro}} > 0$ . However, when the intermediate scale mode is excited  $D^{\text{intermediate}} > 0$ , the micro mode is quenched in the vicinity of the stability boundary  $\gamma_L^{\text{micro}} \sim 0$ , and is excited at finite level only if the growth rate exceeds a substantially larger value,  $\gamma_{\text{crit}}^{\text{micro}}$ . This constitutes an upshift of the boundary for excitation of the turbulence. An analysis of the coupling between ITG and current diffusive ballooning mode is reported in [3.121] and the case of the ITG and ETG is given in [3.123]. These examples also exhibit stability boundary upshifts. (See also the simulation study [3.124, 3.125].)

In the case of drift waves coupled to zonal flow, the 'micro' fluctuation is the drift wave, and the zonal flow plays the role of the 'intermediate scale' fluctuation. For transparency of argument, we take here the limit of vanishing collisional damping of zonal flow, i.e.,

$$\gamma_{\text{damp}} = 0.$$

The shift of the boundary for the excitation of the drift waves from  $\gamma_L^{(\text{DW})} = 0$  occurs if the zonal flow has finite amplitude for very small amplitude of the drift wave [3.126], i.e.,  $\langle U^2 \rangle \neq 0$  at  $\langle N \rangle = 0$ . In the other limit of large growth rate, the increase of the drift wave amplitude  $\langle N \rangle$  by the increase of  $\gamma_L^{(\text{DW})}$  requires self-stabilization of the zonal flow. Examples of such self-nonlinear effects are the  $\gamma_{\text{NL}}(V^2)$  term in Eq.(2.10b) or the  $U^3$  term in Eq.(3.5.29). Summarizing these, the stability boundary for the zonal flow in the  $(U^2, \langle N \rangle)$  plane should have the form as is illustrated in Fig.3.5.15(a). That is, the boundary for the marginal stability condition  $dU_{\text{ZF}}/dt = 0$  (solid line in Fig.3.5.15(a)) intersects the boundary  $\langle N \rangle = 0$  at a finite value of the zonal flow amplitude (denoted by  $U_{\text{crit}}$ ). This allows a finite amplitude of zonal flow at a very low level of drift wave fluctuation. In this circumstance, the boundary for the drift wave excitation shifts from  $\gamma_L^{(\text{DW})} = 0$  to  $\gamma_L^{(\text{DW})} = \gamma_{\text{crit}} > 0$ . The dotted line in Fig.3.5.15(a) illustrates the boundary of the marginality condition for the growth of drift waves from the case of  $\gamma_L^{(\text{DW})} = \gamma_{\text{crit}}$ .

Below the critical value of the growth rate, a steady-state solution is allowed for  $\langle N \rangle = 0$ . Figure 3.5.15(b) illustrates the partition of the energy between drift waves and zonal flow as a function of the growth rate of the drift waves. The waves are not sustained in steady-state below the critical value  $\gamma_L^{(DW)} < \gamma_{crit}$ . After the transient growth of waves, the zonal flow can be sustained at a finite value, and this level is dependent on the initial condition. If the critical growth rate is exceeded, i.e.,  $\gamma_L^{(DW)} > \gamma_{crit}$ , both waves and flows are excited. The estimate of the drift wave amplitude for the case when the excitation of zonal flow is ignored, is denoted by a thin dotted line.

Noting the presence of critical value of zonal flow vorticity  $U_{crit}$ , a phase diagram in the  $(\gamma_L, \gamma_{damp})$  plane is shown schematically in Fig.3.5.16 [3.126].

The mechanism that gives the finite values of the critical vorticity of the zonal flow has been discussed in [3.126]. The key is the determination of the self-nonlinear damping term for the zonal flow growth, e.g.,  $\gamma_{NL}(U_{ZF}^2, \langle N \rangle)$ , as in Eq.(2.10b). The marginal condition for the zonal flow growth is thus expressed as

$$\gamma_{NL}(U_{ZF}^2, \langle N \rangle) = \alpha \langle N \rangle. \quad (3.5.34)$$

### 3.6 Suppression of turbulent transport

Mean shear flow and zonal flow can reduce or quench transport by altering either the turbulent fluctuations amplitude or the wave-particle correlation time, which determines the 'cross-phase' between, say  $\tilde{V}_r$  and  $\tilde{n}$ , in the particle flux  $\Gamma_r = \langle \tilde{n} \tilde{V}_r \rangle$ . Up till now, we have been primarily concerned with effects on the fluctuation intensity. However, both zonal and mean shears can alter the correlation times and thus fluxes, *even at fixed fluctuation amplitude*. In this section 3.6, we examine shear flow effects on transport. We begin by considering the effect of sheared mean and zonal flows on transport of a passive scalar by an otherwise fixed or prescribed ensemble of turbulence.

#### 3.6.1 Passive scalar transport: sheared mean flow

The average cross field flux is given in terms of cross correlations between various fluctuation fields. For instance, the radial particle flux is given by:

$$\Gamma_r = \frac{1}{B} \langle \tilde{n} E_\theta \rangle \quad (3.6.1)$$

This flux, an averaged quantity, is determined by the amplitudes of density and electric field, *and* by the phase between them. In the case of electrostatic fluctuations,  $\Gamma_r$  can be written as:

$$\Gamma_r = \frac{1}{B} |\tilde{n}| |\tilde{E}_\theta| \sin \alpha \quad (3.6.2)$$

where  $\alpha$  is the phase difference between the density and potential fluctuations.  $\alpha$  is determined by the wave-particle correlation time and by the response function.

Obviously, shifting alpha can reduce (or increase) the flux.

Here, we investigate the effect of mean shear on transport by analyzing the response of a passive, phase-space field  $f$  (i.e., a distribution function) to a given ensemble of turbulence. A model equation for the passive advection of  $f$  in the presence of prescribed fluctuating  $\tilde{v}$  is:

$$\frac{\partial f}{\partial t} + v_{\parallel} \hat{b} \cdot \nabla f + \langle V \rangle \cdot \nabla f + \tilde{v} \cdot \nabla f - D_c \nabla^2 f = 0. \quad (3.6.3)$$

Here  $\langle V \rangle = V_y(x) \hat{y}$  is the mean sheared  $E \times B$  flow,  $v_{\parallel}$  is the parallel phase-space velocity and  $D_c$  is the collisional diffusion coefficient. We focus on strong turbulence, and consider the asymptotic limit where  $D_c \rightarrow 0$ . [3.127, 3.128]

Following the standard methodology of renormalized turbulence theory, the equation for the response of  $\tilde{f}$  to  $\tilde{v}$  can be written as:

$$-i \left( \omega - k_{\parallel} v_{\parallel} - k_y x S_v + i/\tau_{ck} \right) \tilde{f}_{k, \omega} = -\tilde{v}_{x, k, \omega} \frac{d}{dx} f_0, \quad (3.6.4)$$

(Here:  $S_v = dV_{E \times B}/dx$  and  $f_0$  is the average part of  $f$ .) Note that Eq.(3.6.4) contains many time scales for irreversible dynamics, which must be considered. These are:

a)  $\Delta\omega_k$  - the mode self-correlation decay rate, or inverse life time, due to nonlinear scrambling;

b) Doppler spread (autocorrelation) rates:

$\left| \frac{d\omega_k^2}{dk^2} \Delta k^2 \right|$  - the spectral self-spreading (autocorrelation) rate, i.e., the inverse lifetime of the spectral pattern (reflects the effect of dispersion - linear process);



$|k_{\parallel} v_{\parallel} \Delta x|$  - the parallel Doppler spread (autocorrelation) rate, i.e., the rate at which parallel Doppler shift  $k_{\parallel} v_{\parallel}$  changes with radius;

$|k_y S_v \Delta x|$  - the shearing Doppler spread (autocorrelation) rate, i.e., the rate at which the sheared  $E \times B$  flow-induced Doppler shift  $k_y V_{E \times B}$  changes with radius;

c) Decorrelation rates

$k_x^2 D_x$  - particle decorrelation rate for radial scattering;

$(k_y^2 D_y S_v^2)^{1/3}$  - particle decorrelation rate for hybrid of radial scattering in sheared flow, i.e., due to random walk in shearing coordinates,

$(k_{\parallel}^2 v_{\parallel}^2 D_x)^{1/3}$  - particle decorrelation rate for radial scattering in a sheared magnetic field.

Here  $\Delta x$  is the radial spectral width,  $D_x$  is the radial test diffusion coefficient,  $k'_{\parallel} = k_{\parallel}/L_s$  and  $L_s$  is the shear length. Hereafter, parallel dynamics are ignored. Shearing becomes of importance when

$$|k_y S_v \Delta x| \geq k_x^2 D_x \sim \frac{D_x}{\Delta x^2}, \quad |k_y S_v \Delta x| \geq \Delta \omega_k \quad (3.6.5).$$

In this case, the relevant decorrelation rate is set by

$$1/\tau_{ck} = (k_y^2 D_y S_v^2)^{1/3}. \quad (3.6.6)$$

A formal solution for  $\tilde{f}_{k, \omega}$  can be written as

$$\tilde{f}_{k, \omega} = \frac{-i \tilde{v}_{x, k, \omega}}{\omega - k_{\parallel} v_{\parallel} - k_y x S_v + i \tau_{ck}^{-1}} \frac{d}{dx} f_0. \quad (3.6.7)$$

The cross field flux of  $f$ ,  $\Gamma_f \equiv \langle \tilde{f}^* \tilde{v}_x \rangle$ , is then given by

$$\Gamma_f = \text{Re} \sum_{k, \omega} \frac{i |\tilde{v}_{x, k, \omega}|^2}{\omega - k_{\parallel} v_{\parallel} - k_y x S_v + i \tau_{ck}^{-1}} \frac{d}{dx} f_0. \quad (3.6.8)$$

For  $k_y S_v \Delta x \gg k_{\parallel} v_{\parallel}$ , but  $|k_y S_v \Delta x|$  or  $|\Delta k d\omega_k/dk|$  greater than  $\Delta\omega_k$  and  $\tau_{ck}^{-1}$ ,  $\Gamma_f$  can be simplified to

$$\Gamma_f \cong -\pi \sum_{k, \omega} |\tilde{v}_{x,k}|^2 \delta(\omega_k - k_y S_v x) \frac{d}{dx} f_0 \quad (3.6.9)$$

(An analytic expression  $\text{Im} \left( \omega - k_y x S_v + i k_y^2 D_y \right)^{-1} \cong -\pi \delta(\omega - k_y x S_v)$  is used.) Note that here  $\mathbf{k} = (m, n)$  and  $x$  is measured relative to the rational surface  $r_{m,n}$  where  $\mathbf{k} \cdot \mathbf{B} = 0$ , so that  $x = r - r_{m,n}$ . Of course,  $\tilde{v}_{x,k,\omega} = \tilde{v}_{x,k,\omega}(r - r_{m,n}) = \tilde{v}_{x,k,\omega}(x)$ . Using the familiar change of integration variables:

$$\iint dm dn = R \iint dm dx \left| \frac{k_y}{L_s} \right|$$

the cross-field flux then reduces to:

$$\Gamma_f \cong -\pi \iint dm d\omega R \left| \frac{k_y}{L_s} \right| \frac{|\tilde{v}_{x,k}|^2}{|k_y S_v|} \frac{d}{dx} f_0. \quad (3.6.10)$$

Note that the flux depends on the spectral intensity at the resonance point  $x_r = \omega/k_y S_v$ . The assumption that this point falls within the spectral envelope is valid if  $x_r < \Delta x$  or equivalently,  $\omega < |k_y S_v \Delta x|$ . Since we are concerned with the regimes of strong shear, this is almost always the case. In such strong shear regimes, then,  $\Gamma_f$  scales inversely with  $S_v$ , i.e.,

$$\Gamma_f \propto S_v^{-1}, \quad (3.6.11)$$

A detailed analysis in [3.128] established that the passive scalar amplitude perturbation scales as

$$\sqrt{\langle (\tilde{f}/f)^2 \rangle} \propto S_v^{-5/6} \quad (3.6.12)$$

so that

$$\sin \alpha \propto S_v^{-1/6}. \quad (3.6.13)$$

Note that the effect of even strong shear on the flux is modest ( $\sim S_v^{-1}$ ) and its impact on the cross-phase is quite weak ( $\sim S_v^{-1/6}$ ). Thus, the theory predicts that suppression of the cross phase is weaker than reduction in turbulence intensity.

It is interesting to examine the scaling of  $D_x$  in the strong turbulence regime, for weak and strong shear. Noting that  $\Gamma_f = -D_x \frac{d}{dx} f_0$ , we have already established that  $D_x \sim S_v^{-1}$  for strong shear and weak turbulence. In the case of strong shear and strong turbulence,  $\tau_{ck}^{-1} > |k_y S_v \Delta x|$ , so  $\Gamma_f$  is given by (from Eq.(3.6.8)):

$$\Gamma_f = -\text{Re} \sum_{k, \omega} \tau_{ck} \left| \vartheta_{x, k, \omega} \right|^2 \frac{d}{dx} f_0 \quad (3.6.14)$$

i.e.,  $D_x = \tau_{ck} \langle \vartheta^2 \rangle$ . Taking Eq.(3.6.6) with  $D_x = D_y$  then gives

$$D_x \sim \frac{\langle \vartheta^2 \rangle^{3/4}}{(k_y S_v)^{1/2}} \quad (3.6.15)$$

which is consistent with the expected scaling  $D_x \sim \omega_b (\Delta x_T)^2$  where  $\omega_b$  is the particle bounce time in a poloidal wavelength, and  $\Delta x_T$  is the resonance width in radii.

Next, for the strong turbulence, weak shear case  $1/\tau_{ck} = k_x^2 D_x$ , so

$$D_x \sim \frac{\langle \vartheta^2 \rangle^{1/2}}{(k_x^2)^{1/2}} \quad (3.6.16)$$

which is the familiar scaling for transport in strong 2D turbulence, first derived by Taylor and McNamara. Finally, we also note that the regime of strong shear (i.e.,

$|k_y S_v \Delta x| > \tau_{ck}^{-1}, \Delta \omega_k, \omega$ ) but with non-resonant response has also been investigated

[3.127]. The predictions are

$$\Gamma_f \sim S_v^{-2} \quad (3.6.17a)$$

and

$$\sin \alpha \propto S_v^{-2} \quad (3.6.17b)$$

The importance of this regime is quite unclear, though, since strong shear naturally favours a large shearing Doppler spread which, in turn, suggests the applicability of standard quasilinear theory, and the occurrence of a resonant interaction.

### 3.6.2 Passive scalar transport: zonal flows

In the previous subsection, we considered the effect of a mean shear flow on passive scalar flux and cross phase. While understanding the case of a mean shear is necessary, it is certainly *not sufficient* for an understanding of the effects of a spectrum of zonal flows upon transport. Two additional features must be considered in the case of zonal flows. These are:

- (a) the flow pattern has a finite lifetime or self-correlation time,  $\tau_{c, ZF}$  ;
- (b) shearing occurs as a *spectrum* of scales, each corresponding to a radial zonal flow wavenumber  $q_r$  . The shearing pattern may be spatially complex.

The implication of differences (a) and (b) are that the effectiveness of shearing will be reduced (relative to that for equal strength mean flow) for short  $\tau_{c, ZF}$  , and that one should expect to find  $S_{v, rms}$  (the root mean square value) replacing  $S_v$  in the quasilinear predictions given above, when  $\tau_{c, ZF} \rightarrow \infty$  . The details of these calculations are presented in the literature. [129]

### 3.6.3 Reduction of turbulent transport

The results in § 3.6.1 and 3.6.2 imply that the scaling of transport in a shear flow is not universal, and turbulent transport must be computed by specifying a relaxation mechanism. In addition, the amplitude of the fluctuating velocity field and characteristic correlation length must be determined simultaneously by considering the effects of  $E_r$  and  $dE_r/dr$  , and their spectra. Some representative analyses of the calculation of turbulent transport are reported here.

Several analyses have been performed for ITG modes, e.g., [3.130-3.132]. An expression for the turbulent transport coefficient has been proposed [3.132]:

$$\chi_{turb} = \frac{(\gamma_L - \omega_{E1} - \gamma_{*1})^{1/2} \gamma_d^{1/2}}{k_y^2} \quad (3.6.18)$$

where  $\gamma_L$  is the linear growth rate in the absence of flow shear,  $\omega_{E1}$  is the  $E \times B$  flow shear frequency

$$\omega_{E1} = \frac{r}{q} \frac{d}{dr} \left( \frac{q E_r}{r B} \right), \quad (3.6.19)$$

$\gamma_{*1}$  is the shear of the diamagnetic flow,  $\gamma_d$  is the damping rate of a representative zonal flow mode. The latter is approximated in [3.132] as

$$\gamma_d \approx 0.3(T/T_e)\omega_M \quad (3.6.20)$$

( $\omega_M$  is the toroidal magnetic drift frequency), and  $k_y$  is the poloidal wavenumber of the most unstable mode. The dependence of  $\chi_{\text{turb}}$  on  $\omega_{E1}$  is adjusted to the results of nonlinear simulation, i.e., the expression represents a fit to data.

In the case of self-sustaining CDIM turbulence, the thermal diffusivity has been predicted to be [3.82, 3.133]

$$\chi_{\text{turb}} \sim \frac{1}{\left(1 + 0.5G_0^{-1}\omega_{E1}^2\right)} \frac{G_0^{3/2}}{s^2} \left(\frac{c}{\omega_p}\right)^2 \frac{v_{Ap}}{a} \quad (3.6.21)$$

where  $\omega_{E1} = k_\theta \tau_{A\theta} E'_r / B$ ,  $G_0$  is normalized pressure gradient and  $\langle k_\perp^2 \rangle \propto \left(1 + 0.5G_0^{-1}\omega_{E1}^2\right) G_0^{-1}$ . As the gradient of radial electric field becomes larger, the correlation length becomes shorter. In toroidal geometry (i.e., CDBM turbulence), the normalized parameter  $\omega_{E1} = \tau_{A\theta} (dE_r/dr) / srB$  controls the turbulence level and turbulent transport [3.74]. The effects of  $E \times B$  flow shear and magnetic shear complement each other. This shear dependence is also found for the case of the ITG mode.

The electron temperature gradient (ETG) mode has a shorter characteristic wave length. This fact suggests that the  $E \times B$  flow shear has a weaker effect. However, extended streamers could be affected by  $E \times B$  shear, and the transport by ETG modes could then also be affected. Current research indicates that some transfer mechanism of ETG energy to longer scale (either, say, by streamer formation or by inverse cascade to  $c/\omega_{pe}$ ) is necessary for ETG turbulence to be of practical interest to tokamak confinement. The electron gyro-Bohm thermal diffusivity, i.e.,  $\chi_{e, \text{GB}} = \rho_e^2 V_{\text{Th},e} / L_{Te} = \sqrt{m_e / m_i} \chi_{i, \text{GB}}$ , is too small to be relevant. Further study is required to understand the relation of transport by shorter wavelength turbulence to electric field shear [3.118, 3.123, 3.134, 3.135].

In addition to the inhomogeneity of flow across the magnetic surfaces, the inhomogeneity on the magnetic surface is also effective in suppression of turbulence. The toroidal flow in tokamaks varies in the poloidal direction if a hot ion component exists. This poloidal dependence suppresses turbulence [3.82].

The dependence of  $\chi_{\text{turb}}$  on  $\omega_{E1}$  has also been explained experimentally. The expression

$$\chi_{\text{turb}} \propto \frac{1}{1 + (\omega_{E1}/\gamma)^h} \quad (3.6.22)$$

has been derived analytically with an index  $h$  ( $\gamma$  is the decorrelation rate or instability growth rate in the absence of  $E \times B$  shear). The index is given as  $h = 2$  in the models [3.73-3.75] and as  $h = 2/3$  in the strong shear limit in [2.7]. A nonlinear simulation has suggested a dependence as that in equation (3.6.13) for the case of ITG mode turbulence. Further elaboration of theory is required in order to derive a formula which is relevant in a wide parameter region. A comparison of the index  $h$  with experimental observations has been reported [3.136] for when the electric field bifurcation is controlled by an external bias current. The result is in the range of  $h \approx 2$  [3.136], but the comparison is not yet conclusive [3.137-3.139].

### 3.6.4 Self-regulated state

The final solution of the turbulent transport problem requires a self-consistent solution for the turbulent heat flux and the zonal flow. The level of the turbulence-generated  $E \times B$  shearing rate in formula in §3.6.3, e.g., Eq. (3.6.22), must be determined *self-consistently* from the dynamics of the drift wave - zonal flow. Here research in this direction is discussed.

Let us illustrate the problem by a model of two scalar variables from the discussion of §3.4, as

$$\frac{\partial}{\partial t} E_{\text{DW}} = \gamma_{\text{L}} E_{\text{DW}} - \alpha E_{\text{ZF}} E_{\text{DW}} - \omega_2 E_{\text{DW}}^2, \quad (3.6.23a)$$

$$\frac{\partial}{\partial t} E_{\text{ZF}} = -\gamma_{\text{damp}} E_{\text{ZF}} + \alpha E_{\text{DW}} E_{\text{ZF}} - \gamma_{\text{ZF}, N2} E_{\text{ZF}}^2, \quad (3.6.23b)$$

where  $E_{\text{DW}}$  and  $E_{\text{ZF}}$  are the quadratic amplitudes (i.e., the fluctuation energy density) of the turbulence and the vorticity of zonal flow. This set of model equations includes processes like the suppression of turbulence by zonal flow ( $\alpha E_{\text{ZF}}$ ), the excitation of zonal flow by turbulence ( $\alpha E_{\text{DW}}$ ), the collisional damping of the zonal flow ( $\gamma_{\text{damp}}$ ), nonlinear damping via self-interaction of drift waves and nonlinear saturation mechanism of the zonal flow. (The nonlinear saturation mechanism is symbolically expressed as  $\gamma_{\text{NL}} = \gamma_{\text{ZF}, N2} E_{\text{ZF}}$  for zonal flow, and  $\Delta\omega_k = \omega_2 E_{\text{DW}}$  for drift waves. Both represent nonlinear transfer to dissipation.) The resulting formula of transport coefficient depends on the competition between the terms  $\gamma_{\text{damp}} E_{\text{ZF}}$ ,  $\alpha E_{\text{DW}} E_{\text{ZF}}$ ,  $\omega_2 E_{\text{DW}}^2$  and  $\gamma_{\text{ZF}, N2} E_{\text{ZF}}^2$ .

#### (i) Collisional damping limit

The simplest case is that for which the quasilinear drive of zonal flow by turbulence is balanced by collisional damping. In this case, Eq.(3.6.23b) gives  $E_{DW} = \gamma_{damp}/\alpha$ . The physics of this result is simple - the fluctuation level adjusts so that the zonal flow is marginally stable. That is, the saturated level of turbulence is independent of the magnitude of the drive of linear instabilities, but is controlled by the damping rate of the zonal flow. Alternatively put, the zonal flow regulates the fluctuation level and the flow damping regulates the flow, so the *flow damping* thus regulates fluctuations and transport. In this case, an analytic result is easily derived, and one obtains a stationary state in a dimensional form

$$\frac{e\tilde{\phi}}{T_e} \approx \sqrt{\frac{\gamma_{damp}}{\omega_*}} \frac{\rho_s}{L_n} \quad (3.6.24)$$

where  $\tilde{\phi}$  is the amplitude of fluctuations in the range of drift wave frequency and  $\gamma_{damp}$  is the damping rate of the zonal flow. The right hand side is reduced by a factor  $\sqrt{\gamma_{damp}/\omega_*}$ , as compared to the mixing length levels, due to zonal flow effects.

Numerical simulations have confirmed the essential weak turbulence limit, i.e.,  $\langle (e\tilde{\phi}/T_e)^2 \rangle \propto \gamma_{damp}/\omega_*$ , not  $|e\tilde{\phi}/T_e|_{rms} \propto \gamma_{damp}/\omega_*$ . The damping rate of the zonal flow ( $\gamma_{damp}$ ) is proportional to the ion-ion collision frequency in the high temperature limit (see §3.1.3). As a result, the level of fluctuations that induces transport is controlled by ion collisions, although the fluctuation spectrum itself is composed of 'collisionless' waves. The transport coefficient follows as

$$\chi_i \approx \frac{\gamma_{damp}}{\omega_*} \frac{\rho_s}{L_n} \frac{T}{eB} \sim \frac{v_{ii}}{\omega_*} \frac{\rho_s}{L_n} \frac{T}{eB} \quad (3.6.25)$$

This scales as a gyro-reduced Bohm thermal diffusivity, 'screened' by the factor of  $\gamma_{damp}/\omega_*$ . Of course, retaining non-adiabatic electron effects complicates the questions of collisionality scaling.

## (ii) Nonlinear saturation mechanism

In high temperature plasmas, where  $v_{ii}/\omega_* \rightarrow 0$  holds, the saturation of the zonal flow is influenced by nonlinear processes. These processes are discussed in §3.4. Possible nonlinear saturation processes include the trapping of drift waves in zonal flows, excitation of *tertiary* instabilities, quenching of zonal flow drive by drift wave spectrum modification, and others. The formal solution of Eq.(3.6.23) can be rewritten

$$E_{ZF} = \alpha \gamma_{ZF}^{-1/2} E_{DW}, \quad (3.6.26a)$$

$$E_{DW} = \frac{1}{1 + \alpha^2 \omega_2^{-1} \gamma_{ZF, N2}^{-1}} \frac{\gamma_L}{\omega_2} \quad (3.6.26b)$$

Because of the production of zonal flow, the usual fluctuation saturation level is 'screened' by the factor of  $\left(1 + \alpha^2 \omega_2^{-1} \gamma_{ZF, N2}^{-1}\right)^{-1}$  as compared to the level  $\gamma_L/\omega_2$ .

Thus, the nonlinear stabilization of turbulence may be dominated by the zonal flows shearing channel, instead of the usual mixing process, i.e.,  $\alpha^2 \omega_2^{-1} \gamma_{ZF, N2}^{-1} > 1$ . (This is the case that is often observed in nonlinear simulations. It is important, however, to keep in mind that most nonlinear simulations address the regime near marginal stability.) In this case, the turbulent transport coefficient is reduced by the factor of  $\alpha^{-2} \omega_2 \gamma_{ZF, N2}$ .

$$\chi_i = \frac{\omega_2 \gamma_{ZF, N2}}{\alpha^2} \chi_{i,0} \quad (3.6.27)$$

where  $\chi_{i,0}$  is the predicted thermal conductivity in the absence of the zonal flow.

Obtaining an explicit formula for the nonlinear suppression mechanism (the term  $\gamma_{ZF, N2}$ ) is a topic of current research, and a final answer has not yet been determined.

However, if one employs one example from the model of nonlinear reduction of zonal flow drive, one has

$$\chi_i = \frac{1}{1 + \tau_c^2 v_z^2 q_r^2} \chi_{i,0} \quad (3.6.28)$$

where  $v_z \simeq V_d$  is the saturation velocity of the zonal flow,  $q_r$  is the wave number of zonal flow, and  $\tau_c$  is the correlation time of turbulence. In the vicinity of the stability boundary, where the correlation time of turbulence is expected to be very long, the reduction of turbulent transport is quite strong. If the drive of turbulent transport becomes stronger (i.e., going further from marginality) and  $\tau_c v_z q_r \simeq 1$  holds, then the parameter dependence of  $\chi_i$  becomes similar to that of  $\chi_{i,0}$ .

### (iii) Role of GAM

When the damping of zonal flow is strong,  $\gamma_{damp} > \gamma_L \alpha / \omega_2$ , the zonal flow may not be excited, but the GAM is still driven. As is discussed in §3.3.2, the fluctuation levels are suppressed by a factor of  $\left(1 + \tau_c \tau_{c, GAM} \left\langle k_\theta^2 \tilde{V}_{GAM}^2 \right\rangle\right)^{-1}$ , where  $\tilde{V}_{GAM}$  is the  $E \times B$  velocity associated with the GAM, and  $\tau_{c, GAM}$  is the autocorrelation time of the GAM. In the large-amplitude limit, the suppression factor is given by Eq.(3.3.35).



This suppression factor is derived for the condition that the source of turbulence is unchanged. As discussed in §3.1.3, the GAM is subject to collisional damping. The saturation mechanism and saturation level of the GAM have not yet been determined. Links between the driven GAM and poloidally-asymmetric cross-field transport have been suggested [3.140]. The accumulation of fluctuation energy in a finite poloidal region, which is coupled to zonal flow dynamics, has also been discussed [3.141]. Calculation of turbulent transport, which is regulated by GAM, is left for future research.

## Chapter 4. Numerical Simulations of Zonal Flow Dynamics

### 4.1. Introduction

Direct nonlinear simulation (DNS) studies have played a crucial role in the development of research on zonal flows. The synergy between the theory and DNS has been a key promoter-of-interest in the physics of the zonal flows. Although the technical details of direct numerical simulation techniques are beyond the scope of this review, the physical results of nonlinear simulations are reviewed here, in order to illustrate elementary dynamics and processes of the drift wave –zonal flow system.

There are several steps in reviewing the understanding which has been facilitated by DNS. These should be addressed in sequence. The first is modeling, i.e., reduction to basic equations appropriate for plasma geometry. Although the rate of development of computational power has been tremendous, the direct computational solution of the primitive nonlinear plasma equations (such as the Klimontovich or Vlasov equations in real geometry and for an actual size) is still far beyond the computational capability of even the foreseeable future. Thus, reduced modelling has been employed to simplify the basic dynamical equations. The main representative models and hierarchical relations among them are explained in Appendix B. (Keywords for various reduced equations are explained in this appendix.) The second is the selection of important elementary processes in zonal flow and drift wave systems. We here focus on following issues:

- i) Generation of zonal flow by turbulence,
- ii) Shearing of turbulence by zonal flow,
- iii) Co-existence of zonal flow and drift waves,
- iv) Nonlinear states,
- v) Collisional damping,
- vi) Dependence on global plasma parameters,
- vii) Nonlinear phenomena.

For these elementary processes, the results of DNS are explained in the following.

Third, several important features of zonal flows have been *discovered* by DNS studies. Therefore, the historical development is also described, though bounded by considerations of brevity.

The observation of zonal flow by DNS has been reported in the last two decades for various types of plasma turbulence. Figure 4.1 is one early example [2.6], in which the formation of a quasi-symmetric isopotential contour, loosely resembling that of the magnetic surface, is demonstrated. These contour structures indicate the presence of a banded poloidal  $\mathbf{E} \times \mathbf{B}$  flow, called a zonal flow.

It should be stressed again that the objective of the explanation here is an illustration of elementary physical processes of zonal flows. The examples are chosen primarily from the DNS of core turbulence, i.e., ‘Gyro-Bohm’ drift-ITG turbulence. It is

well known that the progress in the DNS studies for plasma turbulence and zonal flows is not limited to this class of examples. Readers are suggested to refer to related reviews on DNS of the subject (for instance, see [4.1]). In the following subsections, the progress in DNS of drift-ITG turbulence with zonal flow is reviewed together with the specification of simulation methods.

## **4.2. Ion Temperature Gradient Driven Turbulence**

### **4.2.1 Models and geometry**

Research on zonal flows in plasma physics simulation community has exploded in the 90's and still continues so, to date. This happened as it becomes more obvious that, independent of simulation method, simulation domain, and boundary conditions, zonal flows play a dominant role in regulating ion temperature gradient (ITG) driven turbulence, which is a prime candidate for the anomalous ion heat transport ubiquitously observed in most plasmas in tokamaks[2.16]. This progress also paralleled the advances in both gyrokinetic and gyrofluid simulation methods for various geometries. We summarize the highlights of this story in a roughly chronological order.

Exploiting the governing equations of plasma microturbulence, gyrokinetic simulations are based on the nonlinear gyrokinetic description of plasmas, in which the full charged particle kinetic dynamics in a strong magnetic field is simplified, using the disparity between the spatio-temporal scales of the phenomena of interest, and the scale of the magnetic field inhomogeneity and the gyroperiod as leverage. As a consequence, the gyro-center distribution function is defined in a five-dimensional phase space, after decoupling and elimination of the gyromotion. The perpendicular velocity enters parametrically. The wavelengths of instabilities can be comparable to the size of an ion gyroradius. Some DNS approaches use the particle-in-cell simulation method, which is Lagrangian in character (i.e., particles are pushed) while others use the continuum Vlasov approach which is Eulerian in character (i.e., the gyrokinetic equation is solved as a partial differential equation). While, to date, most simulations in toroidal geometry have used the conventional nonlinear gyrokinetic equation[4.2], which ignores the parallel acceleration nonlinearity which is formally weaker, some simulations[4.3] have used a fully nonlinear energy-conserving form of the nonlinear gyrokinetic equation[4.4]. Gyrofluid models are then derived from the gyrokinetic equations by taking moments[4.5]. Some kinetic effects, such as linear Landau damping and a limited form of nonlinear Landau damping, have been included in gyrofluid models while others have not. Most notably, gyrofluid models do not accurately treat nonlinear wave-particle interaction. (See Fig.4.2.)

Regarding simulation geometry, global simulations typically use a domain which spans a macroscopic fraction of the tokamak volume. Annular domains are sometimes

used as an option. Radial variation of gradient quantities, such as temperature gradient and magnetic shear, is allowed in global simulations. Of course, questions concerning mean profile evolution persist. Flux-tube simulations are restricted to a local domain of a few turbulence correlation lengths and assume the existence of a scale separation between the turbulence and equilibrium profiles, and so do not accurately represent mesoscale dynamics. Typically, radially periodic boundary conditions are used and the gradient quantities are treated as constant within a simulation domain.

#### 4.2.2. Adiabatic electrons and conventional collisionless gyrokinetic ions

We start from the simplest case of the collisionless limit in order to explain some of key elements of zonal flow DNS. In this subsection, illustrations are given on the issues of i) generation of zonal flow by turbulence, ii) shearing of turbulence by zonal flows, iii) coexistence of zonal flow and drift waves, and some aspects of iv) dependence of dynamics on global parameters,.

*Historical overview :* While zonal flows with large radial scales (the system size - so as to render them indistinguishable from mean flows) were observed in ITG simulations in a simple geometry in early 80's[4.8], it was in early gyrofluid[4.9] and gyrokinetic[4.10] simulations of toroidal ITG turbulence, where fluctuating sheared  $E \times B$  flows driven by turbulence with a radial characteristic length comparable to that of ambient turbulence (several ion gyro-radii), began to appear and attract attention. These simulations were either quasi-local in the flux-tube domain [2.15, 2.17, 3.36, 4.7], or in a sheared slab geometry[3.88]. On the other hand, early global gyrokinetic simulations of ITG turbulence either did not address[4.8, 4.9] nor find the effects of fluctuating  $E \times B$  flows[4.10] on turbulence to be significant. The reason for this is as follows. Early global gyrokinetic simulations [4.9, 4.10] had relatively small system size (in ion gyro-radius units), and consequently had rather sharp radial variations of pressure gradient. Zonal flows with scale lengths of the system size have been the dominant feature in these simulations [4.10]. In other words, the simulation domain was so small that it was effectively impossible to distinguish between zonal and mean flows. Even as more codes were independently developed, this qualitative difference between global simulations [4.3, 4.11] and flux-tube simulations [3.36, 4.7] continued, and fomented lingering doubts as to the proper treatment and possible existence of such fluctuating flows. However, as computing power became sufficient to handle larger system size, the finer scale flows began to appear in global gyrokinetic simulations [4.3], although its effect on steady state transport was not observed to be as significant as that seen in the flux tube simulations.

The importance of these small scale zonal flows in regulating turbulence in the tokamak has begun to be widely appreciated, as gyrokinetic simulations[2.16] in both full torus and annulus geometry (with various boundary conditions), for which radial

variations of the pressure gradient are mild, have produced results which exhibit the importance of the fluctuating flows with qualitatively similar characteristics as those in flux-tube simulations[2.17, 2.50, 3.36]. Inclusion of zonal flows in gyrokinetic simulations[2.16] significantly reduces the steady state ion thermal transport, as reported earlier[3.36, 2.50]. Figure 4.3 illustrates some of characteristic results for the effects of zonal flows on ITG turbulence. Isodensity contours are shown. Fluctuations in the presence of zonal flow, Fig.4.3(a), have shorter correlation length and lower saturation level, in comparison to the case where zonal flows are suppressed, Fig. 4.3(b). A similar illustration for noncircular plasma is reproduced as Fig.4.3(c).

The dynamics of coupling between drift waves and zonal flow has been explicitly analyzed by DNS. This simulation has directly tested the physics of modulational instability process, as well. Figure 4.4 illustrates the *generation of zonal flow by turbulence* and the back reaction of zonal flow shear onto that turbulence. In this study, the ITG turbulence freely grows to a saturation, with zonal flows suppressed. This generates a stationary spectrum or 'gas' of ITG modes. (Thick solid line, being followed by thin solid line (c)). In the second run, the turbulence first develops to saturation without zonal flow, but then flow evolution is restored to the system (after  $t \approx 40 L_n/c_s$  in this simulation). The zonal flow *then* starts to grow exponentially (thin solid line (a) plotted on a logarithmic scale), and reaches a new stationary state. As the amplitude of the zonal flow increases, the turbulence level decreases. (Thick solid line (b).) Note that the new stationary level is much smaller than the reference case. The modulational instability of a zonal flow spectrum to a test shear is thus established by the observed exponential growth. The reduction in turbulence level confirms the expectation that the zonal flow shearing will reduce turbulence levels.

*The shearing of turbulence* by zonal flow is also clear. The key mechanism of the turbulence suppression is as explained in §3. One new significant finding from this simulation is a broadening of the  $k_r$  spectrum of turbulence due to self-consistently generated zonal flows, as shown in Fig. 4.5. It is in agreement with the expectation that an eddy's radial size will be reduced as shown by the contours of density fluctuations in Fig. 4.3. These also agree (qualitatively) with theoretical expectations of the reduction of radial correlation length due to the shearing by  $\mathbf{E} \times \mathbf{B}$  flow [2.7, 2.8]. The quantitative analysis of the turbulence shearing rate is explained below.

The zonal flows observed in simulations[2.16, 3.36, 4.12] contained significant energy in  $k - \omega$  bands, with radial scales and frequencies comparable to those of the turbulence. It was therefore of vital importance to extend the nonlinear theory of turbulence decorrelation by the mean  $\mathbf{E} \times \mathbf{B}$  flow shear[2.7, 2.8] to address the effect of rapid-time-varying  $\mathbf{E} \times \mathbf{B}$  flow shear in regulating turbulence. This was needed for a better quantitative understanding of the nonlinear simulation results. An analysis of the nonlinear gyrofluid simulation results indicated that the instantaneous  $\mathbf{E} \times \mathbf{B}$  shearing

rate associated with self-generated zonal flows exceeds the maximum linear growth rate by an order of magnitude, while the turbulence fluctuation amplitude definitely remained above the thermal noise level, and the ion thermal transport remained significantly anomalous[4.12]. This was somewhat puzzling since in the cases with mean  $E \times B$  shear flows, which are now either measured or calculated from data in existing toroidal devices, many leading experimental teams observed that their plasmas made transitions to enhanced confinement regimes[3.137, 4.13] when the  $E \times B$  shearing rate in general toroidal geometry[4.14] exceeded the linear growth rate of microinstabilities in the absence of the  $E \times B$  shear. This puzzle can be resolved by considering the following points.

One thread of thought is to look at fine space-time scales of zonal flow shearing rate. Fluctuating sheared  $E \times B$  flows play an important role in saturating the turbulence[2.15, 2.17, 3.36, 3.88, 4.7]. These flows are typically of radial size  $k_r \rho_i \sim 0.1$ , but contain of a broad  $k_r$  spectrum of shears. Since the  $E \times B$  shearing rate is proportional to  $k_r^2 \phi$ , the high  $k_r$  component of  $\phi$ , although small in magnitude, can contribute significantly to the  $E \times B$  shearing rate. Indeed, for  $|\phi_k|^2 \sim k^{-\alpha}$ , the shear spectrum actually increases with  $k$  (until FLR effects, etc., kick in), i.e.,  $|V_k|^2 \sim k^{4-\alpha}$ , unless  $\alpha > 4$ , which is unlikely. The instantaneous  $E \times B$  shearing rate, which varies in radius and time, can be much higher than the maximum linear growth rate for a significant portion of the simulation domain. An example is shown in Ref.[3.77]. Of course, shearing depends on the lifetime of the shearing pattern, as well as on the shear strength, as discussed in section 3.6.

Specifically, using gyrofluid-simulation zonal flow spectra and time-history data to calculate the correlation time of zonal flows, the effective shearing rate in Ref.[4.12], which reflects the fact that fast-varying components of the zonal flow shear are relatively ineffective in shearing turbulence eddies, has been evaluated for each  $k_r$ . It has a broad peak at low to intermediate  $k_r$ , and becomes smaller at high  $k_r$ , as shown in Fig. 3 of Ref[4.12]. Higher  $k$  components of the shear flows, while strong, have short correlation time. Overall, this rate is *comparable* to the linear growth rate. This seems qualitatively consistent with considerable reduction, but not the complete suppression, of turbulence (as observed in simulations). The expression for the effective shearing rate is presented in Sec.4.5. where we discuss the role of Geodesic Acoustic Modes (GAM) [3.5]. The instantaneous  $E \times B$  shearing rate from global gyrokinetic particle simulations is also dominated by high  $k_r$  components, and varies roughly on the turbulence time scales as reported in Ref.[4.12]. It is much larger than the maximum linear growth rate for a significant portion of the simulation domain.

The other thread of thought is to reconsider the heuristic rule-of-thumb estimate for turbulence quenching,  $\gamma_{E \times B} = \gamma_L$  [2.17]. Though handy and dandy, this formula

has several limitations. First, the nonlinear theory [2.7, 2.8, 2.9] tells that  $\gamma_{E \times B}$  should be compared to the turbulent decorrelation rate,  $\gamma_{NL}$ , not to  $\gamma_L$ . It should be noted that it is much easier to calculate  $\gamma_L$  than  $\gamma_{NL}$ , so that this is one reason why many experimental results were ‘analyzed’ in this simplified context. While  $\gamma_L$  can be used as a rough measure of strength of ambient turbulence when an estimation of  $\gamma_{NL}$  is not available, the limitation of this approximation is obvious.

The dependence on global parameters in the *collisionless* limit is discussed here. One finding of DNS is the complete suppression of the ITG mode near the linear stability boundary. In the regime of a weak linear growth rate, the initial value problem of DNS showed that the ITG turbulence can first grow but is then quenched by the induced zonal flow. This zonal flow can be strong enough to reduce the ion thermal transport to a value which is nearly zero, within the resolution [2.50] of the simulation. Such transient evolution, and later quench of turbulence have been confirmed by DNS. This is the so-called “Dimits shift”, indicating a nonlinear upshift of the threshold for an ITG-driven thermal fluxes. In essence, the Dimits shift regime is one where expansion free energy is transferred to the zonal flows, with relatively little remaining in the drift waves. As a result, the heat flux vs. gradient curve is ‘upshifted’ – hence the name. The Dimits shift regime is, to a large extent, a consequence of the approximation of zero or very low collisionality. A well known example is from a simplified set of equilibrium parameters from the case of DIII-D H-mode plasma [4.15]. For this particular set of parameters, the critical value of the ion temperature gradient has been effectively increased from  $R/L_{Ti} = 4$  to  $R/L_{Ti} = 6$  due to the undamped component of zonal flows. Note that both linear and the up-shifted thresholds are, in general, functions of  $s/q$ ,  $T_e/T_i$ , and  $R/L_n$ . Figure 4.6 illustrates the turbulent transport coefficient in a stationary state as a function of the ion temperature gradient ratio. In collisionless simulations, turbulence is completely quenched slightly above the linear stability threshold. The up-shift of the threshold for the onset of turbulence is observed. When the driving source of turbulence (temperature gradient in this case) becomes larger, the turbulence level starts to increase, as summarized in Fig.4.6

It has been emphasized that low frequency turbulence in confined plasmas should be considered as a self-regulating, two-component system consisting of the usual drift wave spectrum and the zonal flows [2.13]. One of the early indications for the coexistence of the zonal flow and turbulence is shown in Fig.4.7. In this simulation, the co-existence of drift waves (with finite  $k_\theta$ , and frequencies comparable to the diamagnetic frequency) with the poloidally-symmetric ( $k_y = 0$ ) short-scale-length zonal flow perturbations (called radial modes, here) is clearly demonstrated.

The partition of the excited energy between the turbulence and flows is explained in §3. The partition has also been examined in the DNS. While the gyrokinetic approach is desirable for quantitative studies of this issue, as demonstrated in Ref. [4.15], a

simpler model can illustrate the main trend. One of the examples from a fluid simulation of toroidal ITG turbulence is presented in Fig.4.8 [4.16]. Near the linear stability boundary, nearly all of the energy is carried by the flow. When the temperature gradient (and consequently the linear growth rate  $\gamma_L$ ) increases, both the turbulence energy and flow energy increase. As is explained in §3.5, the rate of increment of the turbulence energy and that of flow energy are dependent on the nonlinear saturation mechanism for the zonal flow. Theoretical analysis is in qualitative agreement in this issue of energy partition, but has yet to provide a satisfactory quantitative answer. In particular, the branching ratio between zonal flow and drift wave turbulence is set by the ratio of wave growth to flow damping (collisional and otherwise). For modest collisionality, near threshold,  $E_{\text{flow}}/E_{\text{wave}} \sim \gamma_L/\gamma_{\text{damp}}$ .

An approach to the total quench of turbulence in the Dimits shift regime has also been studied in DNS. Transient bursts of turbulence energy have been observed in direct simulations with various level of modelling. The evolution was studied in the context of various models, e.g., in the convection problem [3.108] and a detailed Vlasov model of 1D ITG turbulence (near the stability boundary) [3.109]. Figure 4.9 illustrates an example of the results of the Vlasov model study.

Before closing this subsection, a distinction caused by models is noted. Global gyrokinetic particle simulations and flux tube gyrofluid simulations display many common features of the physics of zonal flows, despite differences in simulation methods, simulation domains, and boundary conditions. However, the following quantitative difference between them exists. Short wavelength components of zonal flows are more prominent in flux-tube gyrofluid simulations, as compared to gyrokinetic simulations. However, according to estimation from nonlinear gyrofluid simulation, most of the shearing is done by the low to intermediate  $k_r$  part of the zonal flow spectrum. Since the long wavelength components of zonal flows are more prominent in global gyrokinetic simulations, as compared to the flux-tube gyrofluid simulations, one can speculate that the higher value of steady state ion thermal diffusivity typically observed in gyrofluid simulation (in comparison to that seen in gyrokinetic simulation) is partially due to an underestimation of the low  $k_r$  component of the zonal flows. These components of zonal flows which are undamped by collisionless neoclassical process [2.40] were inaccurately treated as completely damped in the original gyrofluid closure [3.36]. This undamped component of the zonal flows (hereafter, we will call it the Rosenbluth-Hinton zonal flow) is of practical importance because it can upshift the threshold value of the ion temperature gradient for ITG instability.

#### **4.2.3. Simulations with additional effects: neoclassical damping of zonal flows, nonadiabatic electrons, and velocity space nonlinearity**



Other fundamental issues of the zonal flow are its neoclassical (both collisional and collisionless) damping, nonadiabatic electron effects, and phase space dynamics. We now discuss these effects.

The aforementioned example of the Rosenbluth-Hinton (RH) zonal flow [2.40] illustrates the importance of a correct treatment of zonal flow damping in predicting the levels of turbulence and transport. This motivated further research on the neoclassical damping of zonal flows and its effect on turbulence. When  $\mathbf{E} \times \mathbf{B}$  flow is initialized in a toroidal plasma and allowed to relax in the absence of turbulence and collisions, its poloidal component is damped due to the variation of  $B$  in the poloidal direction. The damping occurs due to the “transit-time magnetic pumping” [3.9], and in the long term it evolves to a finite RH residual flow level.

The collisionless neoclassical process (transit-time magnetic pumping) induces decay of the flow. The evolution of the flow could be viewed as a superposition of the RH zonal flow of zero frequency and the GAM oscillation, which decays via transit-time magnetic pumping. In Fig.4.10, the evolution of the electrostatic potential (averaged over the magnetic surface) is illustrated, where the initial condition is chosen as a high amplitude zonal flow. A simple adiabatic electron model and the one which includes electron effects and electromagnetic effects are compared in DNS [3.34]. The simple model of adiabatic electrons captures an essential part of the physics, as zonal flows in this system are mostly governed by ion dynamics, more specifically the neoclassical polarization shielding [2.40] and geodesic curvature coupling. In the long term, the flow converges to a level predicted by neoclassical theory [2.40].

In the banana collisionality regime, this short (transit) timescale, collisionless damping accompanied by GAM oscillation is followed by a slower collisional damping. A decay of zonal flows due to ion-ion collisions occurs via a number of different asymptotic phases [2.41], but most of the damping occurs on a time scale  $\tau_{ii} \approx \epsilon/v_{ii}$ , as summarized in Sec. 3.1.5.

The important role of collisional damping of zonal flows in regulating transport has been nicely demonstrated by gyrokinetic particle simulations[2.49]. Even a very low ion-ion collisionality, which is typical of core plasmas in present day tokamaks, was enough to enhance turbulence level by the reducing the amplitude of zonal flows. The changes in the linear growth rates of ITG modes were negligible. Near and beyond the ITG linear threshold, collisional damping of zonal flows was responsible for a non-zero level of ion thermal transport, and thereby effectively softened the nonlinear upshift of the ITG threshold. Equivalently stated, the presence of collisional damping eliminated the Dimits shift regime. Figure 4.11 shows the turbulent transport coefficient as a function of the ion collisionality for the parameters of  $R/L_T = 5.3$ . This parameter is in the “Dimits shift” regime (i.e., practically no turbulent transport, although the ITG is linearly unstable) for  $v_{ii} = 0$ . As the ion collision frequency increases, the level of zonal flow is

reduced, and the turbulent transport increases concomitantly, as predicted by theoretical models. The theory of collisional damping of the zonal flow explains this parameter dependence well. Note again that the linear growth rate  $\gamma_L$  is essentially not influenced by the ion collision frequency, for this set of parameters. The change of the turbulence transport is not caused by a change in  $\gamma_L$ , but by the damping rate of the zonal flow. It is worth emphasizing here that the turbulent transport coefficient often has very different dependence on global parameters, in comparison to those of  $\gamma_L$ . This is a simple consequence of self-regulation – flows damp the drift waves and collisions damp the flows, so collisions (more generally, zonal flow damping) ultimately regulate the turbulence. A schematic drawing of the self-regulation is illustrated in Fig.4.12.

It should be noted that system states are not always fixed points. Near the threshold, the two component system consisting of zonal flows and ambient turbulence has exhibited a bursty cyclic behavior, with a period proportional to the zonal flow decay time  $\sim \tau_{ii} \approx \epsilon/\nu_{ii}$ . It is interesting to note that this is a well-known feature of a predator-prey type dynamical system which has been widely used in transport barrier formation models [4.17, 4.18]. More details on the effect of collisional zonal flow damping on ITG turbulence and transport from gyrofluid simulation with flux boundary conditions were recently reported [4.19]. In this study, the authors reported that the increase in the zonal flow  $\mathbf{E} \times \mathbf{B}$  shearing rate is responsible for the increase in the energy confinement as one decreases the collisionality. It is worthwhile to note that this simulation confirms that the transport reduction occurred via the reduction in fluctuation amplitude, via the shearing mechanism we discussed in detail in Sec 3.6.

We note that a theory [3.127] suggesting that most transport reduction due to  $\mathbf{E} \times \mathbf{B}$  shear flow comes from the change in phase relation between the fluctuating radial velocity (transporter) and the quantity which is transported (transportee) has been proposed. Significant theoretical disagreements have emerged concerning this claim [3.128, 4.20]. Indeed, simulations in Ref. [4.19] show that the change in the cross-phase was negligible while transport varied significantly. An example is quoted in Fig.4.13. The same conclusion can also be drawn [4.21] from the proportionality between transport and fluctuation intensity during the bursting phase observed in Ref. [2.49]. Thus, indications at present favour amplitude reduction as the primary mechanism for transport quenching.

Nonadiabatic electron response (which depends on collisionality) can also change the linear drive of ITG instability. Thus, it is of practical interest to address how the electron-ion collisions can modify transport near marginality i.e., in the Dimits-shift regime via their effect on electrons. For high density core plasmas in tokamaks, such as the one encountered in Alcator C-Mod, the trapped electron response is dissipative (i.e.,  $\nu_{ei}\epsilon^{-1/2} > \omega_{*e}$ ). Thus the additional linear drive of ITG instability, due to trapped electrons, scales roughly with  $\omega_{*e}/(\nu_{ei}\epsilon^{-1/2})$ , modifying the predictions based on a

purely electron adiabatic response. From continuum gyrokinetic simulations in flux-tube geometry [4.22], results indicated that the nonlinear upshift of the ITG threshold *decreases* as the electron-ion collisionality decreases, and the nonadiabatic electron contribution to the linear drive increases. At higher collisionality, nonadiabatic electron effects get weaker, and a significant nonlinear *up*-shift occurs, as predicted by ITG simulation with adiabatic electron response. In the collisionless or low collisionality regime, nonadiabatic trapped electron response can significantly enhance drift-ITG instability drive, even near the ITG marginal point. The concomitant increase in turbulence and zonal flow amplitudes can be sufficient to drive the zonal flows into a strongly nonlinear regime, where collisionless (nonlinear) flow damping significantly exceeds the now familiar collisional damping, thus breaking the scaling of fluctuation intensity with collisionality. Indeed, some hints of a robust nonlinear saturation process for zonal flow were observed in a recent global PIC simulation of collisionless trapped electron mode (CTEM) turbulence [4.23]. In that study, the spectrum of zonal flow was significantly broader in frequency and shorter in radial wavelength than for comparable cases of pure ITG turbulence with adiabatic electrons. The influence of non-adiabatic response of electrons is also illustrated in Fig.4.14. Two cases, without and with, are compared. The two-dimensional power spectrum of the flux-surface-averaged electrostatic potential for electrostatic adiabatic electron turbulence is shown. The zonal flow spectrum is narrowly peaked about  $\omega \approx 0$ , together with the peak at the GAM frequency. The spectrum for electromagnetic kinetic electron turbulence shows a more turbulent zonal flow spectrum. In the presence of nonadiabatic response of electrons, the power spectrum of the zonal flow component becomes wider. [4.23] Thus, seemingly paradoxically, collisionless electron effects can alter the collisionality scaling of drift wave turbulence. Of course, for larger  $v_{ee}$ , the nonadiabatic electron response decreases, thus restoring collisionality dependence via the zonal flow damping.

Some global simulations have suggested there is an interesting link between zonal flows and ‘non-locality’ phenomena in drift or ITG turbulence. ‘Non-local phenomena’ is a catch-all which generically includes mesoscale dynamics associated with avalanches, turbulence spreading, etc. Of particular note here is turbulence spreading [4.24, 4.25], and the mesoscale patterns which form in drift-zonal flow systems. Figure 4.15 shows a spatially inhomogeneous, and in fact highly corrugated and structured, pattern of turbulence level intensity and zonal flow radial electric field. Simply put, the turbulence level is large in the  $E_r$  trough and relatively small in regions of strong  $E_r$  shear. Such a pattern quite likely was formed by a process where by:

- i) a finite region of instability produced growing fluctuations
- ii) these fluctuations naturally drove zonal flow (with preferred radial wave length) growth, implying a concomitant decrease in their intensity levels, and the formation of fluctuation intensity *gradients*,

- iii) the steepened intensity gradient in turn stimulated turbulence spreading via the spatial scattering associated with nonlinear mode coupling,
- iv) the subsequent growth of the zonal flows, following the spreading turbulence.

Such a mechanism could create the corrugated profiles observed in the simulation. Indeed, the corrugated fluctuation intensity profile may be thought of as a “turbulence suppression wave”, which is at first propagating, and later standing. Of course, some additional physics is necessary to explain the apparent quenching of turbulence at  $E_r$  maxima. For this, zonal flow curvature effects on turbulence (which is explained in §3.4.6) are likely candidates. Flow curvature can squeeze or dilate fluctuation wave structures, and thus has an effect which is sign-dependent.

Tertiary instabilities have been discussed in DNS results by a number of authors. For instance, the growth rate of the tertiary instability for an observed zonal flow structure has been reported in [2.51] and is reproduced in Fig.16. The simulation has suggested the possibility that the growth of the zonal flow is quenched by the onset of the tertiary instability. (A similar argument was advanced by [4.27] in the case of ETG.)

Most simulations mentioned above have used the conventional nonlinear gyrokinetic equation [4.2], which ignores the velocity space nonlinearity. The latter is formally smaller than the  $\mathbf{E} \times \mathbf{B}$  nonlinearity. It is commonly believed that this omission of velocity space nonlinearity does not cause a serious problem, if one focuses on practically oriented issues, such as the comparisons of the linear growth rates, turbulence and transport levels in the post nonlinear saturation phase, etc. However, the conventional nonlinear gyrokinetic equation fails to obey the fundamental conservation laws, such as energy (of particles and fluctuation fields), and phase space volume, at a non-trivial order. For longer times, well after the initial nonlinear saturation of turbulence, even very small errors in the governing equation can accumulate in time, regardless of computational method, and muddy the physics predictions. A recent simulation [4.26] in cylindrical geometry used a fully nonlinear energy conserving and phase space conserving form of the nonlinear gyrokinetic equation [4.4]. The importance of using governing equations with proper conservation laws is demonstrated in this series of simulations, with and without velocity space nonlinearity. The authors reported that neglecting velocity space nonlinearity in an ITG simulation resulted in undesirable consequences. The energy was no longer conserved between particles and fluctuating fields, and a precious indicator of the quality of numerical integration was lost. The zonal flow pattern and the radial heat transport pattern were affected as well. The results are presented in Fig. B1, since it highlights an issue related to reduction of equations discussed in Appendix B.

It is worthwhile to note that velocity space nonlinearity of electrons has been considered in the context of the electron drift kinetic equation for the drift wave problem in a sheared slab geometry [4.28]. In this continuum Vlasov simulation, the parallel

trapping of electrons due to velocity space nonlinearity has been resolved by using a sufficient number of grid points ( $\sim 100$ ) in 1-D velocity space. It was found that this velocity space nonlinearity significantly affects the spectral transfer in  $k_{\parallel}$ , especially between convective cells (including zonal flows) and the ambient turbulence. The resulting turbulence and transport levels are also significantly affected. This effect is most pronounced at zero magnetic shear, but gradually gets weaker as magnetic shear increases. Obviously more simulations with sufficient resolution are required to understand the role of velocity space nonlinearity, nonlinear Landau damping [2.18, 4.29] in the presence of zonal flows [4.30, 4.31] and dynamic coupling between zonal flows and phase space granularities (i.e., clumps and holes) [4.32] due to (phase space) trapping.

In this regard, it should be appreciated that, it is not computationally straightforward to reproduce the collisionless limit by the present simulation schemes. In the case of large ion temperature gradient, strong turbulent transport is predicted even in the collisionless limit, as is illustrated in Fig.4.6. Under this condition, Vlasov plasma simulation is performed with a sufficient resolution with the number of grid points in velocity space up to 8000, and an asymptotic limit is shown to reproduce the collisionless limit, as is demonstrated in Fig.4.17.

### 4.3. Electron Temperature Gradient Driven Turbulence

Electron temperature gradient driven (ETG) turbulence is considered to be one the candidates for causing anomalous electron thermal transport. Since it produces little ion thermal transport and particle transport, its possible existence cannot be easily ruled out by a variety of experimental observations on different transport channels. Fluctuations with wavelengths and frequencies as predicted by ETG theory have not been fully observed to date (except that the observed short-wave length fluctuations on TFTR by Wong et al. [4.34, 4.35] has a possibility of being the ETG or current-diffusive ballooning mode [3.74]). There are plans to measure such short-wave-length fluctuations in NSTX [4.36], DIII-D [4.37], and C-Mod [4.38]. ETG is *almost* isomorphic to ITG in the electrostatic limit, with the role of electrons and ions reversed. If this isomorphism were perfect, ETG turbulence at electron gyroradius ( $\sim \rho_e$ ) scale would produce electron thermal transport  $\chi_e^{\text{ETG}} \sim \sqrt{m_e/m_i} \chi_i^{\text{ITG}}$  which is too small to be relevant to tokamak plasma experiment. Here,  $\chi_i^{\text{ITG}}$  is ion thermal transport expected from the electrostatic ITG at the ion gyroradius scale. A more detailed explanation for the isomorphism between ITG and ETG is given in the Appendix C. This isomorphism is broken if one considers zonal flows in the nonlinear regime or Debye shielding effects [2.52]. As stated in the preceding section, for ITG turbulence, a proper electron response with  $\delta n_e/n_0 = e(\phi - \langle \phi \rangle)/T_e$ , was essential to obtaining an enhanced zonal flow

amplitude [4.13]. On the other hand, for ETG turbulence, the ion dynamics asymptotes to a pure adiabatic response  $\delta n_i/n_0 = -e\phi/T_i$ , as it is unmagnetized for  $k_\perp \rho_i \gg 1$ .

Equivalently, *both* ETG mode and ETG-driven zonal flows have adiabatic ions. For this pure adiabatic ion response, the role of the zonal flow in regulating turbulence was expected to be weaker than that for ITG turbulence. This is a consequence of the fact that the adiabatic ion response effectively *increases* the zonal flow inertia. For this case, flux-tube gyrokinetic continuum simulations suggest that radially elongated streamers can be generated and might enhance electron thermal transport significantly [4.39]. At present, there exists significant qualitative differences in ETG simulation results regarding the level of transport produced by ETG turbulence [4.40-4.42], and it is premature to conclude whether the ETG streamers could enhance electron thermal transport up to the level of experimental relevance.

It has been reported [4.39] that transport is reduced significantly for negative or small magnetic shear and large Shafranov shift. A follow-up study on this issue [4.43] attributes the main variations in electron thermal flux (due to ETG turbulence) to the degree to which the relatively long wavelength ETG instabilities contain significant parallel velocity fluctuation (which can be Kelvin Helmholtz (KH) unstable), and to the proximity of the electron temperature gradient to its linear threshold (which depends on the magnetic shear) [4.44, 4.45]. Global gyrokinetic particle [2.52] and global gyrofluid [4.41] simulations in a sheared slab geometry near  $q_{\min}$ , found that transport is substantially reduced in finite magnetic shear regions regardless of its sign, as compared to the region near the  $q_{\min}$  surface. This result is in semi-quantitative agreement with the fact that a state with zonal flows can become unstable to KH instability, but only in the absence of the strong stabilizing influence of magnetic shear [2.7].

An illustration of the zonal flow is reproduced here in Fig.4.18. This case treats the ETG turbulence in the vicinity of the radius where the magnetic shear vanishes (i.e., the 'q-minimum' surface). The horizontal axis indicates the radial direction, and the vertical axis corresponds to the poloidal direction. The center of the horizontal axis of the figure corresponds to the surface of zero magnetic shear. It is noticeable that the zonal flows are reduced in the vicinity of the minimum-q surface. Away from the minimum-q surface, the zonal flow is strongly excited. It has also been noted [2.52] that for some tokamak plasma parameters, the electron Debye length  $\lambda_{De}$  can be larger than the electron gyroradius  $\rho_e$ , and thus can make a quantitative difference in ETG turbulence driven zonal flows.

It is noteworthy that a gyrofluid simulation of ETG turbulence, which completely neglecting ETG zonal flows [4.40], obtained a transport level only a factor of 2 or 3 higher than the insignificant value expected from naive mixing-length estimation based on ETG turbulence at the electron gyroradius scale  $\chi_{e,ML}^{ETG}$  (i.e., 'electron gyro-Bohm scaling'). This level of transport from gyrofluid simulation without zonal flows is much

lower than that obtained from the aforementioned gyrokinetic simulation with zonal flows [4.39]. This current state of discourse is disturbing, because in the ITG case, the higher level of transport from gyrofluid simulations compared to that obtained from gyrokinetic simulation is believed to be due to the incorrect damping of zonal flows in a gyrofluid model. There are undamped Rosenbluth-Hinton zonal flow components in the gyrokinetic simulation. We note that in Ref. [4.39], the radial size of streamers is comparable to the size of simulation domain, invalidating the assumptions of spatial scale separation for flux-tube simulations, and that in Ref. [4.40], unrealistically small system size was assumed. More recent global gyrokinetic particle simulations, with system size comparable to an actual experiment, show that the transport level is quite modest (similar to the result of Ref. [4.40]) even in the presence of radially elongated streamers [4.41]. We note that non-adiabatic ion response due to residual ion magnetization (finite  $1/k_{\perp}\rho_i$  correction), which is typically ignored in simulations, could enhance the level of zonal flows by reducing the effective ion inertia.

Despite recent theoretical progress on electron zonal flow damping [3.39], which is the electron counter-part of the ion zonal flow damping [2.40, 2.41], it appears that understanding of zonal flow physics in ETG turbulence has not matured to the level of understanding of that for zonal flows in ITG turbulence.

#### 4.4. Fluid Simulations with Zonal Flows

Zonal flows have been widely studied in the geophysical and planetary fluid mechanics community, as recently summarized in [4.46]. Zonal flow generation due to inverse cascade has been theoretically predicted [2.2] for the Hasegawa-Mima (HM) system [4.47] which is isomorphic to the quasi-geostrophic or Rossby wave equation first derived by Charney [4.48, 4.49]. Zonal flow generation observed in simulations of the HM-Rossby system as a consequence of inverse cascade is combined with the Rhines scale crossover [4.50] from a dispersive-wave-dominated, weak turbulence regime at large scales to a strong turbulence regime at small scales [4.51]. The Rhines scale is that scale at which the fluid particle circulation frequency (i.e., turbulent decorrelation rate) equals the three-Rossby-wave frequency mis-match. Thus, the Rhines scale  $l_{\text{Rhines}}$  is set by a competition between nonlinearity and dispersion (due to polarization drift). The Rossby dispersion relation,  $\omega = -\beta_R k_y k_{\perp}^{-2}$  (where  $\beta_R$  is a coefficient to show the gradient of Coriolis force and  $k_y$  is the wave number in the longitudinal direction (see §5.2 for more detailed explanation), implies that for scales longer than the Rhines scale, non-zero triad couplings require one component to have  $k_y = 0$ , meaning it is a zonal flow. Thus, for  $l > l_{\text{Rhines}}$ , the dynamically preferred mechanism of nonlinear interaction is seen to involve zonal flow generation. The crucial role of the polarization nonlinearity in zonal flow generation was also confirmed.

Following the pioneering work on the zonal flow self-generation in the Hasegawa-Wakatani (HW) system [2.6], turbulence driven zonal flows have also been observed in the nonlinear simulations of various fluid turbulence models [4.52-4.57]. Their radial scales were typically of the order of a fraction of the simulation domain. In the multi-helicity case, both flows and energy transfer between flows and ambient turbulence oscillate in radius and turbulence suppression by zonal flow was weaker. Large coherent vortices around low-order rational surfaces were found to participate in the generation of zonal flows [4.58].

A new issue of zonal flow is pointed out by Wakatani in conjunction with the control of resistive wall mode (RWM) [4.59]. RWM stability is strongly dependent on plasma rotation. Wakatani showed that the perturbation-driven torque (divergence of the Reynolds-Maxwell stress) tends to decelerate the flow velocity at the rational surface. This would be an origin of the nonlinear instability. That is, when the plasma rotation frequency decreases, RWM becomes more unstable because the lower real frequency enhances the Ohmic dissipation in the resistive wall. The stronger instability will make the Reynolds-Maxwell stress larger so as to decelerate the rotation more effectively. Thus RWM can exhibit a nonlinear instability dynamics.

## 4.5. Edge Turbulence

### 4.5.1. Outstanding Issues

While physical details of zonal flows have been more frequently and thoroughly discussed in the context of core ITG turbulence simulations, as mentioned in Sec.4.2, and the importance of an accurate treatment of zonal flow damping [2.40, 2.41, 3.128] has been emphasized in that context, the causal role of zonal flows in barrier formation from simulation was first claimed to be observed in a Braginskii fluid simulation [4.60]. Ref.[4.60] reported many features appearing in the simulation which are similar to features in experimental observations of the L-H transition [4.61]. However a lack of detailed diagnostics of zonal flows, and absence of follow-up studies have caused a continuing debate in the edge turbulence simulation community, the issues of which are described below.

A different research team also has reported the formation of an  $E_r$  well, which is due to turbulence-driven zonal flows, in Braginskii nonlinear simulations in diverted geometry[4.62]. Yet another independent nonlinear simulation, based on a similar set of equations[4.63], however, has NOT produced the results similar to those of Ref. [4.60], namely that turbulence generated zonal flows play an essential role in the early phase of L-H transition, if a slow heating term is added. Even after an addition of physics relevant to less collisional, so-called transcollisional regimes, a case where self-generated zonal flows suppress turbulence significantly enough to arrive at a H-mode-like state has not been observed [4.64]. Since zonal flows in these edge turbulence simulations contain



significant components with finite frequency, more physics issues, related to the geodesic curvature coupling [4.65] and the Geodesic Acoustic Mode [3.5], must be discussed here. Also, the reader should remember that the L-H or ITB transitions involve mean  $E_r$  dynamics, as well as zonal flow evolution.

#### 4.5.2. Effects of Geodesic Curvature

Figure 4.19 illustrates the co-existence of the dominant zero-frequency zonal flow and the weak GAM oscillation of the flow intensity spectrum in a core, on a linear scale. A different set of edge turbulence simulation results, shown in Fig.4.20, indicates a) that the zonal electrostatic potential spectrum is more continuous and connects directly to a weak GAM, b) the flow spectrum in which the GAM component is almost invisible, even on log scales, and c) the side band ( $m=1$ ) pressure perturbation which shows a dominance of the zero frequency component. At present, long time, high resolution simulations for both core and edge turbulence seem to indicate that the dominant part of zonal flow component is a broad band zero frequency component. Direct measurements of zonal flow potential (either via heavy ion beam probe or Langmuir probe) are more likely to identify GAMs, however, due to their finite frequency.

In the context of the fluid description in toroidal geometry, the axisymmetric ( $n=0$ ) and poloidally symmetric ( $m=0$ ) component of the "zonal" electrostatic potential  $\phi_{0,0}$  is geometrically coupled to the ( $n=0, m=1$ ) component of density fluctuations,  $\delta n_{1,0}$  through the geodesic curvature term in the vorticity equation. Then, through the nonlinear coupling in the continuity equation,  $\delta n_{0,1}$  can connect to the ambient turbulence, say  $\delta n_{n,m}$  and  $\delta \phi_{n,m-1}$ . This particular coupling due to geodesic curvature can provide a channel for a spectral transfer out of the zonal flow which was absent in cylindrical geometry. Reference [4.64] argues that in its toroidal simulations, this "geodesic curvature induced transfer" is responsible for reducing the growth rate of zonal flows by depleting the fluctuation energy from the "zonal"  $\phi_{0,0}$ , thus stopping the turbulence suppression. In two-dimensional drift plane model, where the geodesic curvature coupling is absent, they have observed that the self-generated zonal flows can suppress turbulence, if the collisional damping of zonal flows is weak [4.52]. This is, of course, is eminently consistent with the earlier discussion of the Dimits shift regime and the effects of collisional flow damping on it. Since the geodesic curvature coupling is also responsible for GAMs, as we discuss shortly, it seems to play a subtle dual role of supporting both regulating edge turbulence via GAMs and weakening zonal flows via spectral transfer. The relative strength of these two symptoms may depend sensitively on equilibrium parameters and geometry, as well as the number of modes kept in simulations. One can speculate that this could be the origin of the qualitative differences between Refs. [4.60, 4.62] and Refs. [4.63, 4.64]. The difference could be also due to the differences in boundary conditions, resolution, in the treatment of background

profiles, the heating term and in the sizes and aspect ratio of the flux tube simulation domain [4.65]. At this juncture, it is very important to point out that zonal flows are *not* the only entity which quenches turbulence, and that while the L-to-H transition may involve zonal flows, the mean  $\mathbf{E} \times \mathbf{B}$  flow is essential to complete and 'lock-in' the post-transition, steepened profiles. Indeed, as the transition progresses further, zonal flows must die out, as the driving turbulence is quenched, and dissipation (collisions, neutral friction, etc.) most certainly persists. Thus it seems most unlikely that the L-to-H transition can be explained by the zonal-flow-induced quenching of turbulence, *alone*. Recent theoretical work has suggested that the interplay between zonal and mean flows can produce 'dithering oscillations' near the transition threshold.

One can obtain the Geodesic Acoustic Mode (GAM) by closing the loop between  $\phi_{0,0}$  and  $\delta n_{0,1}$  via a linear coupling to a compressional part of the  $\mathbf{E} \times \mathbf{B}$  velocity in the continuity equation. Then one obtains a damped oscillation with a real frequency  $\omega_{\text{GAM}} \approx 2V_{\text{Th}}/R$ , where the coefficient of the order of 1 depends on the equation of state (i.e., the assumptions on the pressure evolution). Since  $k_{\parallel} = 1/qR$ , the GAM suffers ion Landau damping. The GAM component of the zonal flow (recall that the "zonal"  $\phi_{0,0}$  is typically larger than  $\phi_{0,1}$ ) seems more relevant at the edge than in core for the following reasons. First, the ion Landau damping gets exponentially weaker as the  $q$  value gets higher towards the edge and  $T_i$  decreases. Second, due to the steep pressure gradient at the edge, the characteristic turbulence decorrelation rate  $\Delta\omega_k$  can be greater than  $\omega_{\text{GAM}} \approx V_{\text{Th}}/R$ . This is in contrast to the situation in core turbulence discussed in detail in the context of ITG turbulence in Sec. 4.2. Thus, GAMs can interact with the turbulence. A wave kinetic theory proposed in Ref. [4.12] elucidated why  $\omega_{\text{GAM}} < \Delta\omega_k$  is required for the GAM to efficiently shear the eddies in the ambient turbulence. Specifically, the relevant competition in the wave kinetic equation is between the GAM frequency  $\omega_{\text{GAM}}$ ,  $\Delta\omega_k$  the turbulence decorrelation rate and  $k_{\text{GAM}}V_{\text{gr}}$ , the transit frequency of a drift wave packet through the GAM. For  $\omega_{\text{GAM}} < \Delta\omega_k$ , the drift wave-GAM resonance function is simply  $1/\Delta\omega_k$  to leading order, as it is for the zero frequency zonal flows, rather than  $\Delta\omega_k/\omega_{\text{GAM}}^2$ , as for the 'usual' case of GAMs.

Assuming that the potential for zonal flow varies sinusoidally in time with a characteristic frequency  $\omega_f$ , ref.[4.12] has shown that the fast-varying components of zonal flows are less effective in shearing turbulence eddies. The fundamental reason for this is that the zonal flow shear pattern changes before the eddies can be torn apart. The turbulent eddies can then recover some of their original shape, and the shearing effect is reduced. The following effective shearing rate has been analytically derived [3.77]

$$\omega_{\text{Eff}} = \omega_E \frac{\left( (1 + 3F)^2 + 4F^2 \right)^{1/4}}{(1 + F)\sqrt{1 + 4F}},$$

where  $\omega_E$  is the instantaneous  $\mathbf{E} \times \mathbf{B}$  shearing rate and  $F = \omega_f^2 / \Delta\omega_k^2$ . For  $F > 1$ ,  $\omega_{\text{Eff}}$  is smaller than the instantaneous value  $\omega_E$ . This is the reason why the Geodesic Acoustic Mode (GAM) with  $\omega_{\text{GAM}} \approx V_{\text{Th}}/R$ , which can have a high instantaneous shearing rate, does not quench the ambient turbulence for typical core parameters [4.12]. The adiabatic approximation for zonal flows, focusing on the zero frequency component [2.11], was thus well motivated for core turbulence. At the edge, sharp pressure gradients can make the turbulence decorrelation frequency greater than the GAO (geodesic acoustic oscillation) frequency. Therefore, the GAM could affect the ambient edge turbulence [3.140, 4.63]. It has been noted that including nonadiabatic kinetic electron response for typical core parameters does not affect the GAM frequency and damping [3.34].

## 4.6 Short summary of the correspondence between theoretical issues and numerical results

### 4.6.1 Survey of correspondence

As is stressed throughout this article, the explanation of simulation studies in this chapter does not aim for an exhaustive review of the simulation of zonal flow, but rather strive to illuminate the *understanding* of zonal flow which has emerged together with theory, and to identify to what extent the theoretical understanding has been verified by DNS. For this reason, the emphasis is on the ITG-ZF cases, and the example figures are limited. It would be useful, after listing some DNS results, to summarize the correspondence between theoretical modelling and DNS. Table 4.1 illustrates key issues, sections of this review, and corresponding figures from DNS. It is clear that the theory and simulation has cooperated to advance the understanding of drift wave -zonal flow systems. Further research can be expected to improve understanding considerably.

### 4.6.2 On transport coefficients

The results of global transport studies may attract broader interest, in particular from experimentalists. A short note is added here.

The ITG mode has been studied most intensively. Simulation observations include:

(a) *Upshift of the critical temperature gradient* for the onset of turbulent transport [4.67-4.69]

$$\eta_{c, \text{DNS}} > \eta_{c, \text{lin}}$$

where  $\eta_{c, \text{DNS}}$  is the critical temperature gradient above which turbulent transport occurs and  $\eta_{c, \text{lin}}$  is the linear stability boundary. In between two critical values,  $\eta_{c, \text{DNS}} > \eta_i > \eta_{c, \text{lin}}$ , turbulent transport remains very close to zero but the zonal flow energy dominates, for weak zonal flow damping. The determination of the critical gradient at the onset of turbulence is a subject of current research, and is explained in §3.5.6.

(b) *Recovery* of mixing levels of  $\chi_i$  at higher gradient:

$$\chi_i \propto (\eta_i - \eta_{c, \text{DNS}})^{1-2}$$

as  $\eta_i$  exceeds  $\eta_{c, \text{DNS}}$  [4.16, 4.67-4.69], and

$$\chi_i \propto (\eta_i - \eta_{c, \text{DNS}})^0$$

as  $\eta_i \gg \eta_{c, \text{DNS}}$  [4.67-4.69].

A major gap in the findings from numerical simulations of the physics of drift-ITG - zonal flow turbulence is a *systematic* exploration of at least the two-dimensional parameter space of zonal flow damping ( $\gamma_{\text{damp}}$ ) and deviation from marginal stability (i.e.,  $\delta\eta_i \equiv \eta_i - \eta_{c, \text{lin}}$ ) as is illustrated in Fig.4.21. A possible 'third axis' would measure the strength of non-adiabatic electron effects. Even for the pure ITG case, a systematic exploration of the  $(\gamma_{\text{damp}}, \delta\eta_i)$  parameter space has not been undertaken.

Such a study could help answer many questions, such as:

- (i) finding the cross-over point between collisional and collisionless saturation;
- (ii) understanding and elucidating the relevance of various nonlinear saturation mechanisms for zonal flow, such as trapping, nonlinear scattering, tertiary instability;
- (iii) understanding the effect of nonlinear drift wave noise on zonal flow saturation. The thorough completion of such a study should be a high priority for future DNS investigations.

## 5. Zonal Flows in Planetary Atmospheres

This chapter presents a survey of zonal flow phenomena elsewhere in nature. Special emphasis is placed upon the origin and dynamics of belts and zones in the Jovian atmosphere. The physics of the Venusian super-rotation, is discussed as well. The relationship between zonal flow generation and the magnetic dynamo problem was already discussed in Section 3.2.6.

In this chapter, we begin with an introduction to the mechanics and waves in a thin rotating spherical atmosphere. An introduction to the Rossby wave [4.48] is presented. Then a description of the structures seen on Jupiter and the theoretical understanding of them follows. We conclude with a discussion of the superrotation of Venus.

### 5.1 Waves in a Rotating Atmosphere.

#### 5.1.1 Introduction for rotating coordinates

The observers of geophysical phenomena are rotating in space, with the earth. For understanding the observation of geophysical, planetary and astrophysical objects, which are rotating on their own axes, description using coordinates rotating with the objects is convenient. Thus, we begin with brief introduction of the rotating coordinates.

We consider the rotating sphere as is shown in Fig.5.1.1(a). The radius is given by  $r$ , latitude is given by  $\theta$ , and the distance from the rotation axis is denoted by  $R$ . The point G on the ground has a velocity

$$\mathbf{v}_G = \boldsymbol{\omega}_F \times \mathbf{r} = \boldsymbol{\omega}_F \times \mathbf{R}, \quad (5.1.1)$$

where  $\boldsymbol{\omega}_F$  is the angular frequency of rotation. The acceleration of the point G is given as

$$\frac{d\mathbf{v}_G}{dt} = \frac{d}{dt} (\boldsymbol{\omega}_F \times \mathbf{R}) = \boldsymbol{\omega}_F \times \mathbf{v}_G. \quad (5.1.2)$$

When the observed velocity relative to G (i.e., the velocity in the rotating frame) on the surface is  $\mathbf{v}$ , the total velocity  $\mathbf{v}_{\text{tot}}$  is given by  $\mathbf{v}_{\text{tot}} = \mathbf{v} + \boldsymbol{\omega}_F \times \mathbf{r}$ . The acceleration observed in rotating frame  $\frac{d\mathbf{v}}{dt}$  is then written as

$$\frac{d\mathbf{v}_{\text{tot}}}{dt} = \frac{d\mathbf{v}}{dt} + \boldsymbol{\omega}_F \times \mathbf{v}. \quad (5.1.3a)$$

The motion  $\mathbf{v}_{\text{tot}} = \mathbf{v} + \boldsymbol{\omega}_F \times \mathbf{r}$  has centripetal acceleration  $\boldsymbol{\omega}_F \times \mathbf{v}_{\text{tot}}$ , i.e.,

$$\boldsymbol{\omega}_F \times \mathbf{v}_{\text{tot}} = \boldsymbol{\omega}_F \times \mathbf{v} + \frac{d\mathbf{v}_G}{dt} . \quad (5.1.3b)$$

The total vector acceleration in the lab frame, which balances against external force per mass  $\mathbf{F} / \rho$  ,  $d\mathbf{v}_{\text{tot}}/dt + \boldsymbol{\omega}_F \times \mathbf{v}_{\text{tot}}$  , is given by the relation

$$\frac{d\mathbf{v}_{\text{tot}}}{dt} + \boldsymbol{\omega}_F \times \mathbf{v}_{\text{tot}} = \frac{d\mathbf{v}}{dt} + 2 \boldsymbol{\omega}_F \times \mathbf{v} + \frac{d\mathbf{v}_G}{dt} . \quad (5.1.4)$$

This gives the momentum balance equation:

$$\frac{d\mathbf{v}}{dt} + 2 \boldsymbol{\omega}_F \times \mathbf{v} = \frac{1}{\rho} \mathbf{F} - \frac{d\mathbf{v}_G}{dt} . \quad (5.1.5)$$

Usually the right-hand side denotes the force which includes the centrifugal force, which is additive with pressure. The term

$$\mathbf{f} = -2 \boldsymbol{\omega}_F \times \mathbf{v} \quad (5.1.6)$$

is called the Coriolis force. It is straightforward to see that the Coriolis force for horizontal motion is given as

$$\mathbf{f}_{\perp} = -2 \boldsymbol{\omega}_{F,z} \hat{\mathbf{z}} \times \mathbf{v} \quad (5.1.7)$$

where  $\hat{\mathbf{z}}$  -axis is taken in the vertical direction. Note the structural similarity of the Coriolis force to the Lorentz force.

The equation of motion on a rotating sphere takes the form

$$\begin{array}{cccccccc} \rho \frac{d\mathbf{v}}{dt} & + \rho \mathbf{v} \cdot \nabla \mathbf{v} & - \mathbf{J} \times \mathbf{B} & + \nabla p & - \rho \mathbf{g} & + 2\rho \boldsymbol{\omega}_F \times \mathbf{v}_{\text{tot}} & - \mu \nabla^2 \mathbf{v} & = 0 \end{array} \quad (5.1.8)$$

(1)            (2)            (3)            (4)            (5)            (6)            (7)

where  $\mathbf{g}$  is the gravitational acceleration and  $p$  is the pressure. Combining some of terms in Eq.(5.1.8), various phenomena have been discussed in fluid dynamics. Characteristic examples are listed in table 5.1.1.

### 5.1.2 Rossby wave

The Rossby wave has special importance in geophysical fluid dynamics. This wave has a strong similarity to drift waves in magnetized plasmas and provides a bridge from the study of plasmas to many other applications in nature.

Local Cartesian coordinates are chosen on a rotating sphere. In this review, we choose the x-axis in the direction of latitude (from pole to equator), the y-axis in the direction of longitude (from west to east), and z-axis in the vertical direction. (Fig.5.1.1(b).) This distinction is for the convenience of plasma physicists who are accustomed to using the y-axis for the ignorable coordinate and the x-axis along the direction of inhomogeneity. [The convention in fluid dynamics is to choose the x-axis in the direction of longitude and the y-axis in the direction of latitude.]

Neglecting the gravitational force and viscosity in Eq.(5.1.8), the dynamical equation for the Rossby wave is derived. Rossby waves occur in rapidly rotating systems, where the Coriolis frequency  $\omega_F$  is the fastest in the system. In such a case, the motion is primarily *geostrophic*, so the dominant balance in the momentum equation is between the pressure gradient and the Coriolis force. Such dynamics are classified to as geostrophic, and occur in regimes where  $R_o < 1$ . Here  $R_o$  is the Rossby number, which is the ratio of the vorticity of the motion to the rotation frequency  $\omega_F$ . One may assume incompressible motion on the horizontal plane  $(V_x, V_y)$ . One can then relate the fluid velocity to a stream function

$$V_x = -\frac{\partial}{\partial y} \psi, \quad V_y = \frac{\partial}{\partial x} \psi. \quad (5.1.9)$$

Taking a curl of Eq.(5.1.8) eliminates the pressure term, and assuming independence of the z-direction, one has

$$\frac{D}{Dt} \nabla_{\perp}^2 \psi - 2 \frac{\partial \omega_{F,z}}{\partial x} \frac{\partial \psi}{\partial y} = 0. \quad (5.1.10)$$

Noting that the Coriolis force is stronger near the pole and weaker near the equatorial plane, (i.e.,  $\omega_{F,z}$  is a decreasing function of  $x$ ), the coefficient  $\partial \omega_{F,z} / \partial x$  is negative. If the perturbation is not constant in the z-direction, Eq.(5.1.10) has a form

$$\frac{D}{Dt} \left( \nabla_{\perp}^2 \psi - \frac{\omega_{F,z}^2}{g H_m} \psi \right) - 2 \frac{\partial \omega_{F,z}}{\partial x} \frac{\partial \psi}{\partial y} = 0, \quad (5.1.11)$$

where  $H_m$  is the eigenvalue in the vertical waveform, being of the order of the vertical thickness. This introduces a spatial scale, the Rossby radius,

$$\rho_R = \frac{\sqrt{g H_m}}{\omega_{F,z}}. \quad (5.1.12)$$

Equation (5.1.11) is equivalent to Hasegawa-Mima equation for drift wave turbulence [2.2, 4.47, 4.49]. In the context of geophysical fluid dynamics, the equation is commonly referred to as 'quasi-geostrophic equation', and was first derived by J. Charney [5.2]. The gradient of the Coriolis force in the direction of latitude plays the role of the density gradient in magnetized plasmas. The Rossby radius  $\rho_R$  is the analogue of the gyro-radius for drift wave systems. Taking a perturbation to have the form

$$\psi \propto \cos(k_x x) \exp(ik_y y - i\omega t), \quad (5.1.13)$$

the dispersion relation of the linear perturbation is given as

$$\omega = \frac{2 k_y \rho_R^2}{1 + \rho_R^2 k_\perp^2} \frac{\partial \omega_{F,z}}{\partial x}. \quad (5.1.14)$$

where the quantity  $\left| 2 \rho_R^2 \frac{\partial \omega_{F,z}}{\partial x} \right|$  plays the role of the diamagnetic drift velocity in confined plasmas. The wave is propagating in the  $-y$  direction (westward), because  $\partial \omega_{F,z} / \partial x$  is negative. The propagation of the Rossby wave is illustrated in Fig.5.1.2.

It is useful to evaluate various scale lengths for the earth's atmosphere:

$$\begin{aligned} \text{vertical height: } H_m &\simeq 10^4 \text{ m, angular frequency: } \omega_{F,z} \simeq 1.5 \times 10^{-4} \text{ sec}^{-1}, \\ \text{gradient of frequency: } \frac{\partial \omega_{F,z}}{\partial x} &\sim 10^{-11} \text{ m}^{-1} \text{ sec}^{-1}, \\ \text{Rossby radius: } \rho_R &\sim 2 \times 10^6 \text{ m,} \\ \text{phase velocity: } \left| 2 \rho_R^2 \frac{\partial \omega_{F,z}}{\partial x} \right| &\sim 10^2 \text{ m sec}^{-1} \end{aligned} \quad (5.1.15)$$

The Rossby radius is about 10% of the arc length of the equator.

With the introduction of the normalization

$$\left| 2 \rho_R \frac{\partial \omega_{F,z}}{\partial x} \right|^{-1} t \rightarrow t, \quad \frac{x}{\rho_R} \rightarrow x, \quad \frac{y}{\rho_R} \rightarrow y, \quad \text{and} \quad \left( 2 \left| \frac{\partial \omega_{F,z}}{\partial x} \right| \right)^{-1} \rho_R^3 \psi \rightarrow \psi, \quad (5.1.16)$$

Eq.(5.1.11) takes the form

$$\frac{\partial}{\partial t} (\nabla_\perp^2 \psi - \psi) + [\psi, \nabla_\perp^2 \psi] - \frac{\partial \psi}{\partial y} = 0, \quad (5.1.17a)$$



where

$$[f, g] = (\nabla f \times \nabla g) \cdot \hat{z}. \quad (5.1.17b)$$

### 5.1.3 Rossby wave soliton, zonal flow

Because of the similarity of the normalized equation (5.1.17) to the Hasegawa-Mima equation in plasma dynamics, the understanding of the zonal flow generation, Rossby wave soliton and suppression of Rossby wave by zonal flow is readily extended, using the methods in Chapter 3.

There arises a critical wavenumber  $k_c$ , above which the nonlinear cascade gives a power law spectrum as

$$|\psi_k|^2 \propto k^{-4}. \quad (5.1.18)$$

with

$$k_c = \left( \frac{\rho_R}{4L|\psi|} \right)^{1/3}, \quad (5.1.19)$$

where  $k_c$  is normalized,  $L$  is the horizontal gradient scale length of  $\omega_{F,z}$  (in the direction of latitude) and  $|\psi|$  is the normalized stream function [2.2]. Below this critical wavenumber, global structure such as zonal flow appears. This scale, known as the Rhines scale [4.50], may be estimated by comparing the three-wave frequency mismatch for Rossby wave interaction with the eddy turn-over rate for the 2-D turbulence, i.e.,  $\Delta\omega_{MM} = \omega_k - \omega_{k'} - \omega_{k''}$  vs.  $k\bar{V}_k$ . This comparison effectively locates the scale at which the transition from strong to weak turbulence occurs, and is known as Rhines scale. This is given by  $k_c^{-1}$  (taking  $\Delta\omega_{MM} \sim (k_y \rho_R^2 \partial\omega_F/\partial x) k_\perp^{-2} \rho_R^{-2}$  and noting  $V = \rho_R \nabla\psi \times \hat{z}$ ). Note that for scales smaller than  $k_c^{-1}$ , wave dynamics are effectively irrelevant, as the eddy decorrelation rate exceeds the wave frequency. For scales longer than the Rhines scale, the turbulence is weak, so that the three-wave resonance condition must be satisfied. Since  $k_\perp^2 \rho_R^2$  is finite, dispersion makes this difficult. Thus, three wave resonance is most easily achieved if one mode has  $k_y = 0$ , i.e., is a zonal flow. Note that this picture suggests, then, that:

(a) Zonal flows are the ultimate repository of large scale energy of the 2D inverse cascade in a geostrophic system,

(b) geostrophic turbulence is a *three* component system, composed of eddies, Rossby waves and zonal flows.

The significance of the Rhines length for determining the scale of zonal flow excitation is nicely illustrated in [4.51]. Application to the giant planets, Jupiter and Saturn, has been reported by Hasegawa [5.3].

The nonlinearity becomes important if the normalized amplitude of vorticity  $\nabla^2\psi$  becomes unity. This is the case if the flow velocity reaches the level (in the case of earth, Eq.(5.1.15))

$$V \sim \left| \rho_R^2 \frac{\partial \omega_{F,z}}{\partial x} \right| \sim 50 \text{ m sec}^{-1} \quad (5.1.20)$$

for the horizontal scale length  $k_y \sim \rho_R^{-1} \sim 10^{-6} \text{ m}^{-1}$ . The azimuthal mode number (i.e., corresponding to the poloidal mode number) is in the range of a few to ten.

This estimate implies that the jet streams are associated with the wind speed of the order of  $50 \text{ m sec}^{-1}$  if it is indeed generated by the Rossby waves. Figure 5.1.3 illustrates the zonal flow and giant red spot in planetary atmosphere.

## 5.2 Zonal Belts of Jupiter

One cannot have heard about or contemplate the topic of zonal flows without the vivid image of the belts of Jupiter coming to mind, at least for an instant. Surely these structures are the most famous of all zonal flows! Thus, we spend a significant amount of time on a discussion of their formation and dynamics. While several of the giant planets exhibit zonal flows in their atmospheres, we focus the discussion on the case of Jupiter, in the interests of brevity.

The planet Jupiter consists primarily of a fluid molecular hydrogen, with a solid core of metallic hydrogen. It is enormous, with an equatorial radius of  $7.14 \times 10^4 \text{ km}$  and rotates quite rapidly, so that 1 Jovian day lasts only 9.9 hours. The core of the planet is also very hot, so that the gas envelope is convectively unstable. Thus, the atmosphere is quite dynamic and turbulent. The rich variety of structures we normally tend to associate with the Jovian atmosphere, such as zonal belts, the Great Red Spot vortices, Kelvin-Helmholtz billows, etc., all live in the weather layer, a thin two-dimensional (spherical) surface layer which is stably stratified, and thus acts as a 'rigid lid' on the convectively unstable interior. Thus, the phenomena of the weather layer are the visible projections of the dynamics of the cloud tops, in turn driven by the convective dynamics of the planetary interior, which are hidden from view. Thus, the crucial element in any effort to understand the formation of zonal belt structures is to properly account for the coupling between the (invisible) convective interior and the weather layer and how the former

might trigger zonal flow formation. In this respect, the situation resembles that of solar physics before the start of helioseismology, when researchers were forced to deduce aspects of the convection zone dynamics by watching their photospheric manifestations, or that in radar surveillance of ocean dynamics, where one attempts to uncover the structure of ocean internal waves and currents by studying their modulations of the surface wave field.

The turbulence of Jupiter is driven by thermal buoyancy, and is strongly affected by rotation, so that the Rossby number  $R_o$  is exceedingly low (i.e.,  $R_o \equiv \tilde{\omega}/\omega_F \ll 1$ , where  $\omega_F$  is the planetary rotation rate and  $\tilde{\omega}$  is the vorticity of the fluid motion). Thus, the Taylor-Proudman theorem applies. This theorem states that, in the presence of strong rotation, fluid flow tends to form columnar cells (i.e. "Proudman Pillars") aligned with the axis of rotation, so as to minimize the energy expended on the bending of vortex lines. In case of Jupiter, the Taylor-Proudman theorem implies that the cells in the interior are Taylor columns aligned with the axis of rotation of the planet. As shown in Figure 5.2.1, the lower boundary condition on the columnar motion is the no-slip condition, applied at the surface of the metallic hydrogen core. This, of course, implies an Ekman layer must connect the rigid surface to the rotating columns. The upper boundary condition is  $v_z = 0$  at the weather layer, consistent with the 'rigid lid' imposed by the stable stratification there. The structure of Jovian convection described here is sketched. The basic characteristics and turbulence physics of the Jovian atmosphere are summarized in Table 5.2.1, and are compared to their counterparts in toroidal plasma systems, as well.

The dominant role of rotation in the dynamics of the Jovian atmosphere, together with the rigid lid and no-slip boundary conditions, imply that the evolution may be described using a two-dimensional thermal Rossby wave model, which evolves the fluid potential vorticity and the potential temperature along trajectories determined by geostrophic velocities. In this model, which is structurally similar to the curvature-driven ITG turbulence model, the free energy source is the radial temperature gradient, released by a buoyancy drive process. A critical value of the Rayleigh number  $R_{a, \text{crit}} \sim O(10^4)$  [4.46] must be achieved for instability. Finite frequency, which enters via the diamagnetic frequency in the case of plasmas, appears here via  $\beta$ -effect, i.e. the gradient in the Coriolis frequency. For significant deviations from the critical Rayleigh number  $R_{a, \text{crit}}$ , large transport will result. Thus, it seems likely that the convection system will hover near marginality in the planetary interior, with a large temperature gradient 'held' at the upper and lower boundary layers. In such a case, the temperature in the interior will consist of bursty rising plumes, as well as cellular motions. The Jovian atmosphere is quite strongly turbulent and the effective Reynolds number of the weather layer is high. This is in sharp contrast to the case of a tokamak plasma, where the effective Reynolds number is quite

low, i.e.,  $R_e \sim 10 - 100$ , at most, and the turbulence is more akin to wave turbulence than strong hydrodynamic turbulence.

Given this situation where the essential core dynamics are obscured by cloud cover, it is not surprising that (at least) two schools of thought on the origin of zonal belts have arisen. These are

- i) a secondary bifurcation approach (coherent), developed by Busse and his collaborators [4.46]. This scenario accounts for the appearance of zones via the coherent modulational instability of an array of convection cells.
- ii) the inverse cascade scenario (turbulent), developed by Hasegawa [5.3] and by Marcus and collaborators [5.4], which builds, in part, on the ideas of Rhines. This school seeks to explain the appearance of zonal belts via an inverse energy cascade in  $\beta$ -plane turbulence. Thus 2D turbulence is forced by rising plumes, which impinge on the weather layer, thus energizing its motions.

Here, we briefly discuss the essential features of both approaches. The assumptions and logic of the two scenarios are summarized in Fig.5.2.2. The key elements of Jovian zonal flow physics are listed in Table 5.2.2, which includes a comparison to corresponding aspects of tokamak zonal flow physics.

Figure 5.2.3 encapsulates the quasi-coherent, secondary bifurcation scenario. The idea here is that a modulational (or 'tilting') instability occurs in the array of Taylor columnar vortices. The tilting instability is that originally analyzed by Howard and Krishnamurti, and subsequently studied by many others. As a consequence, the cellular 'footprints' of these columns on the weather layer also undergo tilting instability, thus tending to amplify zonal shears and cause the development of belts. In this scenario, the number of zones is determined by the number of unstable columnar cells which 'fit' into the fluid interior region of the atmosphere. At high latitudes, near the polar regions, granules rather than belts are expected, since the columnar cells sense *both* the no-slip lower boundary condition at the surface of the metallic hydrogen layer, as well as the rigid lid boundary condition at the weather layer. Thus, belts are limited to lower latitudes, where both 'ends' of the Proudman pillar pierce the weather layer. This is consistent with observations of the Jovian atmosphere.

It is interesting to note that, as  $R_a$  is increased, the bifurcation sequence closely resembles that familiar from the formation of the transport barrier. As shown in Figure 5.2.4, starting from  $R_{a, \text{crit}}$ , thermal transport (as quantified by the Nusselt number  $N_u$ ) increases with  $R_a$ . At a second critical Rayleigh number called  $R_{a, \text{bif}}$ , generation of secondary flows begin. This generation is accompanied by an alteration of the convection pattern structure, in that cells are tilted, sheared and distorted by the zonal flows. As  $R_a$  increases beyond  $R_{a, \text{bif}}$ , the Nusselt number decreases with increasing  $R_a$ , while the

zonal flow energy increases, symptomatic of heat transport suppression and the increased channeling of free energy into zonal flows, rather than convection cells. At higher values of  $R_a$ , tertiary bifurcations, vacillations, cyclic phenomena, etc. are predicted to appear, as well. This is shown in Figure 5.2.4. Not surprisingly for this scenario, the mean zonal flow pattern exhibits north-south symmetry, modulo some correction for the effects of the great Red Spot, which appears in the southern hemisphere. This is consistent with Voyager observations. A plot of zonal velocity is shown in Figure 5.2.5.

The second scenario is that of an inverse cascade on a  $\beta$ -plane, as proposed by Marcus, building upon the ideas of Rhines. In this scenario, rising plumes from the convection zone constitute a source of forcing for the 2D inverse cascade on a  $\beta$ -plane. The forcing term is proportional to  $\omega_F \partial V_z / \partial z$ , where  $\partial V_z / \partial z$  is necessarily large in the weather layer, on account of the stable stratification there. On forcing scales, the nonlinearity is strong, so an inverse cascade develops toward large scales, with Kolmogorov spectrum  $E(k) \sim k^{-5/3}$ . Anisotropy develops as a consequence of  $\beta$ , via an extension of the mechanism of Rhines. The Rhines mechanism is based on the observation that on a  $\beta$ -plane the eddies have a finite frequency, corresponding to the Rossby wave frequency  $\omega = \beta k_x k_\perp^{-2}$ . At low  $k$ , such waves are strongly dispersive, so that triad interaction is severely inhibited, except for domains with  $k_x = 0$ . *The preference of nonlinear interaction for such states of high symmetry explains the tendency to form zonal bands.* Note that the Rhines length effectively defines the scale size on which enstrophy enters. The onset of such band formation occurs at large scales when the eddy turn over rate drops to the level of the wave frequency, i.e.  $k \tilde{V} = \beta k_x k_\perp^{-2}$ , so that the 'Rhines scale', which demarks the onset of zonal structure, is  $(\tilde{V}/\beta)^{1/2}$ . The inverse cascade is, in turn, damped by scale independent Rayleigh friction, associated with Ekman damping, etc. Not surprisingly, the frictional damping plays a crucial role in the model, as the Rosenbluth-Hinton scale-independent friction term does in the plasma zonal flow problem. Marcus, et al. emphasize that three conditions are necessary for zonal flow formation, in addition to rapid rotation, convective instability and large  $\partial V_z / \partial z$  in the weather layer, which we have already established. These are that the size of the vorticity advection nonlinearity must

(a) exceed the frictional damping on the forcing scale. Otherwise, energy cannot couple to the Rhines scale and thus anisotropy cannot develop.

(b) exceed the strength of the  $\beta$ -effect, i.e.,  $k_y \partial \omega_F / \partial x$  on forcing scales. Otherwise, energy will be coupled to Rossby waves, rather than zonal flows. Of course, a spectrum of Rossby waves can be unstable too, and thus amplify zonal perturbations, as discussed here. The implications of this secondary mechanism have not been addressed by Marcus, et al.

(c) exceed the viscous damping. Otherwise, energy will be dissipated so that structure formation will not be possible.

In the Marcus scenario, the number of bands is determined via energy balance by the system parameters, such as the forcing strength (related to the heat flux), the frictional damping, etc. In addition, tertiary Kelvin-Helmholtz instability may enter the determination of the band structure by limiting the strength of zonal vorticity. While Marcus and collaborators have assembled quite convincing computational arguments that large scale structure formation will occur if criteria (a)-(c) (above) are satisfied, further research is necessary to clarify the issues related to the details of pattern selection, such as band scale, number of bands, etc.

### 5.3 Superrotation of the Venusian Atmosphere

Another interesting mystery in the dynamics of planetary atmosphere is the superrotation of Venus [5.6, 5.7]. By "*superrotation*", we mean a fast zonal flow with an azimuthal speed in excess of the rotation velocity of the planet itself! Indeed, Venusian winds can reach 100 m/sec at altitudes of 60-70 km, which is about 60 times faster than the speed of the planet. This remarkable observation naturally suggests that the planetary wind results from some processes of self-organization of thermally driven convective flow in the Venusian atmosphere, which is similar to the mechanism of zonal flow generation.

The key questions pertinent to the generation of zonal flows in the atmosphere of the Venus are:

- (a) What is the mechanism of symmetry breaking which seeds zonal flow generation ?
- (b) What are the implications of 3D geometry? In this regard, note that the Venusian atmosphere is *not* thin.

Regarding (a), the conventional wisdom is that superrotation results from a tilting instability, the initial symmetry breaking for which results from the motion of the solar heating. This is called the "moving frame mechanism". Another possibility for symmetry breaking is instability convection between day and night sides of the planet. [5.8]. Other mechanisms involve thermal tidal pumping [5.9] and Hadley circulation pumping mechanism [5.10] which involves a horizontal eddy viscosity. Regarding (b), recent results [5.6] indicate that the moving frame mechanism is viable in 2D (though the cell-temperature perturbation is a critical element of the dynamics, contrary to initial expectations), but fails in 3D, since the basic flow is stable in spherical geometry [5.6]. Thus, attention is shifting to the tidal pumping and Hadley mechanisms. Clearly, much further research is necessary in order to understand the superrotation on Venus.

## 6. Extensions of Theoretical Models

To supplement the theory of zonal flows explained in Chapter 3, some advanced extensions are described in this chapter. The first topic is the streamer, which has a lot of similarity to the zonal flow but can have a quite different influence on the drift wave turbulence and transport. The second issue is the statistical nature of the zonal flow. While the mean field instability growth associated with the negative viscosity effect, explained in Chapter 3, is essential to the dynamics of zonal flow, noise can be important, as well. Thus, the PDF for the dynamical quantities in the system of drift wave -zonal flow can have non-Gaussian properties, and the noise can have greater influence on some global parameter of interest (e.g., heat flux, transition boundary, etc.) The third is the non-Markovian nature of the system dynamics. These issues belong in the realm of advanced research on the zonal flow, and are discussed briefly in this chapter. Finally, a method of theoretical analysis of the zonal flow (based on reductive perturbation theory), which is complementary to the one explained in Chapter 3, is briefly addressed.

### 6.1 Streamers

#### 6.1.1 Illustration

The subject of this review is the zonal flow, but it is worthwhile to give a short discussion of the streamer. The streamer is an intermediate scale perturbation of the electric field, which varies in the poloidal direction but is extended radially,

$$\mathbf{q} \approx (0, q_\theta, 0) \quad , \quad \text{and} \quad \mathbf{\tilde{E}} \approx (0, \tilde{E}_\theta, 0) \quad . \quad (6.1.1)$$

(See figure 6.1.1). The  $\mathbf{E} \times \mathbf{B}$  flow due to this electric field perturbation is in the *radial direction*, at a particular poloidal angle. Like the zonal flow, the streamer is also a highly anisotropic convective cell, albeit one extended radially, rather than poloidally.

The question of the origin of streamer cells is a hotly debated topic of current research. One group of researchers regard the streamer as a residue of the linear ballooning modes, which have the structure of 'twisted eddies', extended in radius. Other researchers conceive of the streamer as a nonlinearly-driven convective cell. From the early days of DNS of drift waves in the absence of magnetic shear, convective cells were found to increase anomalous transport [2.3, 6.1- 6.3]. Such cells associated with radial flows are streamers. Once a streamer is generated, the radial flow of plasma (energy, etc.) can be enhanced. The modification of the density profile due to the streamer can be estimated from the streamer mixing length rule

$$V_{\text{str}} \frac{\partial}{\partial x} T \approx V_{\text{str}} \frac{\partial}{\partial x} \tilde{T}_{\text{str}} \quad . \quad (6.1.2)$$

where the suffix str indicates the streamer. So one has  $\Delta x_{\text{str}}/L_T \sim \tilde{T}_{\text{str}}/\tilde{T}$  and strong gradient modification. The deformed iso-density contours in the presence of a streamer are illustrated in figure 6.1.2. Figures 6.1.2 (left) and (center) show (schematically) the potential perturbation and deformed density contour in toroidal plasmas, respectively. A detailed profile of the density deformation is given in Figure 6.1.2 (right) [6.4].

### 6.1.2 Excitation of streamer by drift wave fluctuations

Although there is on-going debate on the quantitative estimate of the excitation of the streamer, a simple explanation is given here. The streamer can also be induced by modulational instability of drift wave fluctuations. The growth rate for generation of the streamer has been calculated for the case of a coherent monochromatic drift wave (through modulational instability) [3.41] and for the case of drift wave turbulence (through  $k$ -space diffusion) [2.27]. The growth rate of the streamer due to a monochromatic drift wave,  $\gamma_S$ , is given as

$$\gamma_S \sim q_\theta k_r \rho_s c_s \frac{e\tilde{\phi}_d}{T_e}, \quad (6.1.3)$$

where  $q_\theta$  is the poloidal mode number of the streamer, and  $k_r$  and  $\tilde{\phi}_d$  are the radial wavenumber and fluctuation amplitude of the drift wave. In this case, the growth rate  $\gamma_S$  monotonously increases until finite gyroradius effects start to suppress instability, in contrast to the case of zonal flow. The streamer is more easily excited if the radial wavenumber of the drift waves is larger. A generic result for the evolution of secondary vorticity takes the form

$$\frac{\partial}{\partial t} \langle \nabla^2 \phi \rangle = \left( \frac{\partial^2}{\partial x^2} - \frac{\partial^2}{\partial y^2} \right) \langle \tilde{\varphi}_x \tilde{\varphi}_y \rangle + \frac{\partial^2}{\partial x \partial y} \left( \langle \tilde{\varphi}_x^2 \rangle - \langle \tilde{\varphi}_y^2 \rangle \right). \quad (6.1.4)$$

The region of streamer excitation in wave number space is illustrated in Fig.6.1.3. The growth rate  $\gamma_S$  has a value similar to that of  $\gamma_{ZF}$ .

The theory of streamer generation in turbulence has also been developed. The analysis of this process proceeds very similarly to that for zonal flow growth. Thus, drift wave stresses drive radial flows, which in turn modulate the underlying drift wave population. The streamer perturbation is reinforced for  $\partial N / \partial k_\theta < 0$ , and damped for  $\partial N / \partial k_\theta > 0$ . Streamer flows can react back on the drift wave population by driving diffusion in  $k_\theta$ , so that drift wave energy is transferred to high  $k_\theta$ , and thus to damped scales. In the case of streamers, note that sheared radial flow produces high  $k_\theta$ . Additional damping may enter via dissipation on the streamer scales (i.e., Landau damping).



### 6.1.3 Nonlinear drift instabilities

The back-interaction of the streamer on the ambient turbulence is also important. A nonlinear linkage between a streamer and drift-wave turbulence can induce nonlinear instability of the drift waves. A nonlinear link is as follows:

- (i) streamers ( $k_{\parallel} \approx 0$ ) are induced by the drift waves ( $k_{\parallel} \neq 0$ ), and cause a strongly sheared *radial* flow;
- (ii) this system with a radial flow is unstable to drift waves ( $k_{\parallel} \neq 0$ ); and
- (iii) the drift waves regenerate the streamers, closing the nonlinear link.

A set of equations for the coherent interaction of streamer and drift wave has been proposed [3.115]. This system closely resembles that of the tilting instability, proposed as a mechanism whereby convective cells form zonal flows. A potential perturbation of the form

$$\tilde{\phi} = \phi_c \cos \pi y + (\phi_{d1} \cos \pi y + \phi_{d2} \sin 2\pi y) \sin k_z z \exp(ik_x x) \quad (6.1.5)$$

is considered, where  $\phi_c$  is the streamer amplitude,  $\phi_{d1}$  is the least stable drift wave, and  $\phi_{d2}$  denotes the linearly damped drift wave. The original density gradient is in the  $x$ -direction, but a (perturbed) gradient of density in the  $y$ -direction appears, due to the streamer formation. The drift wave in equation (6.1.5) propagates in the  $x$ -direction. The streamer potential  $\phi_S$  grows at the rate given by Eq.(6.1.3), and the density streamer is generated according to Eq.(6.1.2) as  $\gamma_1 \partial \tilde{n} / \partial y = \phi_S^4$ , where the coefficient  $\gamma_1$  is given by the nonlinear interaction terms. Its explicit formula is given in [3.115]. The complex growth rate of the drift wave is calculated by retaining the lowest-order correction due to the streamer as

$$\gamma \left( 1 + k_{\perp}^2 \rho_s^2 + \frac{k_{\perp 1}^2}{k_z^2} \gamma \right) = -ik_x \frac{\partial \tilde{n}}{\partial y}. \quad (6.1.6)$$

From this set of equations, a nonlinear mechanism for self-sustainment emerges: in this mechanism, the drift wave causes convective cells to form, the cells lead to a density streamer; and the density gradient in the  $y$ -direction destabilizes the drift wave. This provides a possibility that the drift waves can be subcritically unstable. Subcritical instability mechanisms are also found to be possible through other mechanisms [2.46, 2.54, 6.5]. At the moment of completing this review, the study of possible subcritical instabilities is on-going, and future research is clearly necessary.

Another route of streamer saturation is back-reaction on the underlying drift wave, via shearing. As mentioned earlier, in this case radially directed, poloidally sheared flows will diffuse drift wave energy, i.e.,  $\langle \delta k_\theta^2 \rangle \sim D_{k_\theta} t$ , where

$$D_{k_\theta} = \sum_{q_\theta} R(\Omega - v_g, \theta q_\theta) k_r^2 q_\theta^2 \tilde{v}_{S, q_\theta}^2 \quad (6.1.7)$$

Thus, high  $k_\theta$  are generated, and the  $k_\theta$  spectral structure is modified.

This discussion naturally leads to the question of what state is induced by the mutual interaction between the drift wave turbulence, zonal flow and streamers. Some research has been done to address this, and an example is illustrated here. Reference [6.6] studies the coupling of zonal flow, streamer and turbulence, in the context of a system of Rayleigh-Taylor instability, with curvature drive. This illustrates the physics of drift wave, zonal flow and streamer in the absence of magnetic shear. A model dynamical system description is proposed:

$$\frac{d}{dt} N = \gamma N - \alpha NV - \beta NS + \delta S^2 \quad (6.1.8a)$$

$$\frac{d}{dt} V = \alpha NV - \nu V \quad (6.1.8b)$$

$$\frac{d}{dt} S = \gamma_s S + \beta NS - \chi VS \quad (6.1.8c)$$

where  $N$ ,  $V$  and  $S$  are squared amplitude of the drift waves, zonal flow and streamer and the coefficients  $\gamma$ ,  $\alpha$  and  $\nu$  denote linear drift wave growth, zonal flow drive and collisional damping. With the introduction of the streamer component, new coupling coefficients  $\beta$ ,  $\delta$ ,  $\chi$  enter, as well. The coefficient  $\gamma_s$  is introduced so that linear instability can exist in the model of Rayleigh-Taylor instabilities. More generally,  $\gamma_s$  - the linear growth rate of the extended radial scale (streamer), could be either positive or negative, depending on the model. This model and generalizations thereof can be used to study the competition between the zonal flow and streamer. A 2-D generalization of this 0-D model would be especially interesting.

Direct numerical simulation of Rayleigh-Taylor turbulence has also been performed. The study contained two control parameters; the collisional diffusivity of particles  $D$  and the molecular viscosity  $\mu$ . When collisional damping is large, the final state is found to be dominated by streamers.

Before closing this subsection, a few words are added concerning the role of magnetic shear for the streamer. If one sticks to a rigorous definition for the streamer, that  $k_\parallel = 0$  holds everywhere with large poloidal mode numbers ( $\partial/\partial\theta \neq 0$ ), it may not

be possible to construct an eigenfunction when magnetic shear is present. In the system with magnetic shear, it might be necessary to extend the definition from  $k_{\parallel} = 0$  to  $k_{\parallel} \approx 0$  for the streamer. With this generalization, one can do the modulational instability calculation for streamers in ballooning representation. This allows streamers to evolve to adjust to shear, i.e., twist with the field line, a la Taylor-Roberts quasimodes [6.7]. Direct numerical simulations have reported observations of streamers [2.52, 4.53, 6.8]. It is also suggested that radially extended structure with high poloidal mode numbers appears as a remnant of the linear mode structure, indicating an importance of geometrical factors [3.124]. This is an important area which requires future research.

## 6.2 Noise Effects and Probabilistic Formulations

Background turbulence that induces zonal flow has a short correlation time, so that the driving force for zonal flow has a component that rapidly changes in time. The driving force by turbulence, on the average, acts to cause the growth of the zonal flow as is explained in Chapter 3. However, in addition to the 'negative viscosity effect', which drives zonal flow growth, there is noise excitation of zonal flow scales due to incoherent emission from drift waves. While generally the mean field instability growth associated with the negative viscosity effect is of greater significance dynamically, noise can be important as well [2.11, 2.40, 2.41, 2.46, 6.9]. Indeed, noise effects are particularly interesting in instances where the zonal flow modulational instability is weak, marginal or weakly damped. In the latter case, large zonal flow fluctuations can occur, due to the weak damping of 'slow modes', even for low levels of noise. This behaviour is rather similar to the well known phenomenon of critical opalescence, close to the critical point for phase transitions.

Schematically speaking, the torque for zonal flow by background turbulence is written as  $F$  with appropriate normalization presumed, i.e.,

$$\frac{d}{dt} V_{ZF} = F, \quad (6.2.1)$$

$F$  is a quadratic nonlinear term in the background fluctuation level and  $V_{ZF}$  is the zonal flow velocity. Then  $F$  can be separated into mean and fluctuating parts,

$$F = \langle F \rangle + \tilde{F} \quad (6.2.2)$$

with  $\langle \tilde{F} \rangle = 0$ , where  $\langle \cdots \rangle$  is an average over time longer than the autocorrelation time of the background turbulence. (Note that the tilde for  $F$  does not mean the drift wave amplitude.) The extensive discussion given in Chapter 3 shows that one may write

$$\langle F \rangle = \gamma_{ZF} V_{ZF} \quad (6.2.3)$$

and also discusses calculation of the zonal flow growth rate  $\gamma_{ZF}$ . The rapidly-varying part  $\tilde{F}$  is treated as noise, and Eq.(6.2.1) takes the form of a Langevin equation, possibly with negative drag (i.e.,  $\gamma_{ZF} > 0$ ):

$$\frac{d}{dt} V_{ZF} - \gamma_{ZF} V_{ZF} = \tilde{F}. \quad (6.2.4)$$

Of course, the analogy with standard statistical mechanics is clearest when  $\gamma_{ZF} < 0$  - i.e., in the slightly over-saturated regime. In such a case, the nonlinear zonal flow saturation must balance both growth and noise emission. The property of the rapidly-varying part  $\tilde{F}$  has been studied, and it is modelled as a noise for the evolution of the zonal flow. The formulation of the noise is discussed below. Of course, one may just simply calculate the noise emission into low  $q_r$  modes via a closure of the 2D fluid equation, treating the background modes as drift waves.

A systematic description of the statistical average  $\langle F \rangle$  and the noise has been given in the literature [2.46, 6.9]. A calculation using the eddy-damped-quasi-normal-Markovian (EDQNM) approach has been discussed in detail in [6.9]. By use of the action of drift waves  $N_k$  and the enstrophy of zonal flows  $Z_q$ , a set of balance equations for the system dynamics has been derived. Detailed calculation is left to the references, but the noise term is explained here. For long wavelength evolution, one finds

$$\frac{\partial}{\partial t} Z_q = 2 \gamma_q Z_q + Z_q^{\text{noise}} \quad (6.2.5)$$

where  $\gamma_q$  is the growth rate of the zonal flow. Note that a stationary solution is possible only when  $\gamma_q < 0$ , which requires confrontation of the problem of nonlinear saturation of zonal flows. Here  $Z_q^{\text{noise}}$  is the long time average magnitude of the mean square of the noise term, i.e.,

$$Z_q^{\text{noise}} = q^4 \sum_q \frac{k_y^2 k_x^2}{(1 + k_\perp^2)^4} \text{Re } \theta_{q, k, -k} N_k^2. \quad (6.2.6)$$

where  $\theta_{k, -k, q}$  is the triad interaction time of three waves [6.9]. This result is also given in [2.11].

Equation (6.2.5) gives a solution for the steady state as

$$Z_q = -\frac{\dot{Z}_q^{\text{noise}}}{2\gamma_q}. \quad (6.2.7)$$

In this expression,  $\gamma_q$  *must* include the effect of nonlinear stabilization, so that  $\gamma_q$  may be negative at finite amplitude, which is necessary for a (meaningful) stationary state. This equation necessarily has the form of an extended *fluctuation-dissipation relation* for zonal flow. By use of such a balance equation, the role of noise pumping has been analyzed [2.46]. The possibility of bifurcation has been pointed out. As mentioned above, the result of Eq.(6.2.7) is strongly dependent upon the knowledge of the damping rate  $\gamma_q$ , which includes all relevant nonlinear as well as linear effects. Obtaining and understanding such a  $\gamma_q$  is a subject for on-going research, and the full solution of this problem is left to future studies.

Equation (6.2.5) provides an expression for the noise term in the Langevin equation for the zonal flow vorticity  $U_{ZF}$ ,  $U_{ZF} = \partial V_{ZF}/\partial x$ , as

$$\frac{d}{dt} U_{ZF} - \gamma_{n, ZF} U_{ZF} = \tilde{S} \quad (6.2.8)$$

with

$$\tilde{S} = \sqrt{\dot{Z}_q^{\text{noise}}} \, \mu(t) \quad (6.2.9)$$

where  $\gamma_{n, ZF}$  includes all relevant nonlinear as well as linear effects, and  $\mu(t)$  is a Gaussian white noise term,  $\langle \mu(t) \mu(t') \rangle = \delta(t - t')$ . The term  $\tilde{S}$  is rapidly changing in time on a scale faster than the autocorrelation time of  $U_{ZF}$ , but does not have the property of white noise. Gaussian white noise is a simplifying approximation.

### 6.3 Statistical properties

As a result of the progress in toroidal plasma experiments, the importance of the tail component of the probability density function in transport problems and in the onset of transport and bifurcation events is gaining in recognition. It is well known that a statistical approach is needed to treat the probability density function. [2.14, 6.10, 6.11] This statistical problem is also relevant to the physics of zonal flows.

The probability density function (PDF) is the fundamental goal of turbulence theory. In order to clarify the implications of statistical theory on the understanding of the relevant phenomena, it is useful to consider models which discuss low dimensional systems. One may write a Langevin equation to study the statistical property of the quantity  $X$  which is the subject of interest:

$$\frac{\partial}{\partial \tau} X + \left[ \Lambda_0(X) + \Lambda_1(X) w_1(\tau) \right] X = w_0(\tau) g . \quad (6.3.1)$$

In this equation  $\Lambda$  is the (nonlinear) damping rate, which can be nonlinear and which can contain multiplicative noise  $w_1(\tau)$ ,  $g$  is the magnitude of the noise source and  $w_0(\tau)$  represents the noise. [It is not necessary to specify the RHS of Eq.(6.3.1) as Gaussian white noise. What is necessary is that the autocorrelation time of the noise must be much shorter than the relevant time scale  $\Lambda^{-1}$ .]

Non-Gaussianity of the PDF is caused either by the nonlinearity in the damping rate  $\Lambda$ , or by the dependence of the noise source  $g$  on the quantity  $X$ , or by multiplicative noise entering via the damping rate. An example of a problem involving multiplicative noise is zonal flow growth in the presence of avalanches. This review gives an extensive discussion on deterministic models for zonal flow growth in terms of quasi-stationary local parameters. However, these parameters may vary stochastically due to intermittent transport event bursts, i.e., due to avalanches. Thus, the relaxation rate  $\Lambda$  should be regarded as noisy. This scenario is a simple example, then, of *multiplicative noise*. Note that multiplicative noise necessarily changes the structure of the Fokker-Planck equation, so that the PDF is, in general, non-Gaussian.

There have been some basic studies of the effect of noise on bifurcation transitions and transport barrier formation [2.4], but in general, the theory of zonal flow and transport barrier dynamics with noise remains *terra nova*. Note that the interplay of avalanches with zonal flows and barriers gives another perspective on the problem of interplay of zonal flows and streamers, discussed previously.

### 6.3.1 Instantons

It has been known that the large amplitude drift wave takes a form of 'modon'. [6.12, 6.13] (The modon is a solitary vortex structure which has a long life time.) Analogous vortical structure has also been found in the nonlinear evolution of the Rossby wave, as is discussed in Chapter 5. Modon solutions can be used as a basis for a theory of instantons in drift wave turbulence. Instantons are temporally localized solutions which correspond to trajectories of least action. Instanton solutions are those of steepest descent, and so dominate the time-asymptotic PDF. They thus serve as tractable models of intermittency phenomena.

Schematically speaking, nonlinear drift waves have an 'anti-shielding effect', which corresponds to vortex coalescence. That is, vortices agglomerate to make a larger vortex. This process sustains the modon against the dispersion of waves. It means that the larger the vortices, the longer the lifetime. (An explicit illustration by direct numerical simulation is seen in [4.50].) Taking this mechanism into account, the formation of a

drift wave modon by random excitation is studied by use of the instanton calculus, for noise with fixed magnitude. A longer life-time is expected for a larger-amplitude modon, so that a stretched, non-Gaussian PDF is obtained [2.53, 6.14, 6.15]. The PDF of the local Reynolds stress  $\mathcal{R}$  is then obtained from the fluctuation PDF. The Reynolds stress PDF  $P(\mathcal{R})$  is

$$P(\mathcal{R}) \sim \exp\left(-\frac{C}{\kappa} \mathcal{R}^{3/2}\right) \quad (6.3.2)$$

where  $\kappa$  is the mean-square noise forcing, and  $C$  stands for a normalization coefficient that includes the effect of the spatial shape of the modon. In this case, a statistical exponential tail is obtained. In addition, as the external forcing becomes larger, the tail extends to larger value of  $\mathcal{R}$ .

The divergence of  $\mathcal{R}$  is the torque that drives plasma flow. This result suggests that the noise source for the zonal flow, which has been discussed in previous sections, is given by a *non-Gaussian* distribution. Further research in this direction is needed in the future.

### 6.3.2 Nonlinearity in noise

Nonlinearity in the noise source gives very prominent tails. In the renormalization model for drift waves,  $g$  is given as a function of the amplitude of the turbulence [2.14, 3.119, 3.120, 6.4, 6.11, 6.16-6.18]. Stronger nonlinear noise appears for stronger fluctuations. This gives small but finite power-law tails in the study of multiple-scale turbulence and bifurcation. The presence of non-Gaussian tails suggests that large-scale but rare events could play a dominant role in determining the average. A detailed calculation of the turbulent noise has been developed in [6.19] and has been applied to the case of zonal flow excitation[2.47, 6.9].

The role of turbulent noise is particularly important when one studies subcritical bifurcation. Including turbulent noise terms, a dynamical model for a relevant, reduced degree of freedom (magnitude of the radial electric field) has been developed for the L-H transition [6.20]. A Langevin equation for the radial electric field in the plasma edge  $X = ep_p E_r / T$  is derived. The damping term in (6.3.1) is given as  $\Lambda X = (1 + 2q^2)^{-1} (qR/\rho_s e c_s n_i) J_r$ , where  $J_r$  is the normalized current. As has been discussed in a model of the L-H transition that focused upon the impact of ion-orbit-loss, the coefficient  $\Lambda$  is dependent on  $X$  and the deterministic equation for steady state thus becomes

$$\Lambda X = 0 \quad (6.3.3)$$

with multiple solutions for  $X$ . The solution is controlled by the ion collision frequency and the pressure gradient at the edge. The noise source is induced by micro-fluctuations. Their amplitude is influenced by the shear of radial electric field. Therefore the noise amplitude  $g$  is dependent on  $X$ , so we have a case of nonlinear noise. The stationary solution for the PDF of  $X$ ,  $P_{eq}(X)$ , may be expressed as  $P_{eq}(X) \propto g^{-1} \exp(-S(X))$  by use of the nonlinear potential

$$S(X) = \int^X 4\Lambda(X')g(X')^{-2}X' dX'. \quad (6.3.4)$$

The minimum of  $S(X)$  (apart from a correction of order  $\ln g$ ), i.e., zero of  $\Lambda$ , predicts the most probable state of  $X$ . The PDF of  $E_r$  and the transition rates between the L-mode and the H-modes are calculated. The phase boundary is obtained by using the statistical average

$$S(X_H) = S(X_L) + \frac{1}{2} \ln(\Lambda_L/\Lambda_H). \quad (6.3.5)$$

where  $\Lambda_{L,H} = 2 \left| X \partial \Lambda_X / \partial X \right|$  at  $X = X_{L,H}$ . This is an extension of the *Maxwell's construction rule* in the thermodynamics. The statistical average of the gradient-flux relation  $Q_r[p']$  is derived. The results are illustrated in Fig.6.3.1. Normalized pressure is defined as  $X_{NC} = -p_0^{-1} \rho_p \nabla p_0$ . We emphasize that the hysteresis is important, due to the fact that the inequality of three holds for the forward and back transition thresholds in the deterministic model. Although a deterministic model predicts hysteresis in  $Q_r[p']$ , the statistical average  $\langle q_r \rangle$  is a single valued function of  $p'$ .

An important property of a nonequilibrium system is the life time of a metastable state. The transition rate from one metastable state to a more stable state is calculated by use of the nonlinear potential [6.20], in a manner similar to the Kramers barrier transition calculation [6.21]. Statistical averages determine the boundary of the phase [6.22].

### 6.3.3 Self-Organized Criticality (SOC) models

The analysis of turbulence has shown that the fluctuations have small but finite radial coherence length, and that they can be excited subcritically. This has motivated the view that fluctuation amplitude and the radial coherence length change nearly simultaneously, and that excitation happens if random kicks of the local gradient exceed some threshold. These properties have stimulated the use of SOC model [6.23] for the dynamics of fluctuations and transport [6.24-6.31]. The correspondence between the SOC model and continuum model has been investigated [6.32]. Schematically, the correspondences are given in Table 6.3.1.



A nontrivial tail of the PDF is obtained in analyses based on the SOC models. The mesoscale dynamics which are inherent to SOC models are realized here as avalanches of transported quantities (heat, particle, etc.). A large avalanche contributes to the tail of the flux PDF and contributes heavily to the total transport. [6.31]

An advantage of the SOC model is that it allows one to easily grasp the nonlocal features of the dynamical phenomena, while retaining a physically plausible picture of localized fluctuation events. Figure 6.3.2 illustrates a gradient-flux relation which is deduced from a SOC model of L-H transitions. The bulk of the PDF exhibits power-law scaling but the tail shows an exponential decay.

#### 6.3.4 Observations of avalanche phenomena in DNS

The PDF of the heat flux  $P(q_r(x, y))$  has been determined from direct nonlinear simulations of drift-ITG turbulence. Here,  $Q_r(x, y)$  is an instantaneous value of the local heat flux at  $(x, y)$ . Abbreviating  $P(Q_r(x, y))$  and  $Q_r(x, y)$  by  $P(Q_r)$  and  $Q_r$ , a power law tail

$$P(Q_r) \propto Q_r^{-\alpha} \quad (6.3.6)$$

was found as the result of direct nonlinear simulation. The power index  $\alpha$  is an important parameter: depending on the condition whether

$$\alpha > 2 \quad \text{or} \quad \alpha < 2, \quad (6.3.7)$$

the statistical average  $\langle Q_r \rangle$  changes its nature. Consider that the power law  $P(Q_r) \propto Q_r^{-\alpha}$  holds in the range  $Q_{\min} < Q_r < Q_{\max}$ . If  $\alpha > 2$  holds, the contribution from the tail to the average is given by  $Q_{\min}^{2-\alpha}$ . That is, the tail does not contribute to the average. If, on the contrary, the relation  $\alpha < 2$  holds, the term  $Q_{\max}^{2-\alpha}$  is dominant. The average is governed by the maximum value of the instantaneous flux. *In that case, rare events (i.e.,  $Q_r \sim Q_{\max}$ ) control the average.* According to the analysis in [3.87, 6.33], the result can be fit to  $\alpha \simeq 1.5$  for the case of weak shear flow, and to  $\alpha \simeq 2.3$  for the case of strong shear flow. In the former case, rare events (probably associated with the larger scale avalanches) play important roles in determining the average flux. It is thus not surprising that gyro-Bohm scaling is broken in this case.

The statistical analysis has also been performed for the bursty flux in the SoL [6.34-6.36]. In this case, an exponential tail for the flux is obtained. These results show that non-Gaussianity in the PDF is frequently observed and is important, and that the

specific form of the tail depends on the explicit form of the nonlinearity that governs the dynamics.

## 6.4 Non-Markovian Theory

The nonlinear analysis explained in §3 was presented in simplified limits. One is the limit where the turbulent decorrelation of drift waves is absent, that is, a drift wavepacket has two integrals of motion. As a consequence, drift wavepackets are considered to move on a surface in phase space set by the initial conditions. These BGK-type solutions are addressed. The other is the limit in which the turbulent decorrelation of drift waves is so fast that the Markovian approximation is used to model nonlinear interactions. In general, the nonlinear decorrelation time of drift waves is not zero, even though it may be short. Non-Markovian theory is necessary to treat the intermediate cases [6.37]. Recent advances in this direction are discussed in this section.

### 6.4.1 Hamiltonian structure of the dynamics

The conservation property of drift waves in the presence of zonal flow is expressed by the invariance of the action along rays, e.g., Eq.(3.4.13). In order to stress the analogy with Hamiltonian dynamics, one may rewrite the  $N$  equation as [3.112]

$$\begin{aligned} \frac{d}{dt} N(x; k, t) &= \mathcal{L}_w N(x; k, t) \\ &\equiv \frac{\partial H(x; k, t)}{\partial x} \frac{\partial N(x; k, t)}{\partial k} - \frac{\partial H(x; k, t)}{\partial k} \frac{\partial N(x; k, t)}{\partial x} \end{aligned} \quad (6.4.1)$$

with

$$H(x; k, t) = \omega_k(k) + k \cdot V_{ZF}(x, t) \quad (6.4.2)$$

where  $\omega_k(k)$  and  $k$  are the frequency and wavevector of drift wave, and  $V_{ZF}$  is the zonal flow velocity.

Equation (6.4.1) is a Hamiltonian equation for the wavepacket density. As is shown in previous subsections, the zonal flow itself has a finite correlation time, even in the situation where the root-mean-square value is stationary. Drift wavepackets in ambient zonal flows are also subject to statistical modulations. In order to consider this statistical dynamics property, the response of wavepackets in the presence of the zonal flow described is reduced perturbatively. One writes

$$N(x; k, t) = \langle N(x; k, t) \rangle + \tilde{N}(x; k, t) \quad (6.4.3)$$

where  $\langle N(x; k, t) \rangle$  is an average over temporal variations with respect to zonal flows, and  $\tilde{N}(x; k, t)$  denotes the deviation. At the same time, the operator  $\mathcal{L}_w$  is separated into

$$\mathcal{L}_w = \mathcal{L}_{w,0} + \mathcal{L}_{w,ZF} \quad (6.4.4)$$

where  $\mathcal{L}_{w,0}$  determines the unperturbed motion of drift wavepackets in the absence of zonal flow

$$\mathcal{L}_{w,0} = -\mathbf{v}_g \cdot \frac{\partial}{\partial \mathbf{x}} \quad (6.4.5)$$

( $\mathbf{v}_g \equiv \partial \omega_k / \partial \mathbf{k}$  : group velocity of wave) and  $\mathcal{L}_{w,ZF}$  describes the perturbation by the zonal flow as

$$\mathcal{L}_{w,ZF} = -\mathbf{V}_{ZF} \cdot \frac{\partial}{\partial \mathbf{x}} - \mathbf{W}_{ZF} \cdot \frac{\partial}{\partial \mathbf{k}}, \quad \mathbf{W}_{ZF} = -\frac{\partial}{\partial \mathbf{x}} (\mathbf{k} \cdot \mathbf{V}_{ZF}). \quad (6.4.6)$$

By the separation in Eqs.(6.4.3) and (6.4.4), Eq.(6.4.1) can be rewritten as

$$\frac{\partial}{\partial t} \langle N(x; k, t) \rangle - \mathcal{L}_{w,0} \langle N(x; k, t) \rangle = \langle \mathcal{L}_{w,ZF} \tilde{N}(x; k, t) \rangle \quad (6.4.7a)$$

$$\frac{\partial}{\partial t} \tilde{N}(x; k, t) - \mathcal{L}_{w,0} \tilde{N}(x; k, t) - \mathcal{L}_{w,ZF} \tilde{N}(x; k, t) = \mathcal{L}_{w,ZF} \langle N(x; k, t) \rangle. \quad (6.4.7b)$$

A solution of Eq.(6.4.7b) can be expressed as a path integral along the characteristics. By combining it with Eq.(6.4.7a), one can derive a non-Markovian equation for wavepackets, as

$$\begin{aligned} & \frac{\partial}{\partial t} \langle N(x; k, t) \rangle - \mathcal{L}_{w,0} \langle N(x; k, t) \rangle = \\ & \int_0^t dt' \left\langle \mathcal{L}_{w,ZF}(x; k, t) \mathcal{L}_{w,ZF}(x(t|t'); k(t|t'), t') \langle N(x(t|t'); k(t|t'), t') \rangle \right\rangle, \end{aligned} \quad (6.4.8)$$

where  $x(t|t')$  and  $k(t|t')$  denote the trajectory of wavepackets in the presence of zonal flow, with the initial conditions

$$x(t|t') = x \text{ and } k(t|t') = k \text{ at } t = t'. \quad (6.4.9)$$

Equation (6.4.8) is an example of a Zwanzig-Mori equation. For a intermediate scale zonal flow,

$$k \gg K_r \gg L_n^{-1}, \quad (6.4.10)$$

the approximation

$$\left\langle N(x(t|t'); k(t|t'), t') \right\rangle \approx \left\langle N(x; k, t') \right\rangle \quad (6.4.11)$$

may be acceptable. Equation (6.4.8) then turns to be a non-Markovian phase-space kinetic equation of the form:

$$\begin{aligned} \frac{\partial}{\partial t} \left\langle N(x; k, t) \right\rangle - \mathcal{L}_{w,0} \left\langle N(x; k, t) \right\rangle = \\ \int_0^t dt' \left\{ \frac{\partial}{\partial x} \cdot \mathbf{D}^{XX}(t-t') \cdot \frac{\partial}{\partial x} + \frac{\partial}{\partial x} \cdot \mathbf{D}^{XK}(t-t') \cdot \frac{\partial}{\partial k} \right\} \left\langle N(x; k, t') \right\rangle + \\ \int_0^t dt' \left\{ \frac{\partial}{\partial k} \cdot \mathbf{D}^{KX}(t-t') \cdot \frac{\partial}{\partial x} + \frac{\partial}{\partial k} \cdot \mathbf{D}^{KK}(t-t') \cdot \frac{\partial}{\partial k} \right\} \left\langle N(x; k, t') \right\rangle, \end{aligned} \quad (6.4.12)$$

where  $\mathbf{D}^{XX}$ ,  $\mathbf{D}^{XK}$ ,  $\mathbf{D}^{KX}$  and  $\mathbf{D}^{KK}$  are 2x2 tensors, given by

$$\mathbf{D}_{i,j}^{XX}(t-t') = \left\langle V_{ZF,i}(x, t) V_{ZF,j}(x(t|t'), t') \right\rangle, \quad (6.4.13a)$$

$$\mathbf{D}_{i,j}^{XK}(t-t') = \left\langle V_{ZF,i}(x, t) W_{ZF,j}(x(t|t'), k(t|t'), t') \right\rangle, \quad (6.4.13b)$$

$$\mathbf{D}_{i,j}^{KX}(t-t') = \left\langle W_{ZF,i}(x, k, t) V_{ZF,j}(x(t|t'), t') \right\rangle, \quad (6.4.13c)$$

$$\mathbf{D}_{i,j}^{KK}(t-t') = \left\langle W_{ZF,i}(x, k, t) W_{ZF,j}(x(t|t'), k(t|t'), t') \right\rangle, \quad (6.4.13d)$$

where  $i, j$  stand for the  $x$  and  $y$  directions. (The tensor form is necessary if one considers poloidal inhomogeneity, as is discussed in §3.3.4 or §6.1.) If the Markovian approximation is now employed, one finds

$$\mathbf{D}_{i,j}^{\alpha\beta} = \int dt' \mathbf{D}_{i,j}^{\alpha\beta}(t-t'), \quad (6.4.14)$$

where  $\alpha, \beta$  vary over  $X, K$ . The two quantities  $D_{x,x}^{XX}$  and  $D_{y,y}^{KK}$  reduce to what has been previously obtained in the limit of short life time of the drift waves.

Equation (6.4.12) describes the evolution of drift waves in the presence of a statistical ensemble zonal flows. First, it is a non-Markovian equation, and includes the finite memory time. Second, this equation includes cross interaction between the wavenumber space and the real space. Note that the cross-interaction terms are also derived in the diffusion approximation. Because of these effects, a deviation from the simple diffusion approximation in phase space arises. As a noticeable consequence of the non-Markovian effect, [6.37] illustrated super-diffusion and sub-diffusion phenomena in the transient response. (The cross-interaction term is small for the pure zonal flow case.)

The Kubo number  $\mathcal{K}$  may be defined as the ratio of the decorrelation time of drift waves to the bounce frequency of wavepackets in the trough of the zonal flow,

$$\mathcal{K} = \frac{\omega_{\text{bounce}}}{\gamma_{\text{drift}}}. \quad (6.4.15)$$

The analyses in §3.5.4, 3.5.5, and 3.5.7 are developed for  $\mathcal{K} < 1$ , while that in §3.5.6 is given for the limit  $\mathcal{K} \rightarrow \infty$ . (For the details of the bounce frequency, see §3.5.6.)

Equation (6.4.12) allows a study that covers a wide range of the Kubo number. Evaluations of the Lagrangian correlations in the RHS of Eq.(6.4.13) have been studied by using of the method of decorrelation trajectories [6.38-6.40]. Analysis of these effects has begun [3.112]. One important fact is that the poloidal wavenumber of drift waves  $k_y$  is no longer constant when the  $\mathbf{E} \times \mathbf{B}$  flow exhibits the poloidal asymmetry. This is in contrast to the case of stationary and purely  $m = 0$  zonal flow. New insights will be given by future research.

#### 6.4.2 Case of multiple fields

One of the key issues in the theory is an extension of the Hamiltonian formalism to the problems with multiple field variables, such as occurs with the inclusion of magnetic perturbations. The transparency of the analysis which was brought by the introduction of the wave kinetic equation could be maintained by introducing Casimir invariants for the Hamiltonian dynamics with multiple fields [6.41]. Research in this direction is on-going, and results from it will be used for the case of zonal flows or for the dynamo problem in electromagnetic turbulence.

### 6.5 Envelope Formalism

The zonal flow problem belongs to the class of problems concerned with understanding interactions in multi-component systems, with each component having its own range of characteristic space-time scales. The ratio of the disparate scales naturally defines one or more expansion parameters, which can then be used to develop perturbative approaches to such multi-scale problems. A number of such multiple time and space scale perturbation theory methods exist. So far, we have discussed two approaches to the multi-scale interaction problem. The first uses parametric (modulational) theory, and is based on a modal interaction expansion. The second is wave kinetics and adiabatic theory, and is based on a description employing rays and eikonal theory. A third multi-scale expansion approach exists, and is commonly referred to as the envelope formalism. This section is devoted to describing the envelope formalism approach to the zonal flow problem.

The envelope formalism uses reductive perturbation theory to develop a description in terms of the dispersion relation of a rapidly varying carrier wave (associated with the primary perturbation) and the amplitude of a slowly varying intensity envelope, associated with the mean field. The envelope evolves slowly in space and time, as compared to the carrier. The envelope formalism complements the parametric and wave kinetic approach in that:

(a) it is not restricted by the structure inherent to a modal expansion, and thus can represent a wider and richer class of nonlinear phenomena (i.e., solitons, collapse, etc.) than simple parametric theory can.

(b) it is not restricted to an eikonal description, and so can capture the physics of the competition between diffraction and nonlinearity, unlike wave kinetics.

Anticipated by Landau, the rigorous envelope formalism was pioneered by Newell and Whitehead [2.33] in 1969, with the aim of describing secondary pattern formation slightly above marginality in Rayleigh-Benard convection. The most notable application of the envelope formalism in plasma physics is to the classic problem of Langmuir turbulence and Langmuir collapse, as studied by Zakharov in 1972 [3.43]. It is worth mentioning here that the Zakharov equations are the coupled envelope equations for the amplitudes of the electric field  $E$  and density perturbation  $\tilde{n}$  in Langmuir turbulence, i.e.,

$$-2i\omega_{pe} \frac{\partial}{\partial t} E = \tilde{n} E - \gamma V_{the}^2 \nabla^2 E, \quad (6.5.1a)$$

$$\frac{\partial^2}{\partial t^2} \tilde{n} - c_s^2 \nabla^2 \tilde{n} = \nabla^2 |E|^2. \quad (6.5.1b)$$

Depending on dimensionality, initial conditions, and the number of degrees of freedom, many different nonlinear phenomena, including soliton formation, collapse, secondary radiation etc., can be described using this simple model. The simplicity and flexibility of the Zakharov equations has greatly stimulated interest in both Langmuir turbulence and in the application of the envelope formalism to other multi-scale nonlinear problems. The first application of the envelope formalism to convective cell dynamics (and thus zonal flows) was by Taniuti and collaborators in 1979. [6.42]

Here, we discuss only an especially simple application of the envelope formalism [6.43, 6.44] to the problem of zonal flow generation in drift wave turbulence. We consider a plasmas in 2D geometry with  $T_i = 0$ , but with a mean  $\mathbf{E} \times \mathbf{B}$  flow. In this case, the basic equations for the fluctuations  $\tilde{\cdot}$  and averaged fields  $\langle \cdot \rangle$  are:

$$\begin{aligned} \frac{\partial}{\partial t} (1 - \rho_s^2 \nabla^2) \frac{e\tilde{\phi}}{T_e} + V_d \frac{\partial}{\partial y} \frac{e\tilde{\phi}}{T_e} + \langle V_E \rangle \cdot \nabla (1 - \rho_s^2 \nabla^2) \frac{e\tilde{\phi}}{T_e} \\ + \tilde{V}_E \cdot \nabla \left( \langle n \rangle - \rho_s^2 \nabla^2 \frac{e\langle \phi \rangle}{T_e} \right) = 0, \end{aligned} \quad (6.5.2)$$

$$\frac{\partial}{\partial t} \nabla^2 \langle \phi \rangle + \langle \tilde{V}_E \cdot \nabla \nabla^2 \tilde{\phi} \rangle = 0, \quad (6.5.3)$$

$$\frac{\partial}{\partial t} \langle n \rangle + V_d \frac{\partial}{\partial y} \frac{e\langle \phi \rangle}{T_e} + \langle \tilde{V}_E \cdot \nabla \tilde{n} \rangle = 0, \quad (6.5.4)$$

where the density  $n$  is appropriately normalized and  $V_d$  is the drift velocity. As in many previous examples, we take the drift waves to be Boltzmann, but not the mean flows. This system can be used to describe simple zonal flow and streamer phenomena. To implement the envelope formalism, we write

$$\frac{e\tilde{\phi}}{T_e} = N \exp i(\mathbf{k} \cdot \mathbf{x} - \omega t) + \text{c.c.} \quad (6.5.5)$$

and assume the drift wave envelope  $N(X, T)$  varies *slowly* in space and time. The fast variation obeys the usual dispersion relation  $\omega = k_\theta V_d (1 + k_\perp^2 \rho_s^2)^{-1}$ . The scale of this variation is, of course, tied to that of the secondary, mean fields  $\langle n \rangle$  and  $\langle \phi \rangle$ . Here, for the slowly varying parameters, the ordering

$$T = \epsilon t, \quad X = (\epsilon x, \epsilon y) \quad (6.5.6)$$

expresses the scale separation. (In this section,  $\epsilon$  is a small parameter, not the inverse aspect ratio.) Note that nonlinearities associated with like-scale interactions are ignored. Now, expanding in  $\epsilon$  throughout yields the equations for the envelope  $N$  and the mean fields  $\langle n \rangle$  and  $\langle \phi \rangle$ , which are

$$\begin{aligned} \frac{i}{\partial \tau} N + \frac{1}{2} \left( \frac{\partial^2 \omega_k}{\partial k_x^2} \frac{\partial^2}{\partial X^2} + \frac{\partial^2 \omega_k}{\partial k_y^2} \frac{\partial^2}{\partial Y^2} + \frac{2 \partial^2 \omega_k}{\partial k_x \partial k_y} \frac{\partial^2}{\partial X \partial Y} \right) N \\ + \rho_s^2 \omega_{ci} \left( k \times \nabla \frac{e \langle \phi \rangle}{T_e} \right) \cdot \hat{z} N - \frac{\rho_s^2 \omega_{ci}}{1 + k_{\perp}^2 \rho_s^2} \left( k \times \nabla \langle n \rangle \right) \cdot \hat{z} N = 0, \end{aligned} \quad (6.5.7a)$$

$$\begin{aligned} \left( \epsilon \frac{\partial}{\partial \tau} - v_g \cdot \nabla \right) \left( \frac{\partial^2}{\partial X^2} + \frac{\partial^2}{\partial Y^2} \right) \frac{e \langle \phi \rangle}{T_e} \\ + 2 \rho_s^2 \omega_{ci} \left( k_x k_y \left( \frac{\partial^2}{\partial Y^2} - \frac{\partial^2}{\partial X^2} \right) + (k_x^2 - k_y^2) \frac{\partial^2}{\partial X \partial Y} \right) |N|^2 = 0, \end{aligned} \quad (6.5.7b)$$

$$\left( \epsilon \frac{\partial}{\partial \tau} - v_g \cdot \nabla \right) \langle n \rangle + V_d \frac{\partial}{\partial Y} \frac{e \langle \phi \rangle}{T_e} = 0. \quad (6.5.7c)$$

These equations are set in the reference frame moving with the wave group velocity, and  $\tau = \epsilon T$ . Note that Eq.(6.5.7b) shows that the structure of the secondary flow is determined, in part, by the anisotropy of the underlying turbulence - i.e., via terms  $\sim (k_x^2 - k_y^2)$ , etc. The system of Eqs.(6.5.7a) - (6.5.7c) constitutes the set of envelope equations for the drift wave - zonal flow system, including the more general case of drift wave - convective cell systems. [6.45-6.50]

For the particular case of zonal flow,  $\partial/\partial Y \rightarrow 0$ , and collisional damping of the zonal flow  $\gamma_{\text{damp}}$  is important, so Eq.(6.5.7b) becomes

$$\left( \epsilon \frac{\partial}{\partial \tau} - \frac{\partial \omega_k}{\partial k_x} \frac{\partial}{\partial X} + \gamma_{\text{damp}} \right) \frac{\partial^2}{\partial X^2} \frac{e \langle \phi \rangle}{T_e} - 2 \rho_s^2 \omega_{ci} k_x k_y \frac{\partial^2}{\partial X^2} |N|^2 = 0. \quad (6.5.8)$$

In the weakly collisional regime, then, the zonal flow potential is slaved to drift wave stresses, via

$$\frac{\partial}{\partial X} \frac{e \langle \phi \rangle}{T_e} = - \left( \frac{2 \rho_s^2 \omega_{ci} k_x k_y}{\partial \omega_k / \partial k_x} \right) |N|^2 = 0 \quad (6.5.9)$$



so that the envelope equation is a cubic nonlinear Schrödinger equation

$$i \frac{\partial}{\partial \tau} N + \frac{1}{2} \frac{\partial^2 \omega_k}{\partial k_x^2} \frac{\partial^2}{\partial X^2} N + \left( \frac{2 \rho_s^4 \omega_{ci}^2 k_y^2 k_x}{\partial \omega_k / \partial k_x} \right) |N|^2 N = 0. \quad (6.5.10)$$

Straightforward analysis then predicts modulational instability for drift wave numbers such that

$$1 + \rho_s^2 k_y^2 - \rho_s^2 k_x^2 > 0. \quad (6.5.11)$$

The most unstable zonal flow wavenumber is

$$q_{x, \max} = \left( \frac{\omega_{ci}^2 (1 + \rho_s^2 k_\perp^2)^5}{V_d^2 (1 + \rho_s^2 k_y^2 - \rho_s^2 k_x^2)} \right) N_0 \quad (6.5.12)$$

where  $N_0$  is the maximum drift wave amplitude. The domains of zonal flow and streamer instability are shown in Fig.6.1.3. A similar analysis for the collisional case has been performed as well. The results are given in [2.27].

It is interesting to note that the results of the envelope expansion may also be used to determine typical zonal flow scales. From the expression for  $q_{x, \max}$ , weakly collisional zonal flow will have radial scale

$$\Delta r \sim \frac{\rho_s^2}{L_n} \left( \frac{\tilde{n}}{n_0} \right)^{-1} F_{ZF}(\rho_s k_\perp). \quad (6.5.13)$$

Here  $F_{ZF}(\rho_s k_\perp)$  is determined by the  $\rho_s k_\perp$ -dependence of  $q_{x, \max}$ . Note that the scale is amplitude dependent. For  $\tilde{n}/n_0 \sim \rho_s/L_n$ ,  $\Delta r \sim \rho_s F_{ZF}(\rho_s k_\perp)$ , so a wide range of zonal flow scales may be excited. In particular, smaller scales producing strong shear are possible. Finally, note that zonal flows will be strongly localized near caustics, where  $\partial \omega_k^2 / \partial k_i^2 \rightarrow 0$ . Strongly anisotropic collapse, to localized, singular shear layers, is possible at caustics.

There is considerable work on the envelope formalism beyond the simple analysis described above. Weiland and collaborators have explored the effect of finite  $T_i$  and ion temperature perturbations [6.51]. More recent extension includes the study of electromagnetic perturbations [6.52]. Spineanu and Vald have studied the structure of zonal flow and have analyzed possible poloidal dependence [3.141, 6.53]. Gurcan, et al.

have examined zonal flow and streamer formation in ETG turbulence, which is isomorphic to quasi-geostrophic turbulence, since both waves and flows have Boltzmann ions [6.54-6.56]. They determined the criterion for collapse to singular shear layers and addressed the problem of pattern competition between streamers and zonal flows using techniques from the Langmuir problem.

## 7. Laboratory Experiments on Zonal Flows Physics

In this chapter, we discuss laboratory experiments relevant to zonal flows. As we have previously noted, the overwhelming preponderance of research on zonal flow phenomena in plasmas has been theoretical or computational, and experimental studies of zonal flows in plasmas are few and far between. Thus, this chapter is written with two aims in mind, namely, both to review existing work and also to outline possible future directions for studies of zonal flows, in the hope that more experimental work will be stimulated. Given the intrinsic difficulty of studying zonal flows in confined plasma, we divide our discussion into sections dealing with direct and indirect measurements. Direct measurements are those which reveal and quantify the nature of potential, electric field, velocity, and density fluctuations etc. which we associate with zonal flows. Indirect measurements are concerned with the study of nonlinear couplings, etc., associated with zonal flow dynamics.

This chapter is organized as follows. Sec 7.1 presents experimental results on determining zonal flow characteristics. Sec 7.2 discusses zonal flow dynamics and their interaction with ambient turbulence. For each section, we first summarize relevant information from theory and simulation, and then present experimental results and progress. We present our suggestions for future experimental research, including possibilities for basic experiments designed for zonal flow measurements, in Sec 7.3.

### 7.1 Characteristics of Zonal Flows

The characteristics of zonal flows are described in Chapters 2, 3 and 4, and are summarized in Table 2.1. Here, we reiterate some of those which are most relevant to experimental measurements and tests [3.77].

#### 7.1.1 Spatial Structure:

In confined plasmas, the equilibrium profile is usually treated as a smooth function of radius, the characteristic scale length of which is less than or equal to the minor radius (excluding the case of transport barriers) or of the barrier thickness (for barriers). In the presence of turbulence, which varies in radial, poloidal and toroidal directions, the flux-surface-averaged flow velocity can vary radially for two reasons. One is the  $\mathbf{E} \times \mathbf{B}$  zonal flow structure, which is discussed in this review. The other possible origin is the corrugation of flux-surface-averaged pressure. If such corrugation occurs, the diamagnetic drift velocity is also modulated, so as to vary in radius. As this is often the case, the fluctuation envelope may, in turn, be localized in radius and decay in a spatially intermittent manner. This latter type of localized diamagnetic flow, which is nothing but a symptom of flux surface-averaged pressure corrugation, must be carefully

distinguished from true zonal flows in experiments. Such pressure corrugations may be induced by avalanches, streamers, and other transport events.

Turbulence-driven zonal flows are radially localized, with a broad spectrum of radial scales ranging from the microscale (i.e., turbulence eddy sizes of  $\Delta r \sim$  several ion gyro-radii) through meso-scales (i.e., a fraction of minor radius). Gyrokinetic simulations of ITG turbulence show that the component of the zonal flow has  $q_r \rho_i \sim 0.1$  [3.77], for typical tokamak core plasma parameters, though the sensitivity of this value to variable system parameters is unclear. The flows are axisymmetric ( $q_\zeta = 0$   $n = 0$ ), and the flux-surface-average of  $\mathbf{E} \times \mathbf{B}$  flows is mainly in the poloidal direction. The associated electrostatic potential  $\phi_{ZF}$  is poloidally symmetric ( $q_\theta = 0$ ).

We note that the magnitude of zonal flow velocity, as predicted from tokamak core turbulence simulations, is typically small (i.e.,  $V_{ZF} = 10^{-2} v_{th,i}$ ), but the associated  $\mathbf{E} \times \mathbf{B}$  shearing rate is significant enough to regulate turbulence and transport [3.77, 7.1]. Obviously, this indicates that the zonal flow shear spectrum peaks at a higher  $q_r \rho_i$ , than the zonal flow velocity and potential spectra. This is apparent from the results of gyrofluid simulations, as shown in Fig. 3 of Ref. [7.1]. This suggests that the difficulties in measuring zonal flows in the experiments come mainly from the fact that it is necessary to simultaneously ensure sensing long correlation lengths in the toroidal direction ( $n=0$ ) and poloidal direction ( $m=0$ ) along with fast radial variation (on the scale of several ion gyro-radii). This constraint poses severe challenges to experimental measurement capabilities. Finally, achieving the goals of detecting the variability of the portion of the zonal flow spectrum responsible for transport regulation and identifying a causal link between flows and turbulence are further complicated by the fact that the 'relevant' shearing scales are determined by their autocorrelation times, as well as their shear strength. Features of the zonal flows contrasting the zero frequency zonal flows from GAM components are listed below in Table 7.1.

### 7.1.2. Temporal behavior:

The frequency spectra of zonal flows and GAMs depend on plasma conditions, and for this reason edge turbulence deserves a later, separate discussion. In the core, the zonal flow frequency spectrum at a fixed  $q_r$  has a broad peak at  $\omega = 0$ , and a width indicating a finite lifetime,  $\tau_{ac,ZF} = (\Delta\omega_{ZF})^{-1}$ . Zonal flows thus have frequency components which significantly outlive the ambient turbulence ( $\Delta\omega_{ZF} < \Delta\omega_{drift}$ , or equivalently  $\tau_{ac,ZF} > \tau_{ac,drift}$ ). Their lifetime  $\tau_{ac,ZF}$  is determined either by collisions, turbulent transfer processes as are explained in Chapter 3, by external noise, which is explained in Chapter 6, or by the instability of the zonal flow pattern.

In general, the question of the nature of zonal flow damping boils down to a comparison between the strength of collisional and nonlinear processes.

### 7.1.3. Toroidal Geometry and GAMs

While the basic nonlinear properties of zonal flows can be most effectively described in a simple geometry, and fundamental contributions to zonal flow physics can be made by basic experiments, it is necessary to characterize the specific geometric effects for each configuration to obtain a proper understanding of the actual experimental results from toroidal devices. In toroidal geometry, the poloidal direction is no longer an ignorable coordinate, and there exists an inevitable poloidal angle dependency of many key quantities (for instance,  $B$  depends on the poloidal angle). While the flux-surface-average of  $\mathbf{E} \times \mathbf{B}$  flows are mainly in the poloidal direction [2.7, 2.8], the toroidal return flow has a  $\sin \theta$  dependence. In general toroidal geometry, the zonal flow magnitude  $V_{ZF} = -E/B = B^{-1} \partial \phi_{ZF} / \partial r$ , i.e.,  $(RB_\theta B^{-1}) \partial \phi_{ZF} / \partial \psi$  ( $\psi$  being the magnetic flux function) has a slight in-out asymmetry due to a flux-expansion factor " $RB_\theta$ " [2.9]. Due to the presence of geodesic curvature in various toroidal devices, the zonal flow contains a linearly damped oscillation called a Geodesic Acoustic Mode (GAM) [3.5], as discussed in Sec 3.1.2 and Sec 4.5.2., in detail. Since GAM pressure fluctuation has dominant mode numbers  $n=0, m=1$  (due to toroidal coupling), it has  $k_{\parallel} = 1/qR$ , so that  $\omega_{GAM} = Gv_{th,i}/R$ . Here  $G$  is a coefficient of the order of 1, and ion Landau damping for GAMs scales like  $\sim \exp \left\{ -\omega^2/2k_{\parallel}^2 v_{th,i}^2 \right\} \sim \exp \left\{ -G^2 q^2/2 \right\}$ . Thus, one would expect a "GAM peak" to be clearly visible in the frequency spectrum when GAM energy is appreciable. In conclusion, some key features of GAM are not only a well-defined linear oscillation frequency,  $\omega_{GAM} = Gv_{th,i}/R$ , but also the existence of side-band pressure fluctuations with  $n=0$  and  $m=1$ . Properly distinguishing between oscillatory GAM's and classical zonal flows (which are quasi-stationary) is a major challenge to experimentalists interested in zonal flow physics. This issue is particularly relevant since the finite characteristic frequency of GAMs renders them easier to detect experimentally than the zero-frequency zonal flows are.

Finally, we briefly remark on stellarators (helical systems). Turbulence-driven zonal flow properties in stellarators have not been discussed widely to date, but have recently begun to be addressed in print [7.2]. The questions of the effective damping and inertia of zonal flows in systems for which axisymmetry is absent, are particularly acute. In particular, new or enhanced damping mechanisms may be present, and the continued status of zonal flows as "modes of minimal inertia" is not certain. For these, experiments on future stellarators with quasi-axisymmetry such as the National Compact Stellarator Experiment (NCSX) [7.4] and CHS-qa [7.5] would be illuminating.

### 7.1.4 Experimental studies of zonal flow structure via potential measurements

### Flux-surface average radial electric field

The most direct evidence of zonal flows comes from measurements of the  $\mathbf{E} \times \mathbf{B}$  flow  $V_{ZF}$ , the associated radial electric field  $E_r$ , or the associated electrostatic potential  $\phi_{ZF}$ . As the importance of the flow shear decorrelation mechanism [2.7-2.9] in enhancing confinement has become widely recognized [3.137, 4.13, 7.6], there have been significant advances in the diagnostic capabilities in measuring  $E_r$  using the motional Stark effect (MSE) [7.7] or the heavy ion beam probe (HIBP) [7.8, 7.9], and in measuring the poloidal velocity  $V_\theta$  of carbon impurity ions using charge exchange recombination spectroscopy (CHERS), and then calculating  $E_r$  from the radial force balance relation [7.10-7.12]. However, an order of magnitude improvement in the *temporal* resolution of these diagnostics is required to distinguish the temporal evolution of zonal flows from that of the mean  $\mathbf{E} \times \mathbf{B}$  flow. Note that the "mean flow" can have a component which is rapidly varying in radius, on account of a fast local variation of the plasma density or temperature profile, especially at transport barriers. For this reason, the "mean equilibrium" profile must also be measured with a radial resolution sufficient to distinguish profile corrugation induced by a spatially intermittent turbulent transport and narrow barrier widths from zonal flows. As discussed at the beginning of this section, while zonal flows are typically long lived as compared to turbulence eddies, their auto-correlation rate can reach 5KHz for typical tokamak core parameters [3.77]

### Identification of zonal flow by use of HIBP

The heavy ion beam probe (HIBP) is capable of measuring the electrostatic potential  $\phi_{es}$ , associated the radial electric field. Its relatively fine temporal resolution has allowed detailed analyses of the edge transport barrier of the H-mode [7.13, 7.14] and the internal transport barrier (ITB) dynamics in stellarators [7.9, 7.15, 7.16]. By use of a single HIBP, the radial resolution of which has not been better than 1cm, the mean  $E_r$  was measured. This is believed to be mainly determined by neoclassical (collisional) particle transport, rather than by turbulence. The identification of the core zonal flow has been achieved very recently by use of a dual-HIBP system, i.e., two HIBP's are set in different toroidal angles, thus allowing the measurement of the toroidally symmetric  $n=0$  component, which is the critical element of the zonal flow measurement. [7.17, 7.18] Improved resolution and S/N ratio allowed the measurement of the local electric field. This has made a path to the direct measurement of zonal flows in the plasma core. Figure 7.1 illustrates the power spectrum of the radial electric field in the core of CHS plasma, indicating the zonal flow component near  $\omega \sim 0$  and the peak of the GAM oscillations. Measuring  $E_r$  at fixed radius  $r_1$  by one HIBP, and  $E_r$  at various radii  $r_2$  by the other HIBP, the coherence of the radial electric field at  $r_1$  and  $r_2$  is directly measured. The low frequency part ( $\omega / 2\pi < 1 \text{ kHz}$ ) has high coherence, demonstrating a long coherence length. Cross-coherence takes a large positive value at  $r_1 = r_2$ , i.e.,  $n=0$ . As the

relative distance  $r_1 - r_2$  varies, the cross coherence-value between two measured electric field varies, alternately, between large positive values and large negative values. By this measurement, the radial wavelength of the zonal flow was identified. In the case of Fig.7.1, the radial wavelength of the zonal flow is about 1-2 cm. This rapid radial variation is another essential feature of the zonal flow. The amplitude of this zonal flow is also observed to be few  $100 \text{ Vm}^{-1}$ , and the  $\mathbf{E} \times \mathbf{B}$  shearing rate remains smaller than the diamagnetic velocity divided by the plasma size. The sample volume still remains of the order of the radial wavelength. This limit of spatial resolution may be an obstacle for measuring the precise peak height of the zonal flow. The decorrelation rate of the zonal flow,  $\Delta\omega_{ZF}$ , is found to be smaller than (or at most)  $2\pi \times 10^3 \text{ s}^{-1}$  in this observation, and is close to the inverse time of the global energy confinement time. (The energy confinement time is a few ms in low density ECH plasmas.) The radial scan of the measurement point has revealed that the zonal flows exist over a wide region of radii. To date, this result seems the most direct and convincing experimental confirmation for the presence of the zonal flow in core plasmas.

#### Measurement at edge

Near the edge of tokamak plasmas, Langmuir probes are applied to the study of long-range electric field fluctuations. In the study of [7.19], radial electric fields are measured at different poloidal angles simultaneously, and the low frequency component is identified. Although the poloidal angle between two forked probes is limited (the distance between them in toroidal direction is about 1/10 of the minor radius), the observation gives a strong support for the presence of the poloidally symmetric, low frequency radial electric field perturbations as is shown in Fig.7.2. The amplitude and radial wavenumber are evaluated as  $\tilde{V}_{ZF}/V_{Thi} \approx 0.5 - 0.9\%$  and  $q_r \rho_i \approx 0.06 - 0.1$ . The half-width at half maximum of the spectrum is not clearly identified.

#### Edge transport barrier

Another measurement of the electric field by use of the HIBP has been performed on the JFT-2M tokamak [7.13, 7.14] in conjunction with the L-to-H transition. The radially-localized response of the electric field structure near the last closed flux surface is precisely measured. The jump of the radial electric field and associated change of the fluctuations have been measured at the onset of the L-H transition. The high temporal resolution of the potential measurement has allowed the determination of the rate of variation of the radial electric field at the onset of the L-H transition. Results indicate  $\dot{E}_r/E_r \approx O(10\mu\text{s}^{-1})$ . This is in the range of theoretical predictions for the rate of radial electric field bifurcation. So far, an accurate decomposition of the measured radial electric field into the zonal flow and the "mean flow" has not been possible. The discrimination of the zonal flow component from the "mean flow" at the transport barrier and other

regions of rapid profile variation remains a significant challenge for future experimental research on zonal flows.

#### Observation of potential fluctuations in GAM frequency range

The long range oscillation in the core plasma, which is attributed to the GAM, has been observed on CHS by use of dual HIBP systems as is illustrated in Fig.7.1. The frequency of  $\omega/2\pi \approx 17 \text{ kHz}$  is close to the GAO frequency at the observed ion temperature [7.20]. The half-width at half maximum of the spectral peak is a few kHz. The measurement of other wave parameters, e.g., the parity of the density perturbation, the radial wavelength, and others, is on-going.

The experimental evidence for the presence of GAMs in tokamaks has also increased. The measurement of potential fluctuations by use of the HIBP has been performed on the JIPP-TIIU tokamak [7.14]. Low frequency fluctuations in the range of 20kHz have been identified in the vicinity of the plasma edge and core, as well [7.8, 7.21]. This was the most advanced measurement of potential fluctuation in the mid 90's. This fluctuation was conjectured to be a GAM oscillation. Further analysis of the measured data is ongoing.

Motivated by the recent community-wide interest in measuring zonal flows, HIBP measurement data obtained from TEXT tokamak plasmas in the early 1990's have been recently re-analyzed in detail [7.22]. The measured potential fluctuation has the following properties. For a range of minor radius from  $r/a = 0.6$  to  $r/a = 0.95$ , the  $m = 0$  component of the potential fluctuation with radial correlation length below 2cm (smaller than the sample volume size) was found to be oscillating with a well-defined frequency which matches that predicted for the GAM [3.5]. Outside of this radial range, no significant  $m = 0$  fluctuation in potential was detected.

It should be noted, however, that conclusive measurements of the long toroidal correlation length ( $n = 0$  component) have *not* yet been completed (except by the dual HIBP measurement on CHS). In particular, the pertinence of the measured potential fluctuations to zonal flows (as opposed to GAMs) is still unclear. Even the dual HIBP experiments need future experiments for more conclusive results. For instance, one would expect that shearing amplitudes can be greater for the zonal flow component. It also remains to be seen whether the potential fluctuation is accompanied by a side-band pressure perturbation. It would also be illuminating to explore, via numerical simulation, whether or not GAMs in that particular frequency and parameter regime could play a significant role in regulating turbulence.

## **7.2. Zonal Flow Dynamics and Interaction with Ambient Turbulence**

As is illustrated in Fig.7.1, the zonal flow amplitude and drift-wave fluctuations are simultaneously measured on CHS by use of the dual HIBP system. This provides a



possibility to identify the causal relation between the zonal flow and ambient turbulent fluctuations. The detailed measurements and analyses are on-going, and a definitive conclusion has not yet been obtained. Therefore, in this section, we discuss indirect measurements on zonal flows. Such experiments attempt to detect and to elucidate the physics of zonal flows by indirect means. In some cases, such indirect approaches strike at the heart of the fundamental physical processes thought to generate zonal flows (i.e., triad interactions between two high frequency drift waves and the zonal flow). In other cases, such approaches look for the “foot print” of the zonal flows in other, more accessible fluctuation measurements channels (i.e., such as the Doppler shifted frequency spectra of density fluctuations presumed to be advected by zonal flows). Thus, these approaches are motivated by concerns of both physics and expediency.

### 7.2.1. Zonal Flow Generation Mechanisms

As discussed in Sec. 3.2, zonal flows in electrostatic turbulence in a simple geometry are generated by the Reynolds' stress associated with the nonlinear coupling of higher- $k$  components of the ambient fluctuations [2.30]. In the more general context of electromagnetic turbulence in toroidal geometry, the evolution of the zonal flow can be written in the following schematic way;

$$\frac{d}{dt} V_{ZF} = \text{Reynolds' + Maxwell's + Stringer-Winsor + damping} \quad (7.1)$$

Most theoretical discussions on zonal flows have focused on the role of Reynolds' stress [the first term on the RHS of Eq. (7.1)], since it is believed to be relevant regardless of geometry, values of the plasma beta, and the nature of fluctuations. However, some [7.23] argued that, in the transition region between the core and edge of tokamak plasmas, the Stringer-Winsor (SW) term [the third term on the RHS of Eq. (7.1)], can play a major role in generation of the GAM component of zonal flows. The Stringer-Winsor mechanism is basically a torque on the plasma pressure column caused by the interaction of pressure inhomogeneity with the in-out asymmetry in magnetic field strength [7.23]. In the results of Braginskii fluid simulation described in Ref. [3.140], it was found that the SW term was greater than the Reynolds' stress term for a typical parameter set for the transition core/edge region. However, more recent related fluid simulations by other teams found that the SW effect has a different sign from that of the Reynolds' stress and can make zonal flow generation weaker [4.64, 7.25].

As discussed in Chapter 3, for electromagnetic turbulence, the Maxwell stress term [the second term on the RHS of Eq. (7.1)] associated with the  $J \times B$  nonlinearity can be appreciable. In the ideal MHD limit of purely Alfvénic turbulence, the Maxwell's stress cancels the Reynolds' stress exactly, and the state is called the purely Alfvénic state. This establishes that zonal flow can be driven only through non-ideal MHD effects.

### 7.2.2. Experimental Studies on Zonal Flow Dynamics

It is encouraging to note that the Reynolds' stress has been measured using Langmuir probes on the TJ-2 stellarator [7.26] and the H-1 tokamak [7.27]. One should note that the dominant nonlinear mode coupling channel for zonal flow generation is the 3 mode coupling involving two high- $k$  fluctuations and the zonal flow, i.e., a nonlocal (distant) interaction in  $k$ . An increase of this nonlinear mode coupling is an indicator, albeit indirect, of increased zonal flow generation [7.28]. The strength of interaction can be quantified by bi-coherence measurements and there have been bi-coherence analyses of the probe measurements on DIII-D edge [7.29-7.31], which support the notion that the nonlinear couplings, which are necessary for zonal flow generation, increases abruptly just prior to the H-mode transition. A relevant experiment has been performed on H-1 heliac [7.32], confirming the dominance of nonlocal interaction in the generation of the poloidally extended structures. The role of geodesic curvature coupling (i.e., the relative importance of Reynolds' stress drive and the Stringer-Winsor drive/damping) have been further investigated on the Kiel stellarator [7.33].

### 7.2.3. Experimental Studies on Zonal Flow Interaction with Turbulence

Given the difficulty in measuring  $\tilde{\phi}$ ,  $E_r$ , etc., most fluctuation diagnostics measure density fluctuations. Therefore, there exist many fusion plasma devices in which zonal-flow-related experiments can be tried via density fluctuation measurements. We summarize some experiments along these lines using different methods. One can try to measure the zonal ( $n=0, m=0$ ) component of density fluctuations associated with the zonal flow potential  $\phi_{m=0, n=0}$ . An experiment and analysis based on line-integrated measurements of density fluctuations on DIII-D tokamak edge using the phase contrast imaging (PCI) [7.34] was able to demonstrate that the fluctuation spectrum as a function of  $k_r$  and  $\omega$ ,  $S(k_r, \omega)$  resembles that obtained from ITG turbulence simulations.

However, this line-integrated measurement could not demonstrate that the observed fluctuations were symmetric in both poloidal and toroidal directions (i.e.,  $m=0, n=0$ ). The estimated upper bounds on the mode number was of the order of 30.

One way of examining zonal flow properties is to estimate the zonal flow velocity (which advects the ambient turbulence) by analyzing the "measured" ambient turbulence density fluctuation spectra. We note that for this approach, the instantaneous Doppler-shift of the density fluctuation with wave vector  $k$  should exceed the decorrelation rates of both the zonal flows and turbulence, thus allowing the use of Taylor's hypothesis [7.35]. Significant progress in this approach has been made by using a 2-dimensional array of beam emission spectroscopy (BES) diagnostics on the plasma edge. BES measurements and analyses have identified that density fluctuations are advected by the zonal-flow-like field [7.36]. The estimated flow amplitude was of the order  $10^{-2} v_{th, i}$

roughly in the range observed in numerical simulations [3.77]. The alleged zonal flow also has a well-defined frequency close to that of the GAM [7.37]. A signal was readily observed at high  $q$  and not observed at low  $q$  [7.38], as expected from the  $q$ -dependence of GAM Landau damping, as discussed in Sec. 7.1.3. Unfortunately, another important aspect of GAM oscillation is that the zonal flow ( $n=0$ ,  $m=0$ ) is accompanied by the  $n=0$ ,  $m=1$  component of density fluctuations. This prediction could not be confirmed. This shortcoming was partly due to the fact that the BES arrays were located near the low field midplane side of the tokamak, where GAM density fluctuations are expected to be very weak. From a simple theory, the GAM amplitude, at a given flux surface, is expected to be highest at the top and at the bottom of the tokamak. The poloidal mode number of density fluctuations from this experiment was predicted to be on the order of 10 [7.37].

Another way of estimating the zonal flow velocity, which of course advects the ambient turbulence, is to measure the Doppler shift of the ambient turbulence density fluctuation frequency spectra, using Doppler reflectometry [7.39]. An oscillation at 20-30 kHz was observed in the core of T-10 tokamak and was attributed to the GAM [7.40]. From a measurement of the edge plasma of ASDEX-U, a coherent peak in the spectrum near the GAM frequency has been observed in addition to a stronger and broader peak at much lower frequency which appears to be “zero frequency” zonal flow [7.41]. The dependence of the peak frequency on the edge electron temperature is in broad agreement with GAM frequency for various operation modes of plasmas including Ohmic, L-mode, and quiescent H(QH)-mode plasmas as reported in Ref [7.41].

#### **7.2.4. Measurements of Zonal Flow Effects on Confinement**

Another indirect way of demonstrating the existence of zonal flow is by identifying the change in transport and confinement due to zonal flows. These include the expected changes in turbulence-driven transport onset conditions (for instance, a change akin to the Dimits shift) and transport scaling with key macroscopic variables (for instance, ion-ion collisions, which damp zonal flows, or parameters which enter the neoclassical dielectric function). Such studies should emerge from systematic dimensionless parameter scans of plasmas.

### **7.3. Suggestions on future experiments and information needed from simulations and theory**

After a summary (not exhaustive) of the recent experimental progress in pursuing the measurements of zonal flows, we discuss some future experimental plans and possibilities for further progress and list key physics information which future experiments will need from numerical simulations and theories for the identification of zonal flows.

We mentioned that an order of improvement in the *temporal* resolution of the present day diagnostics, together with the identification of the  $n = 0$  component, is required to distinguish zonal flows from the “mean  $E \times B$  flows”. Regarding HIBP measurements, two HIBP systems are operating on CHS, providing simultaneous measurements of the electric field perturbation pattern and structure. Initial data from the dual HIBP system has already yielded the essential direct observation of the zonal flow. Future progress on CHS experiments are promising, and will play a central role for the experimental study of zonal flow in core plasmas. Studies of higher resolution are planned on the National Spherical Torus Experiment (NSTX) using a new spectroscopic technique with a higher temporal resolution [7.42] and on the Alcator C-Mod tokamak using a 2-D gas puff image (GPI) of edge turbulence [7.43].

Regarding bi-coherence analysis of turbulence spectra, the conclusive result in this endeavour requires the precise measurement of the zonal flow component, together with the other two 'legs' of the three wave coupling triad that resonate with the measured zonal flow. The coherent part of this nonlinear interaction with the zonal flow of interest must be measured, so as to quantify the acceleration of the zonal flow by the background turbulence. This process can be extended to electromagnetic fluctuations in high  $\beta$  plasmas. Then the incoherent part of the nonlinear interactions must be measured to quantify the stochastic noise term. Through these processes, one has solid understanding of the physical process which governs the generation of the zonal flow

For further elucidation of the implications of the experimental results based on the measurements of density fluctuations, the following information from direct numerical simulations will be extremely useful. First, for an identification of density fluctuations which accompany the zonal flows, simulations should quantify the expected level of density fluctuations not only for the  $n=0, m=0$  mode, but also for the side bands  $n=0, m=1$ , etc. We note that most 'zonal flow characteristics' listed in print to date [3.77] are based on pure ion temperature gradient (ITG) turbulence, with adiabatic electron response where  $\tilde{n}/n=0$  for  $n=0, m=0$  mode. With recent advances in gyrokinetic simulations including more realistic electron dynamics as described in Chapter 4, such information should now be available and should be extremely useful for experiments measuring density fluctuations, such as phase contrast imaging (PCI) [7.44]. Of course, for detailed comparisons between experiment and simulations, more comprehensive spectral information than those usually presented (such as  $S(k_r)$  or  $S(\omega)$  at a fixed  $k_r$ , etc) would be desirable, especially  $S(k_r, \omega)$  and  $S(k_r, \omega, k_\theta)$  for  $m=0, \pm 1, \pm 2 \dots$ , etc. Another way to systematically demonstrate the effects of zonal flows is to scan the plasma parameters and compare the detailed spatio-temporal behavior of the ambient turbulence measured by comprehensive 2-D microwave imaging [7.45] to results from direct numerical simulations. This, however, requires that the simulation code should be validated via comparison to simpler experiments.

Second, for an identification of zonal flows through the measurement of high- $k$  density fluctuations which are advected by the flows, the temporal scale separation of the various physical frequencies required for Taylor's hypothesis [7.45] should be established in order to strengthen the validity of the experiments and analyses. The relevant frequencies involved are:

$k \cdot V_E$ , the instantaneous Doppler-shift of the frequency of ambient turbulence, due to zonal flows,

$\Delta\omega_{\text{drift}}$ , the decorrelation rate of the ambient turbulence,

and

$\Delta\omega_{\text{ZF}}$ , the decorrelation rate of the zonal flow itself.

While the estimate that  $\Delta\omega_{\text{ZF}} < \Delta\omega_{\text{drift}} < k \cdot V_E$  [3.77] is often quoted, this was only one case for a 'typical' set of tokamak core parameters. Preferably, such information should be available from direct numerical simulation, for each experiment.

The reason why the measurement of the zonal flow has been so rare in the experiment of plasma confinement, which has lasted already about five decades, was explained at the beginning of Chapter 7. That is, the need of high resolution of the electric field measurement in radius and time, simultaneous with the capacity to measure long poloidal and toroidal correlation length, is really demanding. These difficulties must be overcome in the future, because the understanding of the drift wave-zonal flow turbulence is a crucial element of the understanding of anomalous transport.

## 8. Summary and Discussion

In this final section, we present the conclusions of this review of zonal flow physics and briefly discuss directions of, and areas for, future research. There is no question that zonal flows exist, are ubiquitous constituents of drift wave turbulence in confined plasma, and also occur many places in nature. Research has also demonstrated that zonal flows are an essential element of the mechanisms of self-regulation of drift wave turbulence and of the formation of edge and internal transport barriers. The development of the understanding of zonal flow phenomena has made a concrete contribution to controlled fusion research, in general, and to the design of ITER and other future experiments, in particular.

The theory of zonal flows is now a well-developed subject. We have shown that it is convenient and illuminating to classify the diversity of zonal flow dynamics according to the degree of stochasticity of drift wave ray propagation in the zonal flow field, and by the ratio of the zonal flow autocorrelation time to the 'bounce time' of a drift wave packet trapped in a zonal flow field. A variety of approximation methods have been utilized to calculate the rate of zonal shear amplification, for both the coherent and the stochastic regimes, and for a variety of different geometries. All of this wide variety of calculational approaches have the common element of their foundation in the disparity of time scales between the primary drift waves and secondary zonal flows. The back reaction of zonal flows onto the primary drift wave spectrum via shearing, both coherent and stochastic, is now well understood. Such insight has facilitated the construction of simple but self-consistent models which describe the various states of the drift wave-zonal flow system. The development of more advanced theories, such as probabilistic approaches and models, is proceeding in the research community.

Numerical simulations of zonal flows have identified their generation in a broad regime of models of low frequency microturbulence. In addition, some aspects of zonal flow structure, generation by modulational instability, and saturation scaling trends have been critically tested by numerical simulation, with a high degree of success. However, the further development and application of detailed computational diagnostics to *quantitative* tests of zonal flow theory is still quite desirable. Experimental research on zonal flow phenomena is still in its youth. While several experiments have identified various elements characteristic of zonal flow phenomena, critical tests of basic zonal flow physics and of the basic theory remain incomplete.

We now discuss some of the frontiers of, and possible future developments in, the physics of drift wave-zonal flow turbulence. In the realm of theory, the critical problem is that of identifying and evaluating zonal flow saturation mechanism in the collisionless regime. Further and deeper work on tertiary shear flow instability, nonlinear wave kinetics, trapped wave packets and turbulent trapping will be valuable and surely

will be forthcoming. Such works need to confront the reality of realistic geometry, including that of the stellarator, as well. The advancement in meeting the challenge of complex geometry and dynamics will strengthen an already powerful theoretical basis, which commonly helps to solve the expected mysteries presented by future space and astronomical observations. In addition, the role of convective cells (i.e., alternatively nonlinear streamers) in the drift wave-zonal flow system must be better understood. General convective cells, which varies in the poloidal direction, can be induced by drift wave turbulence, and may have a strong impact on the dynamical evolution of transport in the system. The structure of convective cells which are rapidly varying in the poloidal direction may be strongly influenced by magnetic shear. The partition of excitation energy between drift waves, zonal flows and convective cells has not been fully addressed, and requires intensive future study. This issue lies at the heart of the 'pattern selection' problem, as to which type of secondary structure is the ultimate 'attractor state' for a given set of system parameters. More generally, the nonlinear theory of wave kinetics, particularly the regime near primary wave marginality (i.e.,  $\gamma_k \rightarrow 0$ ), remains unexplored and thus merits further development. This is a general theme in plasma theory, and progress on this topic will sow the seeds for future benefits in a number of problems. Another area of likely activity is the study of the interaction of zonal flow with mean  $E \times B$  sheared flows and other questions pertinent to confinement, such as turbulence propagation. Also, further study of electromagnetic effects on zonal flows is necessary, including, in particular,  $A_\perp$  effects ( $A_\perp$  is the vector potential in the direction perpendicular to the magnetic field), which are critical to high beta plasmas, such as those found in spherical tori. The more general questions of the interaction between zonal flow dynamics and those of magnetic dynamos, etc., remain to be clarified, as well. Finally, since zonal flow shearing is effectively a process whereby smaller scales are strained by larger scales, it is fundamentally an intermittency phenomenon. Future theoretical research must address such intermittency, in order that predictive capacity be optimized. In particular, the astute reader will surely have noted that all discussion of zonal flow shearing, herein and elsewhere, is, as usual in plasma physics, organized in the either coherent shearing models, where  $k_r V'_{E \times B} t$ , or stochastic shearing models, where  $\delta k_r \sim \sqrt{D_k t}$ . In reality, nondiffusive Levy-flights on  $k_r$ , with  $k_r \sim t^\alpha$   $1/2 < \alpha < 1$ , are surely possible and will appear as intermittent, strong shearing events. To describe such phenomena, a fractional kinetic theory [8.1] will be necessary. Insights from SoC-type models [3.111] may be useful, as well.

Future simulation research must progress further from observation and identification of zonal flow phenomena to quantitative numerical experiments and tests. More advanced numerical diagnostics must be developed, and more systematic regime surveys must be implemented. Though numerical simulation has contributed much to our understanding of drift wave-zonal flow turbulence, its full potential has not yet been

tapped. Finally, it must be said that the greatest opportunities for future research on zonal flows lie in the realm of experiment. Particular challenges include the simultaneous study, correlation and synthesis of generation dynamics in real space (i.e., via vorticity transport) and  $k$ -space (i.e., via nonlinear mode coupling), and the development of methods to control zonal flows. More generally, future experiments must emphasize *challenging* the theory and confronting it with stressful quantitative tests.

Finally, it should be emphasized that the zonal flow dynamics problem represents one well-defined example of a broad class of bifurcation phenomena in confined plasmas. As such, it can and will join with other firm webs of interacting feedback loops which collectively govern plasma dynamics. For example, in burning plasmas, both burning and quenching can be expected to appear as dual, bistable states. Transitions between them, either periodic or intermittent, could be triggered by transport events, for which the dynamics of drift wave-zonal flow turbulence in high temperature D-T plasmas would be of central importance. Internal transport barriers formation in burning plasmas is another example of events from this category. The predictability of such transition phenomena merits intense theoretical study. However, interest in zonal flow physics is not limited to the realm of fusion plasma physics. Zonal flow generation is an example of a broad class of problems dealing with the amplification of an axial vector field with global symmetry by microscopic turbulence which is driven by the gradient of a scalar field. This category of problems also includes the magnetic dynamo (solar, terrestrial and galactic), accretion disk dynamics, jet formation, the global circulation of the ocean, etc. Thus, the study of zonal flows is a splendid opportunity for plasma and fusion science to demonstrate its capability to make a significant contribution to this now classic lore of problems.



## Acknowledgements:

The authors have benefited tremendously from efforts of their collaborators in the course of research on topic related to the material of this review. For their many contributions, we thank (listed alphabetically): M. Beer, K. H. Burrell, B. A. Carreras, S. Champeaux, A. Das, A. Fukuyama, A. Fujisawa, O. Gurcan, K. Hallatschek, C. Hidalgo, F. L. Hinton, C. H. Holland, D. W. Hughes, A. V. Gruzinov, I. Gruzinov, O. Gurcan, E. Kim, Y.-B. Kim, V. B. Lebedev, P. K. Kaw, Liu Chen, Z. Lin, M. Malkov, N. Mattor, R. Moyer, R. Nazikian, M. N. Rosenbluth, H. Sanuki, V. D. Shapiro, R. Singh, A. Smolyakov, F. Spineanu, U. Stroth, E. J. Synakowski, S. Toda, G. Tynan, M. Vlad, M. Yagi and A. Yoshizawa.

We also are grateful for useful and informative discussions with (listed alphabetically): R. Balescu, S. Benkadda, P. Beyer, G. Carnevale, J. W. Connor, A. Dimits, J. F. Drake, X. Garbet, A. Hasegawa, C. W. Horton, K. Ida, Y. Idomura, Y. Kishimoto, Y. Kiwamoto, J. A. Krommes, F. Jenko, E. Mazzucato, G. Mckee, Y. Miura, K. Molvig, V. Naulin, W. Nevins, D. E. Newman, H. Park, F. W. Perkins, T. Rhodes, R. Z. Sagdeev, Y. Sarazin, B. Scott, K. C. Shaing, K.-H. Spatscheck, H. Sugama, R. D. Sydora, S. Tobias, L. Villard, E. Vishniac, F. Wagner, M. Wakatani, W. Wang, T-H Watanabe, J. Weiland, S. Yoshikawa, W. R. Young, M. Zarnstorff, F. Zonca, S. Zweben. We thank authors who permitted reproduction of figures and Mr. S. Keating for careful proof reading of the manuscript.

This work was partly supported by the U.S. DOE under Grant No. FG03-88ER53275. This work was partly supported by the Grant-in-Aid for Specially-Promoted Research (16002005) and the Grant-in-Aid for Scientific Research (15360495) of Ministry Education, Culture, Sports, Science and Technology of Japan, by the Collaboration Programs of NIFS and of the Research Institute for Applied Mechanics of Kyushu University, and by Asada Eiichi Research Foundation. This work was partly supported by the U.S. DOE Contract No DE-AC02-76-CHO-3073. A large part of this article was completed during the stay of three of the authors (PHD, KI and TSH) at Kyushu University, and they gratefully acknowledge the hospitality of and support by Kyushu University.

## References

- [2.1] Arnold V I, Meshalkin: *Uspekhi Mat. Nauk* **15** 247 (1960)
- [2.2] Hasegawa A, MacLennan C G, and Kodama Y, *Phys. Fluids* **22**, 2122 (1979)
- [2.3] Sagdeev R Z, Shapiro V D and Shevchenko V I 1978 *Sov. J. Plasma Phys.* **4** 551
- [2.4] Okuda H and Dawson J M 1973 *Phys. Fluids* **16** 408
- [2.5] Balk A, Nazarenko S V and Zakharov V E 1990 *Sov. Phys.-JETP* **71** 249
- [2.6] Hasegawa A and Wakatani M 1987 *Phys. Rev. Lett.* **59** 1581
- [2.7] Biglari H, Diamond P H and Terry P W 1990 *Phys. Fluids B* **2** 1
- [2.8] Itoh S-I and Itoh K: *J. Phs. Soc. Jpn.* **59** (1990) 3815
- [2.9] Hahm T S and Burrell K H 1995 *Phys. Plasmas* **2** 1648
- [2.10] Terry P W 2000 *Rev. Mod. Phys.* **72** 109
- [2.11] Diamond P H, Rosenbluth M N, Hinton F L, Malkov M, Fleisher J, and Smolyakov A, in *Plasma Phys. and Controlled Nuclear Fusion Research* (IAEA, Vienna, 1998) IAEA-CN-69/TH3/1.
- [2.12] Diamond P H, Rosenbluth M N, Sanchez E, Hidalgo C, Van Milligen B, Estrada T, Brañas B, Hirsch M, Hartfuss H J, and Carreras B A: *Phys. Rev. Lett.* **84** 48 (2000)
- [2.13] Diamond P H et al., *Nuclear Fusion*, Vol. **41** (2001) 1067
- [2.14] Yoshizawa A, Itoh S-I, Itoh K: *Plasma and Fluid Turbulence* (IOP, England, 2002)
- [2.15] Hammet G et al 1993 *Plasma Phys. Control. Fusion* **35** 973
- [2.16] Lin Z, Hahm T S, Lee W W, Tang W M, and White R B, *Science* **281** 1835 (1998).
- [2.17] Waltz R, Kerbel G and Milovich J 1994 *Phys. Plasmas* **1** 2229
- [2.18] Sagdeev R Z and Galeev A A 1969 *Nonlinear Plasma Theory* ed Tom O'Neil and D. L. Book (New York: Benjamin)
- [2.19] Dyachenko A I, Nazarenko S V and Zakharov V E 1995 *Phys. Lett. A* **165** 330
- [2.20] Dubrulle B and Nazarenko S V 1997 *Physica D* **110** 123
- [2.21] Monin A S and Piterbarg L I 1987 *Sov. Phys. Dokl.* **32** 622
- [2.22] Smolyakov A I, Diamond P H: *Phys. Plasmas* **6** (1999) 4410
- [2.23] Chen L, Lin Z and White R B 2000 *Phys. Plasmas* **7** 3129
- [2.24] Tur A V, Chechkin A V and Yanovsky V V 1992 *Phys. Fluids B* **4** 3513
- [2.25] Smolyakov A I, Diamond P H: *Phys. Plasmas* **7** (2000) 1349
- [2.26] Gruzinov A V, Diamond P H, and Lebedev V B: *Phys. Plasmas* **1** (1994) 3148
- [2.27] Champeaux S and Diamond P H 2001 *Phys. Lett. A* **288** 214
- [2.28] Drake J F, Finn J M, Guzdar P, Shapiro V, Shevchenko V, Waelbroeck I, Hassam A B, Liu C S and Sagdeev R 1992 *Phys. Fluids B* **4** 488
- [2.29] Rosenbluth M N and Shapiro V D 1994 *Phys. Plasmas* **1** 222
- [2.30] Diamond P H and Kim Y B: *Phys. Fluids B* **3** 1626 (1991)
- [2.31] Lichtenberg A J and Liebermann M A 1984 *Regular and Stochastic Motion* (Springer, New York).
- [2.32] Rechester A B and Rosenbluth M N: *Phys. Rev. Lett.* **40** (1978) 38
- [2.33] Newell A C and Whitehead J A: *J. Fluid Mech.* **38** (1969) 279
- [2.34] Taniuti T and Wei C C: *J. Phys. Soc. Jpn.* **24** (1968) 941
- [2.35] Satya Y S and Kaw P K: *Phys. Rev. Lett.* **31**(1977) 1453
- [2.36] Kaw P, Singh R, Diamond P H: *Plasma Phys. Contr. Fusion* **44** (2002) 51
- [2.37] Smolyakov A I, Diamond P H, and Malkov M: *Phys. Rev. Lett.* **84**, 491 (2000)
- [2.38] Mima K and Nishikawa K 1984 in *Basic Plasma Physics II* (ed. Galeev A A and Sudan R N, North Holland, Amsterdam) Chapter 6.5
- [2.39] Kraichnan R H: *Phys. Fluids* **10** (1967) 1417
- [2.40] Rosenbluth M N and Hinton F L 1998 *Phys. Rev. Lett.* **80** 724
- [2.41] Hinton F L and Rosenbluth M N 1999 *Plasmas Phys. Control Fusion* **41** A653
- [2.42] Hinton F L: *Phys. Fluids B* **3** (1991) 696
- [2.43] May R: *Stability and Complexity in Model Ecosystems* (Cambridge, 1974)
- [2.44] Diamond P H, Liang Y-M, Carreras B A, Terry P W 1994 *Phys. Rev. Lett.* **72** 2565
- [2.45] Itoh K and Itoh S-I: *Plasma Phys. Contr. Fusion* **38** 1 (1996)

- [2.46] Itoh K, Itoh S-I and Fukuyama A: *Transport and Structural Formation in Plasmas* (IOP, England, 1999)
  - [2.47] Malkov M, Diamond P H: *Phys. Plasmas* **8** 3996 (2001)
  - [2.48] Diamond P H et al.: *Plasma Physics and Controlled Nuclear Fusion Research* 1992 (IAEA, Vienna, 1993) Vol.2, p.97
  - [2.49] Lin Z et al.: *Phys. Rev. Lett.* **83** (1999) 3645
  - [2.50] Dimits A M, Williams T J, Byers J A and Cohen B I 1996 *Phys. Rev. Lett.* **77** 71
  - [2.51] Rogers B N, Dorland W and Kotschenreuther M 2000 *Phys. Rev. Lett.* **85** 5336
  - [2.52] Idomura Y, Wakatani M and Tokuda S 2000 *Phys. Plasmas* **7** 3551
  - [2.53] Kim E and Diamond P H: *Phys. Plasmas* **9** 71 (2002)
  - [2.54] Itoh S-I and Kawai Y ed.: *Bifurcation Phenomena in Plasmas* (Kyushu Univ. 2002).
  - [2.55] Goldman M V 1984 *Revs. Mod. Phys.* **56** 709
  - [2.56] Zel'dovich Ya B and Novikov I D in *The Structure and Evolution of the Universe* (University of Chicago, Chicago, 1983) **242** 2
  - [2.57] Zeldovich Ya B, Ruzmaikin A A, Sokoloff D D: *Magnetic fields in astrophysics* (Gordon and Breach, New York, 1983)
  - [2.58] Moffatt H K 1978 *Magnetic Field Generation in Electrically Conducting Fluids*, N.Y.: Cambridge University Press
  - [2.59] Parker E N 1979 *Cosmical Magnetic Fields* (Oxford: Clarendon)
  - [2.60] Diamond P H, Hughes D W and Kim E-J 2003 "Self-consistent mean field electrodynamics in two and three dimensions," in *The Fluid Mechanics of Astrophysics and Geophysics* ed A M Soward and M Ghil Vol **12** (London: Taylor and Francis)
  - [2.61] Yoshizawa A, Itoh S-I, Itoh K, Yokoi N; *Plasma Phys. Contr. Fusion* **46** (2004) R25
- 
- [3.1] Horton C W: *Rev. Mod. Phys.* **71** (1999) 735
  - [3.2] Okuda H, Chu C, Dawson J M: *Phys. Fluids* **18** (1975) 243.
  - [3.3] Diamond P H: presented at US-Japan workshop on "Transport and structure formation of plasmas" (Kyushu Univ., 2002)
  - [3.4] Galeev A A and Sagdeev R Z, *Sov. Phys. JETP* **26**, 233 (1968).
  - [3.5] Winsor N, Johnson J L, and Dawson J M, *Phys. Fluids* **11**, 2448 (1968)
  - [3.6] Stringer T, *Phys. Rev. Lett.* **22**, 770 (1969).
  - [3.7] Sagdeev R Z and Galeev A A, *Dokl. Akad. Nauk SSSR* **189**, 1204 (1969) [*Sov. Phys. Dokl.* **14**, 1198 (1970)].
  - [3.8] Rosenbluth M N, Rutherford P H, Taylor J B, Frieman E A, and Kovrizhnikh L M, in *Plasma Physics and Controlled Nuclear Fusion Research, 1970* (International Atomic Energy Agency, Vienna, 1971), Vol. 1, p. 495.
  - [3.9] Stix T H, *Phys. Fluids* **16**, 1260 (1973).
  - [3.10] Hazeltine R D: *Phys. Fluids* **17** (1974) 961.
  - [3.11] Hassam A B and Kulsrud R M **21** (1978) 2271
  - [3.12] Hirshman S P: *Nucl. Fusion* **18** (1978) 917.
  - [3.13] Hirshman S P and Sigmar D J, *Nucl. Fusion* **21**, 1079 (1981).
  - [3.14] Hinton F L and Hazeltine R D, *Rev. Mod. Phys.* **48**, 239 (1981).
  - [3.15] Helander P, Sigmar D J: *Collisional transport in magnetized plasmas* (Cambridge University Press, 2002)
  - [3.16] Hassam A B and Drake J F, *Phys. Fluids B* **5**, 4022 (1993).
  - [3.17] Itoh S-I and Itoh K: *Phys. Rev. Letts.* **60** (1988) 2276
  - [3.18] Shaing K S and Grune E C, *Phys. Rev. Lett.* **63**, 2369 (1989).
  - [3.19] Taguchi M, *Plasma Phys. Controlled Fusion* **30**, 1897 (1988).
  - [3.20] Taguchi M, *Plasma Phys. Controlled Fusion* **33**, 859 (1991).
  - [3.21] Hassam A B, Antonsen T M, Drake J F, and Liu C S, *Phys. Rev. Lett.* **66**, 309 (1991).
  - [3.22] Hsu C T, Shaing K C, and Gormley R, *Phys. Plasmas* **1**, 132 (1994).
  - [3.23] Hugill J 1994 *Plasma Phys. Contr. Fusion* **36** B173.
  - [3.24] Wobig H, Kisslinger J 1995 *Plasma Phys. Contr. Fusion* **37** 893.

- [3.25] Rozhansky Y and Tendler M *Plasma Rotation in Tokamaks in Reviews of Plasma Physics* (ed. Kadomtsev B B, Consultants Bureau, New York, 1996) Vol.19, 147.
- [3.26] Galeev A A, Sagdeev R Z, Liu C S, and Novakovskii S V, JETP **82**, 875 (1996).
- [3.27] Morris R C, Haines M G, and Hastie R J, Phys. Plasmas **3**, 4513 (1996).
- [3.28] Lebedev V B, Yushmanov P N, Diamond P H, Novakovskii S V, and Smolyakov A I, Phys. Plasmas **3**, 3023 (1996).
- [3.29] Novakovskii S V, et al.: Phys. Plasmas **4** (1997) 4272
- [3.30] Azumi M: private communications (1989)
- [3.31] Stringer T E: *Nucl. Fusion* **33** 1249 (1993).
- [3.32] Itoh K, Itoh S-I, Yagi M, Fukuyama A: Phys. Plasmas **5** (1998) 4121
- [3.33] Lin Z et al., Phys. Plasmas **7** (1999) 1857
- [3.34] Chen Y, Parker S E et al., Nucl. Fusion **43** (2003) 1121
- [3.35] Candy J et al., J. Comp. Phys. **186**, 545 (2003)
- [3.36] Beer M, Thesis Ph D (1995). Princeton University
- [3.37] Waltz R et al., Proc. Int. IAEA Conf. on Plasma Phys. and Controlled Fusion Research (Montreal, 1996) paper IAEA/CN-64/D1-6
- [3.38] Beer M and Hammett G: Proceedings of the Varenna-Lausanne International Workshop (Societa Italiana di Fisica, Editrice Compositori, Bologna, 1998). p.19
- [3.39] Kim E J, Holland C, and Diamond P H, Phys. Rev. Lett. **91** (2003) 075003
- [3.40] Sagdeev R Z, Shapiro V D, Shevchenko V I, JETP Lett. **27** 1978 [Pis'ma Zh. Eksp. Teor. Fiz. **27** (1978)]
- [3.41] Hallatschek K and Diamond P H, New J. Phys. **5**, 29.1 (2003).
- [3.42] Connor J W, Hastie R J, Taylor J B 1979 *Proc. R. Soc. A* **365** 1.
- [3.43] Zakharov V E: Sov. Phys. JETP **35** (1972) 908
- [3.44] Malkov M, Diamond P H: Phys. Plasmas **9** (2001) 3996
- [3.45] Itoh K, Itoh S-I, Hallatschek K: submitted to Plasma Phys. Contr. Fusion (2004)
- [3.46] Kadomtsev B B 1965 *Plasma Turbulence* (Academic Press, New York)
- [3.47] Chen L: presented at 9th H-mode workshop (San Diego, 2003)
- [3.48] Guzdar P N, Kleva R G, Das A, Kaw P K PRL **87** (2001) 1015001
- [3.49] Some of explicit for has been given in the reduced set of equations in Chap.11 of ref. [2.14]
- [3.50] Yagi M, Itoh S-I, Itoh K and Fukuyama A: Plasma Phys. Contr. Fusion **39** (1997) 1887
- [3.51] Craddock G G and Diamond P H: Phys. Rev. Lett. **67** (1991) 1535
- [3.52] Zonca F: Phys. Plasmas **6** 1917 (1999)
- [3.53] Rebut P H and Hugon M: in *Plasma Physics and Controlled Nuclear Fusion Research 1984* (IAEA, Vienna, 1985) Vol.2, p197; see also J. D. Callen, et al.: in *Plasma Physics and Controlled Nuclear Fusion Research* (IAEA, Vienna, 1986) Vol.2, p157
- [3.54] Gurzinov I and Diamond P H: Phys. letters A **302** (2002) 119
- [3.55] Yoshizawa A, Yokoi N, Itoh S-I and Itoh K 1998 *Phys. Plasmas* **6** 3194
- [3.56] Kuo H L 1963 *Phys. Fluids* **6** 195
- [3.57] Deardorff J W 1965 *Phys. Fluids* **8** 1027
- [3.58] Gage K S and Reid W H 1968 *J. Fluid Mech.* **33** 21
- [3.59] See, e.g., Lehnert B 1966 *Phys. Fluids* **9** 1367
- [3.60] Inoue S, Itoh K and Yoshikawa S 1980 *J. Phys. Soc. Jpn.* **49** 367
- [3.61] Shaing K C 1991 *Comments Plasma Phys. Contr. Fusion* **14** 41
- [3.62] Hassam A B 1991 *Comments Plasma Phys. Contr. Fusion* **14** 275
- [3.63] Sugama H and Wakatani M 1991 *Phys. Fluids B* **3** 1110
- [3.64] Waelbroeck F L et al. 1992 *Phys. Fluids B* **4** 1441
- [3.65] Chu M S et al. 1995 *Phys Plasmas* **2** 2236
- [3.66] Miller R L, Waelbroeck F W, Lao L L, Taylor T S 1994 *International Conf. Plasma Physics and Controlled Nuclear Fusion Research* (IAEA, Seville) Vol.3, p231.
- [3.67] Medvedev M V, Diamond P H 1995 *Phys. Plasmas* **2** 727
- [3.68] Bai L, Fukuyama A, Uchida M 1998 *Plasma Phys. Contr. Fusion* **40** 785
- [3.69] Waltz R E, Kerbel G D, Milovich J Hammett G W 1995 *Phys. Plasmas* **2** 2408

- [3.70] Sanuki H 1984 Phys. Fluids **27** 2500
- [3.71] Itoh S-I, Itoh K, Ohkawa T, Ueda N 1989 in *Plasma Physics and Controlled Nuclear Fusion Research 1988* (IAEA, Vienna) Vol.2, p23
- [3.72] Goldreich P, Linden-Bell D: Mon. Not. Roy. Astron. Soc. **130** (1965) 125
- [3.73] Zhang Y Z, Mahajan S M 1992 Phys. Fluids B **4** 1385
- [3.74] Itoh S-I, Itoh K, Fukuyama A, Yagi M 1994 Phys. Rev. Lett. **72** 1200
- [3.75] Shaing K C *et al* 1989 in *Plasma Physics and Controlled Nuclear Fusion Research 1988* (IAEA, Vienna) Vol.2, p13
- [3.76] Hirshman S P and Molvig K 1979 Phys. Rev. Lett. **42** 648
- [3.77] Hahm T S, Burrell K H, Lin Z, Nazikian R, Synakowski E J 2000 Plasma Phys. Contr. Fusion **42** A205
- [3.78] Krommes J A 2000 Phys. Plasmas **7** 1148
- [3.79] See, *e.g.*, Kubo R, Toda M, Hashitsume N; *Statistical Physics II* (Springer, Berlin, 1985)
- [3.80] Hinton F L and Wong S K: Phys. Fluids **28** (1985) 3082
- [3.81] Connor J W *et al.*: Plasma Phys. Contr. Fusion **29** (1987) 919
- [3.82] Itoh K, *et al.*: Plasma Phys. Contr. Fusion **40** (1998) 661
- [3.83] Hahm T S and Burrell K H: Plasma Phys. Contr. Fusion **38** (1996) 1427
- [3.84] Hahm T S, *et al.*: Plasma Phys. Contr. Fusion **40** (1998) 657.
- [3.85] Mesholkin, Sinai Y; Applied Math and Mechanics, **25**, 1140 (1965).
- [3.86] Kim E J, Diamond P H: Phys. Plasmas **9** (2002) 4530
- [3.87] Holland C, *et al.*: "Investigations of the Role of Nonlinear Couplings in Structure Formation and Transport Regulation: Experiment, Simulation, and Theory", THP1/3
- [3.88] Dorland W, Thesis Ph D, Princeton University, 1993.
- [3.89] Rosenbluth M N: private communications (2002)
- [3.90] Itoh K *et al.*: J. Phys. Soc. Jpn. **73** (2004) in press [Research Report NIFS-786 (2003)]
- [3.91] Diamond P H and Gruzinov A V: Phys. Rev. Lett. **78**, 3306 (1997)
- [3.92] Malkov M, Diamond P H, Rosenbluth M N, Phys. Plasmas **9** (2001) 5073
- [3.93] Breizman B N 1978 Sov. Phys. JETP **45** 271 [Zh. Eksp. Teor. Fiz. **72** (1977) 518]
- [3.94] Itoh K and Itoh S-I 1985 J. Phys. Soc. Jpn. **54** 1228
- [3.95] Bazdenkov S V and Pogutse O P 1990 JETP Letters **57** 410
- [3.96] Itoh S-I, Itoh K, Fukuyama A, Miura Y 1991 Phys. Rev. Lett. **67** 2485
- [3.97] Itoh S-I, Itoh K and Fukuyama A 1993 Nuclear Fusion **33** 1445
- [3.98] Zohm H 1994 Phys. Rev. Lett. **72** 222
- [3.99] Pogutse O P, Kerner W, Gribkov V, Dazdenkov S, Osipenko M 1994 Plasma Phys. Contr. Fusion **36** 1963
- [3.100] Sugama H and Horton W 1995 Plasma Phys. Contr. Fusion **37** 345
- [3.101] Vojtsekhovich L A, Dnestrovskij A Yu, Parail V V 1995 Nucl. Fusion **35** 631
- [3.102] Lebedev V B, Diamond P H, Gruzinova I, and Carreras B A 1995 Phys. Plasmas **2** 3345
- [3.103] Toda S *et al.* 1996 Plasma Phys. Contr. Fusion **38** 1337
- [3.104] Takayama A and Wakatani M 1996 Plasma Phys. Contr. Fusion **38** 1411
- [3.105] Aoyagi T, Yagi M, Itoh S-I 1997 J. Phys. Soc. Jpn. **66** 2689
- [3.106] Thyagaraya A, Haas F A, Harvey D J 1999 Phys. Plasmas **6** 2380
- [3.107] Wersinger J M, Finn J M, and Ott E, Phys. Rev. Lett. **44**, 453 (1980)
- [3.108] Bian N, Benkadda S, Garcia O E, Paulsen J-V, Garbet X: Phys. Plasmas **10** (2003) 1382
- [3.109] Watanabe T-H and Sugama H: **9** (2002) 3659
- [3.110] Marchenko V S, Phys. Rev. Lett. **89**, 185002 (2002)
- [3.111] Diamond P H and Malkov M, Phys. Scr., T **T98**, 63 (2002)
- [3.112] Balescu R: Phys. Rev. E **68** (2003) 046409
- [3.113] Itoh K, Hallatschek K, Toda S, Itoh S-I, Diamond P H, Yagi M, Sanuki H: Plasma Phys. Contr. Fusion **46** (2004) A335
- [3.114] Itoh K, Itoh S-I and Fukuyama A: Phys. Rev. Lett. **69** (1992) 1050

- [3.115] Drake J F, Zeiler A, Biskamp D: Phys. Rev. Lett. **75** (1995) 4222
- [3.116] Walleffe F: Phys. Fluids **9** (1997) 883
- [3.117] Itoh K, Itoh S-I, Fukuyama A, Yagi Toda M S, Kawasaki M: "Modelling of Bifurcations in Magnetic Confinement Plasmas", in *Bifurcation Phenomena in Plasmas* (ed. Itoh S-I and Kawai N, Kyushu Univ., 2002) 416
- [3.118] Itoh S-I and Itoh K: Plasma Phys. Contr. Fusion **43** (2001) 1055
- [3.119] Itoh S-I, Kitazawa A, Yagi M and Itoh K: Plasma Phys. Control. Fusion **44** (2002) 1311
- [3.120] Itoh S-I, Itoh K, Yagi Kawasaki M M, Kitazawa A: Phys. Plasmas **9** (2002) 1947
- [3.121] Kishimoto Y: invited talk at 9th H-mode workshop (San Diego, 2003), to be published in Plasma Phys. Control. Fusion **46** (2004)
- [3.122] Itoh K, Itoh S-I, Spineanu F, Vlad M O and Kawasaki M: Plasma Phys. Control. Fusion **45** (2003) 911
- [3.123] Holland C and Diamond P H: A simple model of interaction between electron temperature gradient model and drift waves" (2003).
- [3.124] Jenko F: presented at 13th Toki Conference (Toki, 2003), paper I-1.
- [3.125] Yagi M et al.: presented at 13th Toki Conference (Toki, 2003), paper I-6.
- [3.126] Malkov M, Diamond P H, Smolyakov A: Phys. Plasmas **8** (2001) 1553
- [3.127] Terry P W, et al.: Phys. Rev. Lett. **87** 185001 (2001)
- [3.128] Kim E-J, Diamond P H: Phys. Rev. Lett. **91** 075001 (2003)
- [3.129] Kim E-J, Diamond P H: submitted to Plasma Phys. Contr. Fusion
- [3.130] Hamaguchi S and Horton W 1992 Phys. Fluids B **4** 319
- [3.131] Kim Y-J, Kishimoto Y, Wakatani M, Tajima T 1996 Phys. Plasmas **3** 3689
- [3.132] Waltz R E, Staebler G M, Dorland W, Hammett G W, Kotschenreuther M, Konings J A 1997 Phys. Plasmas **4** 2482
- [3.133] Itoh K, Itoh S-I, Fukuyama A, Sanuki H, Yagi M 1994 Plasma Phys. Contr. Fusion **36** 123
- [3.134] Li J and Kishimoto Y: Phys. Rev. Lett. **89**, 115002 (2002).
- [3.135] Jenko F, et al.: presented at the 19th IAEA Fusion Energy Conference in Lyon (2002), paper TH/1-2
- [3.136] Weynants R R, Jachmich S, Van Oost G 1998 Plasma Phys. Contr. Fusion **40** 635
- [3.137] Burrell K H: Phys. Plasmas **4** (1997) 1499
- [3.138] Tynan G R, et al.: Phys. Rev. Lett. **68** 3032 (1992)
- [3.139] Shats M G, et al.: Phys. Rev. Lett. **84** (2000) 6042.
- [3.140] Hallatschek K and Biskamp D: Phys. Rev. Lett. **86** (2001) 1223
- [3.141] Spineanu F and Vlad M A: Phys. Rev. Lett. **89** 185001 (2002)
  
- [4.1] Tang W: Phys. Plasmas **9** (2004) 1856
- [4.2] Frieman E A and Chen L, Phys. Fluids **25** 502 (1982).
- [4.3] Sydora R D, Decyk V K, and Dawson J M, Plasma Phys. Controlled Fusion **38** A281 (1996).
- [4.4] Hahm T S, Phys. Fluids **31** 2670 (1988).
- [4.5] Beer M A and Hammett G W, Phys. Plasmas **3** 4046 (1996).
- [4.6] Lee W Tang W W M, and Okuda H, Phys. Fluids **23** 2007 (1980).
- [4.7] Dimits A M, Byers J A, Williams T J *et al.*, in *Plasma Phys. and Controlled Nuclear Fusion Research* (IAEA, Vienna, 1994), Vol. III, p. 457.
- [4.8] Sydora R D, Hahm T S, Lee W W *et al.*, Phys. Rev. Lett. **64** 2015 (1990).
- [4.9] Parker S E, Lee W W, and R.A. Santoro: Phys. Rev. Lett. **71** 2042 (1993).
- [4.10] Cummings J C, Thesis Ph D, Princeton University, 1995.
- [4.11] Kishimoto Y, Kim J Y, Horton W *et al.*, Plasma Phys. Controlled Fusion, **40** A663 (1998).
- [4.12] Hahm T S, Burrell K H, Lin Z *et al.*, Plasma Phys. Controlled Fusion **42** A205 (2000).
- [4.13] Synakowski E J, Batha S, Beer M *et al.*, Phys. Plasmas **4** 1736 (1997).
- [4.14] Mazzucato E, Batha S H, Beer M *et al.*, Phys. Rev. Lett. **77** 3145 (1996).
- [4.15] Dimits A, Bateman G, Beer M *et al.*, Phys. Plasmas **7** 969 (2000).

- [4.16] Hallatschek K: Phys. Rev. Lett. **93** (2004) 065001
- [4.17] Diamond P H *et al.*, Phys. Rev. Lett. **78** 1472 (1997).
- [4.18] Lebedev V B and Diamond P H, Phys. Plasmas **4** 1087 (1997).
- [4.19] Falchetto G L and Ottaviani M, 2004 Phys. Rev. Lett. **92** 25002
- [4.20] Kim E J Diamond P H and Hahm T S 2004 Submitted to Phys. Plasmas
- [4.21] Hahm T S 2003 Plasma Phys. Control. Fusion **44** A87
- [4.22] Mikkelsen D R *et al.* in *Plasma Phys. and Controlled Nuclear Fusion Research* (IAEA, Vienna, 2002) IAEA-CN-69/EXP5/03.
- [4.23] Parker S E, Chen Y, Wan W, Cohen B I and Nevins W M Phys. Plasmas **11** (2004) 2594
- [4.24] Hahm T S, Diamond P H, Lin Z, Itoh K, and Itoh S.-I. 2004 Plasma Phys. Control. Fusion **46** A 323
- [4.25] Zonca F, Chen L, and White R, 2004 Phys. Plasmas **11** 2488
- [4.26] Villard L *et al* 2004 Nuclear Fusion **44** 172
- [4.27] Li J, *et al.*: presented at 13th International Toki Conference (2003, Toki) paper P2-38
- [4.28] Jenko F and Scott B D, Phys. Rev. Lett **80** 4883 (1998).
- [4.29] Tange T *et al* 1977 J. Phys. Soc. Jpn **42** 2006
- [4.30] Hahm T S 1992 Phys. Fluids B **4** 2801
- [4.31] Carreras B A *et al* 1992 Phys. Fluids B **4** 3115
- [4.32] Dupree T H, Phys. Fluids **15** 334 (1972).
- [4.33] Watanabe Tomo-Hiko and Sugama Hideo: Phys. Plasmas **11** (2004) 1476
- [4.34] Wong K-L. *et al.*: Phys. Lett. A **236** (1997) 33
- [4.35] Wong K-L. *et al.*: Phys. Lett. A **276** (2000) 281
- [4.36] Park K-L., Mazzucato E *et al.*, private communications (2004).
- [4.37] Rhodes T, Doyle E *et al.*, private communications (2004).
- [4.38] Porkolab M *et al.*, private communications (2004).
- [4.39] Jenko F *et al.*, Phys. Plasmas **7** 1904 (2000).
- [4.40] Labit B and Ottaviani M, Phys. Plasmas **10** 126 (2003).
- [4.41] Li J and Kishimoto Y 2004 Phys Plasmas **11** 1493
- [4.42] Lin Z *et al.*, 2004 Plasma Phys Controlled Nuclear Fusion IAEA
- [4.43] Jenko F and Dorland W, Phys. Rev. Lett. **89** 225001 (2002).
- [4.44] Hahm T S and Tang W M, Phys. Fluids B **1** 1185 (1989).
- [4.45] Jenko F *et al.*, Phys. Plasmas **8** 4096 (2001).
- [4.46] Busse F H, Chaos **4** 123 (1994).
- [4.47] Hasegawa A and Mima K, Phys. Fluids **21** 87 (1978).
- [4.48] Rossby C G, Meteorol Q J. Soc. Suppl. **66** 68 (1940).
- [4.49] Horton W and Hasegawa A, Chaos **4** (1994) 227
- [4.50] Rhines P B 1975 J. Fluid Mech. **69** 417
- [4.51] Volker Naulin, New Journal of Physics **4** 28.1 (2002).
- [4.52] Scott B D, in *Plasma Phys. and Controlled Nuclear Fusion Research* (IAEA, Vienna, 1995), Vol. III, p 447.
- [4.53] Carreras B A, Lynch V E, and Garcia L, Phys. Fluids B **5** 1795 (1993).
- [4.54] Guzdar P N, Drake J F, McCarthy D, Hassam A B, and Liu C S, Phys. Fluids B **5**, 3712 (1993).
- [4.55] Sugama H, Wakatani M and Hasegawa A, Phys. Fluids ??? (1988)
- [4.56] Sugama H and Horton W, Phys. Plasmas **1** 345 (1994).
- [4.57] Volker Naulin, Phys. Plasmas **10** 4016 (2003).
- [4.58] Sugama H and Horton W, Phys. Plasmas **1** 2220 (1994)
- [4.59] Wakatani M *et al* : "Shear Flow Generation due to Electromagnetic Instabilities", presented at the 19th IAEA Fusion Energy Conference in Lyon (2002), paper TH/P1-18
- [4.60] Rogers B N, Drake J F, and Zeiler A, Phys. Rev. Lett. **81** 4396 (1998)
- [4.61] Rogers B N *et al.*, Phys. Plasma **2**, 2397 (1995).
- [4.62] Xu X Q *et al.*, New journal of Physics **4** 53 (2002).
- [4.63] Scott B D *et al.*, in *Plasma Phys. and Controlled Nuclear Fusion Research* (IAEA, Vienna, 2001)
- [4.64] Scott B D 2003 Phys. Lett. A. **320**, 53.

- [4.65] Scott B D, *Private Communications* (2003).
- [4.66] Scott B D 2004 *Phys. Plasmas*, submitted; "Energetics of the interaction between electromagnetic ExB turbulence and zonal flows".
- [4.67] Dimits A M, et al. *Nucl. Fusion* **40** (2000) 661
- [4.68] Dimits A M, et al, *Phys. Plasmas* **7**, 969 (2000)
- [4.69] Dimits A M, et al.: *Nucl. Fusion* **40** (2000) 1725
  
- [5.1] After Gossard E E and Hooke W H, 'Waves in the atmosphere' Elsevier, 1975, with modifications
- [5.2] Charney J G: *Geophys. Publ. Oslo* **17** (1948) 1
- [5.3] Hasegawa A: *J. Phys. Soc. Jpn.* **52** (1983) 1930
- [5.4] Marcus P S, Kundu T, Lee C: *Phys Plasmas* **7** (2000) 1630
- [5.5] Or A C and Busse R H: *J. Fluid. mech.* **174** (1987) 313.
- [5.6] Takagi M, Matsuda Y: in Reports of RIAM No, S-1 (11-14, Feb. 2003)
- [5.7] Schubert G: in *Venus* (Univ. of Arizona Press, 1983) 681-765
- [5.8] Thompson R, *Atmos J. Sci.* **27** (1970) 1107
- [5.9] Fels S B and Lindzen R E.: *Geophys. Fluid. Byn.* **6** (1973) 149
- [5.10] Gierasch P J: *Atmos J. Sci.* **32** (1975) 1038
  
- [6.1] Horton C W 1984 in *Basic Plasma Physics II* (ed. Galeev A A and Sudan R N, North Holland, Amsterdam) Chapter 6.4
- [6.2] Cheng C Z and Okuda H 1977 *Phys. Rev. Lett.* **38** 708
- [6.3] Sanuki H and Weiland J 1980 *J. Plasma Phys.* **23** 29
- [6.4] Krommes J A 1999 *Plasma Phys. Contr. Fusion* **41** A641
- [6.5] Scott B D 1992 *Phys. Fluids B* **4** 2468.
- [6.6] Das Sen A A, Mahajan S, and Kaw P: *Phys. Plasmas* **8**, 5104 (2001)
- [6.7] Champaux S, et al. APS (2001) invited talk
- [6.8] Carreras B A. *et al* "Anomalous diffusion in plasma turbulence models" in 19th IAEA Fusion Energy Conference in Lyon (2002) *Paper TH/2-3*
- [6.9] Krommes and Kim *Phys. Rev. E* **62** (2000) 8508
- [6.10] Balescu R, *Statistical Dynamics: Matter out of Equilibrium* (Imperial College Press, London, 1997).
- [6.11] Krommes J A: *Phys. Reports* **360** (2002) 1
- [6.12] Makino M, Kamimura Taniuti T T 1981 *J. Phys. Soc. Jpn.* **50** 980
- [6.13] Meiss J D and Horton C W 1983 *Phys. Fluids* **26** 990
- [6.14] Kim E J, Diamond P H : *Phys. Rev. Lett.* **88** 225002 (2002)
- [6.15] Kim E J, et al.: "Intermittency and Structures in Drift Wave Turbulence: Towards a Probabilistic Theory of Anomalous Transport", presented at the 19th IAEA Fusion Energy Conference in Lyon (2002), TH2/4
- [6.16] Itoh S-I and Itoh K 1999 *J. Phys. Soc. Jpn.* **68** 1891; 2661; **69** (2000) 408, 3253
- [6.17] Itoh S-I and Itoh K 2000 *J. Phys. Soc. Jpn.* **69** 427.
- [6.18] Yagi M, et al.: "Multiple-Scale Turbulence and Bifurcation", presented at the 19th IAEA Fusion Energy Conference in Lyon (2002), TH1/4
- [6.19] Bowman J C, Krommes J A, Ottaviani M 1993 *Phys. Fluids B* **5** 3558.
- [6.20] Itoh S-I, Itoh K, Toda S: *Phys. Rev. Lett.* **89** (2002) 215001
- [6.21] Chandrasekhar S: *Rev. Mod. Phys.* **15** (1943) 1
- [6.22] Itoh S-I, Itoh K and Toda S: *Plasma Phys. Control. Fusion* **45** (2003) 823  
See also Itoh S-I, et al.: "Statistical theory of L-H transition and its implication to threshold database", presented at the 19th IAEA Fusion Energy Conference in Lyon (2002), PDP/04
- [6.23] Bak P, Tang C and Wiesenfeld K 1987 *Phys. Rev. Lett.* **59** 381
- [6.24] Diamond P H and Hahm T S: *Phys. Plasmas* **2**, 3640 (1995)
- [6.25] Newman D E, Carreras B A, Diamond P H, and Hahm T S: *Phys. Plasmas* **3**, 1858 (1996)
- [6.26] Carreras B A, Newman D, Lynch V E, and Diamond P H: *Phys. Plasmas* **3**, 2903 (1996)
- [6.27] Dendy R O and Helander P 1997 *Plasma Phys. Contr. Fusion* **39** 1947



- [6.28] Carreras B A et al. 1998 Phys. Plasmas **5** 3632
- [6.29] Carreras B A et al. 1999 Phys. Plasmas **6** 1885
- [6.30] Gruzinov, Diamond P H, and Rosenbluth M N, Phys. Rev. Lett. **89**, 255001 (2002).
- [6.31] Gruzinov I, Diamond P H, and Rosenbluth M N: Phys. Plasmas **10** (2003) 569
- [6.32] Krommes J A 2000 Phys. Plasmas **7** 1752
- [6.33] Nevins W M: Bull. Am. Phys. Soc. (1999)
- [6.34] Krasheninnikov S I, et al.: "Blobs and cross-field transport in the tokamak edge plasmas", presented at the 19th IAEA Fusion Energy Conference in Lyon (2002), TH4/1
- [6.35] Ghendrih Ph, et al. : "Theoretical Analysis of Long Range Turbulent Transport in the Scrape-Off-Layer", presented at the 19th IAEA Fusion Energy Conference in Lyon (2002), THP2/14
- [6.36] Nevins W M, et al.: "Simulations of Boundary Turbulence in Tokamak Experiments", presented at the 19th IAEA Fusion Energy Conference in Lyon (2002), THP3/7
- [6.37] Balescu R, Plasma Phys. Controlled Fusion **42**, B 1 (2000).
- [6.38] Vlad M, Spineanu F, Misguich J H, and Balescu R, Phys. Rev. E **58**, 7359 (1998).
- [6.39] Vlad M, Spineanu F, Misguich J H, and Balescu R, Phys. Rev. E **63**, 066304 (2001).
- [6.40] Vlad M, Spineanu F, Misguich J H, and Balescu R, Phys. Rev. E **67**, 026406 (2003).
- [6.41] Krommes J A; presented at 13th International Toki Conference (2003), paper I-20.
- [6.42] Kodama Y, Taniuti T: J. Phys. Soc. Jpn. **47** (1979) 1706
- [6.43] Nozaki K, Taniuti T and Watanabe K 1979 J. Phys. Soc. Japan **46** 983
- [6.44] Nozaki K, Taniuti T and Watanabe K 1979 J. Phys. Soc. Japan **46** 991
- [6.45] Petviashvili V I, Fiz. Plazmy **3** (1977) 270 [Sov. J. Plasma Phys. **3** (1977) 150].
- [6.46] Flierl G R, Dyn. Atmos. Oceans **3** (1979) 15.
- [6.47] Lakhin V P, Mikhailovskii A B and Onishchenko O G, Phys. Lett. **A119** (1987) 348.
- [6.48] Kono M and Miyashita E, Phys. Fluids **31**, 326 (1988)
- [6.49] Spatschek K H, Laedke E W, Marquardt Chr, Musher S and Wenk H: Phys. Rev. Lett. **64** (1990) 3027.
- [6.50] Spatschek K H: Plasma Phys. Contr. Fusion **41** (1999) A115
- [6.51] Weiland J, Sanuki H and Liu C S 1981 Phys. Fluids **24** 93
- [6.52] Mahajan S and Weiland J, Plasma Physics and Controlled Fusion **42** (2000) 987.
- [6.53] Spineanu F, Vlad M, Itoh K, Sanuki H, and Itoh S-I: Phys. Rev. Lett. **93** (2004) 25001
- [6.54] Gurcan O D and Diamond P H: Phys. Plasmas **11** (2004) 572.
- [6.55] Gurcan O D and Diamond P H: Phys. Plasmas **11** (2004) 332.
- [6.56] Gurcan O D and Diamond P H: "Nonlinear evolution of two dimensional structures in electron temperature gradient driven turbulence" Phys. Plasmas **11** (2004) in press
  
- [7.1] Hahm T S, Beer M A, Lin Z et al 1999 Phys. Plasmas **6**, 922
- [7.2] Jenko F, Kendl A: Phys. Plasmas **8** (2002) 4103
- [7.3] Kendl A, Scott B D et al 2003 Phys. Plasmas
- [7.4] Zarnstorff M et al 2001 Plasma Phys. and Controlled Nuclear Fusion Research (Vienna:IAEA)
- [7.5] Okamura S et al 2001 Plasma Phys. and Controlled Nuclear Fusion Research (Vienna:IAEA)
- [7.6] Ida K 1998 Plasma Phys. Control. Fusion **40**, 609
- [7.7] Levinton F M et al 1998 Phys. Rev. Lett. **80**, 4887
- [7.8] Hamada Y: Fusion Engineering and Design, **34-35** (1997) Pages 25-35
- [7.9] Fujisawa A 2003 Plasma Phys. Control. Fusion **45** (2003) R1
- [7.10] Groebner R J et al 1990 Phys. Rev. Lett. **64**, 3015

- [7.11] Ida K, Hidekuma S, Miura Y, Fujita T, Mori M, Hoshino K, Suzuki N, Yamauchi T and JFT-2M Group: Phys. Rev. Lett. **65** (1990) 1364
- [7.12] Bell R E et al 1998 Phys. Rev. Lett. **81**, 1429
- [7.13] Ido T, Kamiya K and Miura Y et al 2002 Phys. Rev. Lett. **88**, 055006
- [7.14] Miura Y et al.: Nucl. Fusion **41** (2001) 973
- [7.15] Fujisawa A et al 2000 Phys. Plasmas, **7**, 4152
- [7.16] Stroth U et al 2001 Phys. Rev. Lett. **86**, 5910
- [7.17] Fujisawa A, et al.: "Identification of Zonal Flows in a Torus Plasma" Phys. Rev. Lett. (2004) in press
- [7.18] Fujisawa A, et al.: *31st EPS Conf. Contr. Fusion & Plasma Phys.* (London 2004) paper O2-04
- [7.19] Xu G S, Wan B N, Song M, and Li J: Phys. Rev. Lett. **91** (2003) 125001
- [7.20] Hamada Y et al 1994 Plasma Phys. Control. Fusion **36**, 1743
- [7.21] Hamada Y, Nishizawa A, Kawasumi Y, Fujisawa A, Iguchi H and JIPP T-IIU group: Fusion Engineering and Design, **34-35** (1997) 657; 663
- [7.22] Schoch P et al 2003 Submitted to Phys. Rev. Lett.
- [7.23] Hassam A B et al 1994 Phys. Plasmas **1**, 337
- [7.25] Kishimoto Y and Li J Q 2003 Presented at ITC-13
- [7.26] Hidalgo C et al 1999 Phys. Rev. Lett. **83**, 2203
- [7.27] Xu Y H et al 2000 Phys. Rev. Lett. **84**, 3867
- [7.28] Diamond P H et al 2000 Phys. Rev. Lett. **84**, 46042
- [7.29] Tynan G R et al 2001 Phys. plasmas **8**, 2691
- [7.30] Moyer R A et al 2001 Phys. Rev. Lett. **87**, 135001
- [7.31] Holland C et al 2002 Plasma Phys. Control. Fusion **44**, A453
- [7.32] Shats M G and Solomon W M 2002 Phys. Rev. Lett. **88**, 045001
- [7.33] Ramisch M, Stroth U, Niednerand M and Scott B D 2003, New J. Phys. **5**, 12
- [7.34] Coda S, Porkolab M and Burrell K H 2001 Phys. Rev. Lett. **86**, 4835
- [7.35] Taylor G I 1915 Phil. Trans. R. Soc. **A215**, 1
- [7.36] Jackubowski M, Fonck R J and McKee G 2002 Phys. Rev. Lett. **89**, 265003
- [7.37] McKee G R et al 2003 Phys. Plasmas **10** 1712
- [7.38] McKee G R et al 2003 Plasma Phys. Control. Fusion **45**, A477.
- [7.39] Hirsch M and Holzhauer E: Plasma Phys. Control. Fusion **46** (2004) 593
- [7.40] T-10 Team: 'Transport and Turbulence Studies in the T-10 Tokamak' (IAEA 2002.Lyon) paper OV/5-2
- [7.41] Conway G D, Scott B, Schirmer J, Reich M, Kendl A1 & ASDEX Upgrade Team: *31st EPS Conf. Contr. Fusion & Plasma Phys.* (London 2004) paper P4.124
- [7.42] Paul S and Zweben S 2003 private communication
- [7.43] Zweben S 2003 private communication
- [7.44] Porkolab M and Rost C 2003 private communication
- [7.45] Park H Mazzucato E Munsat T et al., 2004 Rev. Sci. Instrum. to appear
  
- [8.1] Zaslavsky G M: Physics Reports, Volume **371** (2002) 461
  
- [B1] Klimontovich Yu L, *The Statistical Theory of Non-equilibrium Processes in a Plasma* (MIT, Cambridge, 1967)
- [B2] Dubin D H et al., Phys. Fluids **26** 3524 (1983)
- [B3] Hahm T S, Lee W W, and Brizard A, Phys. Fluids **31** 1940 (1988)
- [B4] Brizard A, J. Plasma Phys. **41** 541 (1989)
- [B5] Hahm T S, Phys. Plasmas **3** 4658 (1996)
- [B6] Stix T H, *Waves in Plasmas* (American Institute of Physics, New York 1992) 247
- [B7] Dorland W and Hammett G W, Phys. Fluids B **5** 812 (1993)
- [B8] Snyder P B, Hammett G W, and Dorland W, Phys. Plasmas **4** 3974 (1997)
- [B9] Mator N, Phys. Fluids B **4** 3952 (1992)
- [B10] Sugama H, Watanabe T-H, Horton C W: Phys. Plasmas **8** (2001) 2617
- [B10] Braginskii S I, in *Review of Plasma Physics*, edited by M.A. Leontovich (Consultants Bureau, NY 1965) Vol. **1** 205
- [B12] Yagi M and Horton W, Phys. Plasmas **1** 2135 (1994)

- [B13] Scott B, Plasma Phys. Control. Fusion, **39**, 1635 (1997)
- [B14] Zeiler A, Drake J F and B. Rogers, Phys. Plasmas **4** 2134 (1997)
- [B15] Xu X Q et al., Phys. Plasmas **7** 1951 (2000)
- [B16] Simakov A N and Catto P J, Phys. Plasmas **10** 4744 (2003)

**Table 1.1.** Comparison between zonal flow in plasmas, dynamo, electromagnetic (EM) flow generation and flow structure formation.

Name of Concept	Name	Main small-scale fluctuations	Generated global structure	Examples	Equations in fluid limit and fundamental drive	Coverage by this review
Electro-magnetic flow drive	$E \times B$ flow dynamo	EM and pressure fluctuations (drift waves)	$E \times B$ flow	Zonal flow in toroidal plasmas	MHD eq. Plasma response Pressure gradient	Yes
	MHD flow dynamo	EM and flow fluctuations	Magnetized flow	Bipolar jets	MHD eq. Gravitational force Coriolis force	No
Flow generation	Neutral flow dynamo	Small-scale thermal convection	Zonal flow	Jobian belt Tidal current Jet stream, etc.	Navier-Stokes eq. Thermal convection Coriolis force	Yes
	Flow structure formation	Small-scale convection	Structured flow	Swirling flow, Asymmetry in pipe flow	Navier-Stokes eq. Drive of axial flow	Partly
Magnetic dynamo	Dynamo	Fluid motion (thermal convection)	Magnetic field	Geodynamo Solar dynamo	MHD eq. Thermal convection Coriolis force	No
	Magnetic structure formation	Magnetic fluctuations (kink, tearing)	Magnetic field	RFP torus	MHD eq. External toroidal current	No

**Table 2.1. Characteristics of zonal flow**

<b>Spatio-temporal structures</b>	
eigenfunction	electrostatic perturbation is dominant; $\tilde{n}_i/n_0 \approx q_r^2 \rho_s^2 e\tilde{\Phi}/T_e$ or $\tilde{n}_e/n_0 \approx 0$
radial wave length $q_r^{-1}$	$a\rho_i > q_r^{-2} > \rho_i^2$ or $q_r \sim O(0.1) \rho_i^{-1}$ , weak poloidal assymetry
radial coherence length	can be $\sim \sqrt{a\rho_i}$ (See also § 6.4)
real frequency $\Omega_{ZF}$	$\Omega_{ZF} \approx 0$
autocorrelation time	$v_{ii}\epsilon^{-1}$ , and see § 3.5.1
amplitude	average vorticity is order $\rho_i^{-1} V_d$ (§3.5)
<b>Phase diagram for ZF</b>	
appearance:	See §3.2.1, §3.2.2
significant impact for turbulent transort:	$q_r V_{ZF} > \Delta\omega_k$ (See §3.5)
<b>Microfluctuation that is the origin of ZF</b>	
all instability in the range of $\omega_*$ ; $\rho_i$ and $\rho_e$	
partition between ZF and turbulence:	See §3.5.1, §3.5.6
<b>Impact on turbulence</b>	
significant impact if	$q_r V_{ZF} > \Delta\omega_k$ (See §3.5)
scattering of drift wave packet in $(x, k_x)$ space if $\omega_{\text{bounce}} > \Delta\omega_k$	(§3.4.6, §3.4.7)
<b>Interactions between ZFs</b>	
through modifying microfluctuations;	no direct condensation/cascade so far

**Table 2.2:** State of Drift Wave - Zonal Flow System

State	No flow	Flow ( $\alpha_2 = 0$ )	Flow ( $\alpha_2 \neq 0$ )
$N$ (Drift wave turbulence level)	$\gamma/\Delta\omega$	$\frac{\gamma_d}{\alpha}$	$\frac{\gamma_d + \alpha_2\gamma\alpha^{-1}}{\alpha + \Delta\omega\alpha_2\alpha^{-1}}$
$V^2$ (mean square flow)	0	$\frac{\gamma}{\alpha} - \frac{\Delta\omega\gamma_d}{\alpha^2}$	$\frac{\gamma - \Delta\omega\gamma_d\alpha^{-1}}{\alpha + \Delta\omega\alpha_2\alpha^{-1}}$
Drive/excitation mechanism	Linear Growth	Linear Growth	Linear Growth Nonlinear Damping of Flow
Regulation/inhibition mechanism	Self-interaction of turbulence	Random shearing, Self-interaction	Random shearing, Self-interaction
Branching ratio $V^2 / N$	0	$\frac{\gamma - \Delta\omega\gamma_d\alpha^{-1}}{\gamma_d}$	$\frac{\gamma - \Delta\omega\gamma_d\alpha^{-1}}{\gamma_d + \alpha_2\gamma\alpha^{-1}}$
Threshold (without noise)	$\gamma > 0$	$\gamma > \Delta\omega\gamma_d\alpha^{-1}$	$\gamma > \Delta\omega\gamma_d\alpha^{-1}$

**Table 3.2.1:** Analogy Between Weak Langmuir Turbulence and Zonal Flow Generation

Langmuir Turbulence	Drift Waves and Zonal Flows
High Frequency Population	
Plasmon/Electron Plasma $\omega_k^2 = \omega_p^2 + \gamma v_{the}^2 k^2$	Drift Wave $\omega_k = \omega_{*e}/1 + k_{\perp}^2 \rho_s^2$
Low Frequency Structure	
Phonon/Ion Acoustic $\Omega = q c_s$	Zonal Flow $\Omega = 0$
Drive Mechanism	
Ponderomotive Pressure $\frac{\langle E^2 \rangle}{4\pi\omega_p}$	Turbulent Reynolds Stress $\langle \tilde{v}_x \tilde{v}_y \rangle$
Wave Population Distribution	
Action $\leftrightarrow$ Plasmon Number $N = \frac{ E^2 }{\delta\pi} \frac{\partial \mathcal{E}}{\partial \omega}$	Potential Enstrophy $\rightarrow$ Drift-ion Number $N = \left(1 + k_{\perp}^2 \rho_s^2\right)^2 \left \frac{e\phi}{T}\right ^2$
Modulational Instability Criterion	
$d\omega/dk > 0 \rightarrow \frac{d\langle N \rangle}{dk} > 0$	$d\omega/dk < 0 \rightarrow \frac{d\langle N \rangle}{dk} < 0$
Population Inversion Needed	Population Inversion Unnecessary
Regulator	
Ion Landau Damping of Phonon	Collisional Damping of Zonal Flow

**Table 3.4.1:** Analogy of 1D Vlasov and drift Wave - Zonal flow Problems

	1D Vlasov Plasma with Langmuir Waves		Drift Wave Packets in Zonal Flow Field
<i>Constituents</i>	Particle	$\Leftrightarrow$	Drift wave packet
	Langmuir wave spectrum	$\Leftrightarrow$	Zonal shear spectrum
	Particle velocity $v$	$\Leftrightarrow$	Packet group velocity $v$
	real space $x$	$\Leftrightarrow$	wavenumber $k_x$
<hr/>			
<i>Time scales</i>			
<i>Autocorrelation time <math>\tau_{ac}</math></i>			
	$\min \left\{ \left( k \Delta(\omega/k) \right)^{-1}, v \Delta k \right\}$		$\min \left\{ (\Delta\Omega)^{-1}, \left( \Delta(q_x dv_g/dk) \right)^{-1} \right\}$
<i>Nonlinear time</i>	Trapping time $(e\tilde{\Phi}_L/m)^{-1}$		Turnover time $\tau_{\perp} = q_x \tilde{V}_{ZF}, \omega_{\text{bounce}}^{-1}$
<i>Decorrelation time <math>\tau_c</math></i>	$(k^2 D)^{-1/3}$		$\min \left\{ \gamma_k^{-1}, k^2/D_k, \left( q_x^2 D_k (dv_g/dk)^2 \right)^{-1/3} \right\}$
<i>Relaxation time</i>	$\Delta v^2 D_v^{-1}$		$\Delta k^2/D_k$
<hr/>			
<i>Resonance and irreversibility</i>	Wave-particle $\omega/k = v$ ,		Wave packet - Shear flow
	Phase space overlap		$v_g(k) = \Omega/q_x$ ,
	$\leftrightarrow$ Orbit chaos		Group-shear resonance overlap
			$\leftrightarrow$ Ray chaos
<hr/>			
<i>Theoretical Descriptions</i>			
<hr/>			
<i>Stochasticity/Quasi-linear</i>			
	$\tau_{ac} < \tau_{\perp}$ , orbit chaos, Random Acceleration Velocity diffusion		$\tau_{ac} < \tau_{\perp}$ , ray chaos, Random Shearing Diffusive refraction
<hr/>			
<i>Weak turbulence</i>			
	Induced Scattering $\leftrightarrow$ Nonlinear Landau damping of particles		Induced scattering of wave packets in Zonal flow field
<hr/>			
<i>Coherent/Trapping</i>			
	$\tau_{ac} > \tau_{\perp}$ , particle bounce motion Trapping oscillations $\rightarrow$ BGK mode		$\tau_{ac} > \tau_{\perp}$ , Ray trapping Ray trapping oscillations $\rightarrow$ BGK wave packet
<hr/>			
<i>Trapping in turbulence</i>			
	Granulations, clumps $\rightarrow$ Fokker-Planck drag		Wave population granulations $\rightarrow$ Wave kinetic drag



**Table 3.4.2:** Regimes of Zonal flow - Wave kinetics

<b>Regime</b>	<i>Chirikov Overlap Parameter</i> $S = \Delta v_g / \Delta(\Omega/q_x)$	<i>Kubo number</i> $\mathcal{K} = \tau_{ac} / \tau_{\perp}$	<i>Dominant Physical Process</i>
<i>Stochastic</i>	$S > 1$	$\mathcal{K} \ll 1$	Stochastic Rays Random Shearing and Refraction
<i>Turbulent Trapping</i>	$S > 1$	$\mathcal{K} \leq 1$	Stochastic rays, Shearing with Granulated $N$
<i>Coherent</i>	$S \ll 1$	$\mathcal{K} > 1$	Strongly Deflected Rays, Wave Packet Trapping
<i>BGK solution</i>		$\mathcal{K} \rightarrow \infty$	Wave Packet Trapping
Single wave	$S \rightarrow 0$	$\mathcal{K} \rightarrow 0$	Modulational instability

**Table 3.4.3: Comparison of Stochastic Dynamics**

Particles in Electrostatic Wave Spectrum	Drift Wave in Zonal Flow Field
<i>Diffusion Coefficient</i>	
$D_r = \sum_k \frac{e^2}{m^2}  \tilde{E}_k ^2 R(k, \omega)$	$D_x = \sum_{q_x} q_x^2 k_\theta^2  \tilde{v}_q ^2 R(k, q_x)$
<i>Resonance Function</i>	
$R(k, \omega_k) = \frac{\tau_{c,k}^{-1}}{(\omega - kv)^2 + \tau_{c,k}^{-2}}$	$R(k, q_x) = \frac{\gamma_{\text{drift}}}{(\Omega - q_x v_g)^2 + \gamma_{\text{drift}}^2}$
<i>Scattering Field</i>	
Wave spectrum $\sum_k  \tilde{E}_k ^2$	Zonal shear spectrum $ V_{\text{ZF}}' ^2 = \sum_k q_x^2  \tilde{v}_{\text{ZF},q} ^2$
<i>Scattered Field</i>	
Particle $v \rightarrow f(v)$	Drift wave packet $v_g(k) \rightarrow N(k)$
<i>Spectral Autocorrelation Rates</i>	
$\Delta\omega^{-1} \leftrightarrow$ time for fastest slowest waves to cross	$(q_x (dv_g/dk) \Delta k)^{-1} \leftrightarrow$ time for wave packet to disperse while crossing flow layer
<i>Nonlinear Decorrelation Rate <math>\tau_c^{-1}</math></i>	
$k^2 D_r$  time for particle to scatter one wave length	$\max \left\{ \gamma_k, D_k k^{-2}, \left( q_x^2 D_k (dv_g/dk)^2 \right)^{1/3} \right\}$  lower of times for wave packets to diffuse one wavenumber or to scatter through zonal flow scale by wavenumber diffusion and propagation or persistence time of triad

**Table 3.5.1** Short summary of theoretical method and description in this subsection

<b>Theoretical method</b>	<b>Nonlinear process and subsections in §3.4</b>		<b>Self-consistent state explained in §3.5</b>
Parametric instability	tertiary inst.;	3.4.1	-
	dithering;	3.4.2	3.5.2
Random Phase Approximation	predator-prey;	3.4.5	3.5.1
	diffusion model;	3.4.4	3.5.3
Coherent structure	wave trapping;	3.4.6	3.5.4
	saturation;	3.4.7	3.4.5

**Table 4.1:** Correspondence between the presentations of theory and corresponding examples of computational results

<b>Key Issue</b>	<b>Section for theoretical explanation</b>	<b>Example of Computational result (Figure #)</b>
<b>Linear Process</b>		
eigenfrequency	§3.1.1, §3.1.2	4.14, 4.19
collisional damping	§ 3.1.3	4.10
RH undamped flow	§ 3.1.4	4.10
<b>Generation by turbulence</b>	§3.2	4.1, 4.3, 4.4, 4.7
growth rate	§3.2.1, §3.2.2	4.4
<b>Suppression of turbulence</b>	§ 3.3	4.3, 4.4, 4.6
stretching vortex	§ 3.3.2	4.5
effect on cross phase	§ 3.6.2	4.13
<b>Nonlinear interaction</b>		
tertiary instability	§ 3.4.1	4.16
RPA and diffusion approach	§3.4.3, §3.4.4	4.4
wave trapping	§3.4.6, §3.4.7	4.15
broadening of ZF spectra	§3.4.8	4.20
dynamical evolution	§3.5.1, §3.5.3	
<b>Steady state and energy partition</b>		
weak instability case		
complete suppression	§3.5.1, §3.5.6	4.6
role of collisional damping	§3.5.1	4.11
quench via transient burst	§3.5.1	4.9
strong instability	§3.5.3-3.5.5	4.6, 4.8
coherent structure	§3.4.6, §3.4.7	
<b>Other effects</b>		
Non adiabatic electrons		4.14, 4.20
electromagnetic effects	§3.2.6	4.14
<b>ETG mode</b>	Appendix C	4.18
Collisionless dissipation		4.17

**Table 5.1.1** Terms in dynamical equation (5.1.8) and related equations, flow and waves [5.1]

(1)	(2)	(3)	(4)	(5)	(6)	(7)	
			◇	◇			Hydrostatic equilibrium
	◇		◇	◇			Bernoulli equation
◇	◇		◇	◇		◇	Navier-Stokes equation
			◇	◇	◇		geostrophic and thermal wind eq.
	◇		◇		◇		gradient-driven flow
	◇				◇		inertial flow
			◇			◇	Stokes flow
					◇	◇	Eckman spiral
◇	◇					◇	Fick's law
◇	◇		◇				Sound wave
◇	◇				◇		Rossby wave
◇	◇	◇					Alfven wave

**Table 5.2.1** Comparison and Contrast of Jovian Atmosphere and Toroidal System Dynamics

	Jupiter	Toroidal System
<b>Basic Characteristics</b>		
<i>Free energy</i>	$\nabla T$	$\nabla T$ , $\nabla n$ , etc.
<i>Rotation</i>	$\Omega_{\text{rot}} \gg \omega_k$	$\Omega_{\text{c}, i} \gg \omega_k$
<i>Rossby number</i>	$R_o \equiv \tilde{\omega} / \Omega_{\text{rot}} \ll 1$	$R_o = k_{\perp}^2 \rho_i^2 e \tilde{\phi} / T \ll 1$
<i>Effective Reynolds number</i>	strong turbulence	$R_{\text{eff}} \sim 10 - 100$ wave turbulence
<i>Velocity</i>	Geostrophic	$\boldsymbol{E} \times \boldsymbol{B} B^{-2}$
<b>Turbulence Physics</b>		
<i>Instability</i>	Thermal Rossby	Drift- ITG
<i>Frequency</i>	$\beta$ -effect	Diamagnetic
<i>Cell Structure</i>	Taylor-Proudmann Columns	Ballooning modes, extended along $\boldsymbol{B}_0$
<i>Threshold</i>	$R_a > R_{a, c}$	$R/L_{Ti} > R/L_{Ti} \Big _{\text{crit}}$
<i>Eddy</i>	Rising Thermal Plumes	Ballooning envelope fragments
<i>Transport</i>	turbulent transport	$D, \chi \sim D_{\text{gyroBohm}}$

**Table 5.2.2** Comparison, continued

	<b>Jupiter</b>	<b>Toroidal System</b>
<i>Basic structure</i>	Belts, Zones	$n = 0$ , $k_r$ finite, electrostatic fluctuations
<i>Location</i>	Surface, "Weather Layer"	Core and Edge of Confined Plasmas
<i>Mechanism for Generation</i>	i) Secondary bifurcation of Convection Column Tip Cells ii) Inverse Cascade in Weather Layer with $\beta$ -effect	Modulational instability of Wave spectrum
<i>Large Scale Dissipation</i>	Eckman Friction	Rosenbluth-Hinton Friction
<i>Anisotropy</i>	$\beta$ -effect	Flow - Minimal Inertia
<i>Flow and Fluctuation model</i>	Same	Flow 2D ( $n = 0$ ) and Fluctuation 3D, with $k_{\parallel} v_{th,e} > \omega_k$
<i>Bifurcated State</i>	Belt Formation	L-mode, ITB, ETB

**Table 6.3.1** Correspondence between the SOC model and continuum model (based on [6.25])

<i>model of continuous media</i>		<i>SOC models</i>
Localized fluctuation (eddy)	↔	Grid site (cell)
Local turbulence mechanism	↔	Automata rules:
Critical gradient for local instability	↔	Critical sandpile slope
Local eddy-induced transport	↔	Number of grains moved if unstable
Heating noise	↔	Random rain of grains
Energy/particle flux	↔	Sand flux
Mean temperature/density profiles	↔	Average slope of sandpile
Transport event	↔	Avalanche
Sheared electric field	↔	Sheared flow (sheared wind)



**Table 7.1. Experimental characteristics of zonal flows**

	<b>Zonal flow (narrow sense)</b>	<b>GAMs</b>
<i>fluctuation structure</i>	$m = n = 0$ for $\tilde{\phi}$ $\hat{n} \ll \hat{\phi}$	$m = n = 0$ for $\tilde{\phi}$ $m = 1, n = 0$ for $\tilde{n}$ $ \tilde{n}/n_0  = \sqrt{2} q r \rho_s  e\tilde{\phi}/T_e $
<i>real frequency</i>	$\Omega_{ZF} = 0$	$\omega_{\text{GAM}} = v_{\text{Th}}/R$
<i>autocorrelation time</i>	$\epsilon v_{ii}^{-1}$ , or other (TBD)	$v_{ii}^{-1}$ , or other (TBD)
<i>radial wavelength</i>	$a\rho_i > q_r^{-2} > \rho_i^2$	←
<i>radial coherence length</i>	several tens of $\rho_i \sim \sqrt{a\rho_i}$	←
<i>amplitude (vorticity)</i>	order of $\rho_i^{-1} V_d$	TBD

## Appendix A Ray of Drift Wave Packet and Trapping

A ray of drift wave packet in the presence of zonal flow is calculated by assuming that the autocorrelation time of drift wave  $\tau_{ac}$  is much longer than the dynamical time of the zonal flows. The drift kinetic equation for the drift-wave action density is given as

$$\frac{\partial}{\partial t} N_k + \mathbf{v}_g \cdot \frac{\partial N_k}{\partial \mathbf{x}} = k_\theta \frac{\partial N_k}{\partial k_r} \frac{\partial V_{ZF}}{\partial x}, \quad (\text{A.1})$$

When a screening effect of the finite gyroradius effect is kept,  $V_{ZF}$  is replaced by  $\bar{V}_{ZF}$ , which is given as

$$\bar{V}_{ZF} = V_{ZF} + \rho_s^2 \frac{d^2 V_{ZF}}{dx^2}. \quad (\text{A.2})$$

In comparison with Eq.(3.4.13), the linear growth and nonlinear damping terms of drift wave are dropped in Eq.(A1), because the case with coherent waves is studied here.

### (i) Stationary State

A coherent and stationary structure for the zonal flow is considered here in Eq.(A1). A stationary solution which is propagating in the  $x$  direction with the speed  $u$  is analyzed by the transformation of

$$\frac{\partial}{\partial t} \rightarrow -u \frac{\partial}{\partial x}. \quad (\text{A.3})$$

Equation (A.1) is rewritten as

$$(v_g - u) \frac{\partial N_k}{\partial x} + k_y \frac{d\bar{V}_{ZF}}{dx} \frac{\partial N_k}{\partial k_x} = 0. \quad (\text{A.4})$$

Equation (A.4) shows that the drift wave action is constant along the characteristics

$$k_y = k_{y0} \quad (\text{A.5})$$

and

$$\frac{\partial k_x}{\partial x} = \frac{k_y}{v_g - u} \frac{d\bar{V}_{ZF}}{dx}. \quad (\text{A.6})$$

Integrating Eq.(A.6) once over  $x$ , Eq.(A.6) gives

$$\omega_k - u k_x - k_y \bar{V}_{ZF} \equiv \omega_{k0} \quad (\text{A.7})$$

with

$$\omega_k = k_{y0} \left( 1 + k_{y0}^2 + k_x^2 \right)^{-1/2}. \quad (\text{A.8})$$

Equations (A.5) and (A.7) show two integrals of motion. The integral constant  $\omega_{k0}$  is the initial frequency, and the LHS of Eq.(A.7) is kept constant during the evolution of the system. This means that the wave-packet of drift wave moves in the phase space  $(x, k_x, k_y)$  while keeping  $k_y$  and the screened frequency (A.7) constant. It is straightforward to see that  $k_y$  is constant, because the zonal flow does not violate the symmetry in the  $y$ -direction.

### (ii) Ray of Drift Wave-Packet

Equations (A.7) and (A.8) describe the ray of the wave-packet of drift waves. In a case of the inhomogeneous zonal flow like Fig.A.1(a), the wave-packet moves in the phase space  $(x, k_x)$ . The trajectory is illustrated in Fig.A.1(b) for the case of  $u = 0$ . Note that the group velocity of the wave in the  $x$ -direction is opposite to the phase velocity. The wave-packet with positive  $x$ -direction (i.e.,  $k_x < 0$ ), the velocity decreases, and is reflected.

The trajectory Fig.A.1(b) explains the mechanism of linear instability of zonal flow. The wavevector of the drift wave starts to increase when the test zonal flow ( $d\bar{V}_{ZF}/dx > 0$ ) is imposed. The distribution function  $N(k_x)$  which is symmetric in  $k_x$  starts to deform. Figure A.2 illustrates the change of distribution function after the imposition of the zonal flow like Fig.A.1(a). The original symmetric one (solid line) deforms as is shown by dashed line. As a result,  $N(k_x)$  becomes larger for  $k_x > 0$  and decreases for  $k_x < 0$ . The difference of  $N(k_x)$  after the imposition of the zonal flow is positive for  $k_x > 0$ . This is an alternative explanation for the source term illustrated in Fig.3.2.4.

### (iii) Reflection and Trapping of Drift Waves

If the inhomogeneity is localized in space, the trajectories are categorized in two groups. One is the transit orbit, moving in all places. The other is reflected trajectory. By this reflection of wave-packets, the inhomogeneity of zonal flow velocity is sustained. Figure A.3 shows an example of the localized inhomogeneity of zonal flow and the reflection of waves.

The preceding analysis leads to the fact that (a) the drift wave-packet can be labeled by the initial frequency  $\omega_{k0}$  and that (b) the wavefrequency  $\omega_k$  and the wavenumber  $k_x$  are modified along the path of drift wave-packet according to Eq.(A.7).

The trapping of the drift wave-packet in the trough of zonal flow velocity is derived. Figure A.4 illustrates the rays of drift wave-packets in the phase space for the case that the screened velocity  $\bar{V}_{ZF}$  has a sinusoidal dependence in the  $x$ -direction. Near the minimum of the zonal flow velocity, the wave-packets follow the bouncing orbit. At the maximum, the separatrix appears. If the initial value of  $k_x$  is large, the wave-packets are not trapped but follow the transit orbit. Thus the wave-packets are divided in to the class of trapped waves and the class of transit waves. They are also called the bounded quasi-particles and free quasi-particles.

The trapped region is determined by the difference between maximum and minimum of  $\bar{V}_{ZF}$ ,  $\Delta\bar{V}_{ZF}$ . The wavenumber on the separatrix at the minimum of  $\bar{V}_{ZF}$  is given as

$$k_{x0, sep}^2 = \frac{\Delta\bar{V}_{ZF} (1 + k_{y0}^2)^2}{1 - \Delta\bar{V}_{ZF} (1 + k_{y0}^2)} \quad (A.9)$$

for a simple case of  $u = 0$ . Wave packets which satisfy

$$k_{x0}^2 < k_{x0, sep}^2 \quad (A.10)$$

are trapped in the inhomogeneous zonal flow. As is the case of particle trapping in the waves of collisionless plasmas, the width of the trapping region in the phase space of quasi-particles is in proportion to the square-root of the amplitude of the zonal flow.

The bounce motion of wave-packets is analyzed. As is explained in Eq.(A.10), the 'acceleration' of the wave-packet in  $k_x$  space is given as  $k_0 d\bar{V}_{ZF}/dx$ . Therefore the dynamical equation of the wave-packets are given as

$$\frac{dx}{dt} = v_g \quad (\text{A.11a})$$

$$\frac{d}{dt} k_x = k_y \frac{d}{dx} \bar{V}_{ZF} \quad (\text{A.11b})$$

Expanding Eq.(A.11a) and (A.11b) near the O-point of the trapped particle orbit at the bottom of  $\bar{V}_{ZF}$ , one has a linearized equations

$$\frac{dx}{dt} = \frac{-2\omega_{k0}}{1 + k_y^2} k_x \quad (\text{A.12a})$$

$$\frac{d}{dt} k_x = \left( k_y \frac{d^2}{dx^2} \bar{V}_{ZF} \right)_m x, \quad (\text{A.12b})$$

where the subscript m indicates that the derivative is taken at the minimum of the zonal flow velocity. The bounce frequency is derived as in a dimensional form

$$\omega_{\text{bounce}}^2 = \frac{2\rho_s^2 k_y K_r}{1 + \rho_s^2 k_y^2} \omega_{k0} \left. \frac{d\bar{V}_{ZF}}{dr} \right|_{\text{max}}. \quad (\text{A.13})$$

As is the case of the trapping of resonant particles by waves in collisionless plasmas, the bounce frequency of quasi-particles (wave-packets) has a dependence like

$$\omega_{\text{bounce}} \propto \sqrt{V_{ZF}}. \quad (\text{A.14})$$

The bounce frequency away from the O-point is evaluated by use of the elliptic functions. The bounce frequency becomes lower as the trajectory approaches the separatrix.

Appendix B: Hierarchy of Nonlinear Governing Equations

In this appendix, the hierarchy of nonlinear governing equations is explained. Steps for reduction, and physics lost due to reduction is also listed.

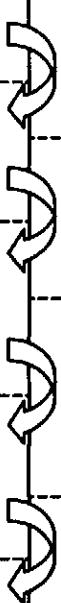
Nonlinear equations: From fundamental, primitive to reduced, simplified	Steps for reduction	Physics lost due to reduction
Vlasov-Klimontovich equation [B1]	 <div>Remove high frequency terms (<math>\geq \omega_{ci}</math>)</div> <div>Neglect velocity space nonlinearity</div> <div>Take moments in velocity space</div> <div>Expansion in finite Larmor radius terms; Ordering for collisional plasmas</div>	High frequency phenomena [B6]
Gyrokinetic Equation: Conservative [4.4, B2-B5]		
Gyrokinetic Equation: Conventional [4.2]		Conservation of energy between particles and fields, of phase-space volume, nonlinear trapping of particles along $B$ . (Influence is illustrated in Fig.B.1.)
Gyrofluid Equation [4.7, B7, B8]		Some nonlinear kinetic effects including inelastic Compton scattering [B9], accuracy in damping rates of zonal flow [2.40, 2.41] and damped mode [B10]
Fluid Equations [B11-B16]		Most kinetic effects associated with long mean free paths and finite size orbits.

Table B.1 Hierarchy of governing equations

As is explained in the main text, most simulations mentioned above have used the conventional nonlinear gyrokinetic equation[4.4], which ignores the velocity space nonlinearity, which is formally smaller than the  $E \times B$  nonlinearity. The conventional nonlinear gyrokinetic equation fails to obey the fundamental conservation laws, such as energy (of particles and fluctuation fields), and phase space volume at a non-trivial order. For longer times, well after the initial nonlinear saturation of turbulence, even very small errors in the governing equation can accumulate (in time, regardless of computational method) and muddy the physics predictions. A recent simulation [4.48] in cylindrical geometry used a fully nonlinear energy conserving and phase space conserving form of the nonlinear gyrokinetic equation [4.6]. The importance of using governing equation with proper conservation laws is demonstrated in this series of simulations, with and without velocity space nonlinearity. The authors reported that neglecting velocity space nonlinearity in an ITG simulation resulted in undesirable consequences. The energy was

no longer conserved between particles and fluctuating fields, and a precious indicator of the quality of numerical integration was lost. The zonal flow pattern and the radial heat transport pattern were affected as well. The results are presented in Fig. B.1; it highlights an issue related to reduction of equations.

**Appendix C: Near-Isomorphism between ITG and ETG**

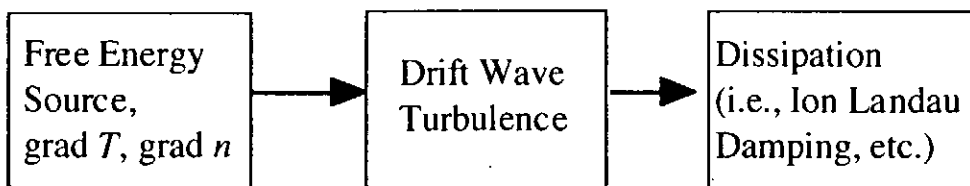
Here the quasi-isomorphism between ITG and ETG are tabulated in Table C.1.

Key issue		ITG	ETG
Linear response in the electrostatic limit	$\tilde{n}_i$	From gyrokinetic equation	$-e\phi/T_i$ : pure adiabatic
	$\tilde{n}_e$	$e(\phi - \langle \phi \rangle)/T_e$ : adiabatic with zonal flow	From gyrokinetic equation
Disparity in transport channels caused by particular turbulence		$\chi_i \sim \chi_\phi > \chi_e, D$	$\chi_e \sim \chi_J > D, \chi_i, \chi_\phi$
Zonal flow strength in nonlinear regime		Typically strong	Typically weaker
Radial correlation length of ambient turbulence at nonlinear saturation		Several $\rho_i$	Uncertain – current research
Isomorphism breaker		Zonal flow	- residual magnetization of ion response - electromagnetic effect - Debye shielding

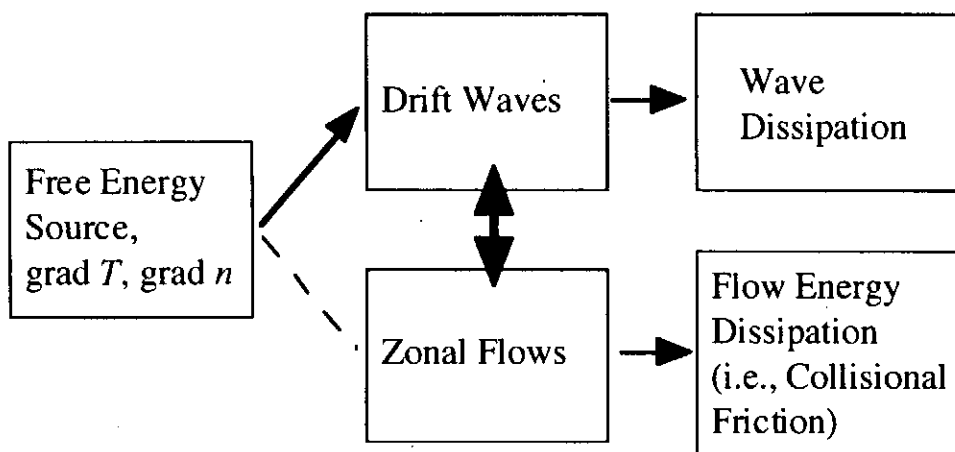
**Table C.1** Quasi-isomorphism between ITG and ETG

In this table,  $D$ ,  $\chi_\phi$  and  $\chi_J$  are diffusivities of particle, momentum and current. Note that ETG will transport current much like ITG transport momentum.  $\chi_J$  is like hyper-resistivity.





Classic Paradigm of Drift Wave Turbulence



New Paradigm of Drift Wave-Zonal flow Turbulence

**Fig. 1.1** New paradigm for the plasma turbulence

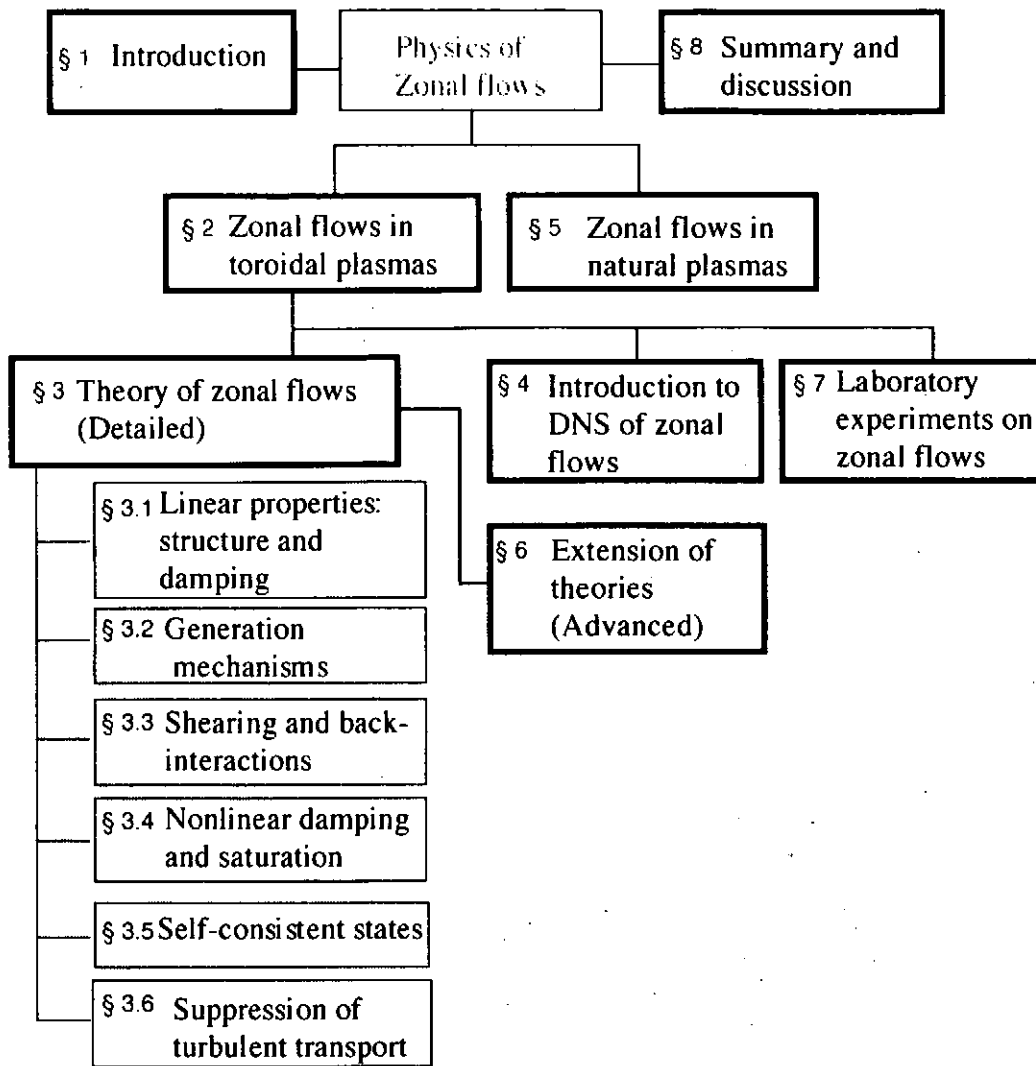


**Fig.1.2** Road Map for the review

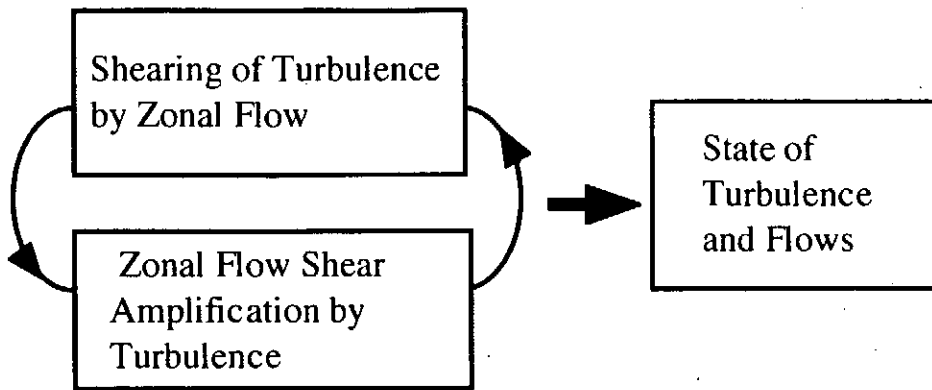


**Fig.2.1** Mutual interaction of drift waves and zonal flows

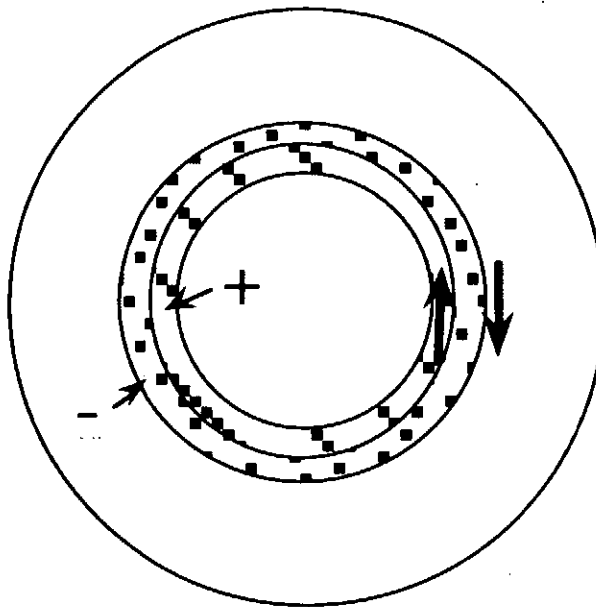


**Fig.2.2.** Zonal electric field and zonal flow. The poloidal crosssection of toroidal plasma is illustrated. Hatched region and dotted region denote the positive and negative charges, respectively. Plasma flow is in the poloidal direction as is shown by the arrow.

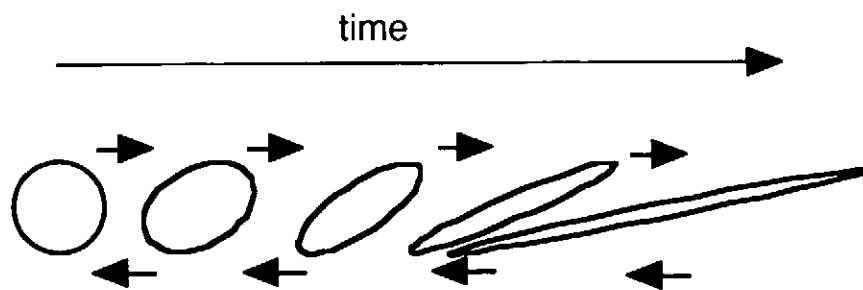


**Fig.2.3** Shearing of the vortex

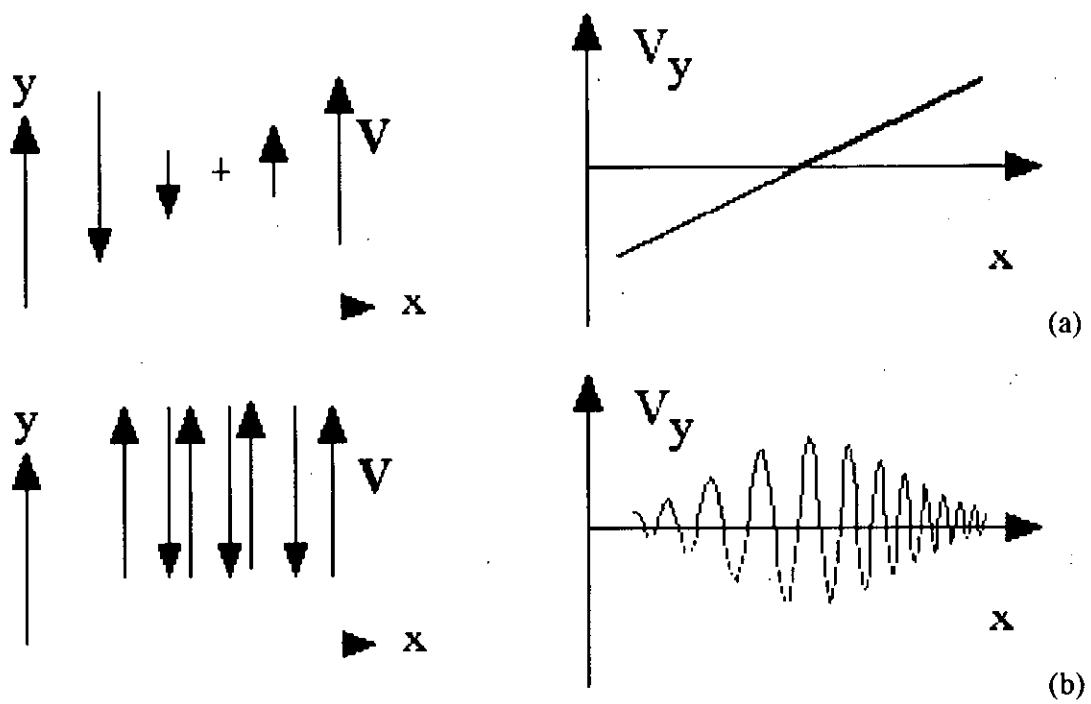


**Fig.2.4** Sheared mean flow (a) and zonal flows (b) are illustrated.

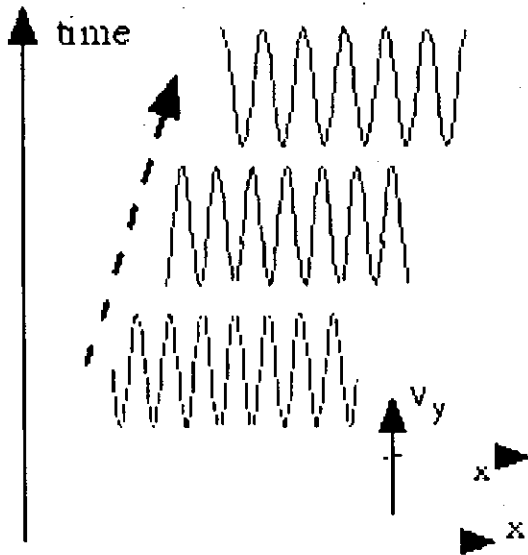


**Fig.2.5** Drift wave in sheared flow field. When a drift wave packet is propagating in the  $x$ -direction in the presence of flow shear,  $dV_y/dx > 0$ , the wave number  $k_x$  changes.

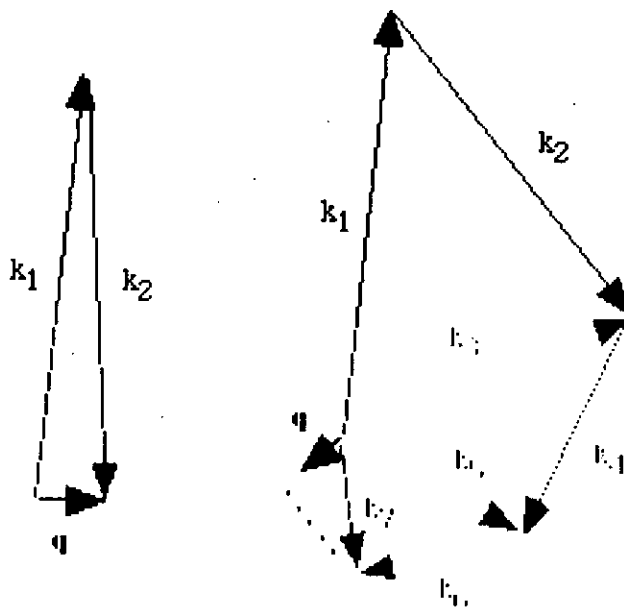


**Fig.2.6** Short wavelength fluctuations ( $k_1$ ,  $k_2$ ) generate the long wave length component ( $q$ ) by nonlocal interaction in the wavenumver space.(left). The local interactions in the wavenumber space generates the long wavelength component, i.e., inverse cascade (right).

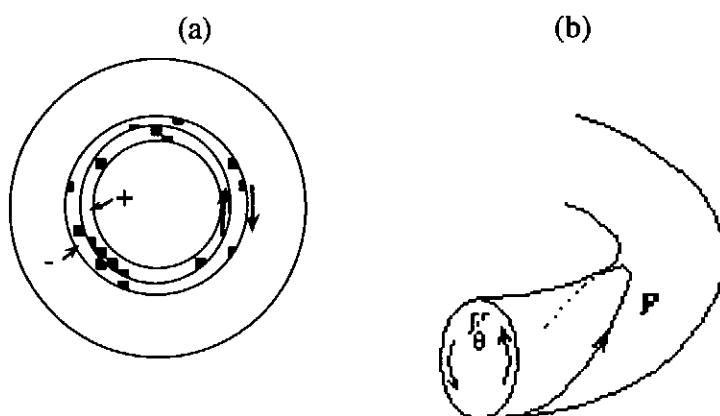


**Fig.3.1.1** (a) The flow perturbation in the poloidal cross-section. The bird-eye view of the net flow associated with the zonal perturbation is illustrated in (b).

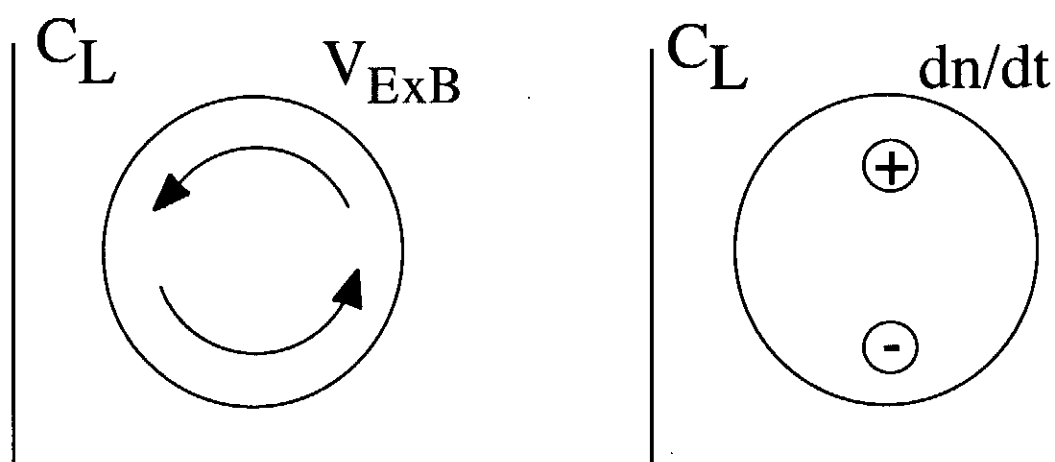


**Fig.3.1.2** GAM flow pattern and the rise of density

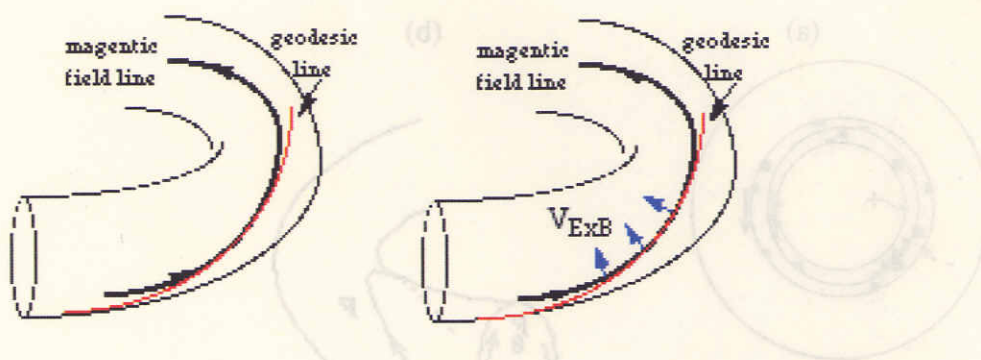


**Fig.3.1.3** Magnetic field line (thick solid line, black) and geodesic line (thin solid line, red) on a toroidal magnetic surface (a). Geodesic curvature is also shown. If geodesic curvature exists, i.e., the magnetic field line is not the geodesic line, the  $E \times B$  velocities (written in the right figure) are not parallel to each other. That is, the divergence of the  $E \times B$  does not necessarily vanish and can induce compression. (b)

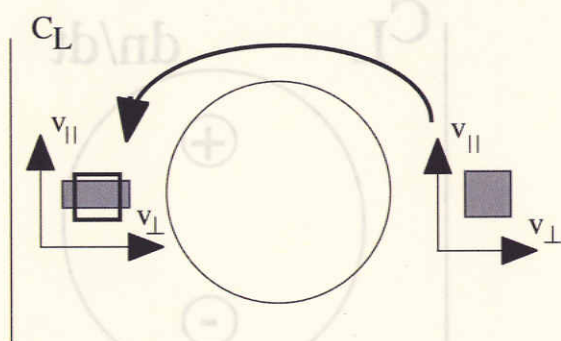


**Fig.3.1.4** Schematic drawing of the phase-space distribution of ions. Hatched square shows collisionless case. [3.30]

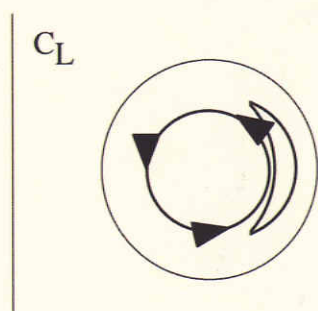


**Fig. 3.1.5** Transiting ions and trapped ions. Trapped ions do not rotate in the poloidal direction.

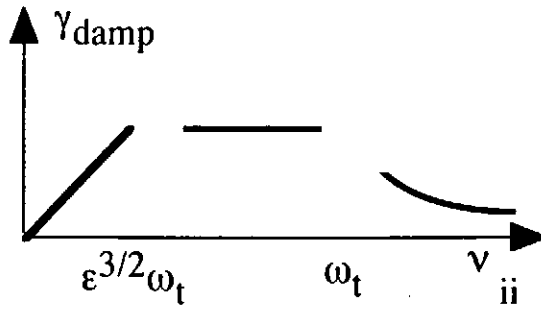


**Fig. 3.1.6** Schematic drawing of the collisional damping rate for the zonal flow.

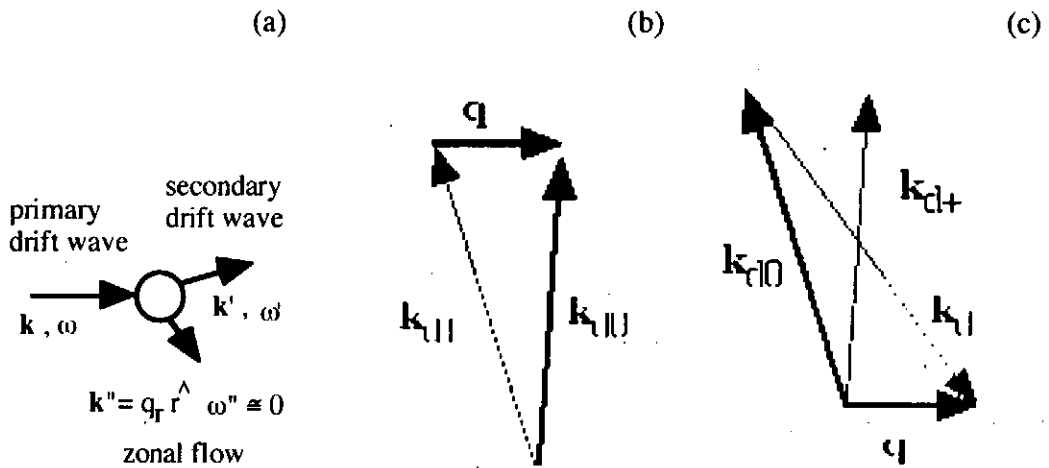


**Fig.3.2.1** Parametric instabilities of a drift wave (a). (b) Parametric decay of the primary drift wave (denoted by  $k_{d0}$ ) into a convective cell (denoted by  $q$ ) and the secondary drift wave ( $k_{d1}$ ): Structure of the wave numbers selection rule is shown in (b) and (c) for decay case and for modulational instability, respectively. (c) Parametric modulational instability of the primary drift wave (denoted by  $k_{d0}$ ) generating a convective cell (denoted by  $q$ ) and the secondary drift waves ( $k_{d+}$  and  $k_{d-}$ ).



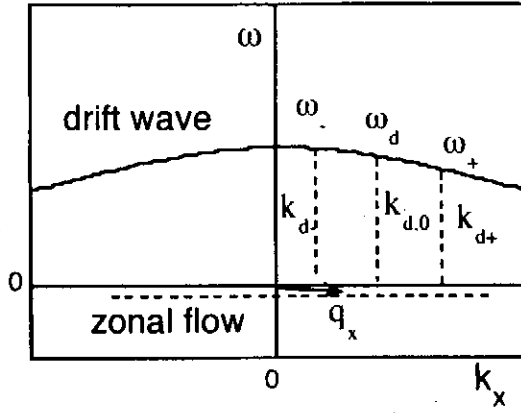


**Fig.3.2.2** Eigen frequencies of drift waves (solid line) and zonal flow (dashed line) plotted vs  $k_x$ . The frequency of the zonal flow is exaggerated.

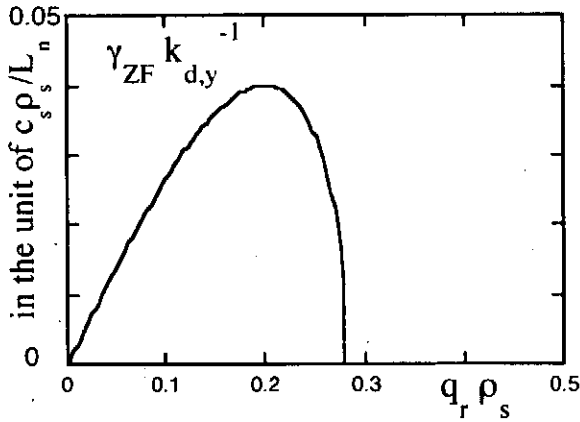


**Fig.3.2.3** Growth rate of the zonal flow for the parametric modulational instability. A case of  $e \tilde{\phi}_{d0}/T_e = 0.2 \rho_s/L_n$  and  $k_{d,x} = 0$  is shown.

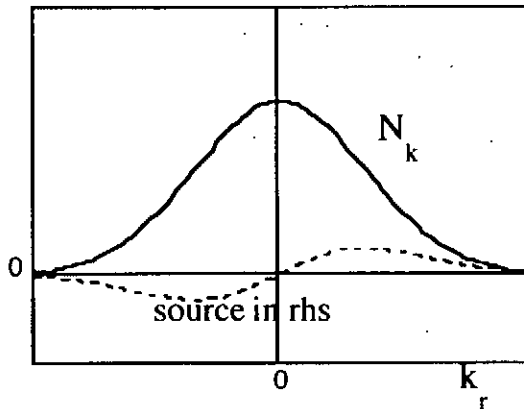


**Fig.3.2.4** Conceptual drawing of the distribution of the drift wave action  $N_k$  and the right hand side of Eq.(3.2.51). (The sign of the term  $k_\theta dV_{ZF}/dr$  is chosen negative.)

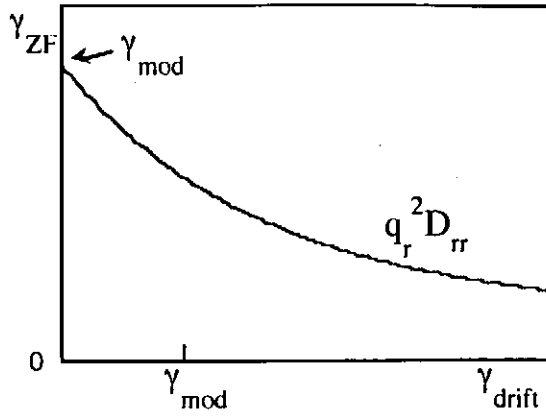


**Fig.3.2.5** Illustration of the growth rate of the zonal flow as a function of the inverse of the life time of the primary drift wave,  $\gamma_{drift}$ . ( $\gamma_{mod}$  is given by Eq.(3.2.60c).) When the life time is long,  $\gamma_{drift} \ll \gamma_{mod}$ , the growth rate of the modulational instability is recovered. In the opposite case, the diffusive growth occurs.

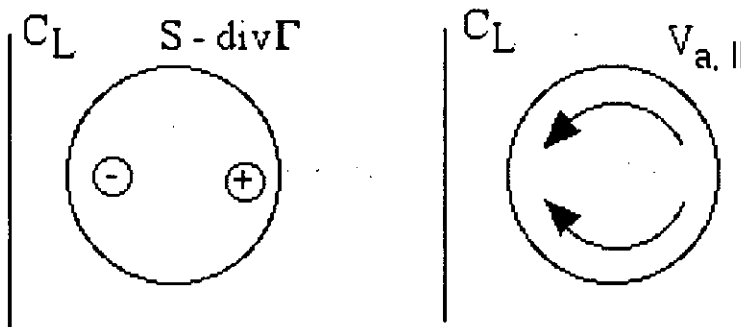


**Fig.3.2.6** Poloidal inhomogeneity of the excess source  $S - \nabla \cdot \Gamma$  (left), and the secondary flow on magnetic surface  $V_{a,||}$  (right).

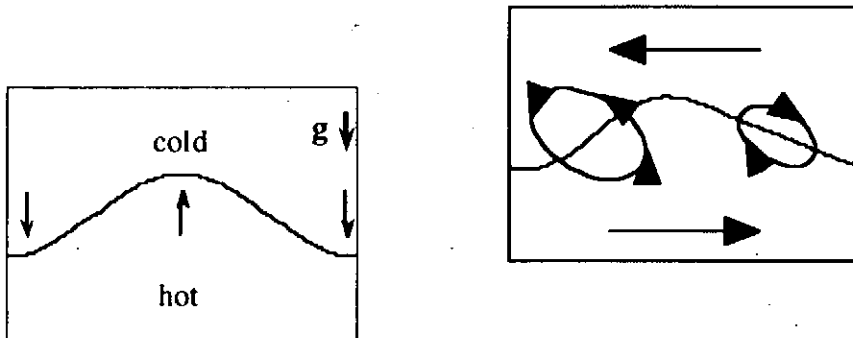


**Fig.3.3.1** Rayleigh-Benard instability in the presence of gravity (a) and the KH instability in the presence of sheared flow (b).

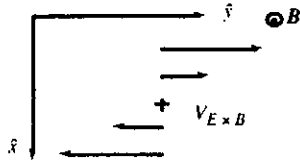


**Fig. 3.3.2** Flow in the y-direction, which is inhomogeneous in the x-direction

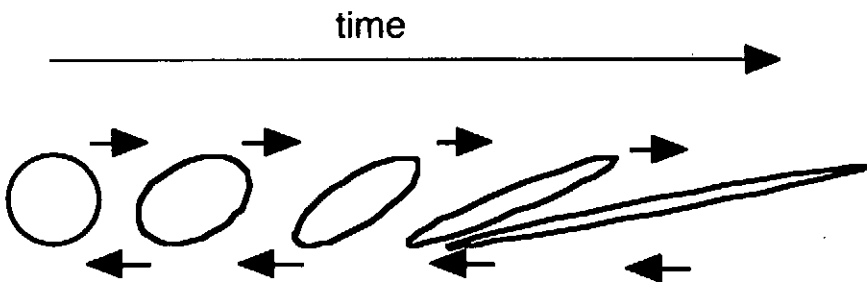


**Fig.3.3.3** Stretching of eddy by shear flow which is constant in time. Thick arrows indicate the sheared flow.

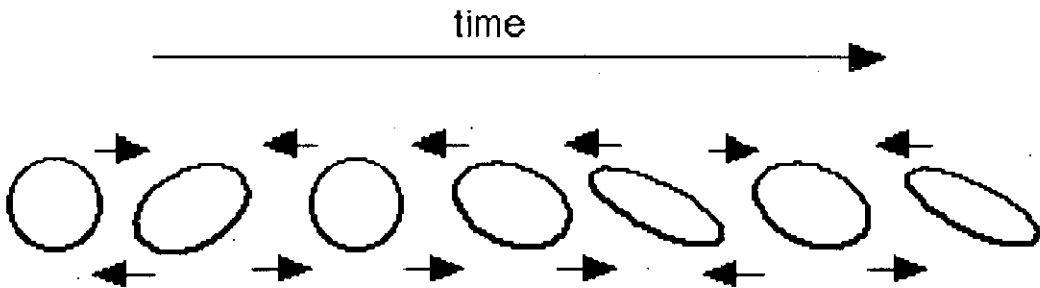


**Fig.3.3.4** Random shearing flow and stretching. Shear flow (denoted by blue arrows or red arrows) is rapidly changing in time.

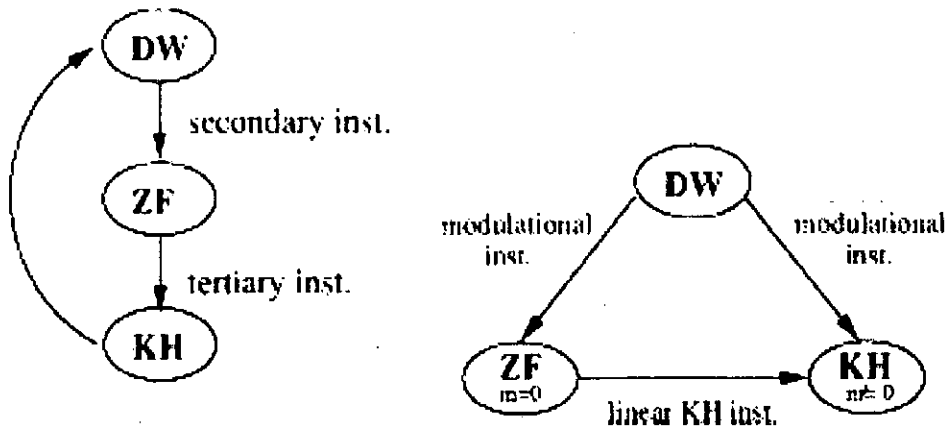


**Fig. 3.4.1** The contrast of the linear view of the GKH modes (a) to a more general case where GKH modes are generated by both linear and nonlinear modulatory instabilities (b). The linear view is hierarchical in that GKH is generated by the linear instability of zonal flows (ZF), which are already generated by DW. In general, GKH modes can, however, be generated directly from DW by modulatory instability.

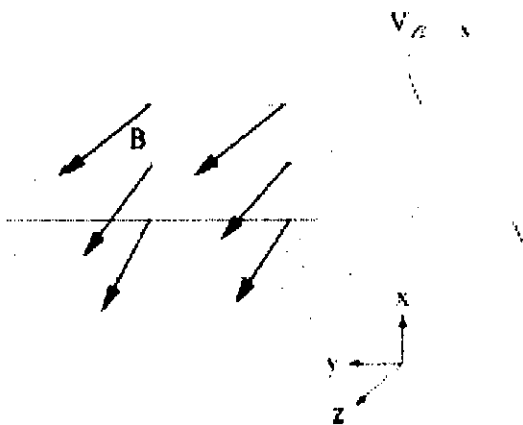


**Fig.3.4.2.** A schematic picture showing the magnetic shear and zonal flow profile; the exchange of two vortices requires the alignment of those vortices with tilted magnetic field lines.

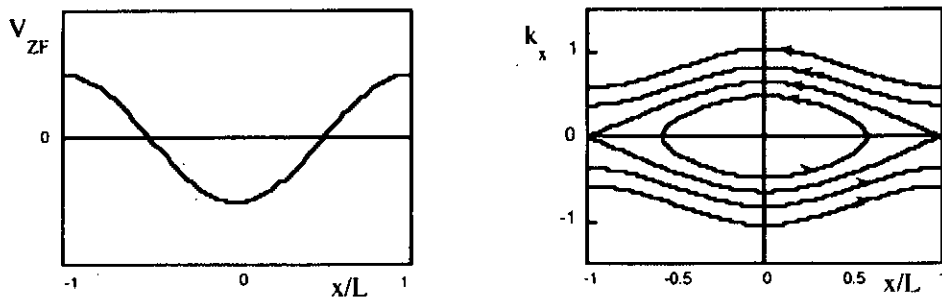


**Fig.3.4.3** Trapping of wave-packets in the trough of zonal flow velocity. The spatial profile of zonal flow velocity (a) and trajectories in phase space (b).

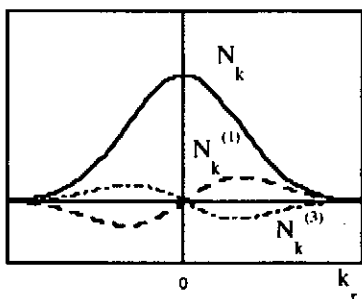


**Fig.3.4.4** Linear response of the distribution function  $\hat{N}_k^{(1)}$  (dashed line) and the third order response  $\hat{N}_k^{(3)}$  (broken line). The nonlinear term tends to cancel the linear drive.

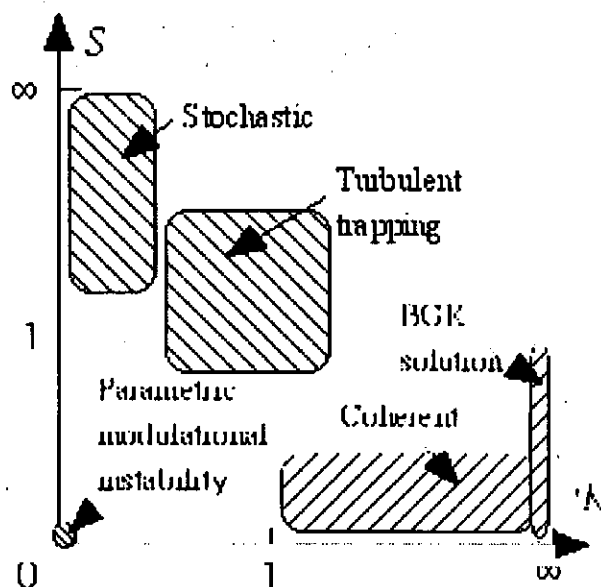


**Fig.3.4.5** Parameter domains for various theoretical approaches

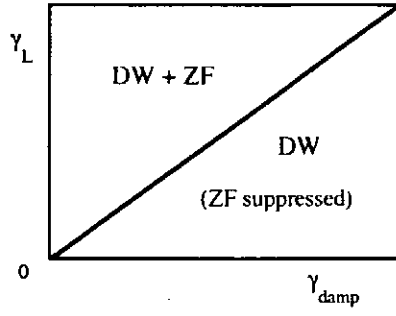


**Fig.3.5.1** Phase diagram of the predator-prey model for the system of drift waves and zonal flow. In the region of low damping rate,  $\gamma_{damp} < C_d \rightarrow Z\gamma_L/\gamma_2$ , the zonal flow coexists with drift waves. In this regime,  $\langle U^2 \rangle/N \sim \gamma_L/\gamma_{damp}$ .

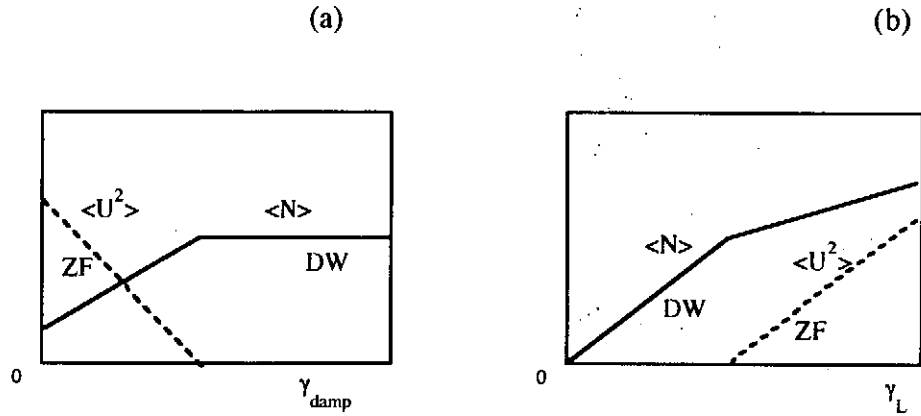


**Fig.3.5.2** Amplitude of drift waves  $\langle N \rangle$  and that of zonal flow  $\langle U^2 \rangle$  for the case where the self-nonlinear stabilization effect of zonal flow (e.g., the  $\gamma_{NL}(V^2)$  term in Eq.(2.10b)) exists. (a) shows the  $\gamma_{damp}$ -dependence with fixed  $\gamma_L$ , and (b) shows the  $\gamma_L$ -dependence with fixed value of  $\gamma_{damp}$ .

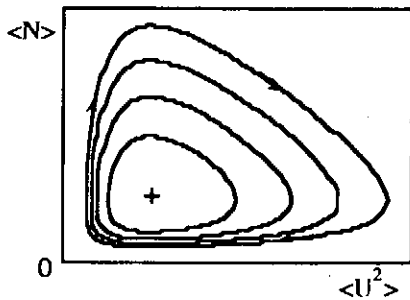


**Fig.3.5.3** Phase portrait in the absence of nonlinear stabilization effect of drift waves,  $\gamma_2 = 0$ . [2.14]

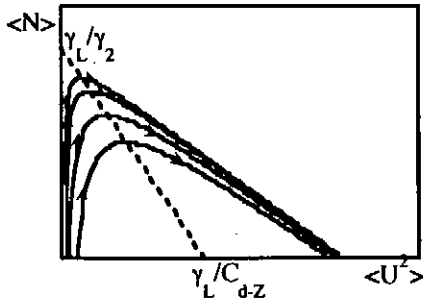


**Fig.3.5.4** Trajectory in the case of no zonal flow damping  $\gamma_{\text{damp}} = 0$ . Depending on the initial conditions, the system reaches different final states, in which the waves are quenched.

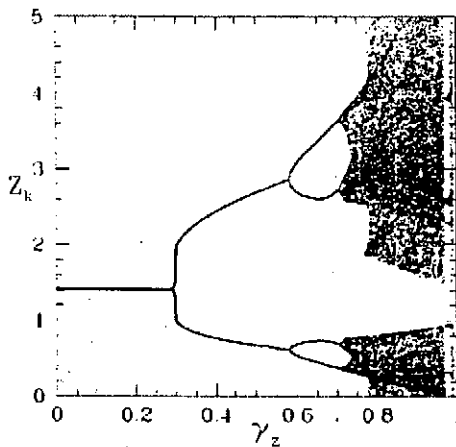


**Fig.3.5.5** Normalized amplitude of zonal flow  $Z_k$  as a function of the normalized damping rate  $\gamma_z = \gamma_{\text{damp}} / \gamma_L$ . Quoted from [2.23].

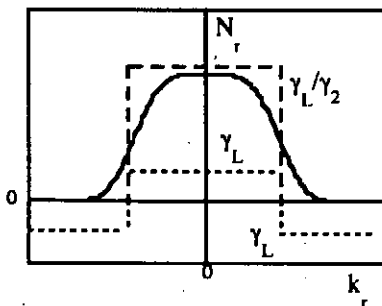


**Fig.3.5.6** Spectrum of drift waves in a stationary state (solid line). Linear instability exists in the lower  $|k_r|$  region. The local balance of self-nonlinearity,  $\gamma_L = \gamma_{\text{NL}}$  is denoted by the thick solid line.

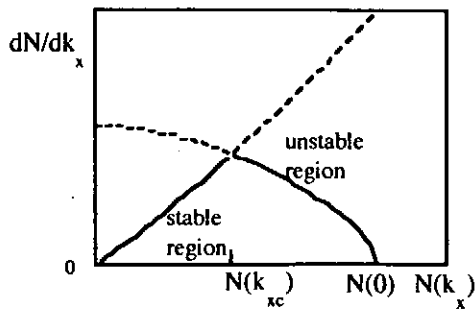


**Fig.3.5.7** Relation (3.5.19). Thin lines fall in the region of linear stability,  $|k_r| > k_{rc}$ , and thick lines fall in the unstable region,  $|k_r| < k_{rc}$ . Solid lines define the solution.

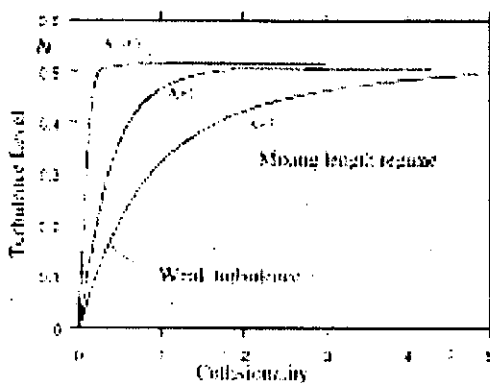
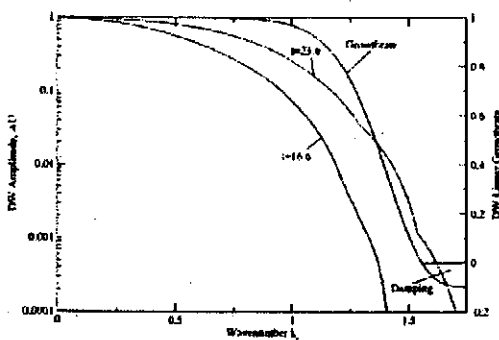


**Fig.3.5.8** Amplitude of drift waves (normalized to  $2\gamma_L/\gamma_2$ ) in the stationary state as a function of the collisional damping rate of zonal flow  $\gamma_{\text{damp}}$ . The horizontal axis is taken  $\gamma_{\text{damp}}/\gamma_L$  in the unstable region  $|k_r| < k_{rc}$ . In this figure,  $A$  is a parameter that is in proportion to  $C_d \rightarrow z/\gamma_2$ . (quoted from [3.44].)



**3.5.9** Linear growth rate and spectrum of drift waves. [3.92]



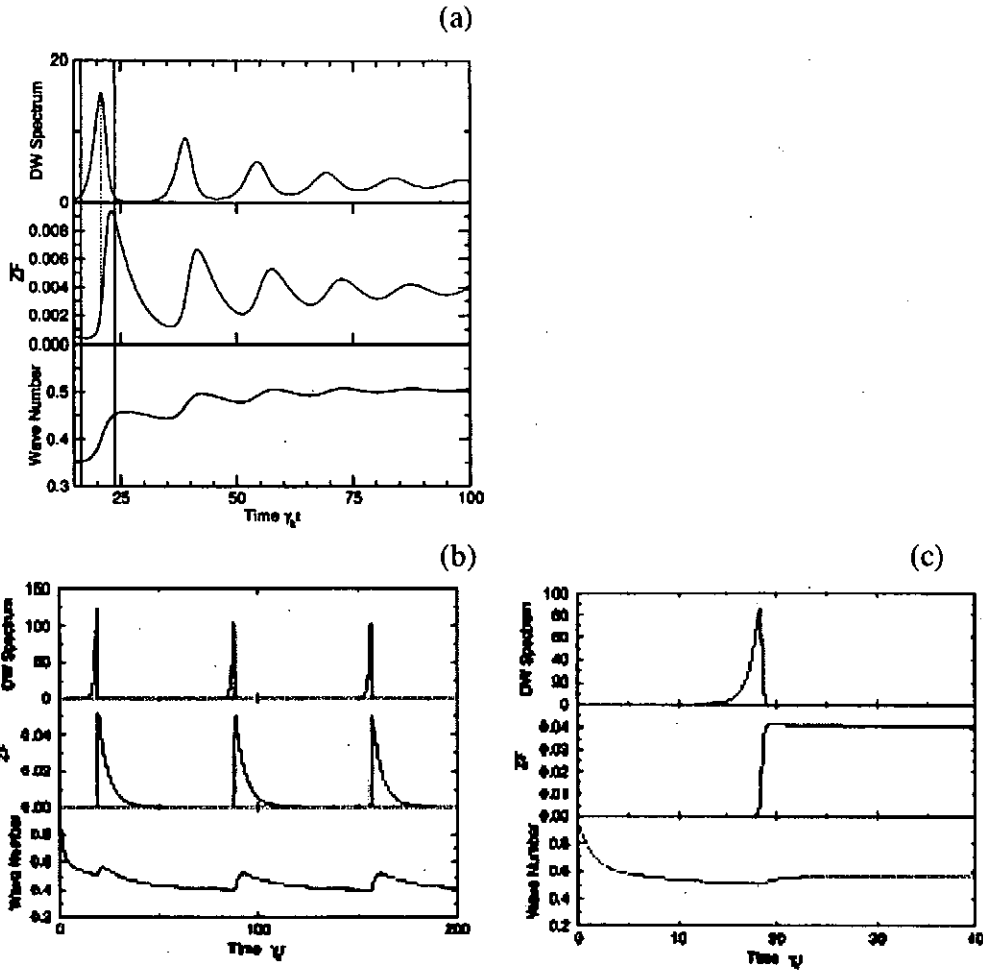


**Fig.3.5.10** Temporal evolution of drift wave energy, zonal flow and the average wave number. cases of  $\gamma_L \neq 0, \gamma_{damp} \neq 0, \gamma_2 \neq 0$  (a),  $\gamma_2 = 0$  (b) and  $\gamma_{damp} = 0$  (c) are shown. [3.92].

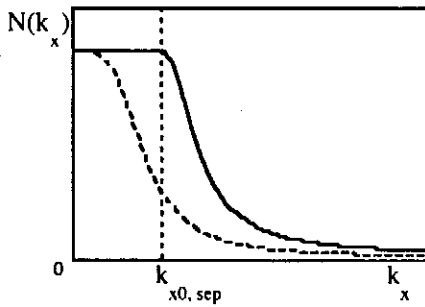


**Fig.3.5.11** Example of the distribution function of  $N(k_x)$  for the case of Lorentzian shaped distribution in  $w$ . The distribution function in the trough (solid line) and that at the peak (dashed line) are shown. (Zonal flow is given as in Fig.3.4.5)

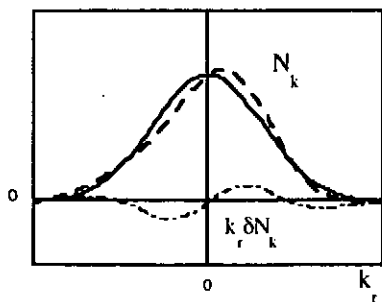


**Fig.3.5.12** Deformation of the spectrum function  $N(k_y)$  by zonal flow. In the absence of zonal flow (solid line) and in the presence of finite amplitude zonal flow (dashed line). Difference is also shown.

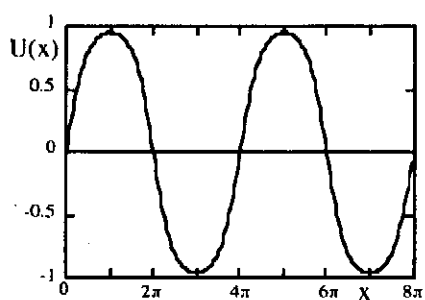


**Fig.3.5.13** Coherent profile of normalized zonal flow vorticity.

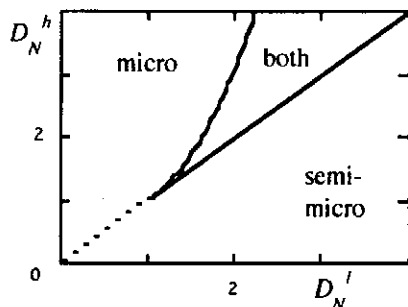


**Fig.3.5.14** Phase diagram for the case of mutual interactions between intermediate scale and micro modes.

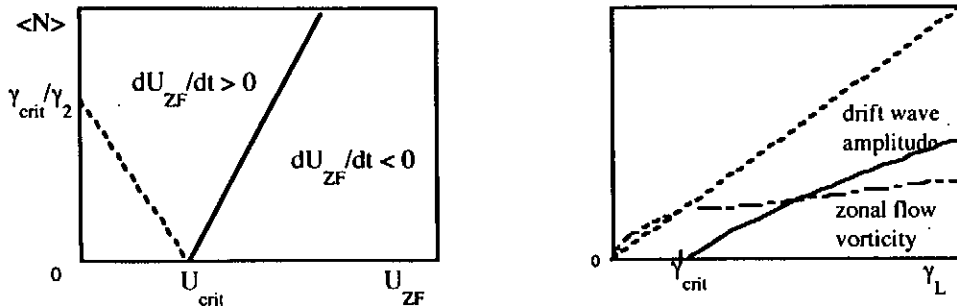


**Fig.3.5.15** Marginal stability boundary for the growth of the zonal flow is shown by the solid line in the limit of  $\gamma_{damp} = 0$  (a). Dotted line indicates the marginal stability condition for the drift waves (a). The excited energy of waves and flows as a function of the growth rate of drift waves, in the limit of  $\gamma_{damp} = 0$  (b).

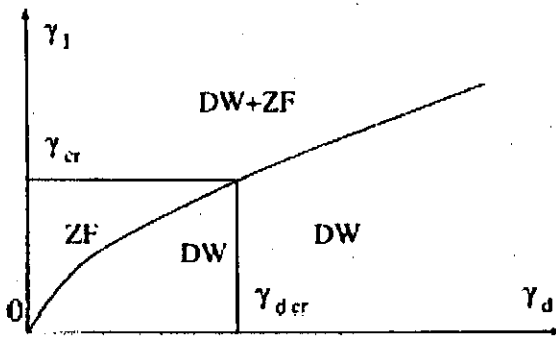


**Fig.3.5.16** The diagram, indicating the regions of residual drift wave, and zonal flow turbulence as well as the region where they coexist in the  $(\gamma_L, \gamma_{damp})$  plane.

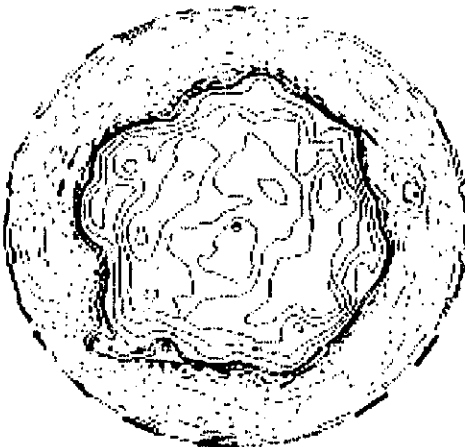


**Fig.4.1** Contour of electrostatic potential from the simulation of [2.6].

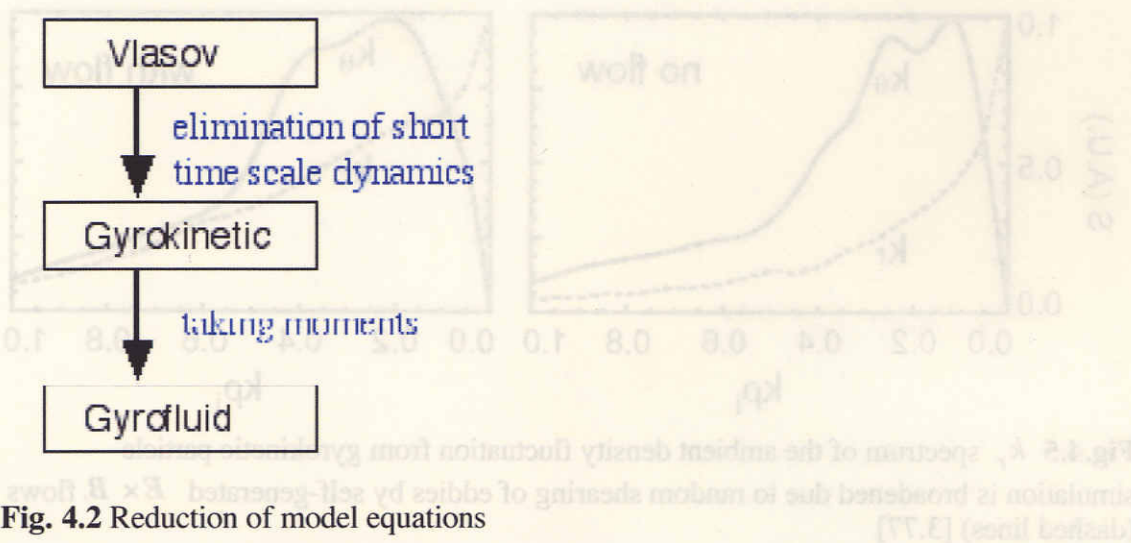


**Fig. 4.2** Reduction of model equations

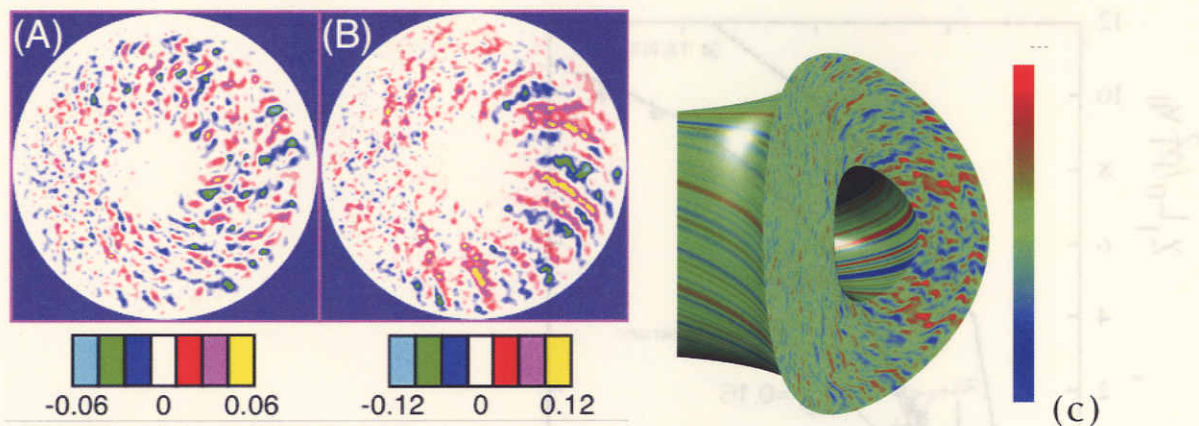


**Fig. 4.3** Radial size of turbulent eddies shown in colored contour of ambient density fluctuation gets reduced due to the random shearing by self-generated  $E \times B$  zonal flows from gyrokinetic particle simulation, (a) and (b) (from [2.16]). (c) is quoted from [http://fusion.gat.com/comp/parallel/gyro\\_gallery.html](http://fusion.gat.com/comp/parallel/gyro_gallery.html).

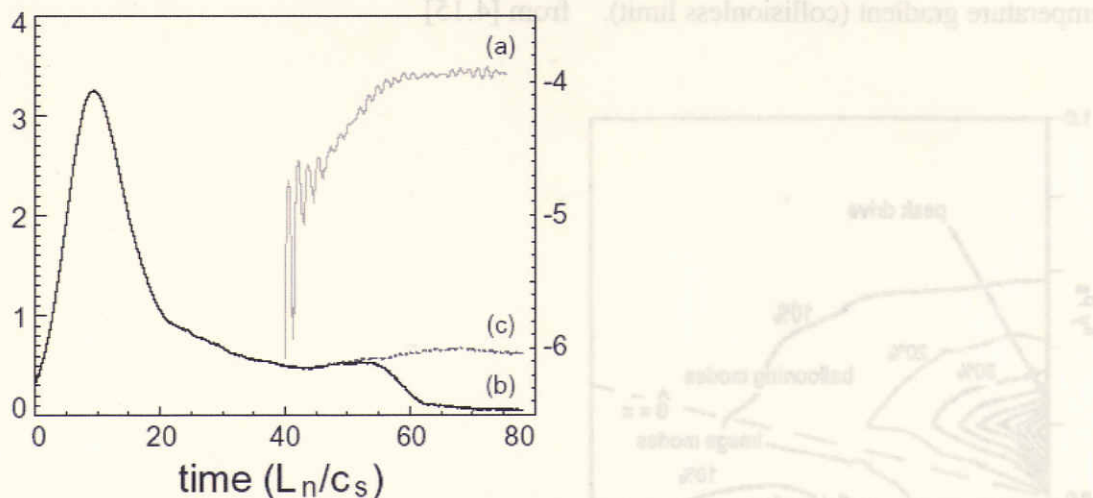


**Fig.4.4.** Temporal evolution of the amplitude of the zonal flow, on log scale (a), and turbulence level (b) and (c) on linear scale [2.13].

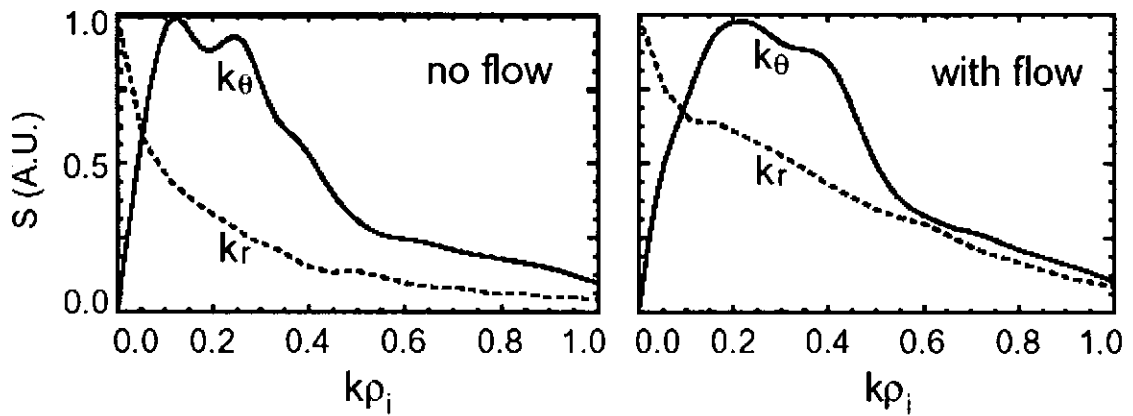


**Fig.4.5**  $k_r$  spectrum of the ambient density fluctuation from gyrokinetic particle simulation is broadened due to random shearing of eddies by self-generated  $E \times B$  flows (dashed lines) [3.77]

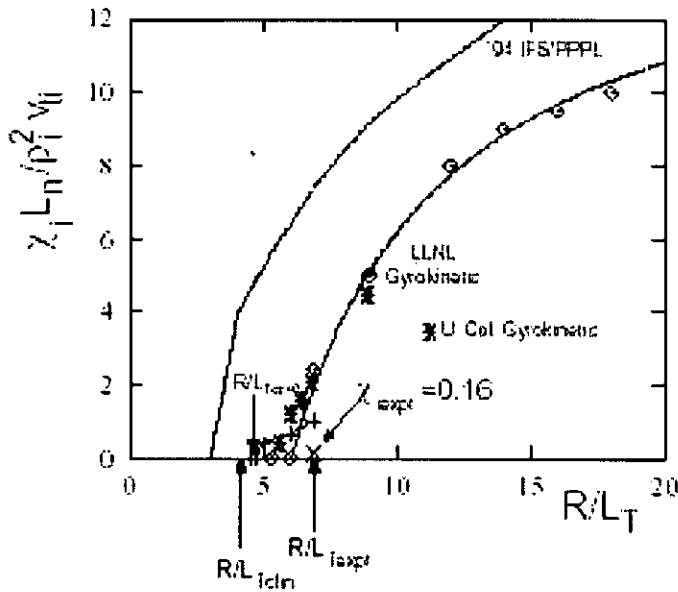


**Fig.4.6** Dependence of ion thermal conductivity by ITG turbulence on the ion temperature gradient (collisionless limit). from [4.15]

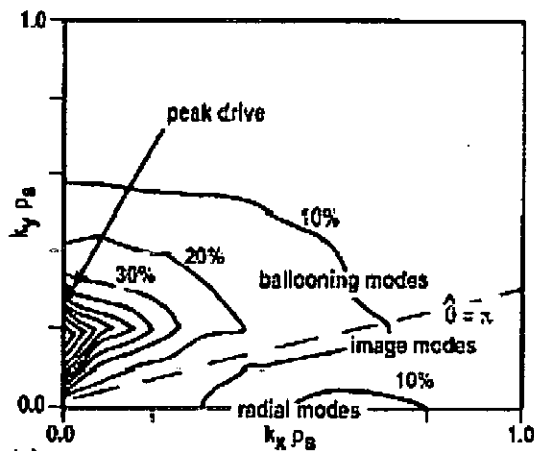


**Fig. 4.7** Contour of fluctuation spectrum from [2.17].

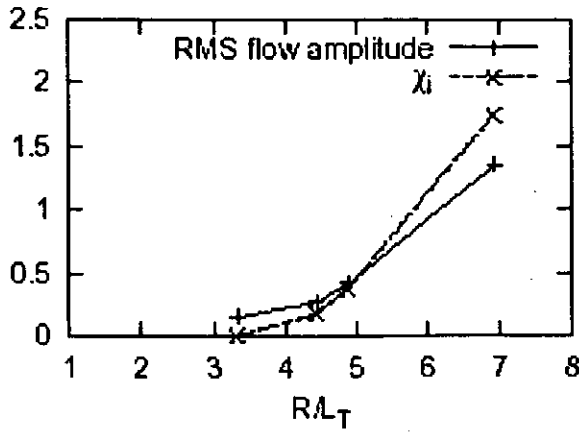


**Fig.4.8** Dependence of the turbulence level (shown by ion thermal conductivity) and zonal flow amplitude on the ion temperature gradient. (from [4.16])

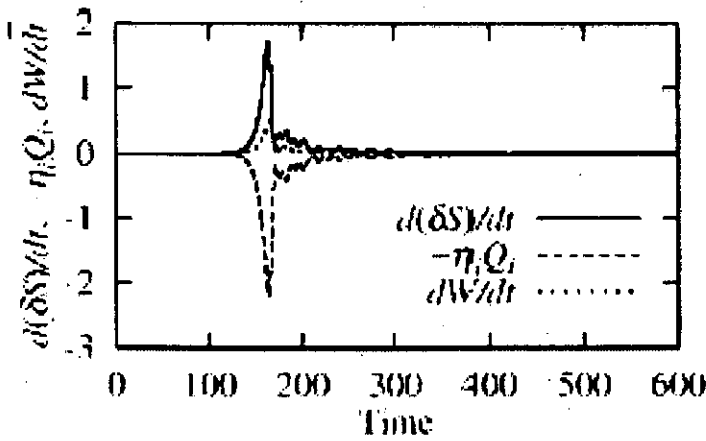


**Fig.4.9** Transient burst of ITG turbulence and associated transport in the collisionless limit. [3.109]

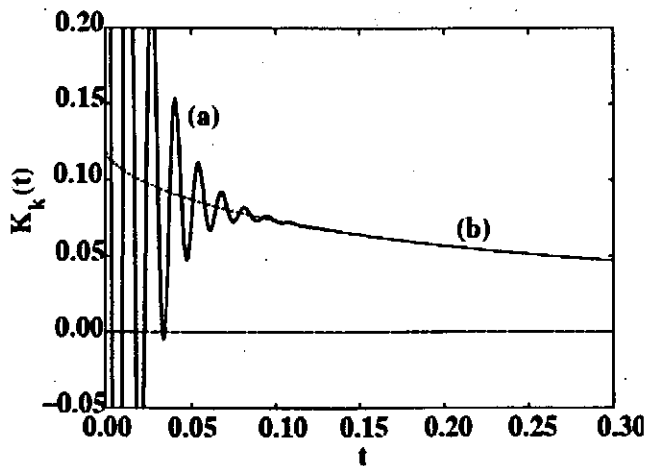


**Fig.4.10** Transient evolution of the poloidal flow and approach to the R-H zonal flow.  $K(t) = \phi(t)/\phi(0)$  is the normalized potential and time is normalized to  $\tau_{ii}$ . (from [2.37])

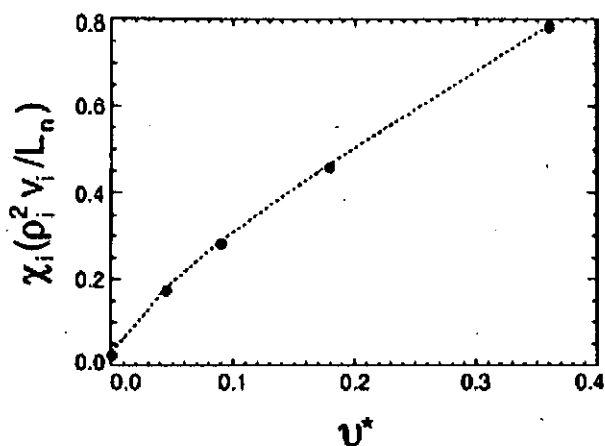


**Fig. 4.11** Ion heat conductivity in nonlinear gyrokinetic simulations with  $R/L_T = 5.3$  vs the ion-ion collision frequency [2.49].

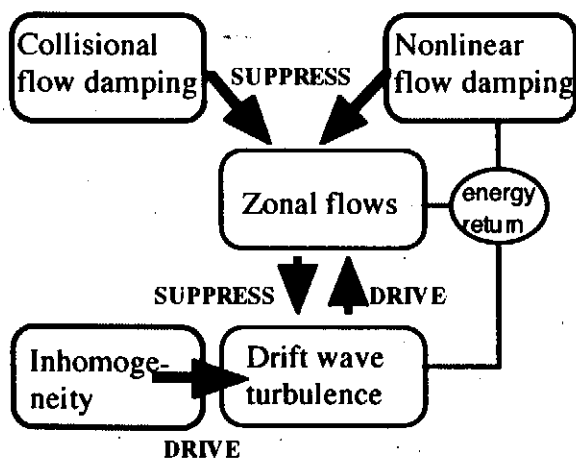


**Fig. 4.12** Schematic illustration of the self-regulation. In the right circle, 'energy return' indicates the process of energy return to drift waves (being investigated.)

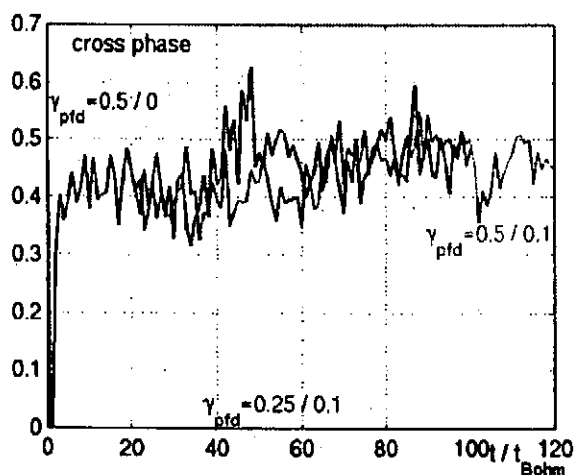


**Fig. 4.13** Cross phase evaluated at the radial position where the ZFs are persistently localized ( $r/a = 0.8$ ) for all the simulations with  $\rho_* = 0.02$  versus time.  $\gamma_{ptd}$ , the poloidal damping rate normalized to  $c_s/qR$ , is varied as indicated. [4.19].

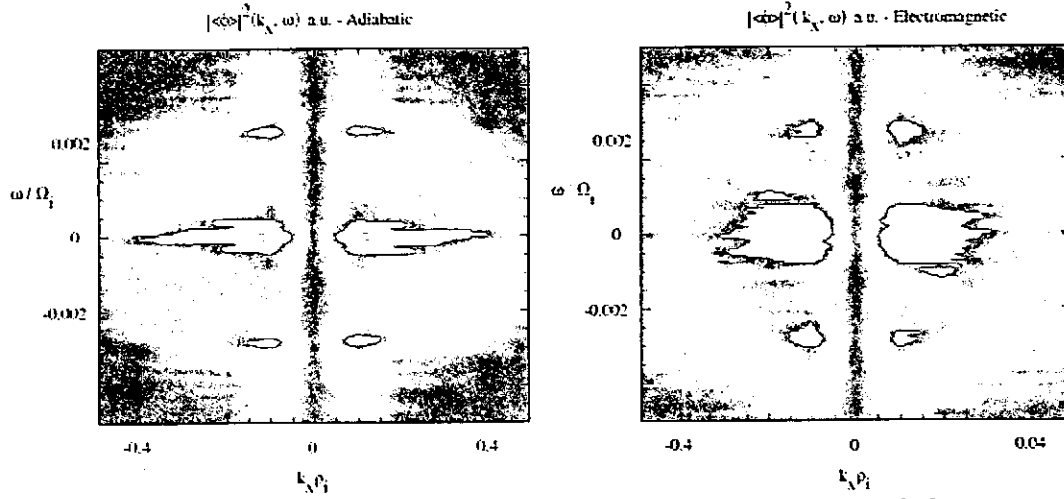


**Fig.4.14** Frequency spectrum of the zonal flows in collisionless trapped electron mode (CTEM) turbulence. Note a peak of pure zonal flow near  $\omega = 0$  and that at GAO frequency  $\omega_{\text{GAO}} = v_{\text{Thi}}/R$ . The influence of non-adiabatic response of electrons is illustrated. The case without (left) and with (right) are shown. In the presence of nonadiabatic response of electrons, the power spectrum of zonal flow component becomes wider. [4.23]

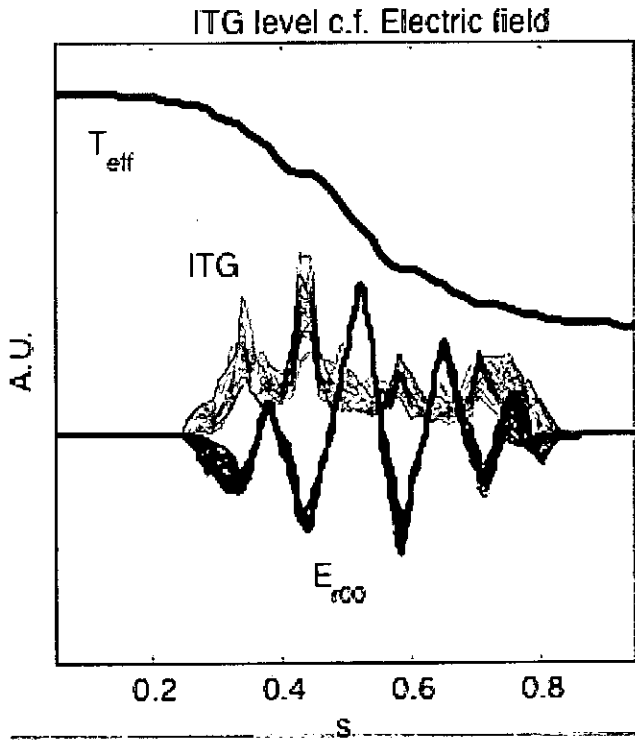


**Fig.4.15** Snapshots of the zonal  $E \times B$  flow, ITG amplitude, and effective temperature profile in the nonlinear stage. [4.26]



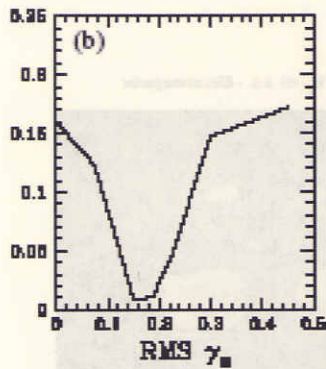


**Fig.4.16** Growth rate of tertiary instability [2.51]

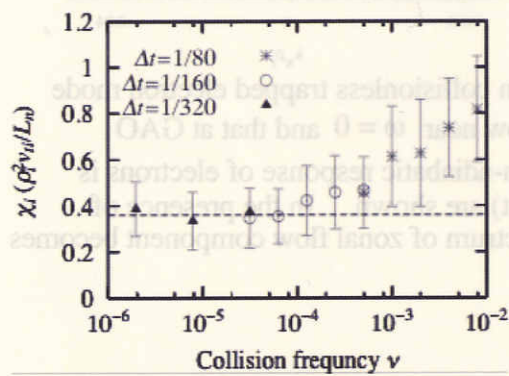


**Fig.4.17** Asymptotic convergence of the turbulent transport in the collisionless limit. from [4.33]

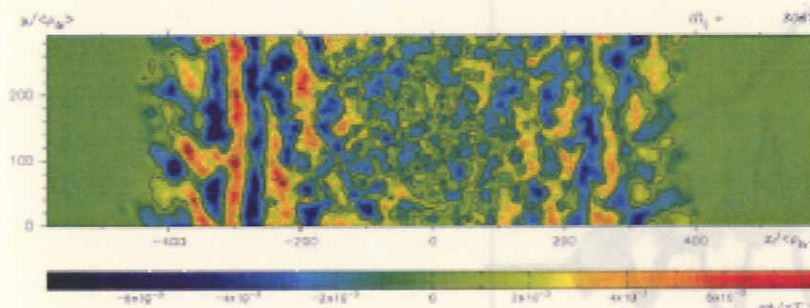


**Fig.4.18** Two dimensional contour of the electrostatic potential perturbation of ETG turbulence near the q-minimum surface  $x = 0$ . [2.52]

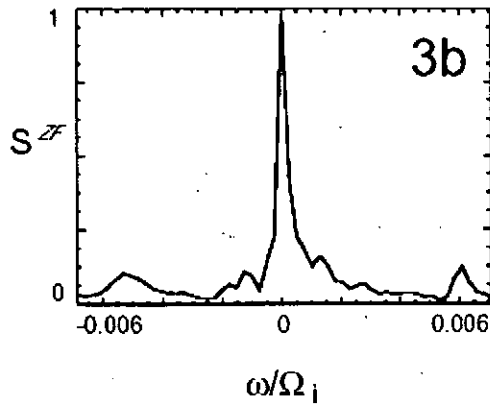


**Fig.4.19** Frequency spectrum of the zonal flows from gyrokinetic particle simulation of ITG core turbulence. Note a peak at GAO frequency  $\omega_{\text{GAO}} = v_{\text{Thi}}/R$  is subdominant to a broad peak at zero frequency [4.12].

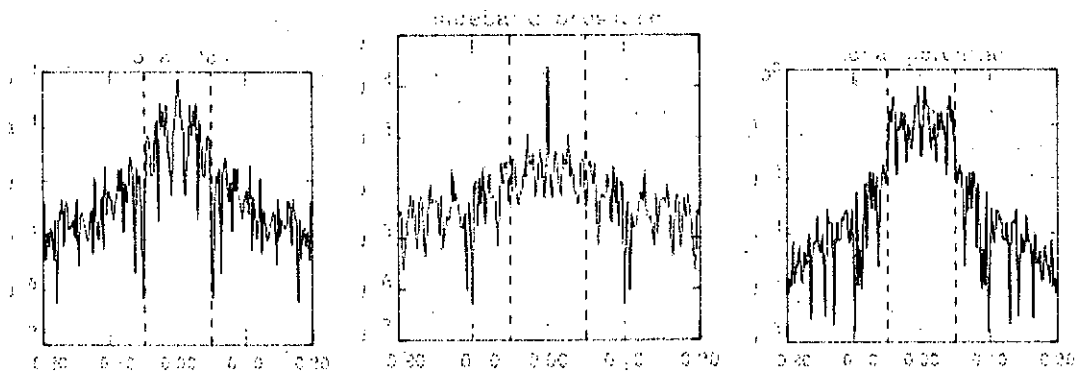


**Fig.4.20** Frequency spectrum of the zonal flows from gyrofluid simulation of edge drift-Alfven turbulence [4.66]. Note a significant intensity spectrum from zero frequency all the way up to the GAO frequency  $\omega_{\text{GAO}}$ , without a distinct single peak.

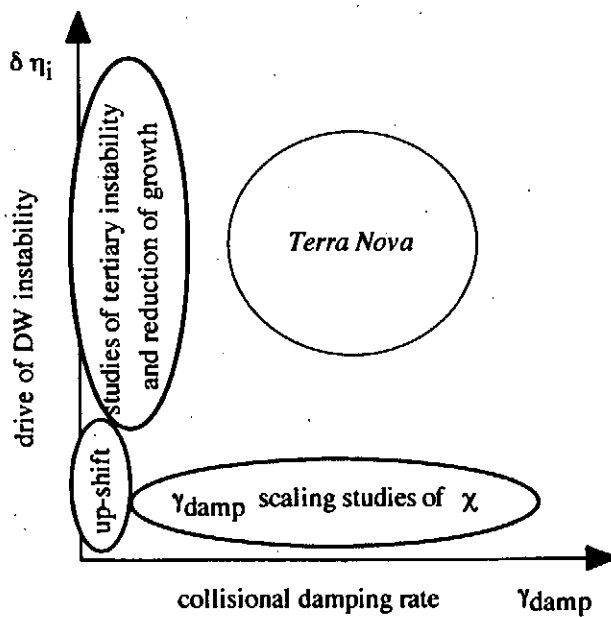
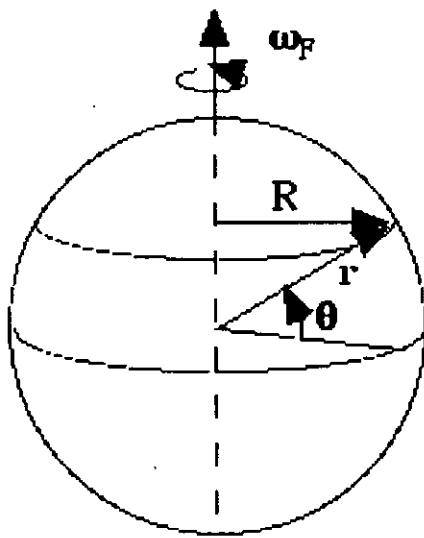
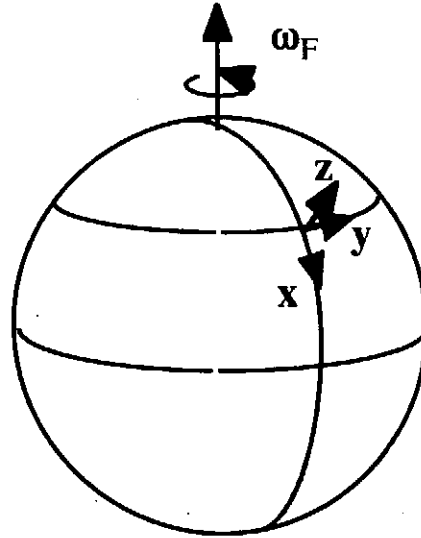


**Fig.4.21** Schematic drawing for the systematic exploration of zonal flow dynamics.



(a)



(b)

**Fig.5.1.1** Rotating sphere (a). Coordinates on a rotating sphere (b). The x-axis in the direction of latitude (from pole to equator), y-axis in the direction of longitude, and z-axis in the vertical direction.

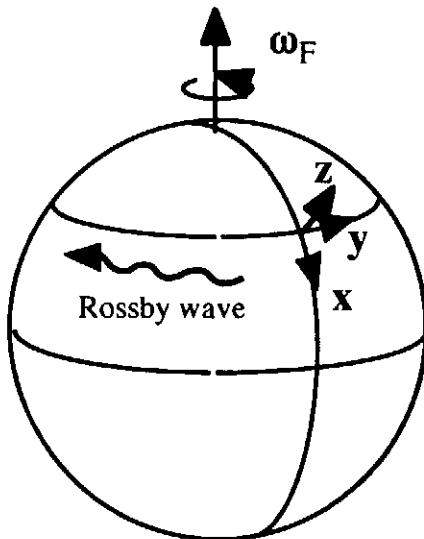


**Fig. 5.1.2** Propagation of Rossby wave in the westward direction.

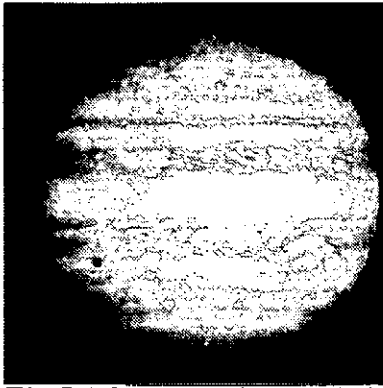


**Fig.5.1.3** Zonal flow and giant spot in planets. [quoted from <http://nssdc.gsfc.nasa.gov/planetary/factsheet/jupiterfact.html>]

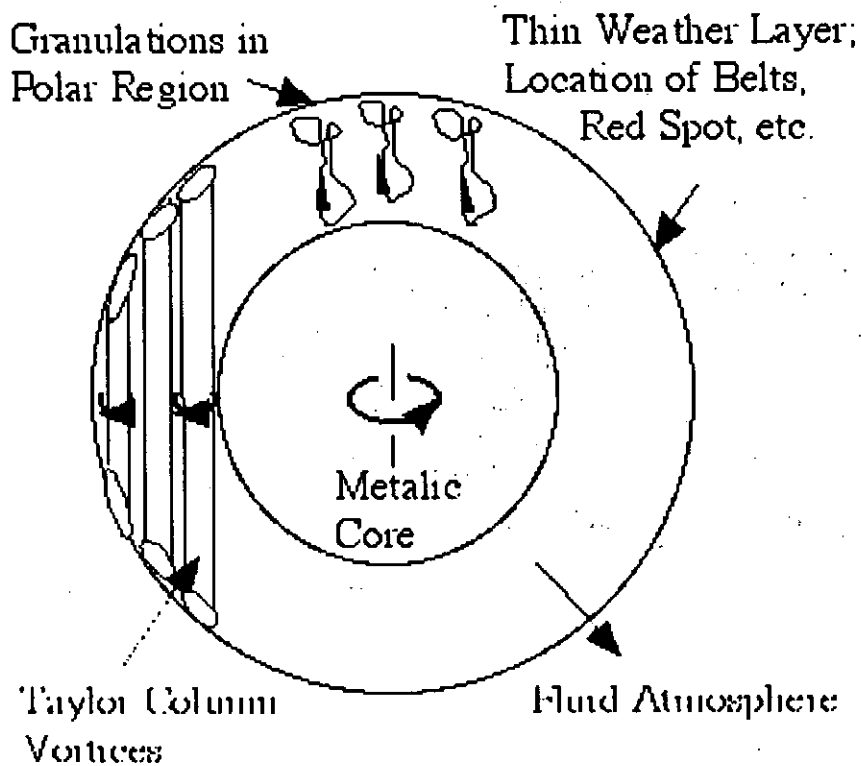


**Fig.5.2.1** Schematic drawing of convection phenomena in Jovian atmosphere. (Based on [4.46].)

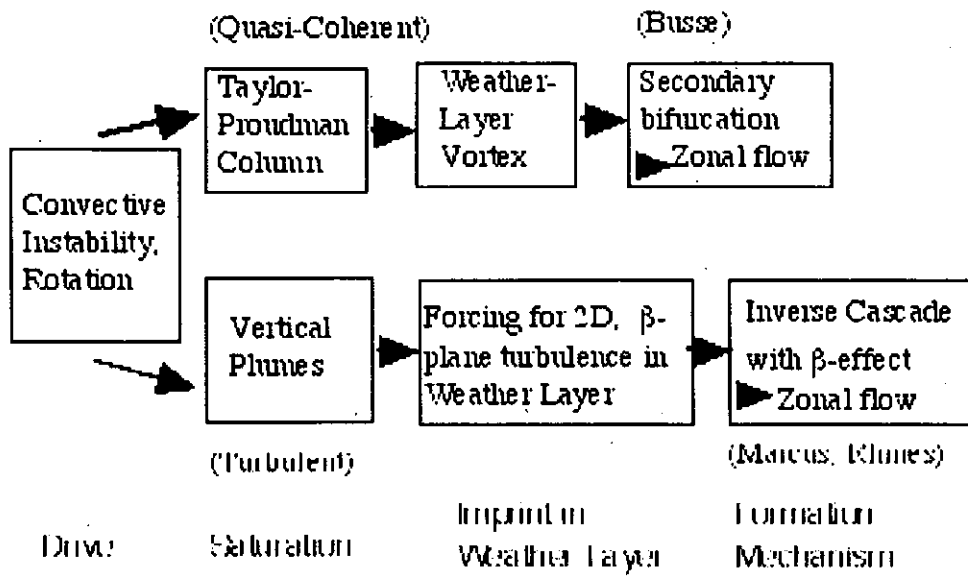


Fig.5.2.2 The assumptions and logic of the two scenarios.

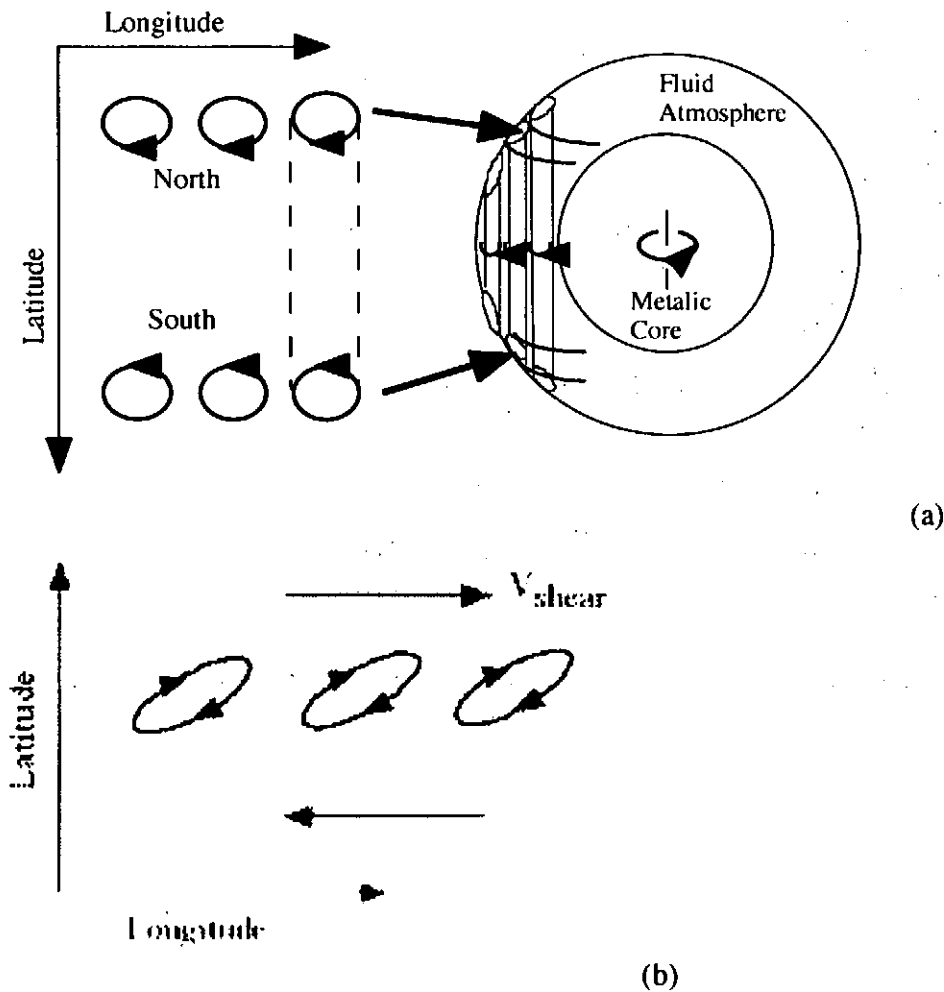


Fig.5.2.3 Schematic depiction of zonal belt formation in secondary bifurcation scenario. (a) Northern and southern projections of Taylor column onto Weather Layer. (b) After tilting modulation and bifurcation.

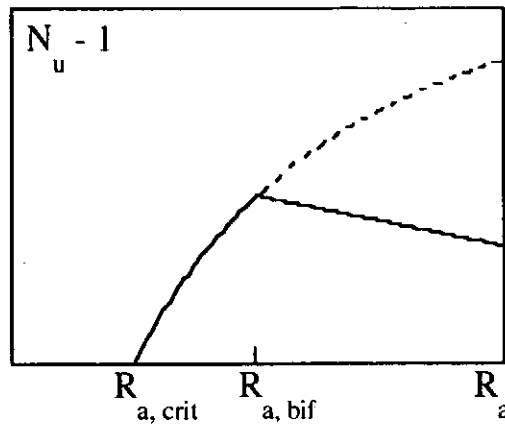


Fig.5.2.4 Cartoon of secondary bifurcation scenario, after Fig. 6 of [5.5].

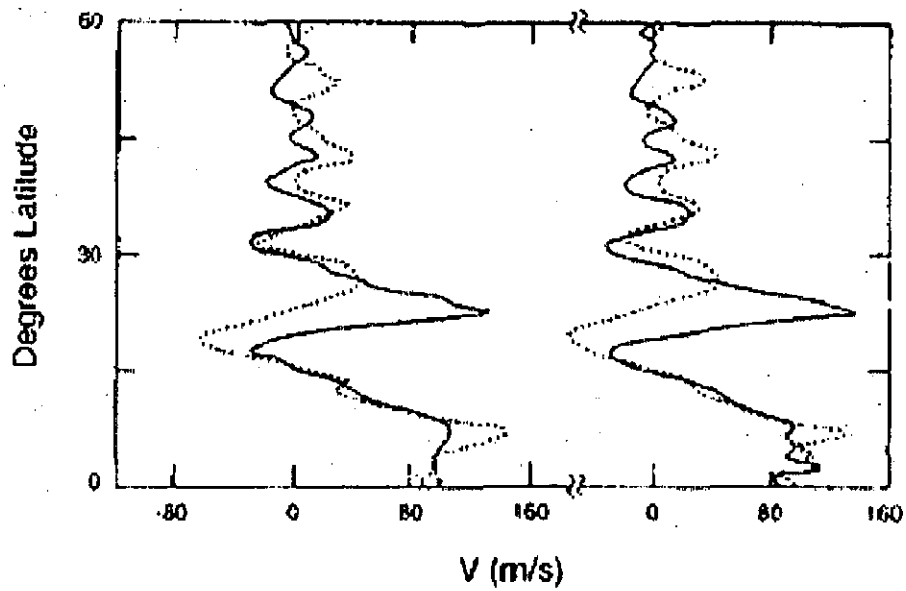
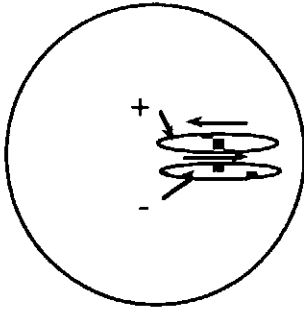
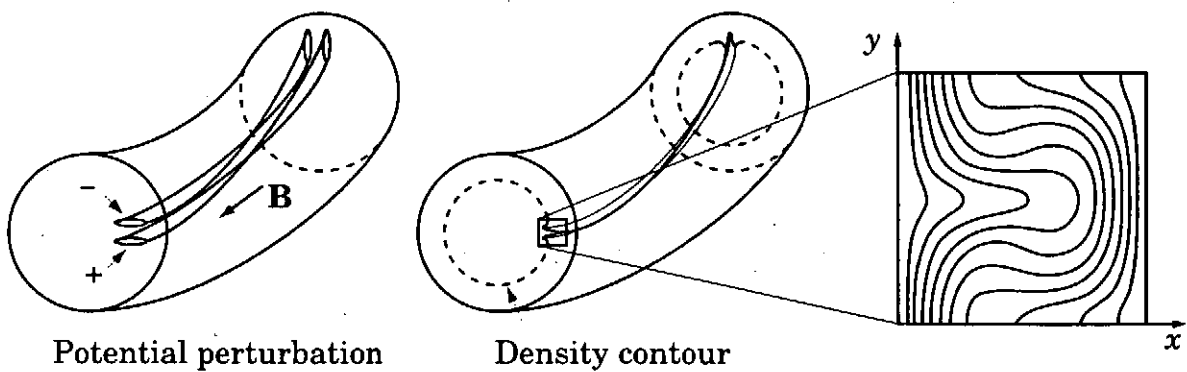


Fig.5.2.5 Mean zonal flow pattern, from Voyager observations. Solid and dashed lines for northern and southern hemisphere, respectively. The left data is from Voyager 1, and the right from Voyager 2, respectively. (Reproduced from [4.46].)



**Fig.6.1.1** The streamer as an example of convective cell formation. Poloidally-inhomogeneous radial flow occurs for a streamer.



**Fig.6.1.2** Illustration of density contour in the presence of a streamer. Potential perturbation (left) and density contour (center). Contour of unperturbed state is denoted by dashed curve and deformed one by solid line. Expanded view of density contour (right). Quoted from [2.14] and is also based on [6.4].

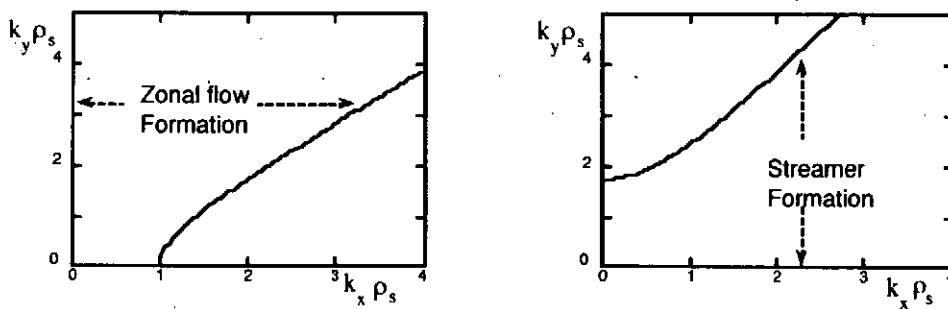


**Fig.6.1.3** Region of wavenumber of drift waves for the excitation of zonal flow (a) and streamer (b). Zonal flow is generated by waves with larger poloidal mode number  $k_\theta$ , but the zonal flow is excited by drift waves with larger radial modenumber  $k_r$ . (Based on [2.27])

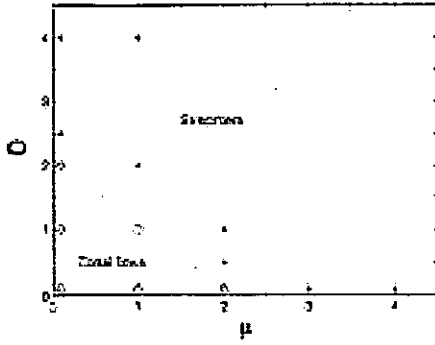


**Fig.6.1.4.** A consolidated phase diagram in  $D, m$  space delineating regions corresponding to the predominance of zonal and streamers structures in the final state. The circles and asterisks represent the values of  $D$  and  $m$  where the numerical simulation was actually carried out leading to the formation of zonal and streamer structures, respectively. (quoted from [6.6].)

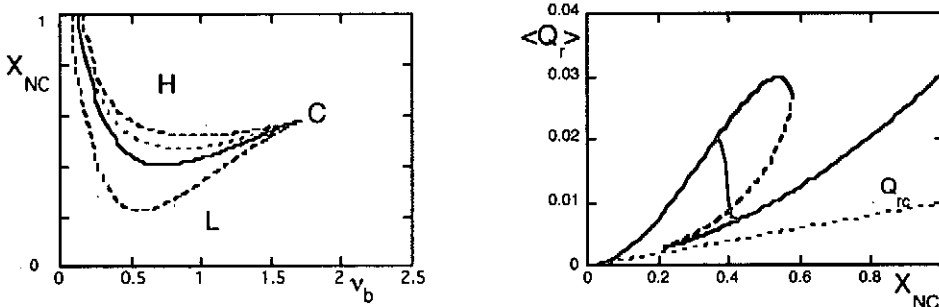


**Fig.6.3.1** (a) Phase boundary on the plane of PDF of normalized collision frequency of banana  $X_{NC}$ . Dashed lines for deterministic model,  $\Lambda X = 0$ , and the solid line shows the statistical average. (b) Normalized heat flux  $\langle Q_r \rangle$  as a function of global gradient  $X_{NC}$ . Deterministic model shows the cusp catastrophe (thin line). Ensemble average is shown by the thick solid line. (Quoted from [6.20].)

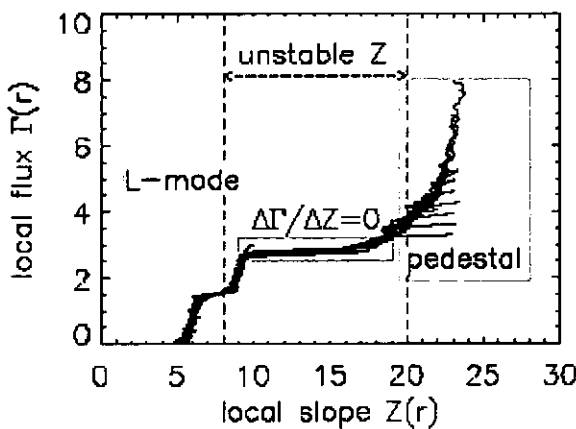


**Fig.6.3.2.** Family of parametric plots of local flux  $\Gamma_r$  versus local slope  $Z(r)$  function  $\Gamma(Z)$  is multivalued for  $\Gamma > 3$ . (quoted from [6.29].)



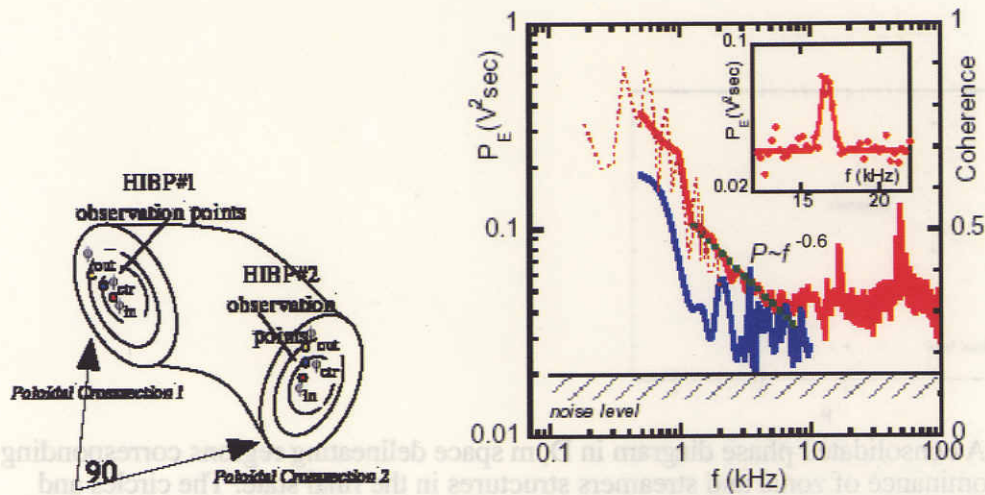


**Fig.7.1** Identification of zonal flow on CHS. Geometry of measurements and fluctuation spectra. (a) Observation points of dual heavy ion beam probes in CHS. (b) Power spectra of a electric field, and coherence between electric fields from the HIBPs. In the frequency range from 0.3 kHz to 1 kHz, the activity to show long range correlation is found to be zonal flow. A peak at the GAM frequency is shown by an insert. Fluctuations in the range of tens of kHz are drift-wave turbulence. [7.17]

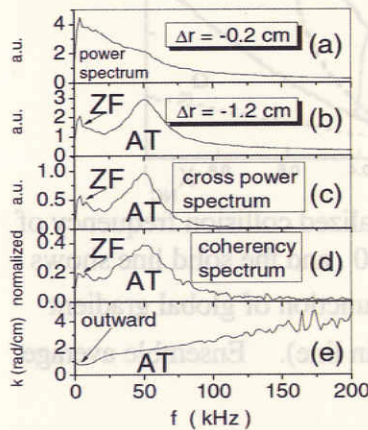


**Fig. 7.2** Spectra measured with the modified forked probe. Peaks of zonal flow and ambient turbulence (AT) are shown. (a) Auto power spectrum of  $\tilde{V}_{01}$  ( $\Delta r = -0.2$  cm ). (b) Auto power spectrum of  $\tilde{V}_{02}$  ( $\Delta r = -1.2$  cm ). (c) Cross power spectrum. (d) Coherency spectrum. (e) Wave number spectrum. (c), (d). and (e) were calculated from the long distance correlation between  $\tilde{V}_{01}$  and  $\tilde{V}_{02}$ . [7.19]

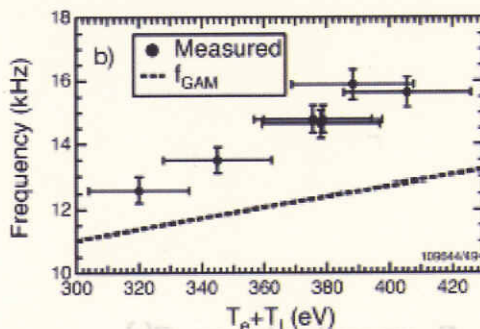


**Fig.7.4** Frequency of observed oscillations (attributed to GAM) and it dependence on temperature. Measurement of D III-D is compared to the calculated GAM frequency (left) [7.37].

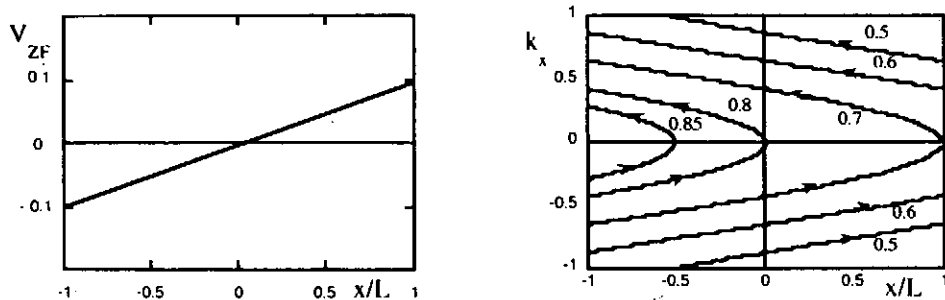


**Fig.A.1** Case of constant gradient of the zonal flow (a). The trajectory of the wave-packet (b). (The unit of velocity is diamagnetic drift velocity.)

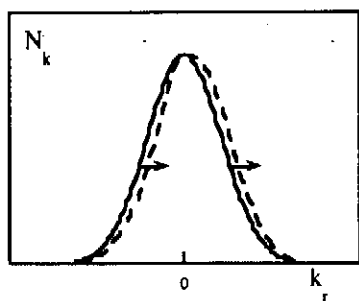


**Fig.A.2** Change of distribution function after the imposition of the zonal flow like Fig.A.1(a). Original symmetric one (solid line) is shifted and deformed as is shown by dashed line.

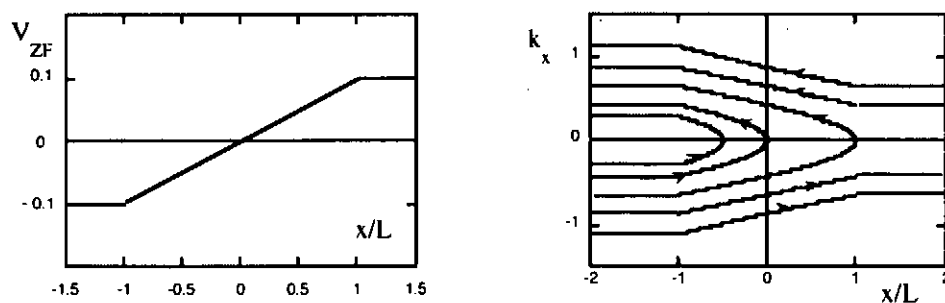


**Fig.A.3** Schematic drawing of the localized inhomogeneity of the flow (a) and the reflection orbit (b).

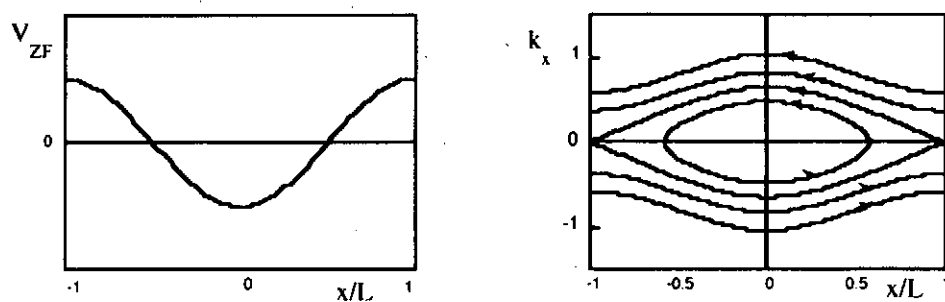


**Fig. A.4** Trapping of wave-packets in the trough of zonal flow velocity. The spatial profile of zonal flow velocity (a) and trajectories in the phase space (b).

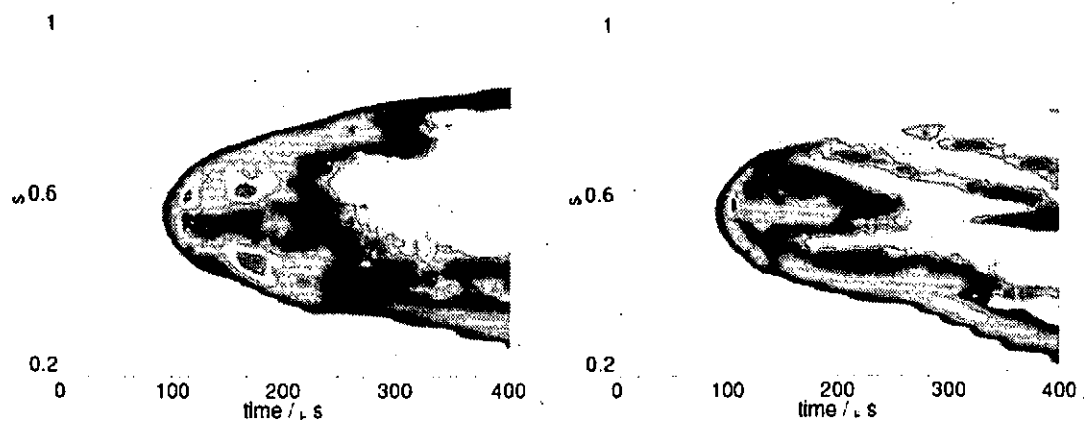


**Fig. B1** Time evolution of the radial heat flux, with (left) and without (right)  $V_{\parallel}$  nonlinearity. [4.47]

## Recent Issues of NIFS Series

- NIFS-781 Ya. I. Kolesnichenko, K. Yamazaki, S. Yamamoto, V.V. Lutsenko, N. Nakajima, Y. Narushima, K. Toi, Yu. V. Yakovenko  
Interplay of Energetic Ions and Alfvén Modes in Helical Plasmas  
Aug. 2003
- NIFS-782 S.-I. Itoh, K. Itoh and M. Yagi  
Turbulence Trigger for Neoclassical Tearing Modes in Tokamaks  
Sep. 2003
- NIFS-783 F. Spineanu, M. Vlad, K. Itoh, H. Sanuki and S.-I. Itoh  
Pole Dynamics for the Flierl-Petviashvili Equation and Zonal Flow  
Sep. 2003
- NIFS-784 R. Smirnov, Y. Tomita, T. Takizuka, A. Takayama, Yu. Chutov  
Particle Simulation Study of Dust Particle Dynamics in Sheaths  
Oct. 2003
- NIFS-785 T.-H. Watanabe and H. Sugama  
Kinetic Simulation of Steady States of Ion Temperature Gradient Driven Turbulence with Weak Collisionality  
Nov. 2003
- NIFS-786 K. Itoh, K. Hallatschek, S. Toda, H. Sanuki and S.-I. Itoh  
Coherent Structure of Zonal Flow and Nonlinear Saturation  
Dec. 2003
- NIFS-787 S.I. Itoh, K. Itoh, M. Yagi and S. Toda  
Statistical Theory for Transition and Long-time Sustainment of Improved Confinement State  
Dec. 2003
- NIFS-788 A. Yoshizawa, S.-I. Itoh, K. Itoh and N. Yokoi  
Dynamics and MHD Theory of Turbulence Suppression  
Dec. 2003
- NIFS-789 V.D. Pustovitov  
Pressure-induced Shift of the Plasma in a Helical System with Ideally Conducting Wall  
Jan. 2004
- NIFS-790 S. Koikari  
Rooted Tree Analysis of Runge-Kutta Methods with Exact Treatment of Linear Terms  
Jan. 2004
- NIFS-791 T. Takahashi, K. Inoue, N. Iwasawa, T. Ishizuka and Y. Kondoh  
Losses of Neutral Beam Injected Fast Ions Due to Adiabaticity Breaking Processes in a Field-Reversed Configuration  
Feb. 2004
- NIFS-792 T.-H. Watanabe and H. Sugama  
Vlasov and Drift Kinetic Simulation Methods Based on the Symplectic Integrator  
Feb. 2004
- NIFS-793 H. Sugama and T.-H. Watanabe  
Electromagnetic Microinstabilities in Helical Systems  
Feb. 2004
- NIFS-794 S.I. Kononenko, O.V. Kalantaryan, V.I. Muratov and C. Namba  
Spectral and Angular Characteristics of Fast Proton-Induced Luminescence of Quartz  
Mar. 2004
- NIFS-795 K. Itoh, K. Hallatschek and S.-I. Itoh  
Excitation of Geodesic Acoustic Mode in Toroidal Plasmas  
Mar. 2004
- NIFS-796 A. Shimizu, A. Fujisawa, S. Ohshima and H. Nakano  
Consideration of Magnetic Field Fluctuation Measurements in a Torus Plasma with Heavy Ion Beam Probe  
Mar. 2004
- NIFS-797 M.I. Mikhailov, K. Yamazaki  
Fast Particles Confinement in Stellarators with Both Poloidal-Pseudo-Symmetry and Quasi-Isodynamicity  
Apr. 2004
- NIFS-798 T. Takahashi, T. Kato, N. Iwasawa and Y. Kondoh  
Power Deposition by Neutral Beam Injected Fast Ions in Field-Reversed Configurations  
Apr. 2004
- NIFS-799 V.S. Voitsenya, D.I. Naidenkova, Y. Kubota, S. Masuzaki, A. Sagara, K. Yamazaki  
On the Possibility to Increase Efficiency of Conditioning of Vacuum Surfaces by Using a Discharge in a Hydrogen-noble Gas Mixture  
Apr. 2004
- NIFS-800 S.-I. Itoh, K. Itoh, A. Yoshizawa and N. Yokoi  
Periodic Change of Solar Differential Rotation  
May 2004
- NIFS-801 V.S. Voitsenya, A. Sagara, A.I. Belyaeva  
Effect of Exposure inside the LHD Vessel on Optical Properties of Stainless Steel Mirrors  
Jun 2004
- NIFS-802 T.J. Dolan and K. Yamazaki  
Upgrade and Benchmarking of the NIFS Physics-Engineering-Cost Code  
July 2004
- NIFS-803 Contributions to 31st European Physical Society Conference on Plasma Physics (London, UK, 28 June to 2 July, 2004) from NIFS  
Aug. 2004
- NIFS-804 M. Tanaka  
A Cluster of Personal Computers Equipped with Low-Latency Communication Software  
Aug. 2004
- NIFS-805 P.H. Diamond, S.-I. Itoh, K. Itoh and T.S. Hahm  
Review of Zonal Flows  
Oct. 2004